

Alkali Metal Zincate Chemistry: The Importance of Structure and Stoichiometry on Reactivity

Emma Herd

August 2014

A thesis submitted to the Department of Pure and Applied Chemistry, University of Strathclyde, in part fulfillment of the regulations for the degree of Doctor of Philosophy.

This thesis is the result of the author's original research. It has been composed by the author and has not been previously submitted for examination which has lead to the award of a degree.

The copyright of this thesis belongs to the author under the terms of the United Kingdom Copyright Acts as qualified by University of Strathclyde Regulation 3.50. Due acknowledgement must always be made of the use of any material contained in, or derived from, this thesis.

Acknowledgements

Many people have been complicit in the creation of this masterpiece, and unfortunately it would be impossible to list them all. At the top of the shortlist are undoubtedly my supervisors, Professors Hevia and Mulvey, without whom there would have been no funding, no research and a significantly shorter thesis. I thank them for having sufficient faith in my abilities to seek out the funding which enabled me to complete my PhD; and the University of Strathclyde for generously providing the funds. Credit must also go to Dr. Thomas Cadenbach, Dr. Alberto Hernán-Gomez and Dr. Alan Kennedy for the valuable provision of X-ray data and to Dr. David Armstrong for performing his ~~magical~~ theoretical calculations. Likewise, many thanks are due to Janie-Anne Pickrell for keeping everything running, and to Mayte Muñoz for performing the groundwork on the bis(amido)silyl complexes.

I would also like to recognize all members (past and present) of the Hevia, Mulvey, O'Hara and Robertson research groups for their general help and support. In particular, I would like to express my gratitude to my partners in crime Dr. Jenni Garden, Donna Ramsay, Sarah Leenhouts and Marina Uzelac for being my loyal support group, and Dr. Tobias Blümke my occasional psychotherapist and regular drinking buddy. You guys deserve a medal, but owing to budget restrictions I hope that you will accept this namedrop in lieu of any actual reward.

Finally, I must thank my family; my parents Bob and Mags Herd for being there in my darkest hour and supporting me no matter what, and my long-suffering other half Dr. Dave Bowes for his constant love, encouragement and for bearing the brunt of my insanity throughout the writing of this, my opus. I owe each of you more than I can ever hope to repay.

Abstract

Focusing on the area of cooperative bimetallic reagents, this report aims to advance our understanding on the construction and reactivity of alkali metal zincates. Extending previous studies on the synthesis of dialkyl(amido)zincates, unsolvated lithium zincate [LiZn(HMDS)Me₂] **4a** was prepared by a cocomplexation approach, and its interaction with a range of Lewis basic solvents of varying denticity was examined. The effect of these donors on constitution and stability was assessed, resulting in the determination of a novel dialkyl(amido)zincate, [(PMDETA)LiZn(HMDS)Me₂] **5**, containing an unusual terminal amido ligand.

The influence of the amido group in these mixed-metal systems was also studied. Using the amide [NHDipp], a new family of lithium zincates has been synthesised, leading to the characterisation of the first dialkyl(amido)zincates based on a primary amide – [(PMDETA)LiZn(NHDipp)Me₂] **10** and [(THF)₃LiZn(NHDipp)(Me)₂] **11**. X-ray crystallographic studies evidenced that, depending on the donor solvent employed, novel zincate formulations can be accomplished – as demonstrated by the isolation of the unprecedented zinc-rich zincate [LiZn₂(NHDipp)₂(Me)₃(THF)₃] **12**, containing an unusual 2:1 zinc to lithium ratio.

By synthesising the homoaryl lithium zincates [LiZnPh₃] **15** and [Li₂ZnPh₄] **16**, and investigating their reactivity towards several electron-deficient *N*-heterocycles, a new transition metal free method enabling the efficient, regioselective arylation of acridine has been developed. Isolation of key reaction intermediates such as [(THF)₃Li(NC₁₃H₉-9-Ph)] **17**, has provided important clues as to how these bimetallic systems operate. The reactivity of trimetallic mixtures based on [Zn(OPiv)₂·2LiCl] **27** and ArMgCl towards *N*-heterocyclic molecules was also investigated. Although unreactive towards arylation, new light has been shed on the constitution, reactivity and stability of these multi-component reagents.

Finally, the bulky bis(amido)silyl ligand $[\text{Ph}_2\text{Si}(\text{NDipp})_2]^{2-}$ has been successfully incorporated into two novel zincates, $[\{\text{Na}(\text{THF})_6\}^+\{(\text{Ph}_2\text{Si}(\text{NDipp})_2)\text{ZnEt}\}^-]$ **29** and $[(\text{Ph}_2\text{Si}(\text{NDipp})_2)\text{Zn}(\text{TMP})\text{Na}(\text{THF})]$ **30**, which have been employed in the regioselective zincation of benzothiazole and pyrrole, yielding the novel compounds $[\text{Na}(\text{THF})_2\text{Zn}(\text{Btz})_3]_2$ **31** and $[\text{Na}_2(\text{THF})_4\text{Zn}(\text{NC}_4\text{H}_4)_4]_\infty$ **32**.

Publications

Publications in Peer Reviewed Journals

1. Organozinc Pivalate Reagents: Segregation, Solubility, Stabilization and Structural Insights.

Alberto Hernán-Gómez, Emma Herd, Eva Hevia, Alan R. Kennedy, Paul Knochel, Konrad Koszinowski, Sophia M. Manolikakes, Robert E. Mulvey, Christoph Schnegelsberg, *Angewandte Chemie International Edition*, **2014**, 53, 2706.

2. Donor-Dictated Interlocking Co-Complexation Reactions of LiNHDipp with Dimethylzinc: Synthesis and Structures of New Methyl(amido)zincates.

William Clegg, David V. Graham, Emma Herd, Eva Hevia, Alan R. Kennedy, Matthew D. McCall, Luca Russo, *Inorganic chemistry*, **2009**, 48, 5320.

3. Synthesis and structural elucidation of solvent-free and solvated lithium dimethyl (HMDS) zincates.

David R. Armstrong, Emma Herd, David V. Graham, Eva Hevia, Alan R. Kennedy, William Clegg, Luca Russo, *Dalton Transactions*, **2008**, 1323.

Conference Presentations (Oral)

4. Investigating Direct Arylation Reactions of *N*-Heterocycles Using Polar Organometallic Reagents

Universities of Scotland Inorganic Conference, University of Edinburgh, July **2013**.

5. Investigating Direct Arylation Reactions of *N*-Heterocycles Using Polar Organometallic Reagents

University of Strathclyde Inorganic Section Meeting, June **2013**.

Conference Presentations (Poster)

6. Transition Metal-free Direct Arylation of Electron Deficient Heterocycles using Lithium Zincates

Thomas Cadenbach, Emma Herd, Eva Hevia, Alan R. Kennedy, Universities of Scotland Inorganic Conference, University of St. Andrews, August **2012**.

Table of Common Abbreviations

acac	Acetylacetonate
Acr	Acridine
AMMZn	Alkali Metal Mediated Zincation
Ar	Aryl
Bu	Butyl
^t BuCN	<i>tert</i> -butylcyanide
Btz	Benzothiazole
Btz*	Benzothiozoyl
Bz	Benzyl
CCDB	Cambridge Crystallographic database
CIP	Contacted ion-pair
<i>cis</i> -DMP	<i>cis</i> -2,6-Dimethylpiperidide
COSY	Correlation Spectroscopy
D	Donor
DA	Diisopropylamide
DDQ	2,3-Dichloro-5,6-dicyano-1,4-benzoquinone
DFT	Density Functional Theory
DihydroAcr	9-Phenyl-9,10-dihydroacridine
DihydroEtAcr	9-ethyl-9,10-dihydroacridines
DihydroQuin	2-Phenyl-1,2-dihydroquinoline
Dipp	2,5-diisopropylphenyl
DMG	Direct metallating group
DoM	Directed <i>ortho</i> metallation
dpa	2,2-dipyridylamine
E ⁺	Electrophile
ESI-MS	Electrospray Ionisation – Mass Spectrometry
Et	Ethyl
h	Hours
HMDS	Hexamethyldisilylazide
HMPA	Hexamethylphosphoramide

HOESY	Heteronuclear Overhauser Effect Spectroscopy
HSQC	Heteronuclear Single Quantum Correlation Spectroscopy
ⁱ Pr	<i>iso</i> -Propyl
L	Ligand
LDA	Lithium Diisopropylamide
LUMO	Lowest unoccupied molecular orbital
M	Metal
Me	Methyl
MW	Microwave
NBoc	-NCO ₂ ^t Bu
NCS	<i>N</i> -Chlorosuccinimide
NHDipp	2,6-Diisopropylanilide
NH ₂ Dipp	2,6-Diisopropylaniline
NK ₃	Mammalian tachykinin receptor
NMR	Nuclear Magnetic Resonance
NOE	Nuclear Overhauser effect
NR ₂	Amide
Nu ⁻	Nucleophile
OMs	-OSO ₂ Me
OPiv	-OC(O) ^t Bu
OTBS	-OSiMe ₂ ^t Bu
Ph	Phenyl
PhAcr	9-Phenylacridine
PhPyr	2-Phenylpyrazine
Ph ₂ Pyr	2,5-Diphenylpyrazine
PhQuin	2-Phenylquinoline
PMDETA	<i>N,N,N',N'',N'''</i> -Pentamethyldiethylenetriamine
ppm	Parts per million
<i>p</i> -Tol	<i>para</i> -tolyl
Py	Pyridine
Pyr	Pyrazine
Quin	Quinoline

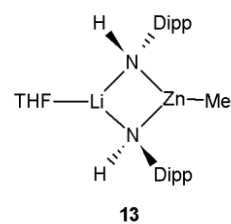
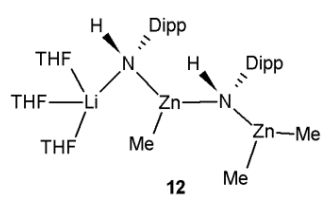
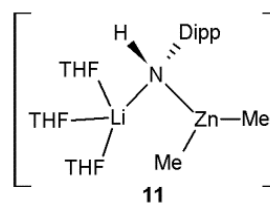
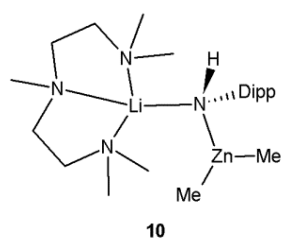
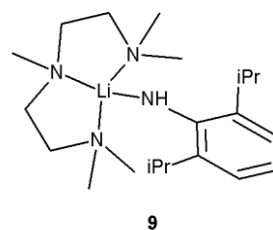
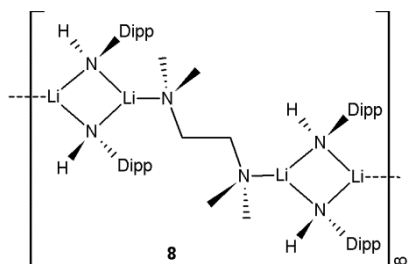
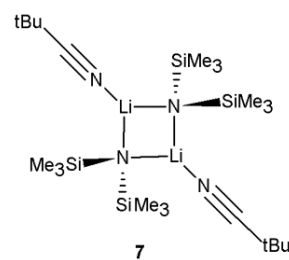
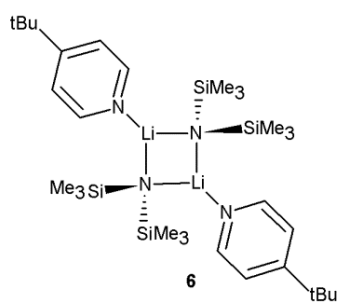
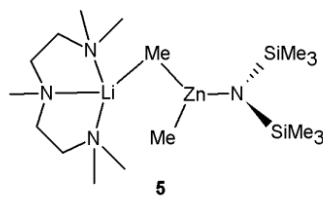
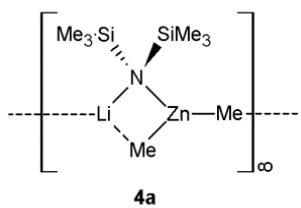
R	Alkyl
rt	Room temperature
SET	Single electron transfer
SM	Starting material
SSIP	Solvent separated ion-pair
^t Bu-py	4- <i>tert</i> -Butylpyridine
THF	Tetrahydrofuran
TMEDA	<i>N,N,N',N'</i> -Tetramethylethylenediamine
TMP	2,2,6,6-Tetramethylpiperidide
TMP(H)	2,2,6,6-Tetramethylpiperidine
TMS	trimethylsilane
TMTA	1,3,5-Trimethyl-1,3,5-triazinane
X	halide

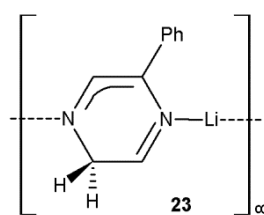
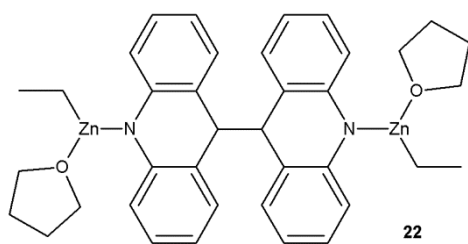
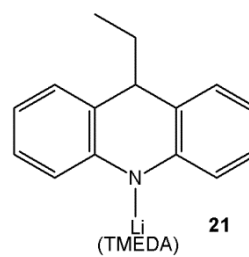
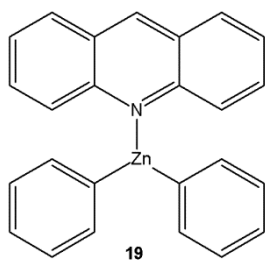
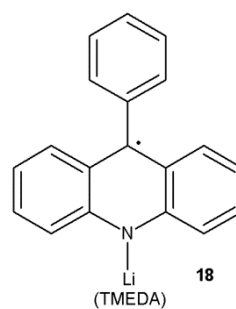
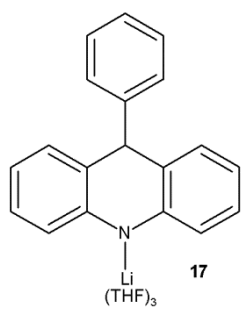
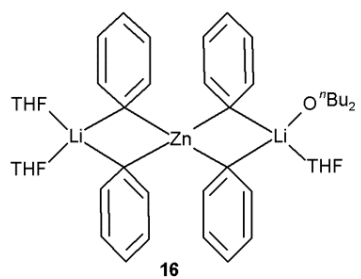
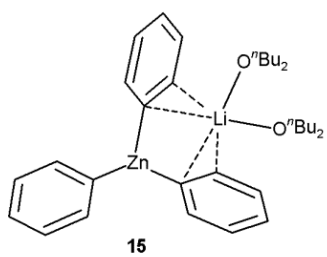
Table of Numbered Compounds

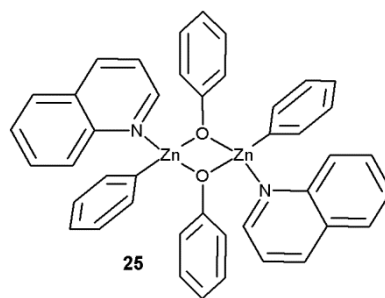
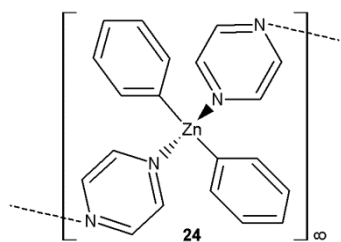
1	[Li(TMP)Zn ^t Bu ₂]
2	[(TMEDA)Na(TMP)Zn(^t Bu) ₂]
3a	[Li(TMP)ZnMe ₂]
3	[(TMEDA)Li(TMP)ZnMe ₂]
4a	[Li(HMDS)ZnMe ₂]
4	[Li ₂ (HMDS) ₂ (Me) ₂ Zn(TMEDA)]
5	[(PMDETA)LiZn(HMDS)Me ₂]
6	[(^t Bu-py)Li(HMDS)]
7	[(^t BuCN)Li(HMDS)]
8	[{Li ₂ (NHDipp) ₂ TMEDA} _∞]
9	[(PMDETA)Li(NHDipp)]
10	[(PMDETA)LiZn(NHDipp)Me ₂]
11	[(THF) ₃ LiZn(NHDipp)(Me) ₂]
12	[LiZn ₂ (NHDipp) ₂ (Me) ₃ (THF) ₃]
13	[(THF)LiZn(NHDipp) ₂ Me]
14	[(PMDETA)LiZn ^t Bu ₃]
15	[LiZnPh ₃]
15·LiCl	[Ph ₃ LiZn·2LiCl]
16	[Li ₂ ZnPh ₄]
16·LiCl	[Ph ₄ Li ₂ Zn·2LiCl]
17	[(THF) ₃ Li(NC ₁₃ H ₉ -9-Ph)]
18	[{(TMEDA)Li(THF)} ⁺ {NC ₁₃ H ₈ -9-Ph} ^{-*}]
19	[Ph ₂ Zn(NC ₁₃ H ₉)]
20	[LiZnEt ₃]
21	[(TMEDA)(THF)Li(NC ₁₃ H ₉ -9-Et)]
22	[(THF) ₂ Zn(Et)] ₂ [μ-(NC ₁₃ H ₉ -C ₁₃ H ₉ N)]
23	[(THF) ₂ Li(N ₂ C ₄ H ₄ -2-Ph)] _∞
24	[Ph ₂ Zn(Pyr) ₂] _∞
25	[(Quin)Zn(OPh)Ph] ₂

- 26 $[(\text{THF})_6\text{Mg}_{16}(\text{OPiv})_{12}(\text{O}_2)_4(\text{OH})_{12}]$
- 27 $[\text{Zn}(\text{OPiv})_2 \cdot 2\text{LiCl}]$
- 28 $[\{\text{Na}(\text{THF})_6\}^+ \{(\text{Ph}_2\text{Si}(\text{NDipp})_2)\text{MgBu}(\text{THF})\}^-]$
- 29 $[\{\text{Na}(\text{THF})_6\}^+ \{(\text{Ph}_2\text{Si}(\text{NDipp})_2)\text{ZnEt}\}^-]$
- 30 $[(\text{Ph}_2\text{Si}(\text{NDipp})_2)\text{Zn}(\text{TMP})\text{Na}(\text{THF})]$
- 31 $[\text{Na}(\text{THF})_2\text{Zn}(\text{Btz})_3]_2$
- 32 $[\text{Na}_2(\text{THF})_4\text{Zn}(\text{NC}_4\text{H}_4)_4]_\infty$
- 33 $[\{(\text{THF})_2\text{NaZn}(\text{THF})(\text{NC}_4\text{H}_4)_3\}_\infty]$

Compounds Prepared in this Thesis







26

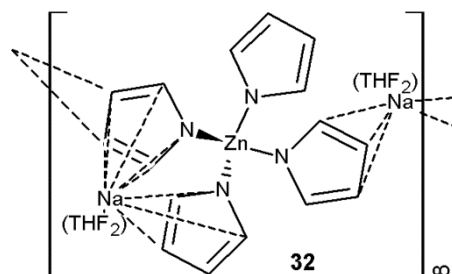
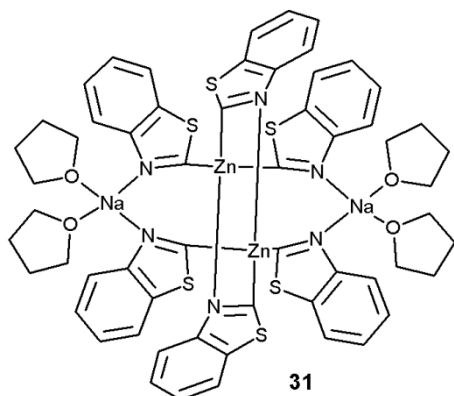
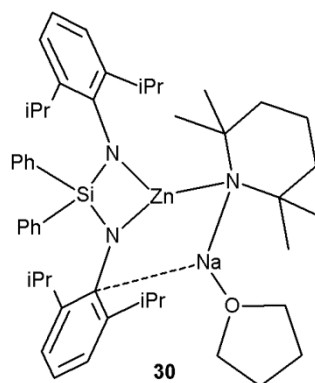
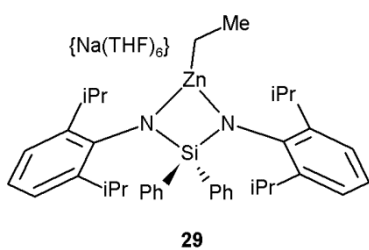
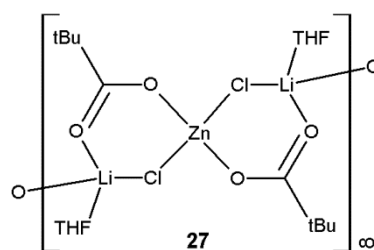


Table of Contents

Acknowledgements	iii
Abstract	iv
Publications	vi
Table of Common Abbreviations	viii
Table of Numbered Compounds	xi
Compounds Prepared in this Thesis	xiii
Table of Contents	xvi
Chapter 1 An Introduction to Alkali Metal Zincate Chemistry	1
1.1 Organometallic Chemistry	1
1.2 Organozinc reagents	2
1.2.1 The Reformatsky Reaction	2
1.2.2 The Negishi Cross-Coupling Reaction	3
1.2.3 Simmons-Smith Cyclopropanation Reaction	5
1.3 Alkali Metal Organozincates	6
1.4 Preparation of Organozincates	7
1.5 Application of Organozincates in Synthesis	10
1.5.1 Metal-Halogen Exchange	10
1.5.2 1,4-Conjugate Addition and 1,2-Addition	16
1.5.3 Deprotonative Metallation	19
1.5.3.1 Directed <i>ortho</i> Metallation (DoM)	20
1.6 Structural Diversity in Organozincate Chemistry	31
Chapter 2 Solvated and Solvent-free Lithium Dimethyl HMDS Zincates	38
2.1 The Unsolvated Zincate [LiZn(HMDS)Me ₂] 4a	39
2.2 The Effect of the Donor Solvent	43
2.2.1 PMDETA	44
2.2.2 Monodentate Donors	50
2.3 Conclusions	54
Chapter 3 Donor-Dictated Co-Complexation Reactions: The Structures of New Methyl(NHDipp) Zincates	56
3.1 The Effect of the Donor Solvent	57
3.1.1 TMEDA	57
3.1.2 PMDETA	60
3.1.3 THF	66
3.2 Conclusions	73

Chapter 4 Arylation Studies of Electron-deficient <i>N</i>-Heterocycles	75
4.1 The Use and Reactivity of <i>N</i> -Heterocyclic Compounds	75
4.2 Direct C-H Arylation vs. Addition/Rearomatisation	77
4.3 Synthesis and Characterisation of Tri- and Tetraphenyl Lithium Zincates 15 and 16	84
4.4 Reactivity of Zincates 15 and 16 towards Electron-deficient <i>N</i> -Heterocycles	93
4.4.1 Acridine	93
4.4.2 Pyrazine	115
4.4.3 Quinoline	123
4.5 Zinc Pivalates as Arylating Reagents	125
4.6 Conclusions	131
Chapter 5 Synthesis of Zincates Containing Bulky Bis(amido)silyl Ligands	134
5.1 Zinc-Zinc Bonding and the use of Bulky ligands	134
5.2 Synthesis of Sodium Zincates based on Ph ₂ Si(NHDipp) ₂	136
5.2.1 Synthesis of Ph ₂ Si(NHDipp) ₂	136
5.2.2 Synthesis of [$\{Na(THF)_6\}^+ \{ (Ph_2Si(NDipp)_2)ZnEt \}^-$] 29	137
5.2.3 Synthesis of [(Ph ₂ Si(NDipp) ₂)Zn(TMP)Na(THF)] 30	140
5.3 Reactivity Studies Assessing the Metallating Ability of Zincates 29 and 30	145
5.3.1 Reaction with Benzothiazole	145
5.3.2 Reaction with Pyrrole	149
5.3.3 Reaction with Anisole	154
5.4 Conclusions	157
Chapter 6 Conclusions and Future Work	158
Chapter 7 Experimental Procedures	166
7.1 General Experimental Techniques	166
7.1.1 Schlenk Techniques	166
7.1.2 Glove Box	167
7.1.3 Purification of Solvents and Reagents	168
7.1.4 Standardisation of Organometallic Reagents	169
7.1.5 Instrumentation	169
7.2 Synthesis of Common Starting Materials	170
7.2.1 Preparation of ZnPh ₂	170
7.2.2 Synthesis of BuNa	171
7.2.3 Synthesis of [Ph ₂ Si(NHDipp) ₂]	171
7.2.4 Synthesis of Zn(TMP) ₂	172
7.3 Synthesis of Numbered Compounds	172
Synthesis of [LiZn(HMDS)Me ₂] 4a	172
Synthesis of [(PMDETA)Li(μ-Me)Zn(HMDS)Me] 5	173
Synthesis of [^t Bu-py)Li(HMDS)] 6	173
Synthesis of [^t BuCN)Li(HMDS)] 7	174

Synthesis of [$\{\text{Li}_2(\text{NHDipp})_2(\text{TMEDA})\}_\infty$] 8	174
Synthesis of [(PMDETA)Li(NHDipp)] 9	175
Synthesis of [(PMDETA)LiZn(NHDipp)(Me) ₂] 10	176
Synthesis of [(THF) ₃ LiZn(NHDipp)(Me) ₂] 11	176
Synthesis of [(THF) ₃ LiZn ₂ (Me) ₃ (NHDipp) ₂] 12	177
Synthesis of [(THF)LiZn(NHDipp) ₂ Me] 13	178
Synthesis of Ph ₃ LiZn(THF) ₃ 15·THF ₃	178
Synthesis of Ph ₄ Li ₂ Zn(THF) ₃ (O ⁿ Bu) ₂ 16	179
Synthesis of 9, 10-dihydro-9-phenylacridine	180
Synthesis of 9-phenylacridine	180
Synthesis of [(THF) ₃ Li(NC ₁₃ H ₉ -9-Ph)] 17	181
Synthesis of [$\{\text{(TMEDA)Li(THF)}\}^+ \{\text{NC}_{13}\text{H}_8\text{-9-Ph}\}^-$] 18	181
Synthesis of [Ph ₂ Zn(NC ₁₃ H ₉)] 19	182
Synthesis of [(TMEDA) ₂ LiZnEt ₃] 20	183
Synthesis of 9-ethylacridine	183
Synthesis of [(TMEDA)(THF)Li(NC ₁₃ H ₉ -9-Et)] 21	184
Synthesis of [(THF) ₂ Zn(Et) ₂][μ -(NC ₁₃ H ₉ -C ₁₃ H ₉ N)] 22	184
Synthesis of [(THF) ₂ Li(N ₂ C ₄ H ₄ -2-Ph)] _∞ 23	184
Synthesis of [Ph ₂ Zn(Pyr) ₂] _∞ 24	185
Synthesis of 2-Phenylpyrazine	185
Synthesis of 2,5-Diphenylpyrazine	186
Synthesis of 2-Phenylquinoline	186
Synthesis of [$\{\text{Na(THF)}_6\}^+ \{\text{(Ph}_2\text{Si(NDipp)}_2\text{)ZnEt}\}^-$] 29	187
Synthesis of [Ph ₂ Si(NHDipp) ₂ Zn(TMP)Na(THF)] 30	187
Synthesis of [Na(THF) ₂ Zn(NSC ₇ H ₄) ₃] ₂ 31	188

Bibliography **190**

Appendix of Crystallographic Data **205**

Chapter 1 An Introduction to Alkali Metal Zincate Chemistry

This chapter is designed to outline the evolution of mixed alkali metal zinc complexes (zincates), and highlight the advantages which these unique reagents can offer. Thus, the more traditional organometallic compounds will be discussed, followed by a comparison with heterobimetallic reagents; contrasting their reactivities and cataloguing their applications.

1.1 Organometallic Chemistry

Organometallic reagents are critical to the process of chemical synthesis, enabling the functionalisation of countless numbers of compounds. As an illustration of their synthetic relevance, it has been noted that greater than 95% of all natural products synthesised will have been treated with a lithium reagent at some stage in their construction.^[1] Organolithium reagents in particular are commonplace – owing to the convenience of being widely commercially available – and are most often the "go to" reagents for performing deprotonative metallation,^[2] or the preparation of low polarity organometallics via salt-metathesis.^[3] However, despite their widespread application, these reagents are not without limitation. Due to the presence of a highly polarised metal-carbon bond such species are incredibly reactive; which leads to problems with chemoselectivity, unwanted side reactions – with sensitive functional groups, reaction intermediates or solvents – and the requirement of cryogenic conditions.^[4]

The kinetic reactivity of an organometallic species is largely dictated by the degree of polarisation of the metal-carbon bond which it contains – the more electropositive the metal, the more ionic (and therefore reactive) the M-C bond will be.^[5] This means that the alkali metals form highly polarised bonds to what may be formally

considered an organic anion, thus imparting the high reactivity which has led to the ubiquity of organolithium reagents in synthesis. Conversely, less electropositive metals such as magnesium and zinc form more covalent metal-carbon bonds, resulting in a more stable compound overall. Therefore Grignard reagents exhibit greater functional group tolerance than organolithium reagents, and can be used at higher temperatures,^[2f, 5-6] while organozinc reagents display even more covalent character, and are therefore more compatible with a wide range of sensitive functional groups, such as carboxylates, amides and carbonyls. Organozinc reagents do however suffer from limited kinetic reactivity. This reduction in reactivity means that zinc reagents tend to be restricted to carbon-carbon bond forming reactions which require transition metal catalysis, such as palladium-catalysed cross-coupling reactions.^[2f]

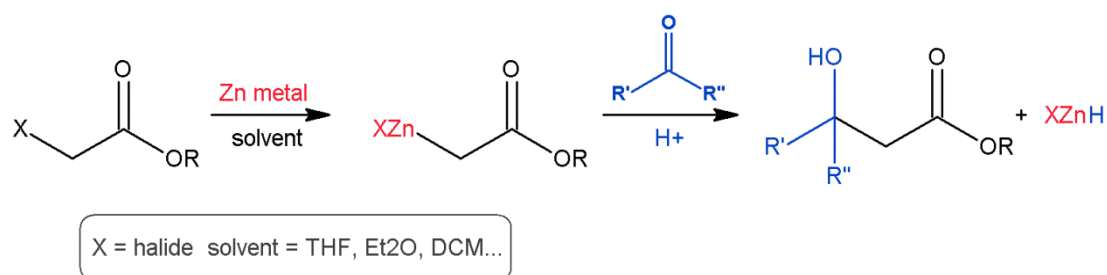
1.2 Organozinc reagents

Neutral organozinc reagents have three core uses; as soft nucleophiles for performing addition reactions such as the Reformatsky reaction,^[7] in transition metal catalysed C-C bond forming reactions such as the Negishi cross-coupling,^[8] and in the formation of cyclopropane rings via the Simmons-Smith reaction.^[9]

1.2.1 The Reformatsky Reaction

The Reformatsky reaction, dating from 1887, is one of the earliest uses of organozinc compounds. Developed shortly after Frankland's pioneering synthesis of diethylzinc in 1849,^[10] it remains a very powerful method for the preparation of α -ester organometallic intermediates. The reaction involves the condensation of an aldehyde or ketone with an α -haloester to yield a β -hydroxyester (Scheme 1.1).^[7] The initial step involves the synthesis of an alkylzinc halide by the insertion of zinc metal into the carbon-halide bond of the α -haloester. This can be a slow process, due to the

build up of zinc oxides on the metal surface, and many methods of activating the zinc towards insertion have been employed;^[11] including the use of Rieke-Zn^[12] – prepared by the reduction zinc halide salts with an alkali metal – and zinc-copper alloys, formed by treating zinc dust with hydrochloric acid and copper sulfate solutions.^[13] More recently the process has been performed using dialkylzinc reagents in the presence of a transition metal catalyst.^[7b, 14]

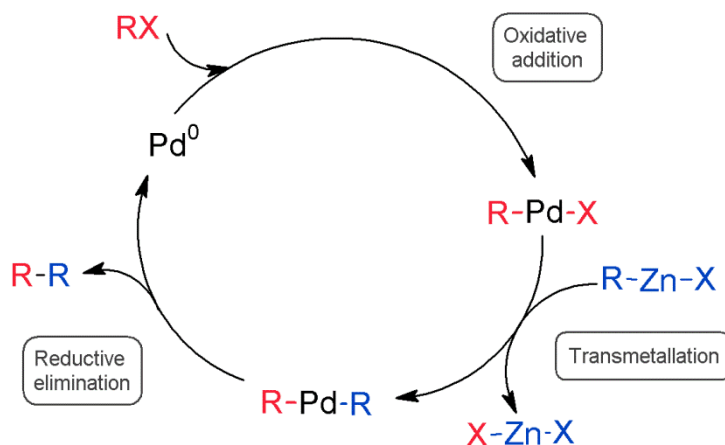


Scheme 1.1 The Reformatsky reaction.

Once formed the organozinc compound performs a nucleophilic addition reaction to the aldehyde or ketone, leading to the subsequent isolation of the β -hydroxyester product.^[7] Such reactions are testament to the high functional group tolerance of zinc, which allows the sensitive ester functionality to remain intact, whereas lithium and magnesium compounds decompose via self-condensation.^[11a]

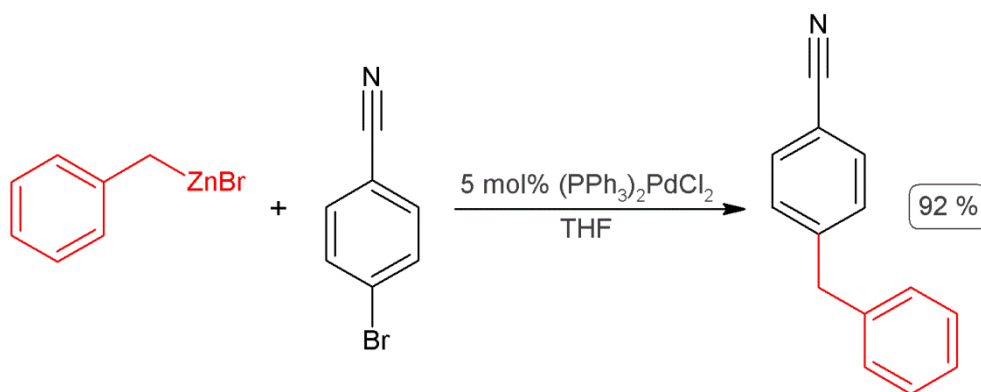
1.2.2 The Negishi Cross-Coupling Reaction

Another notable feature of organozinc reagents is their ability to undergo transmetalation with transition metal complexes^[11a, 11c] – this facilitates their use in catalytic cross-coupling reactions. In 2010 Negishi, Suzuki and Heck were jointly awarded the Nobel prize for developing the palladium catalysed cross-coupling reactions which bear their names. The mechanism of these reactions is general, differing only in the organometallic compound employed, and the mechanism of the Negishi reaction –involving zinc – is depicted below (Scheme 1.2).^[8]



Scheme 1.2 General catalytic cycle for the palladium-catalysed Negishi cross-coupling.

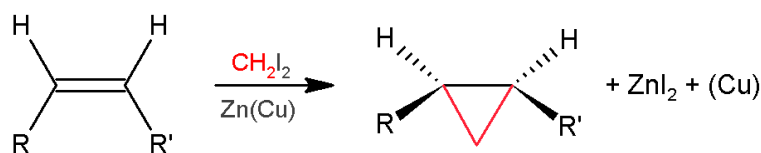
The catalytic cycle can be summarised in three steps; the oxidative insertion of the transition metal catalyst, generally Pd^0 (or Ni^0), into an R-X bond (where X is a halide and R is any organic fragment), the transmetalation of this Pd^{II} species with the organozinc compound to give a zinc halide salt as a by-product, and finally the reductive elimination of the coupled product which serves to regenerate the Pd^0 catalyst. The low nucleophilicity of zinc, in comparison to metals such as lithium and magnesium, enables the use of various functional groups and the likelihood of side-reactions is greatly reduced.^[8] Thus, the coupling of organic fragments can be achieved in excellent yield, for example the reaction of benzylzinc bromide and *para*-bromobenzonitrile occurs at room temperature furnishing the biaryl product after one hour (92 %).^[8a]



Scheme 1.3 Negishi cross-coupling of *para*-bromobenzonitrile and benzylzinc bromide.^[8a]

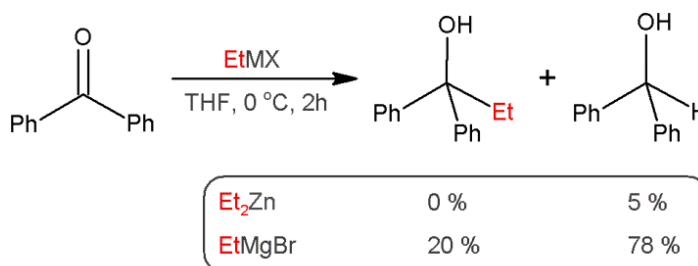
1.2.3 Simmons-Smith Cyclopropanation Reaction

In the late 1950s Simmons and Smith discovered that iodomethylzinc iodide reacts with alkenes in order to furnish cyclopropane rings (Scheme 1.4).^[9] This chemoselective reaction is compatible with a variety of alkenes and functional groups, and has been studied extensively with regards to the activation of zinc towards insertion into the C-I bond.^[11c] The most notable alternative to the traditional zinc-copper couple is the Furukawa reagent,^[15] which involves the use of diethylzinc rather than zinc metal, thus facilitating homogeneous reactions and the use of non-ethereal solvents.^[3, 11c, 16] This results in a faster rate of reaction, and often better yields.



Scheme 1.4 The Simmons-Smith cyclopropanation reaction.

Despite possessing the ability to perform these important synthetic transformations, the use of organozinc species in synthesis is limited due to their low kinetic reactivity; this is neatly illustrated by the reduction of benzophenone with diethylzinc in comparison to EtMgBr (Scheme 1.5).^[17] As such, organozinc reagents are often overlooked in preference of the more reactive s-block compounds – organolithium and Grignard reagents.^[3, 11a, 16]

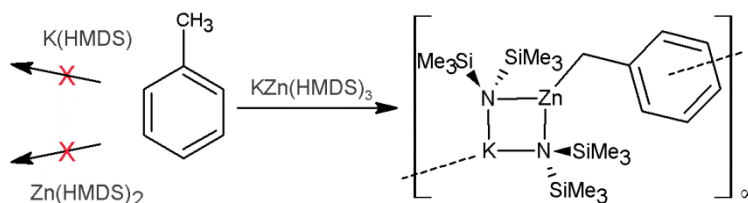


Scheme 1.5 Reduction of benzophenone with Et₂Zn and EtMgBr.^[17]

1.3 Alkali Metal Organozincates

Alkali metal zincates are the earliest class of heterobimetallic (ate) complex, known since the preparation of sodium triethylzincate NaZnEt_3 by Wanklyn in 1858.^[18] Much like their monometallic organozinc forbearers, however, ate complexes were largely disregarded by the synthetic community due to the introduction of Grignard reagents in the early 1900s.^[11a, 16] Indeed, the successful synthesis of the tetra(alkyl)zincate $[\text{Li}_2\text{ZnMe}_4]$, published by Hurd in 1948,^[19] and the conception of the term “ate complex” – prompted by Wittig’s synthesis of lithium triphenylzincate and the analogous magnesiate in 1951^[20] – occurred almost a century after their initial discovery. Nonetheless, over the last decade organozincates have begun to be appreciated for their scope in synthesis, being utilised in many fundamental organic transformations such as deprotonative metallation,^[2i, 2j, 21] catalysis,^[22] metal-halogen exchange^[23] and nucleophilic exchange.^[24]

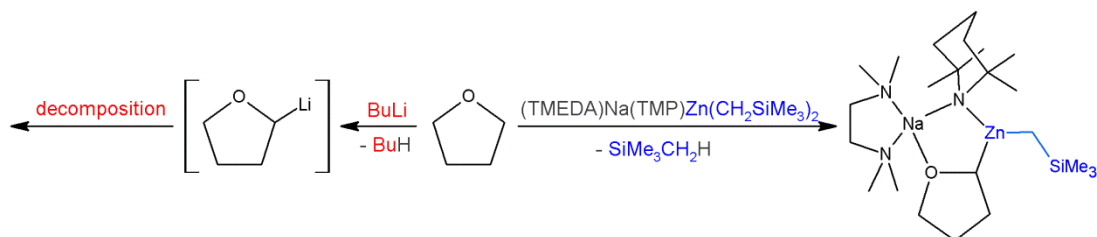
Maintaining some of the advantages of classical organozinc reagents – in terms of functional group tolerance, stability and selectivity – these heterobimetallic reagents exhibit greatly enhanced reactivities, displaying unique chemical profiles which cannot be replicated by their monometallic counterparts.^[2i, 21] Potassium zinc silylamide $\text{KZn}(\text{HMDS})_3$, for instance, possesses the ability to deprotonate toluene, despite neither KHMDS or $\text{Zn}(\text{HMDS})_2$ being able to do so unaided (Scheme 1.6).^[25]



Scheme 1.6 The synergistic deprotonation of toluene.

Furthermore, this bimetallic approach has revealed unusual reactivity patterns – such as the *meta* deprotonation of toluene by $[(\text{TMEDA})\text{NaMg}(\text{TMP})_2\text{Bu}]$ ^[26] and *N,N*-

dimethylaniline by $[(\text{TMEDA})\text{Na}(\text{TMP})\text{Zn}^t\text{Bu}_2]$ ^[27] – and an ability to stabilise extremely sensitive intermediates, as exemplified by the isolation of the α -metallated THF anion (Scheme 1.7).^[28] Despite the tendency of THF to undergo spontaneous ring opening when deprotonated by organolithium reagents (*vide infra*), when the same reaction is performed by the TMP zincate $[(\text{TMEDA})\text{Na}(\text{TMP})\text{Zn}(\text{CH}_2\text{SiMe}_3)_2]$ the α -zincated THF anion can be isolated intact due to a stabilising coordination with sodium.



Scheme 1.7 Trapping of the α -zincated THF anion with $[(\text{TMEDA})\text{Na}(\text{TMP})\text{Zn}(\text{CH}_2\text{SiMe}_3)_2]$.^[28]

1.4 Preparation of Organozincates

Alkali metal zincates can be divided into two major categories; those of formulation MZnR_3 , known as triorganozincates, and those of type M_2ZnR_4 , termed higher order, or tetraorganozincates.^[23b] Additionally, these may exhibit either (i) a contacted ion-pair (CIP) structure – which tend to form in the absence of a strongly coordinating Lewis base – forming a discrete molecular structure in which both metals are connected via bridging ligands, or (ii) a solvent separated ion-pair (SSIP) structure whereby the alkali metal cation (coordinated to a Lewis base or donor solvent) is complemented by the anionic zinc-based counter-ion.^[29]

The specific structure adopted by a zincate is dependent upon a variety of factors, including the presence of a Lewis base, the nature of the anionic ligands and even the choice of solvent. A more delocalised the charge on the anion, and hence a weaker anion-cation interaction, or an increase in solvent polarity, both increase the

likelihood of SSIP structure formation.^[30] This concept is demonstrated neatly by the triorganozincate LiZnMe_3 , which has been found to adopt a CIP structure in the presence of the chelating tridentate *N*-donor PMDETA, and an SSIP structure in the presence of a two molar excess of the related oxygen donor diglyme, which coordinates to lithium to form $[\text{Li}(\text{diglyme})_2]^+[\text{ZnMe}_3]^-$ (Figure 1.1).^[31]

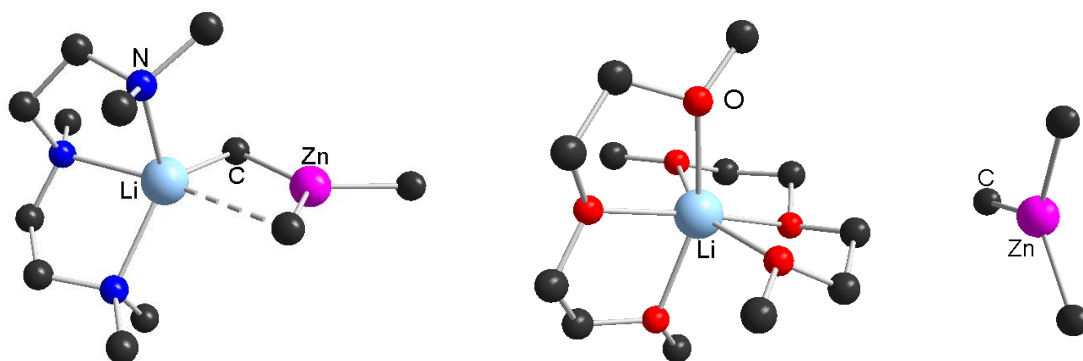


Figure 1.1 Molecular structures of the CIP $[(\text{PMDETA})\text{LiZnMe}_3]$ (left) and SSIP $[\text{Li}(\text{diglyme})_2]^+[\text{ZnMe}_3]^-$ (right).

There are several common methods for the preparation of alkali metal zincates,^[11a] the most general of which are summarised below in Scheme 1.8. One of the most frequently encountered methods is the co-complexation of an organozinc reagent with an alkali metal species (Scheme 1.8(a) co-complexation).^[11c] While Scheme 1.8(a) depicts the formation of a triorganozincate MZnR_3 , it is also possible to generate tetraorganozincates by altering the stoichiometry of the reaction to a 2:1 ratio of alkali metal to organozinc reagent. However, it is also possible that the formation of one zincate is more energetically preferred than the other, and that ultimately a redistribution reaction will occur in solution.^[23d, 29d, 32] The solution chemistry of zincates is highly complex; the equilibrium between LiZnMe_3 and Li_2ZnMe_4 , for example, greatly favours the triorganozincate,^[33] whereas the higher order zincate dominates in the solid state, it being the first lithium zincate to be structurally characterised in 1968.^[34]



Scheme 1.8 Common methods for the synthesis of organozincates; (a) co-complexation of monometallic components, (b) salt metathesis and (c) transmetallation.

A variety of organozincates can be prepared by the transmetallation of zinc salts (such as ZnCl_2) with three equivalents of organolithium or Grignard reagent (Scheme 1.8(b) salt metathesis).^[11a, 11c] As above, it is possible to preferentially form either higher order or lower order zincates by controlling the ratio of monometallic reagents; however, this method requires the use of ethereal solvents, which are vulnerable to attack by the alkali metal precursor, producing side-products (*vide infra*). Furthermore, this reaction results in the formation of two equivalents of alkali metal halide, the presence of which has been shown to affect the reactivity of the mixed-metal complex significantly, in certain cases.^[35] For instance, Knochel has reported that functionalised aryl- and benzylic zinc reagents show improved reaction rates (and yields) towards aldehydes and ketones in the presence of magnesium salts.^[35a]

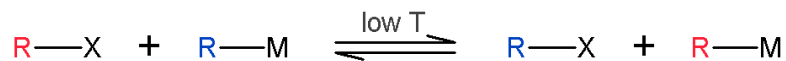
An alternative zincate synthesis is the reduction of a dialkylzinc reagent by the alkali metal itself (Scheme 1.8(c) transmetallation),^[36] the same method used by Wanklyn for the synthesis of the original alkali metal zincates NaZnEt_3 and KZnEt_3 in 1858.^[18] The main drawback of this method is that only homoleptic zincates can be prepared in this fashion and forcing reaction conditions are needed, which in some cases induces side reactions with the solvents employed.^[36]

1.5 Application of Organozincates in Synthesis

As discussed above in section 1.1 Organometallic Chemistry, polar organolithium and Grignard reagents have found widespread application in organic synthesis. Due to the highly reactive nature of such species, however, many functional groups are vulnerable to attack, and cryogenic reaction conditions are generally required. In contrast to these polar compounds, neutral organozinc reagents are soft nucleophiles which exhibit good functional group tolerance. As the combination of an alkali metal and zinc within an organozincate reagent combines this high reactivity with the added benefit of greater functional group tolerance, these reagents have been used to improve the scope of transformations traditionally performed by polar organometallic species.

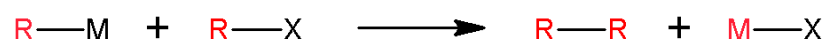
1.5.1 Metal-Halogen Exchange

Metal-halogen exchange is one of the most powerful processes for the preparation of organometallic compounds, and indeed it is one of the most common uses of organolithium reagents in synthesis.^[2d, 37] This process involves the transformation of a C-X bond (where X is a halide, most commonly Br or I) to a more polar (and therefore more reactive) C-M bond (Scheme 1.9). As the metal displaces the halide atom the reaction is regiospecific, often exerting more control than deprotonative metallation, due to the surplus of carbon-hydrogen bonds available in organic substrates.



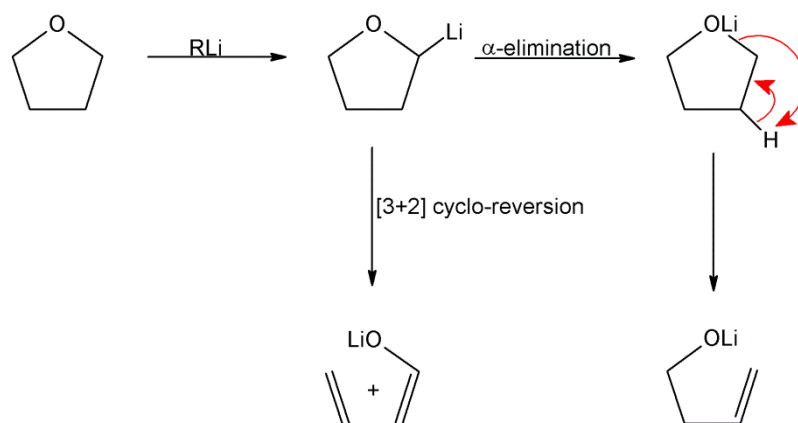
Scheme 1.9 General equation detailing metal-halogen exchange.

The highly polar nature of organolithium compounds leads to high reactivity towards aryl-, heteroaryl-, vinyl- and alkylhalides;^[2d, 37a] however, an excess of the organolithium species is generally required to prevent side-reactions involving the lithiated intermediates. As metal-halogen exchange is a kinetic process, driven by the stability of the newly generated organometallic species, the substrate may be left open to attack if the equilibrium lies to the right.^[38] This leads to the coupling of alkyl fragments and formation of the thermodynamically favoured metal halide salt (Scheme 1.10).^[37a]



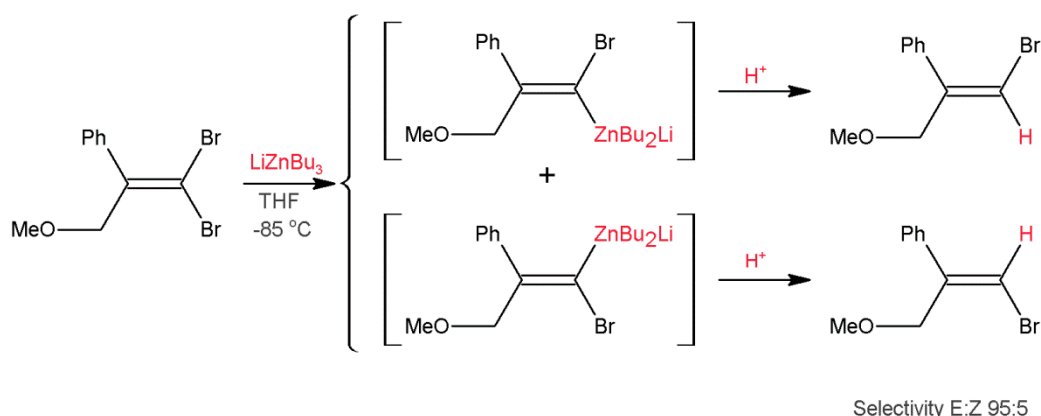
Scheme 1.10 Coupling of alkyl fragments resulting in the precipitation of halide salt MX.

As such, subambient temperatures are required, which can also prevent any unwanted deprotonation or addition reactions. The choice of halogen is also an important factor; the observed order of reactivity being $\text{I} > \text{Br} > \text{Cl} > \text{F}$. Iodine- and bromine-lithium exchange occur readily; however, chlorine-lithium exchange proceeds more slowly and the competing process of hydrogen-lithium exchange, or metallation, is generally favoured.^[39] Etheral solvents may also be utilised to hasten the reaction rate, which compensates for the harsh cooling employed,^[40] although side-reactions with such solvents are common (Scheme 1.11).^[41]



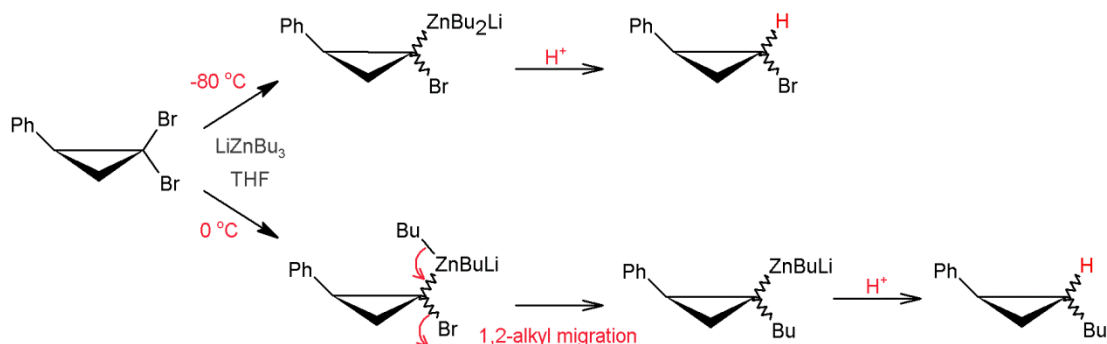
Scheme 1.11 Decomposition of THF in the presence of organolithium reagents.

In contrast to the highly polar organolithium reagents, neutral organozinc reagents are largely unreactive in regard to metal-halogen exchange, being limited to iodo-compounds and/or requiring catalysts to effect the transformation.^[3, 11c, 23b, 42] However, alkali metal zincates have been shown to facilitate direct zinc-halogen exchange.^[43] Harada and Oku reported the first successful attempts to perform both Zn-Br and Zn-Cl exchange with 1,1-dibromocyclopropane^[44] and 1,1-dihaloalkenes respectively, using triorganozincate LiZnBu_3 .^[45] They noted that the exchange reaction occurred at the most sterically hindered bromine of a variety of 1,1-dibromoalkenes, and that subsequent quenching takes place stereospecifically with retention of the carbenoid carbon configuration (Scheme 1.12).



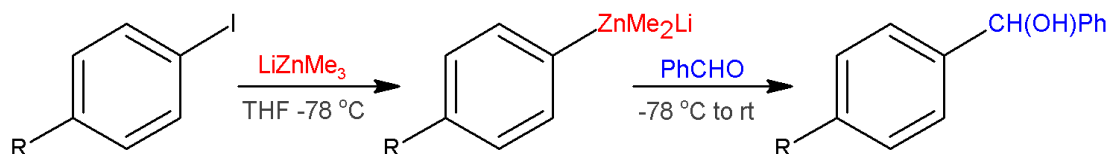
Scheme 1.12 Selective zinc-bromine exchange with 1,1-dibromoalkenes quenched with H^+ .

Equally, if the zinc-bromine exchange reaction of 1,1-dibromocyclopropane is performed under cryogenic conditions – thus stabilising the intermediate zincate carbenoid – the reaction may simply be quenched with a suitable electrophile. The resulting carbenoid, however, can also undergo a 1,2-alkyl migration with the loss of a second halogen atom when the reaction is performed at higher temperatures. The cyclopropylzinc species can then be quenched to form the alternative product (Scheme 1.13).



Scheme 1.13 Zinc-bromine exchange of 1,1-dibromocyclopropane with LiZnBu_3 at variable temperatures followed by quenching with H^+ .

Sakamoto has reported a straightforward method for the zinc-halogen exchange of various *para*-substituted arylhalides with lithium trimethylzincate, noting that arylbromides do not react, but that the iodides work efficiently.^[46] Good functional group tolerance was observed and yields of up to 74 % product were isolated on subsequent reaction with benzaldehyde (Scheme 1.14).

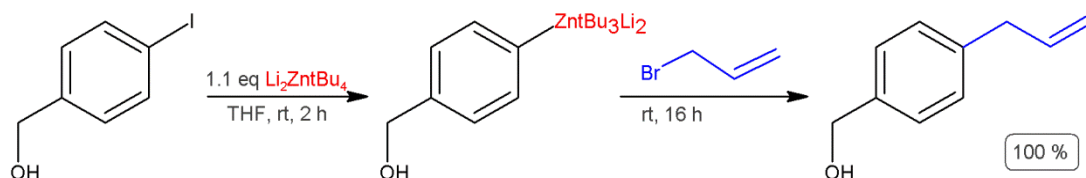


Scheme 1.14 Zinc-iodine exchange of arylhalides followed by electrophilic quenching with benzaldehyde.

Zinc-bromine exchange with bromobenzene can be achieved when the higher order tetramethylzincate Li_2ZnMe_4 is utilised.^[23b] The greater reactivity of the tetramethylzincate over the trimethylzincate has been attributed to the greater anionic nature of the higher order bimetallic species. Under the same reaction conditions neither LiZnMe_3 nor LiMe were found to react with bromobenzene, illustrating the enhanced reactivity of such mixed-metal species.

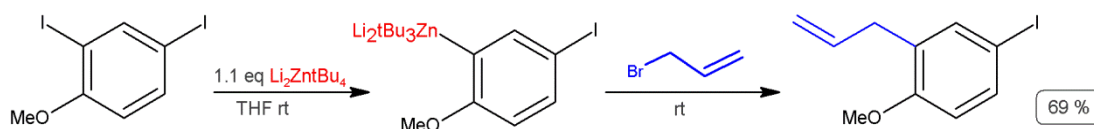
The higher order *t*-butylzincate $\text{Li}_2\text{Zn}^t\text{Bu}_4$ has also been recognised as a useful reagent, able to promote zinc-halogen exchange at ambient temperatures.^[23d] Neither

of its component monometallic reagents demonstrate the ability to undergo metal-iodine exchange under these reaction conditions, yet the tetraorganozincate was found to transform a range of aromatic substrates in almost quantitative yields (Scheme 1.15). Additionally, a wide range of functional groups were tolerated, including terminal alkynes, acidic protons and electrophilic groups such as esters and amides.



Scheme 1.15 Zinc-Iodine exchange with $\text{Li}_2\text{Zn}'\text{Bu}_4$ with 4-iodobenzyl alcohol followed by reaction with allyl bromide.

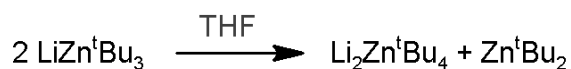
More highly substituted aromatic molecules such as 2,4-iodoanisole and 3-iodoquinoline can be functionalized by this method, and in the case of diiodo-substituted substrates it is the position *ortho* to the best directing group which undergoes Zn-I exchange (Scheme 1.16). Zinc-bromine exchange can also be achieved with $\text{Li}_2\text{Zn}'\text{Bu}_4$, and although a reaction temperature of 60 °C is required, yields of 74-98 % can be accomplished.



Scheme 1.16 Selective zinc-iodine exchange with $\text{Li}_2\text{Zn}'\text{Bu}_4$.

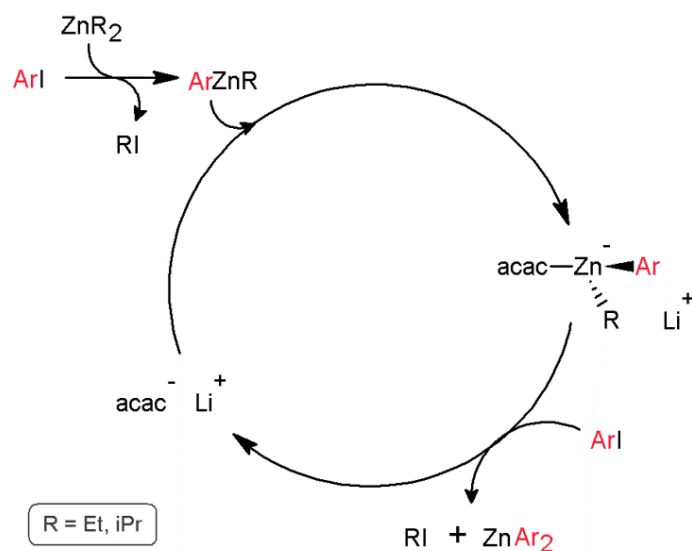
From NMR and ESI-MS studies of $\text{Li}_2\text{Zn}'\text{Bu}_4$, it has been proposed that the integrity of the zincate structure is retained in THF solution, as no equilibrium between the trialkylzincate and $\text{Li}'\text{Bu}$ was observed. Contrastingly, low temperature NMR studies indicate that the trialkylzincate itself was found to disproportionate to $\text{Zn}'\text{Bu}_2$ and the higher order zincate $\text{Li}_2\text{Zn}'\text{Bu}_4$, suggesting that $\text{LiZn}'\text{Bu}_3$ does not exist in THF solution (Scheme 1.17). Further evidence was obtained from theoretical studies

involving DFT calculations which indicate that the disproportionation to the higher order zincate is thermodynamically favourable ($\Delta E_{\text{rel}} = -6.9 \text{ kcal mol}^{-1}$).



Scheme 1.17 The disproportionation of LiZn^tBu_3 in THF solution.

Alkali metal catalysed zinc-iodine exchange reactions have been reported by Knochel,^[22] who observed that ZnEt_2 and Zn^iPr_2 were inert towards zinc-halogen exchange with aryl iodides in ether or THF solution. Yet in a 1:10 mixture of Et_2O and *N*-methylpyrrolidinone the exchange to the mixed diorganozinc reagent ArZnR ($\text{R} = \text{Et}$ or ^iPr) occurs at room temperature. Thus a catalytic cycle was proposed, whereby the addition of substoichiometric amounts of $\text{Li}(\text{acac})$, as a nucleophilic catalyst, may facilitate transfer of the remaining alkyl group from ArZnR via the formation of a zincate complex (Scheme 1.18). The elimination of the spectator ligands improves the atom efficiency of the metal-halogen exchange process, generating ZnAr_2 and recycling the lithium salt, thus propagating the catalytic cycle.



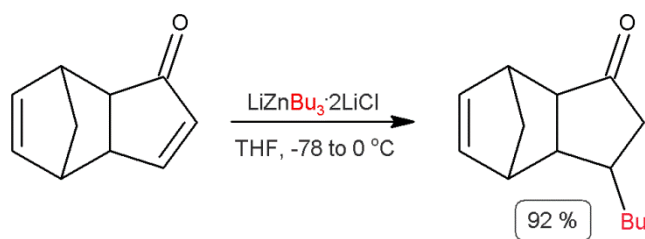
Scheme 1.18 Proposed catalytic cycle of the zinc-iodine exchange reaction of R_2Zn and $\text{Li}(\text{acac})$.

It was noted that bulkier alkyl groups led to greater reactivity, with Zn^iPr_2 and Zn^sBu_2 outperforming ZnMe_2 and ZnEt_2 .^[22] It has also been observed that the rate of zinc-iodine exchange can be enhanced by the addition of magnesium salts,^[47] which subsequently led to the discovery that the magnesium zincate $[\{\text{Mg}_2\text{Cl}_3(\text{THF})_6\}^+ \{\text{Zn}^t\text{Bu}_3\}^-]$ displays activation of all three alkyl groups under mild conditions, and can subsequently be employed in Pd catalysed Negishi cross-coupling reactions leading to good yields of biaryl products.^[48]

Uchiyama and Kondo have shown that zinc-halogen exchange can be successfully accomplished in the solid-phase, with lithium tri-*tert*-butyl zincate and immobilised organic halides,^[49] and although the reaction rate appears sluggish in comparison to the solution-phase reaction (which it is now recognised would involve the more activated tetraorganozincate due to disproportionation,^[23d] *vide supra*), this reduces the need for harsh cooling (0 °C *cf.* -78 °C). The immobilised zincate can be subsequently reacted with benzaldehyde and subjected to Negishi cross-coupling with iodobenzene, resulting in good yields following cleavage from the resin support.

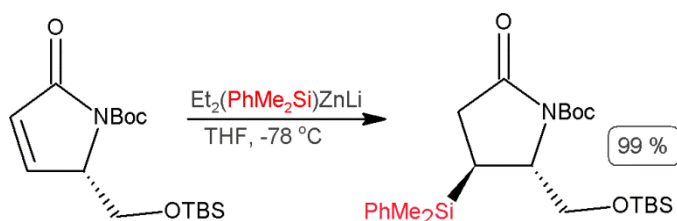
1.5.2 1,4-Conjugate Addition and 1,2-Addition

In 1951 Wittig reported that LiZnPh_3 added to PhCH=CHCOPh to give both 1,2- and 1,4-addition products, whilst ZnPh_2 was unreactive.^[20] It has since been observed that triorganozincates react with α,β -unsaturated ketones by 1,4-addition,^[50] as shown by the reaction of various lithium zincates with cyclopentadiene-1-one (Scheme 1.19). No evidence of the 1,2-addition products were observed so long as the correct stoichiometry for the triorganozincate was implemented.



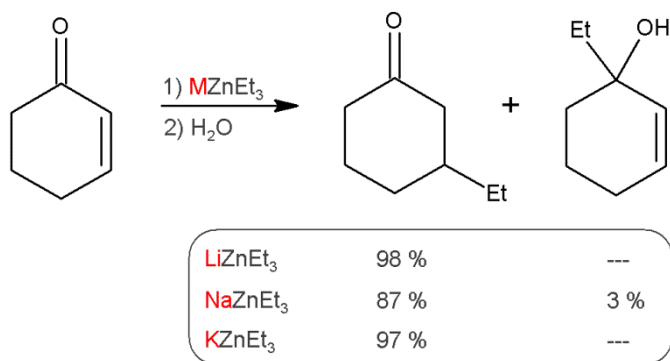
Scheme 1.19 1,4-addition of LiZnBu_3 to cyclopentadiene-1-one.

Many other examples of triorganozincates implementing conjugate addition have since been reported.^[51] This includes asymmetric additions, for example in 1990 Barrett reported the total synthesis of the anti-fungal compound (–)-Pramanicin based on the addition of lithium diethyl(dimethylphenylsilyl)zincate to a γ -lactam (Scheme 1.20). This resulted in the isolation of a single diastereoisomer – as confirmed by X-ray analysis of the subsequently deprotected amido alcohol – in quantitative yield.^[52]



Scheme 1.20 The asymmetric Michael addition of $\text{LiZnEt}_2(\text{SiMe}_2\text{Ph})$.

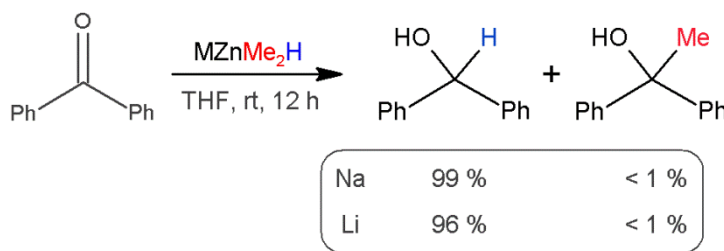
A study of the reactivity of zincates of type MZnEt_3 (where $\text{M} = \text{Li}, \text{Na}$ or K)^[53] has shown that, in contrast to the homometallic diethylzinc, LiZnEt_3 reacts rapidly with aldehydes and ketones at room temperature affording 1,2-addition products in good yields. Contrastingly, the sodium and potassium variants – although noted to add rapidly to substrates – also competitively metallate those with α -hydrogens. Only an α,β -unsaturated substrate (2-cyclohexenone) gave the 1,4-addition product for all three zincates (Scheme 1.21).



Scheme 1.21 Addition of various alkali metal zincates to cyclohex-2-ene-1-one.

While homometallic ZnEt₂ is unreactive towards these substrates, the use of organolithium reagents often leads to side-reactions, such as β-hydride elimination and aldol condensation.^[48a, 54] With the use of these triethylzincates only trace amounts of such by-products were ever observed, although the reaction of the sodium and potassium zincates with hexan-2-one do produce the aldol product in notable quantities (23% and 28% respectively).^[53]

Working on the premise that on modifying the environment of the zinc centre – by changing the ligands bound to it – the reactivity of novel bimetallic species can be finely tuned, Uchiyama and Sakamoto designed various dialkylzinc hydride ate complexes, to be used for the reduction of carbonyl compounds (Scheme 1.22).^[24a] The 1,2-addition reaction of the dimethylzinc hydrides were discovered to produce the benzhydrol as a sole product, preferentially transferring the hydride ligand and not a methyl group, while with the corresponding ethyl and *tert*-butyl complexes a significant proportion of the alkylated product accompanied the generation of the benzhydrol species. A wide variety of aldehydes and ketones were successfully reduced by the dimethylzinc hydride complexes, and the reaction can even be performed catalytically, using 20 mol% of ZnMe₂.^[24a]

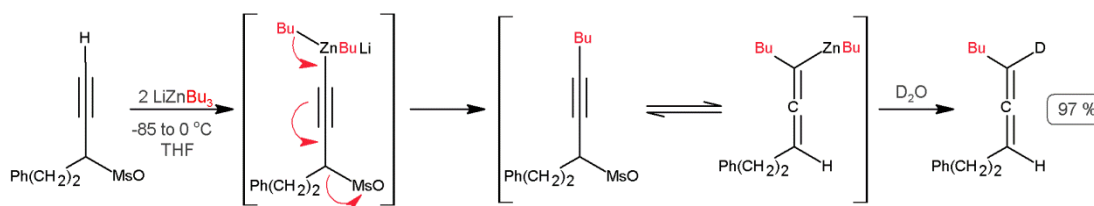


Scheme 1.22 Reduction of benzophenone with dimethylzinc hydride ate complexes.

Since neither the lithium or sodium hydrides, from which these ate complexes were prepared, reacted under the same conditions, hydride activation through complexation with the dialkylzinc was proposed. Furthermore, variable chemoselectivity – shown to be dependent on the alkyl group – demonstrates the versatility of such reagents.

1.5.3 Deprotonative Metallation

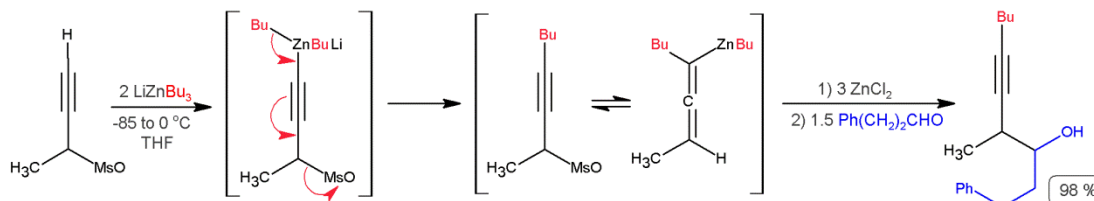
Homoleptic alkylzincates have limited basicity; however, Harada *et al.* have demonstrated that they are reactive enough to promote the zincation of alkynes^[55] to generate allenyl zinc reagents via a 1,2-migration of the alkynyl zincate intermediate (Scheme 1.23) in an analogous fashion to the rearrangements discussed above (see 1.5.1 Metal-Halogen Exchange). These allenic zinc reagents react regio- and stereoselectively to yield a variety of propargylic halides, silanes and ketones.



Scheme 1.23 Formation of allenes by deprotonation of alkynes with LiZnBu_3 .

The same research group has also found that by utilising this 1,2-migration a three-carbon homologation reaction of propargylic reagents was possible,^[56] with the

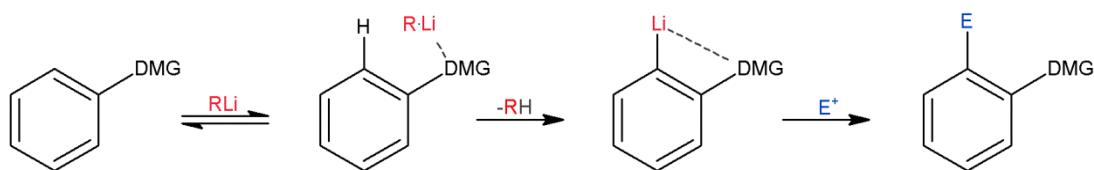
allenyl zinc intermediates coupling to a variety of electrophiles regioselectively at the γ -position (Scheme 1.24). Thus, it is therefore possible to smoothly introduce both a nucleophile and an electrophile to the 1- and 3-positions of a propargylic substrate in a one pot protocol.



Scheme 1.24 Deprotonation of alkynes with LiZnBu_3 and trapping with $\text{Ph}(\text{CH}_2)_2\text{CHO}$.

1.5.3.1 Directed *ortho* Metallation (DoM)

Directed *ortho* metallation (DoM) constitutes one of the most important and widely employed methodologies for the regioselective functionalisation of aromatic molecules.^[2c, 2d] The presence of a certain functional group, generally containing a heteroatom, facilitates the selective removal of an aromatic proton *ortho* to that group (a direct metallating group (DMG), Scheme 1.25),^[2d] leading to the *ortho*-metallated species. Upon treatment with an electrophile the 1,2-disubstituted product is subsequently obtained.



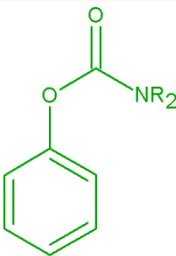
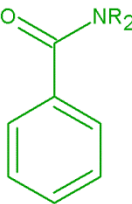

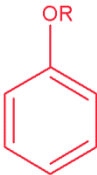
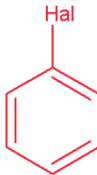
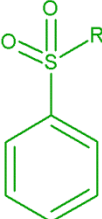
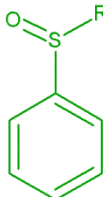
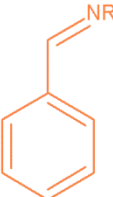
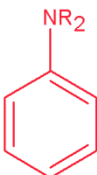
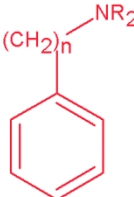
Scheme 1.25 Proposed mechanism for DoM.

Direct metallating groups must provide a coordination site for the organometallic base which directs the metal towards the adjacent (*ortho*) site to itself, thus regulating the stereoselectivity of the reaction by controlling the position of the

metallating agent.^[2c, 2d] Additionally, since the DMG is electron-withdrawing, it has the ability to acidify adjacent protons via inductive effects, and hence activate those protons *ortho* to itself towards metal-hydrogen exchange, with respect to the *meta* and *para* protons.

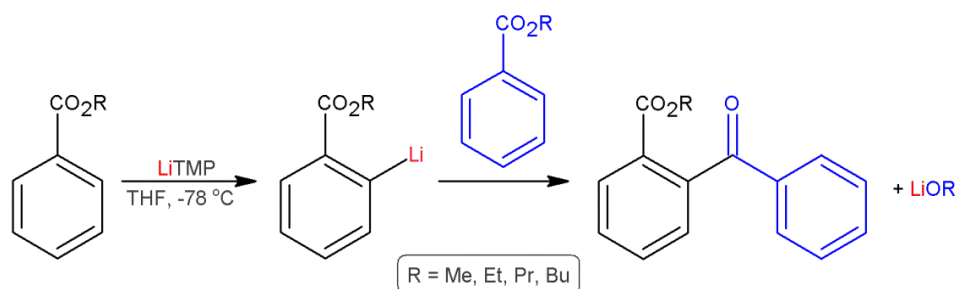
As a result of the effectiveness of a DMG being dependent on a combination of these two effects, they can be grouped into different categories (strong, moderate and weak) based upon their overall ability to promote *ortho* lithiation (Table 1.1).^[2c] The stronger DMGs (such as amides and sulfones) are powerfully electron withdrawing and contain a basic heteroatom; hence, these substrates require the use of cryogenic conditions to prevent side-reactions with the electrophilic functionalities. Less effective DMGs, however, (for example halogens or ethers) work mainly by acidifying the adjacent protons, via the inductive effect of their electronegative elements, and as a result these reactions can tolerate higher temperatures.

Table 1.1 Substituted aromatic substrates ranked according to their ability to facilitate DoM.^[2d]

Strong		Moderate	Weak	
				
				

Amongst the most commonly used metallating reagents, the utility amide LiTMP (TMP = 2,2,6,6-tetramethylpiperidide) is capable of the deprotonation of an array of organic substrates.^[2i, 2j, 5] It can, however, produce unwanted side reactions, even

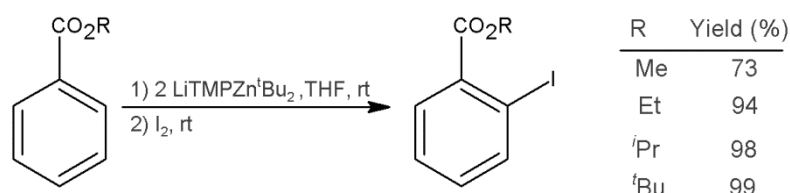
despite the use of cryogenic conditions. It has been noted for example that the *ortho*-lithiated aryl compounds of a variety of benzoate esters unavoidably undergo condensation reactions with the starting material yielding the corresponding *ortho*-benzoyl benzoate when deprotonated by LiTMP (Scheme 1.26).^[4b]



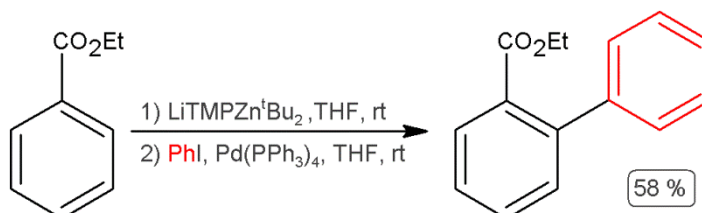
Scheme 1.26 Directed *ortho*-metallation of aryl carboxylic esters and the unwanted condensation of the lithiated intermediate with the starting material.

Contrastingly, regioselective deprotonation of this substrate takes place at ambient temperature when LiTMP is incorporated into a bimetallic framework. Thus in 1998, Kondo and Uchiyama reported the use of heteroleptic $[\text{Li}(\text{TMP})\text{Zn}^t\text{Bu}_2]$ (TMP-zincate **1**) to chemoselectively functionalise a variety of arenes containing sensitive directing groups.^[57] The same substrates which form *ortho*-benzoyl benzoate esters when treated with LiTMP at $-78\text{ }^\circ\text{C}$, can be cleanly deprotonated (and subsequently iodinated) in near quantitative yields, at ambient temperature, when treated with TMP-zincate **1** (Table 1.2).

Table 1.2 Yield of iodated product following *ortho* deprotonation with TMP-zincate **1**.



These *in situ* prepared arylzincates can also be successfully employed in Pd-catalysed Negishi cross-coupling reactions, affording the relevant bis(aryl) species in moderate yields (Scheme 1.27).^[8]



Scheme 1.27 Negishi cross-coupling of *in situ* prepared TMP arylzincates.

This bimetallic approach can also be employed for the effective deprotonation of several sensitive *N*-heterocyclic molecules.^[57] The α -metallation of pyridine, and selective deprotonation of isoquinoline and quinoline (~70:30 C8 *versus* C2 metallation) is of particular interest (Figure 1.2), since the use of organolithium species with such electron-deficient *N*-heterocycles generally results in nucleophilic addition to the carbon-nitrogen double bond.^[58]

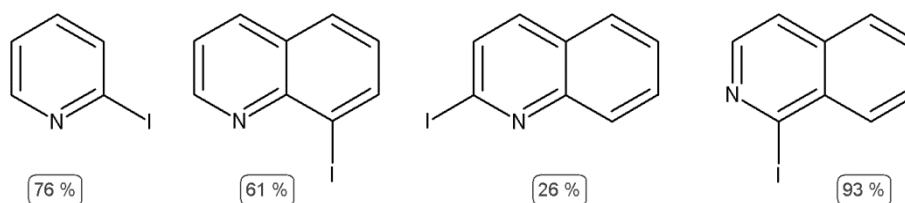
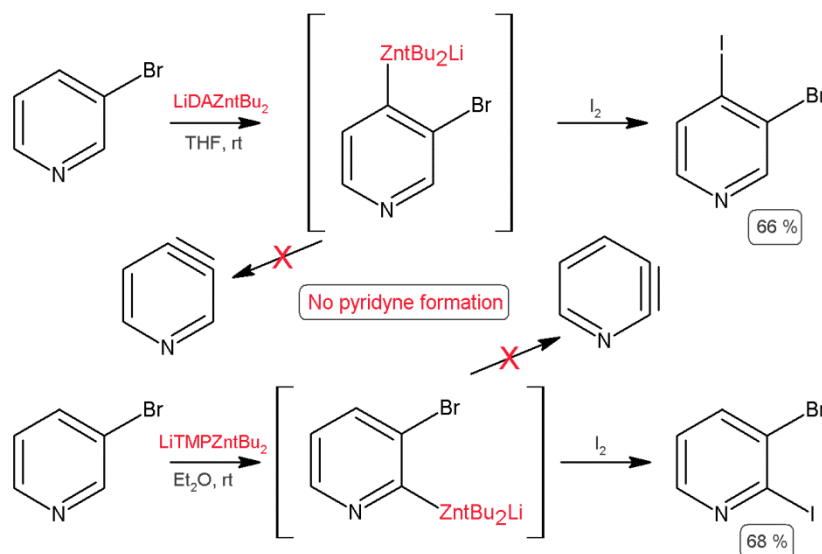


Figure 1.2 Deprotonation of pyridine, quinoline and isoquinoline with TMP-zincate **1** followed by quenching with iodine at room temperature.^[57]

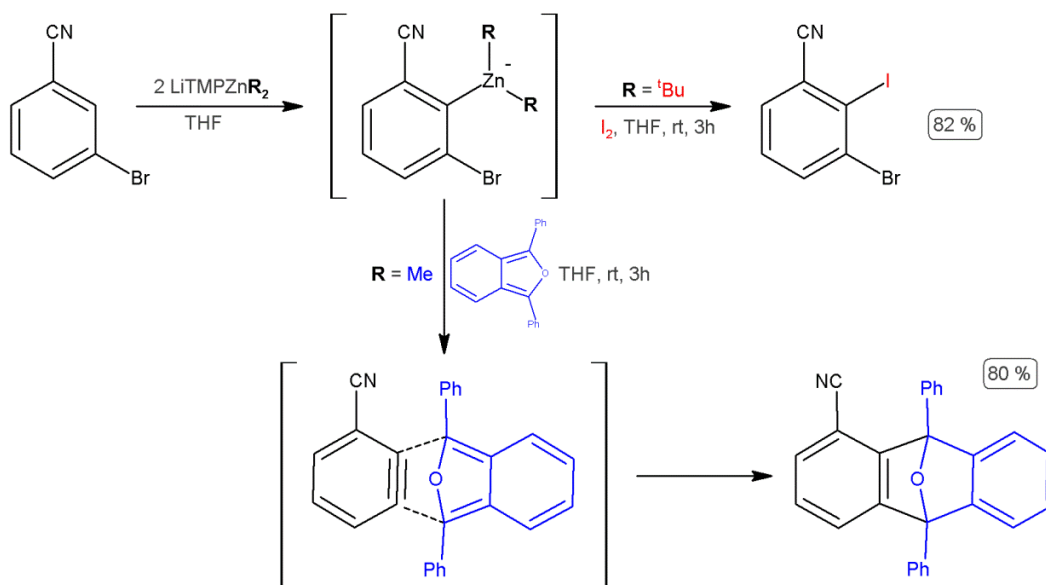
The reactivity of **1** towards the DoM of anisole has also been investigated, with DFT calculations suggesting that the modification of alkyl ligands and alkali metal may be instrumental in tuning the reactivity and selectivity of such reagents.^[59] Furthermore, Kondo has reported the contrasting regioselectivities of TMP-zincate **1** and the closely related lithium di-*tert*-butyldiisopropylaminozincate (DA-zincate) in the zincation of 3-bromopyridine (Scheme 1.28),^[60] noting that the choice of both ligand

and solvent has a considerable impact on the regioselectivity of the reagent. Zincate **1** was found to deprotonate 2-bromopyridine at the 6-position, leading to an 86% yield of 2-bromo-6-iodopyridine following an iodine quench. Contrastingly, by replacing the TMP anion with a diisopropylamido group metallation of the same substrate ultimately results in the isolation of a 72% yield of 2-bromo-3-iodopyridine. Furthermore, this approach also has the added advantage of suppressing pyridyne formation (via MX elimination), a common complication associated with organolithium reagents.



Scheme 1.28 Selective iodination of 3-bromopyridine.^[60]

The effect on modifying the alkyl groups in these dialkyl(amido)zincates has also been assessed.^[61] TMP-zincate **1** chemo- and regioselectively deprotonates 3-substituted bromobenzene compounds at C2 leading ultimately to the corresponding 2-iodo derivatives. Conversely, when the *t*-butyl ligands are substituted for methyl groups, as in Li(TMP)ZnMe₂, the same bromobenzene substrates yield a Diels-Alder product in the presence of a diene, indicating the formation of benzyne intermediates (Scheme 1.29).



Scheme 1.29 Deprotonation of 3-bromobenzenes with $\text{LiTMPZn}^t\text{Bu}_2$ and LiTMPZnMe_2 and trapped with iodine and 1,3-diphenylisobenzofuran respectively.

The structure of TMP-zincate **1** was crystallographically characterized in 2006.^[62] In the solid state it displays a CIP structure whereby both metals are connected by a bridging TMP group. A secondary long distance electrostatic interaction^[63] between lithium and a methyl carbon of one of the *tert*-butyl groups completes a five-membered $[\text{LiNZnCC}]$ cyclic foundation, and the remaining alkyl group sits in a terminal position on the zinc while the lithium coordinates to a single molecule of THF - $[(\text{THF})\text{Li}(\text{TMP})\text{Zn}^t\text{Bu}_2]$ **1** (Figure 1.3).

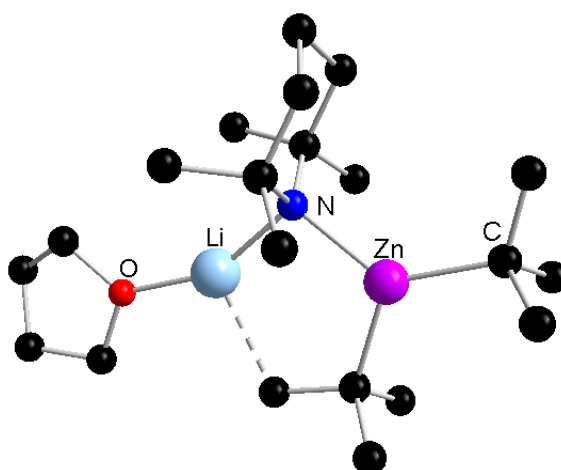
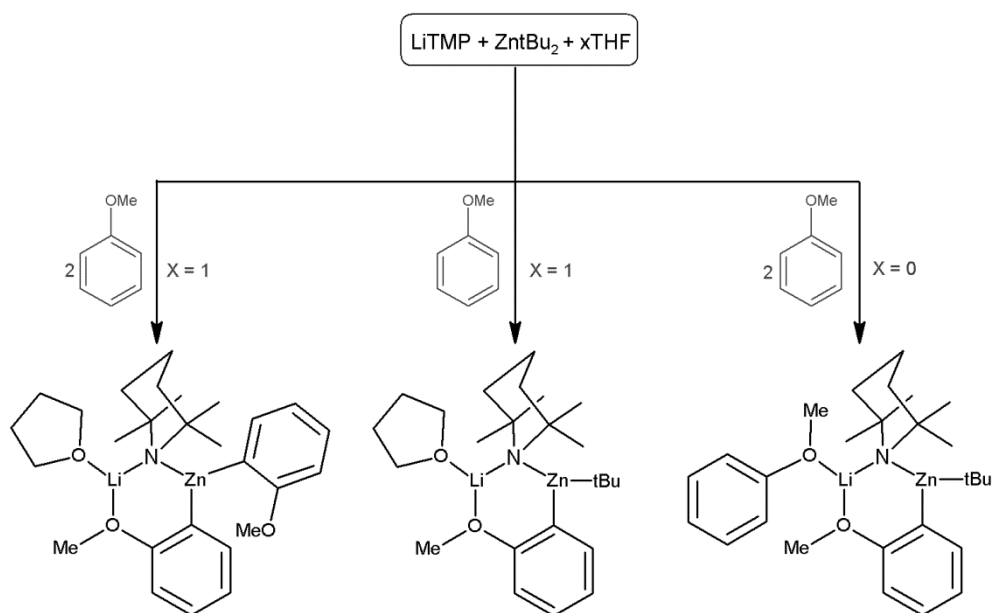


Figure 1.3 Molecular structure of $[(\text{THF})\text{Li}(\text{TMP})\text{Zn}^t\text{Bu}_2]$ **1** with H atoms omitted for clarity.

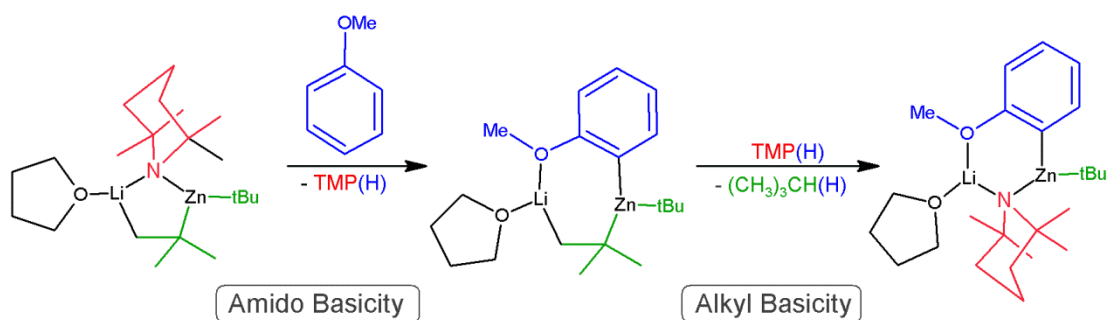
Structural, spectroscopic and theoretical studies carried out by the groups of Mulvey, Hevia, Uchiyama and Wheatley have demonstrated that the deprotonation reactions carried out by these heterobimetallic reagents are indeed direct Zn-H activations.^[64] Building on reports which have shown the ability of **1** to *ortho*-deprotonate aromatic substrates,^[57] the reactivity of the structurally defined lithium zincate **1** has further been assessed with the principal DoM substrate anisole (Scheme 1.30).^[65] The lithiation of anisole has been already been well studied;^[66] spectroscopically by NMR,^[67] through semi-empirical calculations,^[67-68] kinetic isotope effects,^[69] X-ray crystallography and rate studies,^[70] and was therefore the obvious choice for such an investigation.



Scheme 1.30 DoM of anisole with $[(\text{THF})\text{Li}(\text{TMP})\text{Zn}(\text{tBu})_2]$ **1** in hexane.

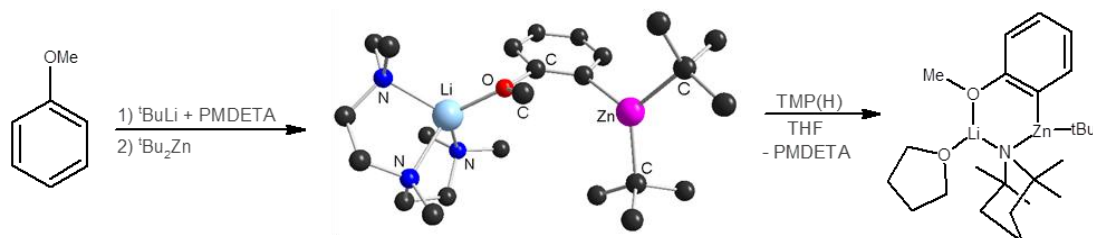
Interestingly, although these structural studies suggest that heteroleptic reagent **1** acts as an alkyl base – using one of the *t*Bu groups to deprotonate the aromatic substrate with concurrent formation of isobutene – DFT studies have revealed that from a kinetic perspective, amido basicity involving the TMP group should be more favourable. Following several theoretical (DFT) studies on a selection of DoM substrates – including anisole,^[59] benzonitrile,^[71] methyl benzoate^[71] and *N,N*-

diisopropyl benzamide^[72] – which indicate a preference for amido basicity, conflicting with the experimentally observed alkyl basicity,^[65] a two-step mechanism was proposed (Scheme 1.31).^[73] This involves the initial deprotonation of the arene by the amido ligand generating a putative $[\text{Li}(\text{areneide})(^t\text{Bu})\text{Zn}(^t\text{Bu})]$ intermediate, which may then react with the TMP(H) produced on deprotonation, resulting in the formation of the isolated $[\text{Li}(\text{TMP})(\text{areneide})\text{Zn}(^t\text{Bu})]$ product and isobutane.



Scheme 1.31 Proposed two-step mechanism for the DoM of anisole by TMP zincate **1**.

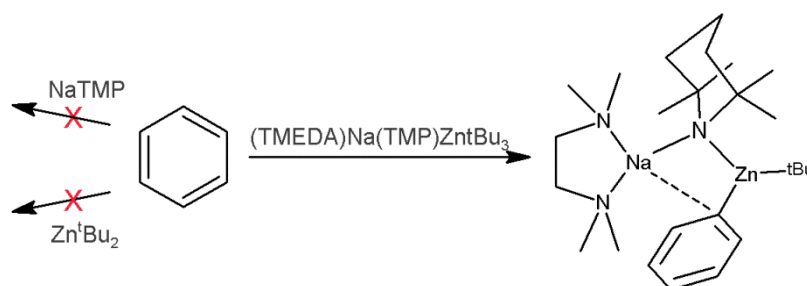
This hypothesis explains both the calculated predilection for amido basicity and the eventual formation of the product of alkyl basicity, although no direct experimental evidence could be found. However, using a co-complexation approach it has been possible to synthesise some surrogate intermediate species;^[74] $[(\text{D})_n\text{Li}(\text{C}_6\text{H}_4\text{-OMe})(\text{Me})\text{Zn}(\text{Me})]$ (where $\text{D} = \text{THF}$, $n = 2$ or $\text{D} = \text{TMEDA}$, $n = 1$) to mimic the species used in the computational model^[73] and $[(\text{PMDETA})\text{Li}(\text{C}_6\text{H}_4\text{-OMe})(^t\text{Bu})\text{Zn}(^t\text{Bu})]$ to better gauge the influence of the alkyl group.^[74] On treatment with TMP(H) it was found that this *tert*-butyl compound reacts to form the previously characterized *ortho*-zincated TMP zincate – providing the first experimental evidence of a two-step mechanism (Scheme 1.32).



Scheme 1.32 Alternative synthesis of $[\text{Li}(\text{TMP})(\text{C}_6\text{H}_4\text{-OCH}_3)\text{Zn}(^t\text{Bu})]$.

The isolation and crystallographic determination of reaction intermediates confirm that the deprotonation of the substrate is indeed a zincation, and that the lithium remains a spectator, albeit a not entirely innocent one. The role of the lithium in coordinating with the DMG, whilst leaving the zinc to perform the metallation, is central to the concept of alkali-metal-mediated-zincation (AMMZn).^[21] This term was coined on observation that the presence of one metal is necessary for the other to react; the alkali metal does not participate in the transformation yet it is crucial to the process.

Consequently, another feature to investigate with regards to the affect on the reactivity of such mixed-metal species, is the nature of the alkali metal. In practice, when sodium is substituted for lithium in the TMP-zincate the resulting sodium zincate [(TMEDA)Na(μ -TMP)Zn(*t*Bu)₂] **2** possesses the ability to deprotonate benzene at room temperature,^[75] something which neither NaTMP nor Zn*t*Bu₂ can achieve under the same conditions (Scheme 1.33).



Scheme 1.33 The Alkali Metal Mediated Zincation of Benzene.

This sodium diorgano(amido)zincate was also one of the first to be structurally characterized – displaying a CIP structure which is essentially isostructural to **1** – and the intermediate phenylzinc species was also characterized crystallographically (Figure 1.4). The resulting structure displays the same configuration as the starting zincate, with the exception that the bridging *tert*-butyl group has been replaced by the benzene ring. Zinc, having deprotonated the benzene, displays a σ -bond to the ring carbon, whilst sodium π -bonds to the ring (Na-C_{ipso} 2.706(3) Å). The retention

of the TMP backbone, alongside the substitution of the alkyl group for the phenyl, indicates that the zincate acts as an overall alkyl base with the loss of a ^tBu ligand as isobutane. However, this does not exclude the possibility of a two-step mechanism, as discussed above for TMP zincate **1**.^[73-74]

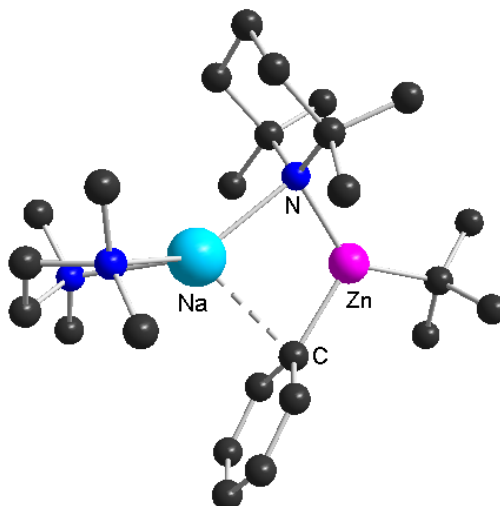


Figure 1.4 Molecular structure of [(TMEDA)Na(TMP)Zn(C₆H₅)(^tBu)] with H atoms omitted for clarity.

Sodium TMP-zincate **2** has been used to both mono- and dizincate unactivated benzene (Figure 1.5)^[76] and naphthalene,^[77] selectively *meta*-zincate aniline^[27] and *meta/para*-zincate toluene (in a ratio of ~ 1:2),^[78] leaving the acidic methyl protons intact (see Scheme 1.34). It has also been employed to *ortho* zincate phenyl *O*-carbamate,^[79] *N,N*-diisopropylbenzamide^[80] and benzyl methyl ether,^[81] in this instance without eliminating the highly acidic benzyl protons which are most commonly removed. The selective C2-zincation of 1-methylindole,^[82] has also been reported.

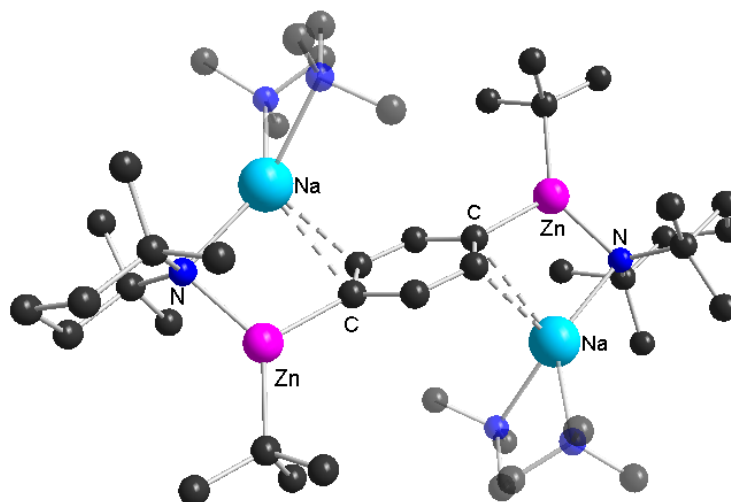
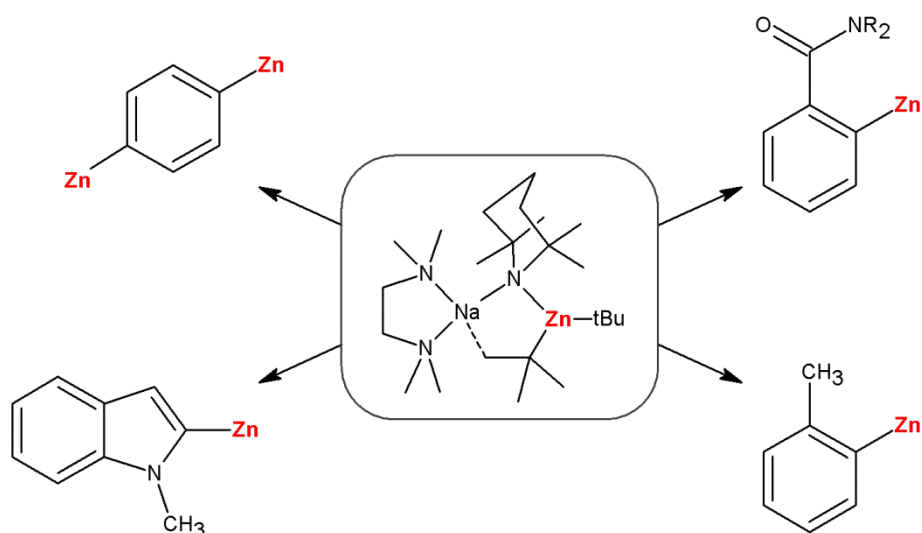


Figure 1.5 Molecular structure of dizincated benzene. H atoms have been omitted for clarity.

Thus, **2** provides an efficient route to carbon-zincated aromatics which would otherwise be difficult or impossible to achieve, eliminating the need to perform the metathesis of a carbon-lithiated species, and invoke cryogenic temperatures. Due to this efficiency and regioselectivity, sodium-TMP zincate **2** has proved to be a useful and highly versatile metallating reagent (Scheme 1.34).

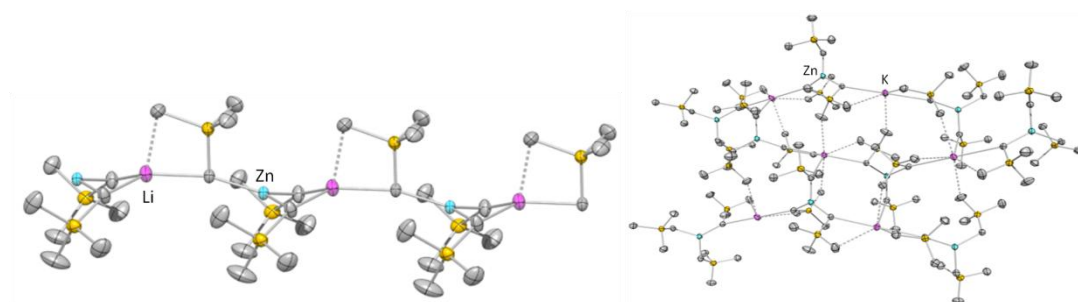


Scheme 1.34 Selective deprotonation of a variety of substrates by $[(\text{TMEDA})\text{Na}(\text{TMP})\text{Zn}(\text{tBu})_2]$ **2**.

1.6 Structural Diversity in Organozincate Chemistry

The capacity to finely tune these zincate reagents through relatively small ligand and donor modifications,^[60-61] coupled with their enormous synthetic potential,^[2i] makes them an interesting, and potentially beneficial, prospect for synthesis.^[2i] Their synthetic relevance notwithstanding, the structural information available on the constitution of these heterobimetallic reagents remains limited.^[83] This section highlights some recent structural advances in alkali metal zincate chemistry which reflect the vast structural diversity available to these compounds.

There are relatively few examples of structurally characterised alkali metal zincates, and most known examples incorporate some form of Lewis basic donor solvent.^[84] In certain cases a donor solvent is required to initiate the co-complexation of the two separate homometallic compounds;^[29c] however, Lewis bases are also employed in order to control the degree of aggregation and improve solubility of such species.^[31] As implied, those bimetallic complexes which do form in the absence of a Lewis base tend to form highly aggregated assemblies, which are largely insoluble in the non-polar solvents often required for their synthesis.^[29c, 85] Despite this, an homologous series of non-solvated zincates of type $[M\text{Zn}(\text{CH}_2\text{SiCH}_3)_3]$ ($M = \text{Li}, \text{Na}, \text{K}$) has recently been crystallographically characterised.^[84] These homoleptic zincates display a variety of supramolecular architectures; ranging from a linear polymer with lithium, to two- or three-dimensional networks with the larger alkali metals, potassium and sodium respectively (Scheme 1.35).



Scheme 1.35 Extended structures of $[\text{LiZn}(\text{CHSiCH}_3)_3]$ (left) and $[\text{KZn}(\text{CHSiCH}_3)_3]$ (right).

These highly aggregated structures are broken down considerably on the addition of a chelating donor solvent, resulting in the formation of monomeric zincates $[(\text{PMDETA})\text{LiZn}(\text{CH}_2\text{SiCH}_3)_3]$ and $[(\text{TMEDA})_2\text{NaZn}(\text{CH}_2\text{SiCH}_3)_3]$;^[84] however, supramolecular structures which incorporate donor molecules are not unknown. For instance the two-fold deprotonation of *N,N*-diethylthiophene-2-carboxamide by $[(\text{TMEDA})\text{Na}(\text{TMP})\text{Zn}^i\text{Bu}_2]$ **2** results in a tetrameric macrocycle in which the sodium atoms are coordinated to two donor atoms; either from the chelation of TMEDA, or coordination to two molecules of THF (Figure 1.6).^[86]

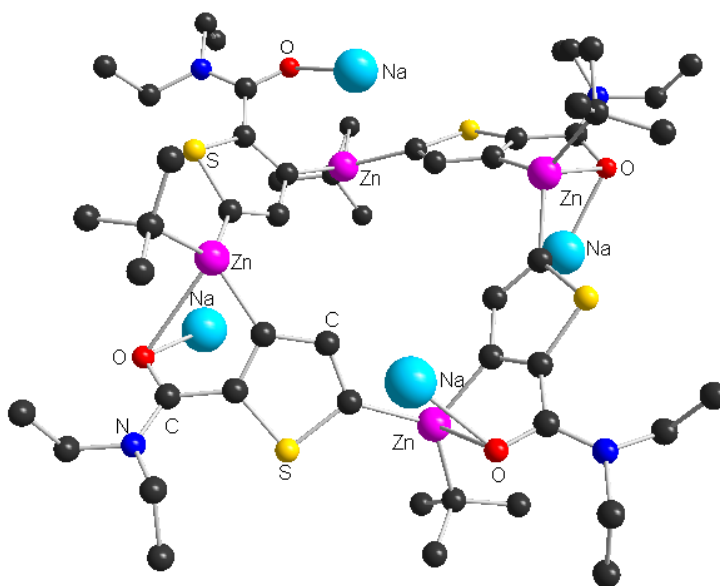


Figure 1.6 Molecular structure of 3,5-dizincated *N,N*-diethylthiophene-2-carboxamide. H atoms and TMEDA/THF donors on Na have been omitted for clarity.

Higher degrees of aggregation have also been observed. For example the cyclopentadienyl sodium compound $[(\text{THF})_2\text{NaZn}(\text{C}_5\text{H}_5)_3]$ ^[87] forms an infinite polymeric chain, propagated by the π -interaction of the THF solvated sodium atoms and the cyclopentadiene rings, which themselves bond to zinc in an η^1 -fashion (Figure 1.7, left). The addition of an extra molar equivalent of $[\text{Zn}(\text{C}_5\text{H}_5)_2]$ to this compound however results in the formation of $[\{\text{Na}(\text{THF})_6\}^+\{\text{Zn}_2(\text{C}_5\text{H}_5)_5\}^-]$ which adopts a solvent-separated structure incorporating the unusual dizinc anion $\{\text{Zn}_2(\text{C}_5\text{H}_5)_5\}^-$ (Figure 1.7, right).^[87]

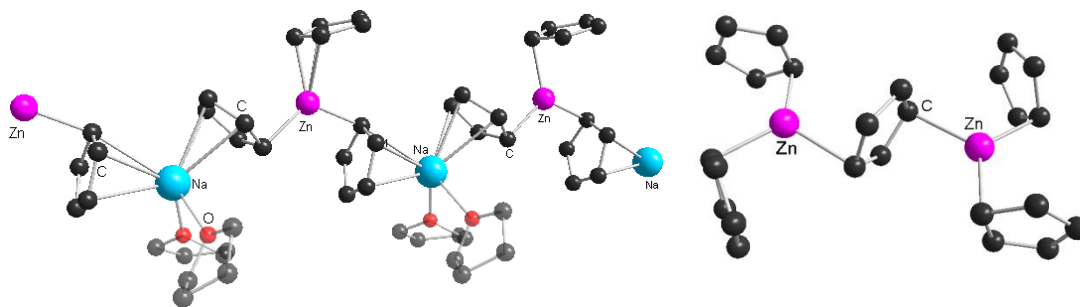


Figure 1.7 Molecular structure of $[(\text{THF})_2\text{NaZn}(\text{C}_5\text{H}_5)_3]_\infty$ (left) and the $\{\text{Zn}_2(\text{C}_5\text{H}_5)_5\}^-$ anion (right) with H atoms omitted for clarity.

The formulation of $[\{\text{Na}(\text{THF})_6\}^+\{\text{Zn}_2(\text{C}_5\text{H}_5)_5\}^-]$ is of further interest as it can be distinguished from both tetraorganozincates $[\text{M}_2\text{ZnR}_4]$ and triorganozincates $[\text{MZnR}_3]$ in the ratio of the metals to anionic ligands. This compound displays a 1M:2Zn:5R (where M = Na and R is an anionic ligand) constitution which is rarely observed in zincate chemistry, being restricted to only a handful of examples, including the lithium anilido zincate $[(\text{THF})_3\text{LiZn}_2(\text{NHDipp})_2(\text{Me})_3]$ **12** (see Chapter 3.1.3 THF)^[88] and the SSIP 2,2'-dipyridylamine (dpa) complexes $[\{\text{M}(\text{THF})_6\}^+\{\text{Zn}^i\text{Bu}_2(\text{dpa})\text{Zn}^i\text{Bu}_2\}^-]$ (M = Na, K)^[89] where the bis-*N*-heterocycle bridges between two zinc atoms through the chelation of one zinc by the two pyridyl nitrogens, whilst the other zinc centre bonds to the central amide nitrogen (Figure 1.8).

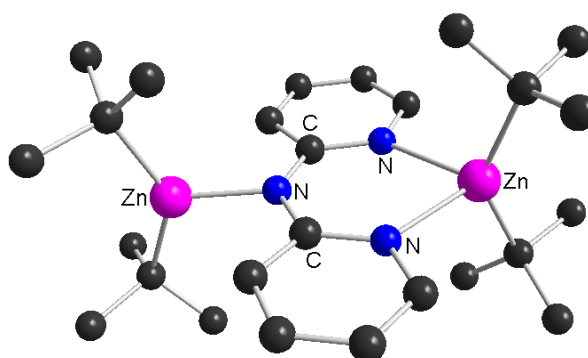


Figure 1.8 Molecular structure of the $\{\text{Zn}^i\text{Bu}_2(\text{dpa})\text{Zn}^i\text{Bu}_2\}^-$ anion of $[\{\text{K}(\text{THF})_6\}^+\{\text{Zn}^i\text{Bu}_2(\text{dpa})\text{Zn}^i\text{Bu}_2\}^-]$ with H atoms omitted for clarity.

The dpa ligand possesses the ability to coordinate in a variety of conformations; *syn/syn*, *syn/anti* and *anti/anti*. Both the sodium and potassium variants of $[\{M(\text{THF})_6\}^+\{Zn^t\text{Bu}_2(\text{dpa})Zn^t\text{Bu}_2\}^-]$ display the same *anti/anti* conformation seen in Figure 1.8; however, if the donor solvent THF is replaced with TMEDA the sodium system then produces $[(\text{TMEDA})_2\text{Na}_2(\text{dpa})_2Zn^t\text{Bu}_2]$, which incorporates two molecules of dpa, each exhibiting a different bonding mode – *syn/syn* and *anti/anti* (Figure 1.9).

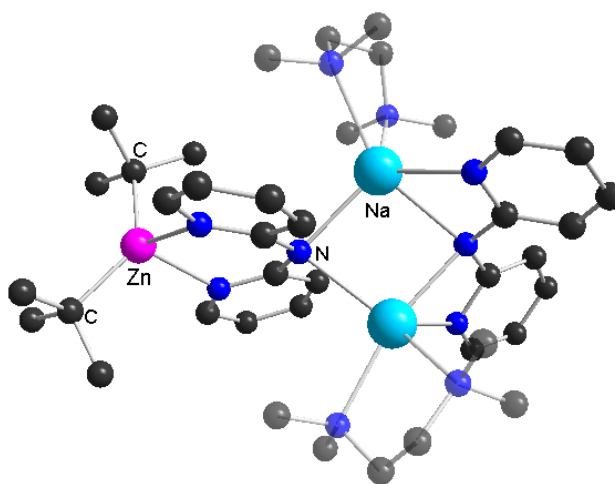
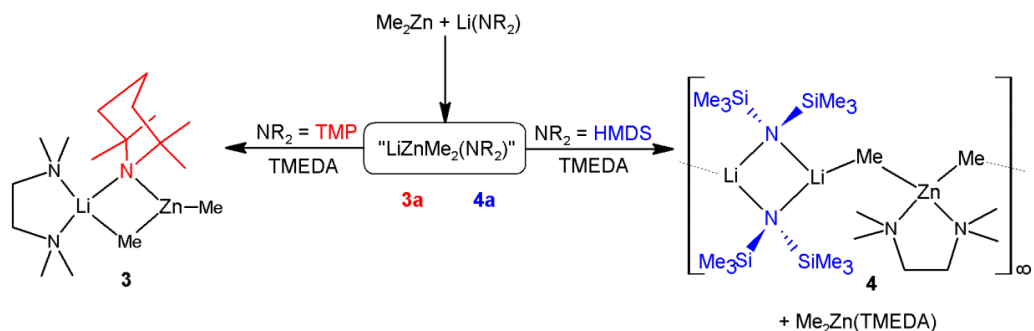


Figure 1.9 Molecular structure of $[(\text{TMEDA})_2\text{Na}_2(\text{dpa})_2Zn^t\text{Bu}_2]$ with H atoms omitted for clarity.

Although $[(\text{TMEDA})_2\text{Na}_2(\text{dpa})_2Zn^t\text{Bu}_2]$ shares the same formulation as the higher order zincates $[M_2ZnR_4]$, with a ratio of 2M:1Zn:4R (M = Na and R is an anionic ligand), the structure is distinctly different to the Weiss motif generally adopted by higher order ate complexes.^[2j, 83, 89-90] In this instance, it would appear that rather than containing the charged anionic zinc of a zincate species, this structure is in fact a neutral dialkylzinc species coordinated to a complex metalloligand donor.^[89]

The addition of a Lewis base may have a far more dramatic effect on a structure than straightforward deaggregation.^[29c, 85] The substitution of one donor for another can result in dramatic structural changes; for example, when the highly aggregated zincate species $\text{LiZn}(\text{NR}_2)\text{Me}_2$ ($\text{NR}_2 = \text{TMP } \mathbf{3a}$, $\text{HMDS } \mathbf{4a}$) are treated with the chelating donor TMEDA two very distinct structures result (Scheme 1.36).^[29c]



Scheme 1.36 Formation of zincates $[\text{LiZn}(\text{TMP})(\text{Me})_2]$ **3** and $[\text{LiZn}(\text{HMDS})(\text{Me})_2]$ **4**.

The structure of $[(\text{TMEDA})\text{Li}(\text{TMP})\text{ZnMe}_2]$ **3** (Figure 1.10) displays the same cyclical motif seen in other monomeric TMP-dialkyl zincates.^[62, 75] A $[\text{LiNZnC}]$ ring is formed whereby the two metals are bridged by the amido nitrogen and closed by an interaction between the methyl carbon and the lithium.

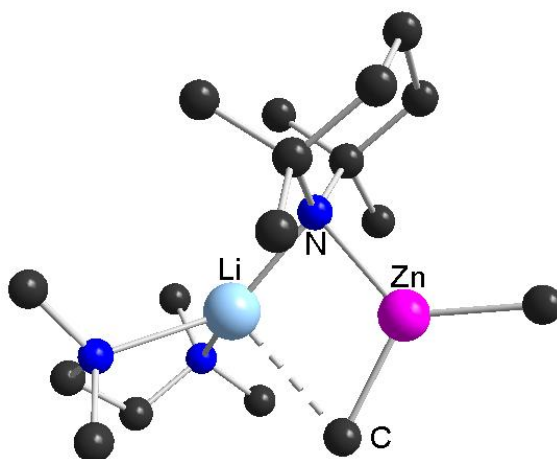


Figure 1.10 Molecular structure of $[(\text{TMEDA})\text{Li}(\text{TMP})\text{ZnMe}_2]$ **3** with H atoms omitted for clarity.

However, the structure of $[(\text{TMEDA})\text{Li}_2(\text{HMDS})_2\text{ZnMe}_2]$ **4** (Figure 1.11) does not display the same cyclical assembly as its TMP analogue – rather, the structure obtained is best described as an inverse zincate. Despite the stronger Lewis acidity of zinc, here it is the lithium which bonds to three anionic ligands, while the chelating donor binds to the zinc. This is a highly unusual preference in zincate chemistry where normally the zinc binds exclusively to anionic ligands.

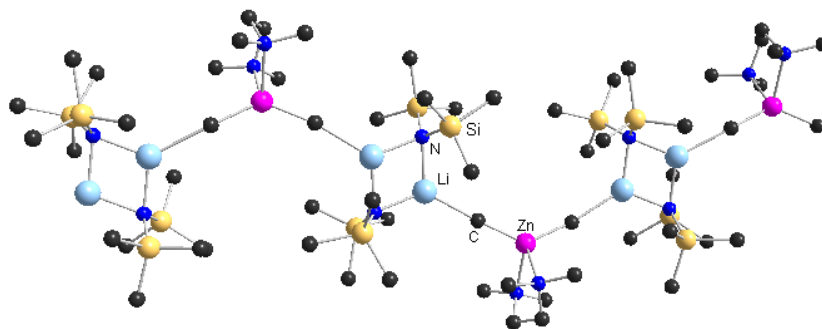


Figure 1.11 Molecular structure of $[(\text{TMEDA})\text{Li}_2(\text{HMDS})_2\text{ZnMe}_2]$ **4** with H atoms omitted for clarity.

In this inverse zincate the lithium amide has formed $[\text{LiHMDS}]_2$ dimers, whilst the donor solvent has chelated to zinc. The dimethylzinc then acts as a donor itself, linking the lithium amide dimers via interactions with its methyl groups and thus propagating a polymeric chain. This polymeric motif, whereby LiHMDS dimers are linked by a donor molecule, has been previously observed in the monometallic system with Lewis bases such as dioxane.^[29c]

Since both zincates **3** and **4** were prepared via the same co-complexation procedure (Scheme 1.36 *vide supra*) it appears that the addition of the diamine TMEDA triggers the disproportionation of the mixed-metal complex $[\text{Li}(\text{HMDS})\text{ZnMe}_2]$ **4a**, whereas it simply solvates $[\text{Li}(\text{TMP})\text{ZnMe}_2]$ **3a**. This difference has been attributed to the basicity of the amido ligand. Since TMP is more basic than HMDS it forms stronger bonds to the dimethylzinc, and as HMDS interacts less strongly this allows the nitrogen-zinc bond to cleave in the presence of the donor. However, since **4** is the only example of such an inverse zincate, no firm conclusions can be reached; although, if said hypothesis is correct then the possibility exists that other amines, which are also less basic than TMP, may form similar structures under the same conditions.

Building on such precedents in this rapidly evolving area, this thesis aims to advance our understanding of the synthesis, structure and reactivity of alkali metal zincate reagents. The first part of this report focuses on the synthesis of novel heteroleptic

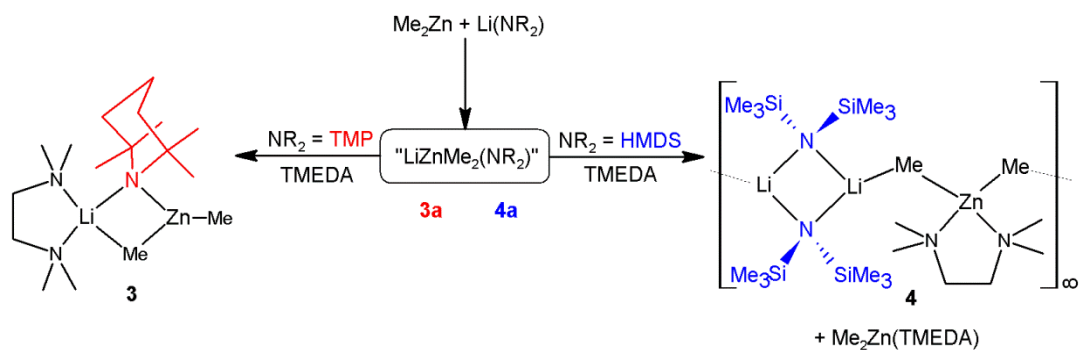
alkyl(amido) alkali metal zincates, probing the effect that the various ligands may have on the overall structure, and consequently reactivity, of the bimetallic species generated. Combining X-ray crystallography, NMR spectroscopy and DFT studies the effect of different donor solvents on the structure of [Li(HMDS)ZnMe₂] **4a** was investigated, revealing that the nature of the amide ligand is critical to the result (Chapter 2). Next, the influence of the amide ligand was explored by incorporating a primary amide – 2,6-diisopropylanilide [NHDipp⁻] – into the bimetallic system. Again a variety of Lewis basic donors were employed and their impact on the zincate formation and structure was determined (Chapter 3).

The remainder of the report concentrates on developing new synthetic applications for alkali metal zincates. Firstly, the homoleptic tri- and tetraphenyl lithium zincates **15** and **16** were synthesised, and their application towards the functionalisation of electron-deficient *N*-heterocyclic molecules by nucleophilic addition was studied (Chapter 4). This chapter also includes studies on the constitution and reactivity of trimetallic mixtures combining PhMgCl and [Zn(OPiv)₂·2LiCl] **27**. Finally, a bulky, chelating bis(amido)silyl ligand was employed to prepare the bis(amido)alkyl- and tris(amido)zincates $[\{\text{Na}(\text{THF})_6\}^+\{(\text{Ph}_2\text{Si}(\text{NDipp})_2)\text{ZnEt}\}^-]$ **29** and $[(\text{Ph}_2\text{Si}(\text{NDipp})_2)\text{Zn}(\text{TMP})\text{Na}(\text{THF})]$ **30**, which were employed in the deprotonation of various aromatic compounds (Chapter 5).

Chapter 2 Solvated and Solvent-free Lithium Dimethyl HMDS Zincates

As discussed above (see 1.6 Structural Diversity in Organozincate Chemistry) the addition of a Lewis base donor solvent to a mixed-metal species can have a major influence on the structure of the resulting compound. The TMEDA solvation of [LiZn(TMP)Me₂] **3a** and [LiZn(HMDS)Me₂] **4a**, for example, results in the isolation of two very different structures,^[29c] a monomeric molecular structure where the diamine coordinates to lithium (see Chapter 1, Figure 1.10), and a polymeric structure where TMEDA chelates to the zinc centre, respectively (see Chapter 1, Figure 1.11), with the latter exhibiting a novel inverse zincate motif (Scheme 2.1).

Since both of these contrasting structures were prepared using the same synthetic approach – *to wit* the co-complexation of the alkali metal amide with the dialkylzinc reagent (Scheme 2.1) – it appears that the inclusion of a donor solvent can have a significant impact on the overall structure of the resulting complex. Given the important role of the donor solvent in determining the ultimate configuration of a structure, an investigation into their influence on bis(alkyl)lithium HMDS zincates was carried out.

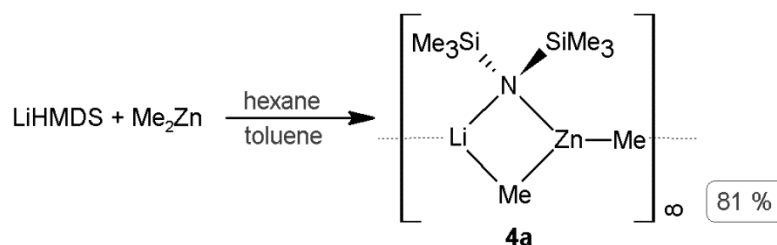


Scheme 2.1 Formation of zincates [LiZn(TMP)(Me)₂] **3** and [LiZn(HMDS)(Me)₂] **4**.

In the original report of **4**, both solvent-free zincates ($[\text{LiZn}(\text{NR}_2)_2\text{Me}_2]$, $\text{NR}_2 = \text{TMP}$ **3a**, HMDS **4a**) were identified and fully characterised by multinuclear (^1H , ^{13}C and ^7Li) NMR spectroscopy; however, their solid state structures remained undetermined. Suspecting that both reactants had formed a co-complex – as indicated by the NMR data – dismutation of the unsolvated HMDS zincate **4a** on the addition of TMEDA was proposed to explain the intriguing structure of the solvated zincate $[\text{Li}_2(\text{HMDS})_2(\text{Me})_2\text{Zn}(\text{TMEDA})]$ **4**. However, in order to understand this process in more detail the architecture of the non-solvated zincate had to be established. Inspired by these initial findings, it was decided to perform the systematic study of the synthesis of the donor-free precursor to zincate **4** – $[\text{LiZn}(\text{HMDS})\text{Me}_2]$ **4a** – and investigate its reactivity with a range of neutral Lewis donors.^[85]

2.1 The Unsolvated Zincate $[\text{LiZn}(\text{HMDS})\text{Me}_2]$ **4a**

The investigation began by studying the co-complexation reaction of LiHMDS and dimethylzinc in the absence of any donor. Thus, equimolar quantities of both homometallic components were mixed in the non-polar solvent hexane, leading to the formation of a white solid. Considering that both LiHMDS and dimethylzinc are soluble in hexane, the instantaneous precipitation of this powder is indicative of the formation of a new species. Addition of toluene and gentle heating of the reaction mixture led to the eventual isolation of $[\text{LiZn}(\text{HMDS})\text{Me}_2]$ **4a** as colourless crystals in a yield of 81% (Scheme 2.2).



Scheme 2.2 Formation of unsolvated zincate $[\text{LiZn}(\text{HMDS})\text{Me}_2]$ **4a**.

The full characterisation of **4a** by ^1H , ^{13}C and ^7Li NMR spectroscopy evidenced its bimetallic constitution in C_6D_6 solution.^[29c] Hence, the ^1H NMR spectrum indicated the presence of the methyl groups with a singlet at -0.67 ppm – a similar, though significantly different shift, to the corresponding signal of the dimethylzinc starting material in the same solvent (-0.52 ppm, Table 2.1). This shows that, despite now being part of a mixed-metal compound, the methyl groups retain a large proportion of their “zinc character”, in agreement with a trend previously observed in zincate chemistry,^[29c, 91] by virtue of the carbophilic nature of zinc, the alkyl groups remain strongly bound to the metal – a feature common amongst dialkyl-amido zincates. Regarding the amido ligand, the HMDS resonance of **4a** occurs at 0.15 ppm – intermediate to the corresponding signals of the homometallic amides (0.12 ppm and 0.20 ppm for LiHMDS and $\text{Zn}(\text{HMDS})_2$ respectively, Table 2.1). Further, the presence of a signal in the ^7Li NMR spectrum at 0.46 ppm confirms the inclusion of lithium in **4**. The ^{13}C NMR spectrum also supports the presence of a Zn-Me bond, as a signal at -6.7 ppm is also observed (*cf.* -4.7 ppm in ZnMe_2). A further resonance at 5.5 ppm was assigned to the HMDS methyl carbon by comparison to that of the homometallic $\text{Zn}(\text{HMDS})_2$ in the same solvent (5.1 ppm).^[92] All of the above is in accordance with the spectroscopic data previously published for **4a**.^[29c]

Table 2.1 Comparison of ^1H NMR shifts (in ppm) for the methyl and HMDS protons in zincates **4a** and **4** with other related species in C_6D_6 solution.

Compound	δ (Zn-CH ₃)	δ (HMDS)
LiHMDS		0.12
$\text{Zn}(\text{HMDS})_2$		0.20
ZnMe_2	-0.52	
[Li(HMDS)ZnMe ₂] 4a	-0.67	0.15
[Li ₂ (HMDS) ₂ (Me) ₂ Zn(TMEDA)] 4	-0.52	0.28

The bimetallic composition of **4** was confirmed by X-ray crystallographic studies and the structure of **4a** was also determined by X-ray crystallography (Figure 2.1); however, disorder between the metal sites and the terminal methyl ligand affected the precision of the structure, preventing the discussion of any geometrical parameters.

The data collected was, however, sufficient to establish the connectivity of the atoms, and zincate **4a** was found to adopt a CIP structure, based around a four membered [LiNZnC] ring. The lithium and zinc are bridged by the amide with one methyl ligand closing the four-membered ring, while the remaining methyl adopts a pseudo-terminal position on the zinc, coordinating to the lithium centre of a neighbouring unit. This propagates a linear polymeric chain structure by satisfying the otherwise coordinatively unsaturated lithium atom, resulting in both metals having tricoordinate environments (Figure 2.1). Interestingly, the arrangement of the HMDS ligands was found to be cisoid, with all of the amide groups lying on the same side of the Li \cdots Zn-C vector. Similar 1D polymeric systems have been observed for the related zincate [LiZn(HMDS)₂Me] (Li \cdots C = 2.435 Å)^[93] and the unsolvated TMP zincate [LiZn(TMP)Et₂], where the amido groups also sit in a cisoid configuration.^[94]

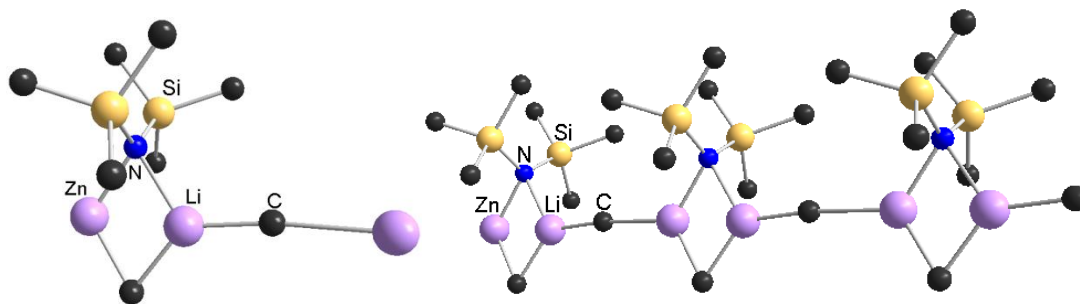
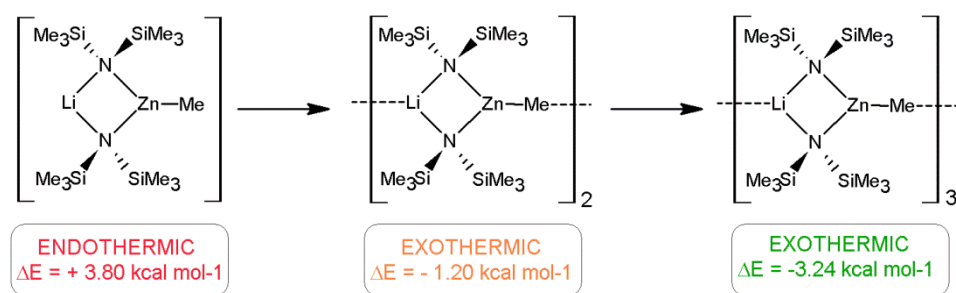


Figure 2.1 Molecular structure of the asymmetric unit of **4a** (left) and the extended polymeric chain (right) with H atoms omitted for clarity. There is disorder between the metal sites.

The formation of **4a** via co-complexation contrasts with previous reports on related TMP-zincates – such as [Li(TMP)Zn^tBu₂] and [Na(TMP)Zn^tBu₂] – which fail to form in the absence of a Lewis basic solvent such as TMEDA or THF.^[29c] Westerhausen has also reported the homoalkyl [LiZn{CH(SiMe₃)₂}₃],^[95] which is known to form solvent separated molecules with polydentate *N*-donors such as TMEDA or TMTA, but has only recently been found to adopt a similar 1D polymeric arrangement to that of **4a** (see 1.6 Structural Diversity in Organozincate Chemistry).^[84]

In order to develop our understanding of the formation of **4a**, a theoretical study into the reaction of lithium HMDS with dimethylzinc was then carried out.^[85] Exploratory *ab initio* calculations at the Hartree Fock (HF) level were performed using the 6-31G* basis set, and the resultant optimised geometries were subject to frequency analysis and then refined further by density functional theory (DFT) calculations using the B3LYP functionals and the 6-311G* basis set (Scheme 2.3). The lithium amide was modelled as a cyclic trimer, since this is the arrangement that it exhibits in the absence of any neutral donor ligand,^[96] and dimethylzinc was modelled as a simple linear monomer.^[97]



Scheme 2.3 Relative energies of modelled DFT reaction to yield **4a**.

When the product **4a** was modelled as a dinuclear monomer the co-complexation reaction was calculated to be endothermic by $+3.80 \text{ kcal mol}^{-1}$. The thermodynamics are observed to reverse, however, when modelled in a higher aggregation state; on modelling as a dimer the reaction becomes slightly exothermic ($-1.20 \text{ kcal mol}^{-1}$) and as a trimer the energy gain increases further to $-3.24 \text{ kcal mol}^{-1}$ (Scheme 2.3). When modelled, both the dimer and trimer adopted a linear structure and, in contrast to the related magnesiate $[\text{LiMg}(\text{HMDS})_3]$,^[98] no agostic interactions between the lithium and the trimethylsilyl groups of the amide ligand were observed. According to these results it would appear that the probability of a non-solvated zincate forming is dependent on the ability of said species to aggregate: thus the infinite aggregation of the polymeric structure of **4a** is thermodynamically favoured.

These results seem to suggest that the potential for an unsolvated zincate to aggregate may be critical in facilitating the co-complexation reaction of its homometallic

components. This offers an explanation as to why the solvent-free zincate $[\text{LiZn}(\text{TMP})\text{Et}_2]_\infty$ ^[94] (Figure 2.2 (right)) has been found to adopt a similar polymeric structure, and yet Zn^tBu_2 will not complex with LiTMP in the absence of a donor solvent.^[29c] The steric congestion around the quaternary carbon of a *tert*-butyl group would most likely prevent any effective interaction with the coordinatively unsaturated lithium centre of a neighbouring unit, greatly limiting the ability to form a highly aggregated structure.

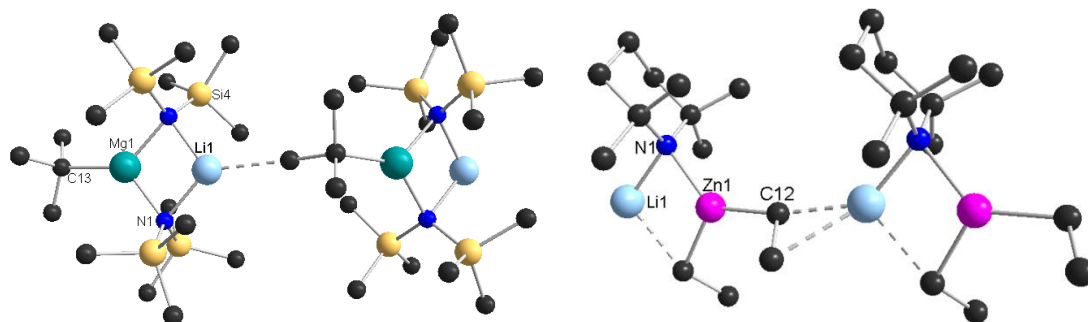


Figure 2.2 Molecular structure of solvent-free species $[\text{LiMg}(\text{HMDS})_2^t\text{Bu}]_\infty$ (left) and $[\text{LiZn}(\text{TMP})\text{Et}_2]_\infty$ (right) showing the agostic aggregation of the repeating units. H atoms have been omitted for clarity.

The lithium magnesiate $[\text{LiMg}(\text{HMDS})_2^t\text{Bu}]_\infty$ ^[99] is known to propagate a polymer by interactions between the alkali metal and one of the methyl groups on the terminal *tert*-butyl group ($\text{Li}\cdots\text{C} = 2.563 \text{ \AA}$, Figure 2.2 (left)); however, these interactions are much weaker and less energetically preferred than those found in **4a** or $[\text{LiZn}(\text{TMP})\text{Et}_2]_\infty$ ($\text{Li}\cdots\text{C} = 2.374 \text{ \AA}$), where the interaction with the lithium occurs through a more anionic carbon, bearing most of the negative charge of the alkyl group.

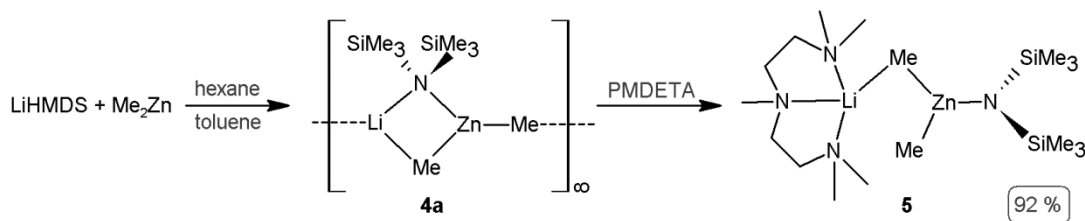
2.2 The Effect of the Donor Solvent

As noted above, the addition of one molar equivalent of TMEDA to **4a** yields the inverse zincate **4**,^[29c] where the roles of the lithium and the zinc are reversed with respect to those of conventional zincates, and TMEDA preferentially bonds to zinc

(See 1.6 Structural Diversity in Organozincate Chemistry, Figure 1.11). The reactivity of **4a** towards other neutral nitrogen donors was therefore investigated. Focusing mainly on the influence of donor denticity, the tridentate nitrogen donor PMDETA and monodentate donors 4-*tert*-butylpyridine and *tert*-butylcyanide were employed.

2.2.1 PMDETA

Starting with PMDETA – one equivalent of which was added to a freshly prepared suspension of **4a** in hexane-toluene mixture – colourless crystals were isolated in near quantitative yield (92%, Scheme 2.4). These crystals were spectroscopically identified as [(PMDETA)LiZn(HMDS)Me₂] **5**. Thus, the ¹H NMR spectrum in C₆D₆ displays a singlet at -0.53 ppm corresponding to the methyl groups – this is almost identical to the chemical shift of the Zn-Me groups of the precursor ZnMe₂, and of inverse zincate **4** (both -0.52 ppm), indicating that the methyl groups still retain much of their zinc character, in accordance with the observations discussed above.^[29c, 91] A resonance at 0.50 ppm assigned to the trimethylsilyl groups of the amido ligand appears significantly downfield with respect to the monometallic species (0.12 ppm for LiHMDS and 0.20 ppm for Zn(HMDS)₂). This suggests that the bond between amide and metal is more covalent in **5** than in either monometallic compound.^[85] The relevant signals for a single equivalent of PMDETA were also present; a singlet at 1.87 ppm and 1.85 ppm corresponding to the methyl groups on the terminal and central N atoms respectively, and another broad singlet centred at 1.72 ppm corresponding to the methylene protons. The ¹³C NMR spectrum shows signals at -6.99 ppm – indicative of a carbon bound to zinc (*versus* -6.67 ppm for **4a**) – and 6.69 ppm corresponding to the methyl groups of the HMDS (*cf.* 5.51 ppm in **4a** and 6.28 ppm in **4**), whilst the inclusion of lithium is revealed by a resonance in the ⁷Li NMR spectrum at 0.67 ppm. Interpretation of this spectroscopic data indicated a 1:1:2 ratio of donor to amide to alkyl group.



Scheme 2.4 Co-complexation to afford **4a** and its subsequent chelation with PMDETA to yield **5**.

X-ray crystallographic studies established the molecular structure of [(PMDETA)LiZn(HMDS)Me₂] **5** – exhibiting a discrete monomeric arrangement, which in contrast to the TMEDA adduct **3**, displays a CIP motif with an open structure, rather than the closed ring structure of other zincates (Figure 2.3, Table 2.2). The connectivity of the two metals is now via a bridging alkyl ligand, which was surprising considering the superior bridging ability of an amide ligand in comparison to a methyl group.

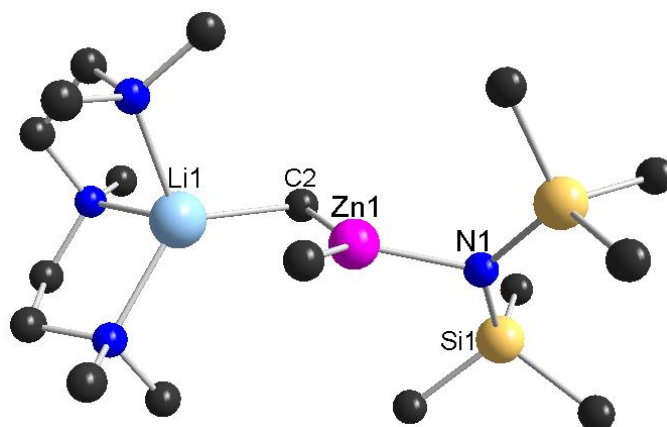


Figure 2.3 Molecular structure of [(PMDETA)LiZn(HMDS)Me₂] **5** with H omitted for clarity.

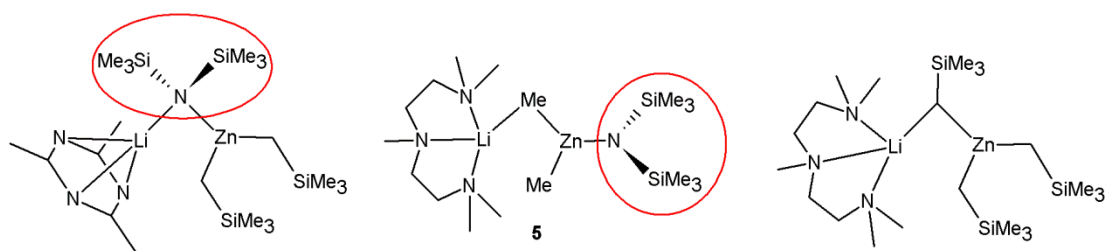
Despite the unconventional bridging arrangement in **5**, the geometry about the zinc remains almost perfectly trigonal planar (sum of the angles about zinc: 359.91°), and the Zn-N1 distance (1.9851(10) Å) is similar to those of other zinc compounds which feature a terminal HMDS, yet appreciably longer than in the monomeric [Zn(HMDS)₂]^[92] (average of 1.832 Å). The Zn-C bonds are, as expected, unequal in length with the bridging methyl bond being slightly elongated (Zn-C2 = 2.0361(15)

Å versus Zn-C1 2.0074(14) Å). Both distances are comparable to the related bond lengths in inverse zincate [Li₂(HMDS)₂(Me)₂Zn(TMEDA)] **4** (average Zn-C distance 2.005 Å)^[29c] and conventional zincate [(TMEDA)Li(μ-TMP)(μ-Me)Zn(Me)] **3** (average Zn-C distance 2.014 Å).^[29c] The Li-C2 bond, at 2.335(2) Å, is almost identical to that of **4** (mean Li-C distance of 2.375 Å) where the methyl groups also bridge between the two metals, although both of these structures display marginally elongated Li-C contacts with respect to the homometallic [{LiMe(THF)}₄] in which each methyl anion bridges to three lithium atoms (average Li-C distance 2.240 Å).^[100]

Table 2.2 Selected bond lengths (Å) and angles (°) for [(PMDETA)LiZn(HMDS)Me₂] **5**.

Zn1 – C1	2.0074(14)	Li1 – C2	2.335(2)
Zn1 – C2	2.0361(15)	Li1 – N2	2.196(2)
Zn1 – N1	1.9851(10)	Li1 – N3	2.132(2)
Li1 ... C1	3.084(3)	Li1 – N4	2.113(2)
C1 – Zn1 – C2	132.64(6)	N2 – Li1 – N3	84.22(8)
C1 – Zn1 – N1	114.59(6)	N2 – Li1 – N4	87.12(8)
C2 – Zn1 – N1	112.68(5)	N3 – Li1 – N4	121.97(10)

The distance between Li and the remaining methyl group (Li1-C1 3.084(3) Å) is too elongated to indicate any type of significant interaction hence, rather than the closed cyclic structures of **3** and **4a**, **5** displays the same type of open structure seen in the TMTA zincate [Li(μ-HMDS)Zn(CH₂SiMe₃)₂(TMTA)]^[101] (Scheme 2.5). The lithium carbon contact of 2.736 Å in this structure is appreciably shorter than that of the corresponding distance in **5** (3.084(3) Å), and despite displaying the same open arrangement, due to the large steric bulk of the donor, the bulk of the alkyl ligand dictates that the HMDS is not forced into a terminal position in this instance.



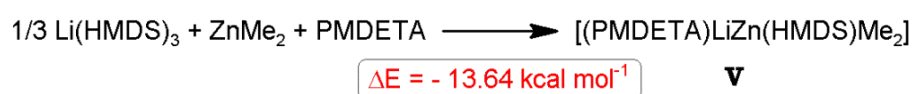
Scheme 2.5 Comparison of the structure of **5** (centre) with $[\text{Li}(\mu\text{-HMDS})\text{Zn}(\text{CH}_2\text{SiMe}_3)_2(\text{TMTA})]$ (left) and $[(\text{PMDETA})\text{LiZn}(\text{CH}_2\text{SiMe}_3)_3]$ (right).

Closely related to the TMTA compound, the homoleptic lithium zincate $[(\text{PMDETA})\text{LiZn}(\text{CH}_2\text{SiMe}_3)_3]^{[84]}$ and the isostructural magnesiate $[(\text{PMDETA})\text{LiMg}(\text{CH}_2\text{SiMe}_3)_3]^{[102]}$ also display an open structural motif, which has been described as intermediate between an SSIP and CIP structure (Scheme 2.5). Thus, although the TMTA and PMDETA donors are both tridentate there is not such a significant relief of steric hindrance on reversing the roles of the alkyl and amido ligands within the heteroleptic TMTA structure, due to the increased size of the alkyl group in relation to those of **5** – CH_2SiMe_3 *versus* CH_3 . It can therefore be concluded that it is the greater ability of the amide to bridge which dictates the overall structure of $[\text{Li}(\mu\text{-HMDS})\text{Zn}(\text{CH}_2\text{SiMe}_3)_2(\text{TMTA})]$, whilst the reduction of steric congestion (Me *vs.* CH_2SiMe_3) prevails in compound **5**, resulting in a switching of ligand roles.

As mentioned above, the ^1H NMR spectrum of **5** in C_6D_6 shows a single resonance for both methyl groups at -0.53 ppm, indicating that the solution structure either undergoes a rapid exchange between the terminal and bridging function of the methyl groups, or adopts a solvent separated structure $[(\text{PMDETA})\text{Li}(\text{C}_6\text{D}_6)_x]^+[\text{Zn}(\text{HMDS})\text{Me}_2]^-$, resulting in the chemical equivalence of both groups at room temperature.

The terminal position of the amide ligand and bridging alkyl ligand in this structure is a feature which has no precedent in dialkyl(amido)zincate chemistry. The

tridentate coordination and steric bulk of the PMDETA donor has seemingly forced the larger HMDS ligand into a terminal position, overcoming both the electronic preference of the nitrogen to bridge between the metal centres and the jealously carbophilic nature of zinc. In order to ascertain the process behind the formation of **5** another theoretical study was carried out at the same level as described above for **4a**. Thus, the modelled reaction between lithium HMDS and dimethylzinc in the presence of PMDETA was calculated as exothermic by $-13.64 \text{ kcal mol}^{-1}$ (Scheme 2.6).



Scheme 2.6 Modelled reaction between Li(HMDS) and ZnMe₂ in the presence of PMDETA.

The product was modelled as two regioisomers **Va** with a terminal amido group, and **Vb** with a bridging amide ligand (Figure 2.4). The calculated bond lengths for both models are given in Table 2.3 alongside the bond lengths determined crystallographically.

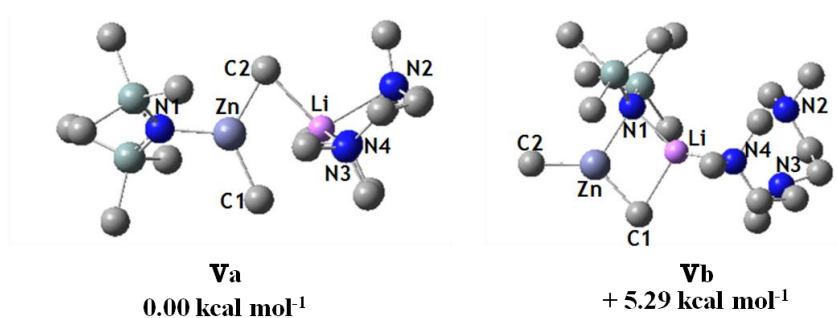


Figure 2.4 Modelled structures of **V** with terminal HMDS (left) and bridging HMDS (right).

Table 2.3 Comparison of the calculated bond distances (Å) of **Va** and **Vb** with the crystallographic data for **5**.

	5	Va	Vb
Zn-C1	2.0074	2.067	1.981
Zn-C2	2.0361	2.042	2.057
Zn-N1	1.9851	1.975	2.143
Li-C2	2.335	2.271	
Li···C1	3.084	2.671	2.569
Li-N1			1.978
Li-N4	2.113	2.256	2.130
Li-N3	2.132	2.251	3.711
Li-N2	2.196	2.362	5.035

The most stable isomer was found to be **Va**, by a difference of 5.29 kcal mol⁻¹. This corresponds to the structure found experimentally, and the calculated and observed bond lengths are also in good agreement (Table 2.3). With the exception of the longer lithium carbon interaction, which is stronger in the modelled structure (2.671 Å *versus* 3.084 Å), the remainder of the bond distances are reasonably close to the experimentally obtained values. Again, despite the superior ability of the amide ligand (with two lone pairs of electrons) to construct a bridge, it is the isomer with the electron deficient alkyl bridge which is energetically preferred in this instance.

Furthermore, the absence of PMDETA in the calculations reverses the relative stabilities of the two isomers, with [Li(μ-HMDS)(μ-Me)Zn(Me)] **Vb*** which contains a bridging amide ligand being more stable than [Li(μ-Me)₂Zn(HMDS)] **Va*** by 14.01 kcal mol⁻¹, proving that the presence of the PMDETA has a significant and defining effect on the structure (Figure 2.5).

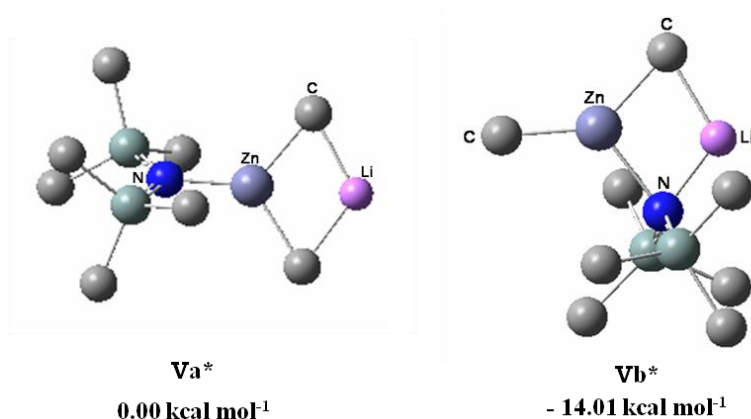
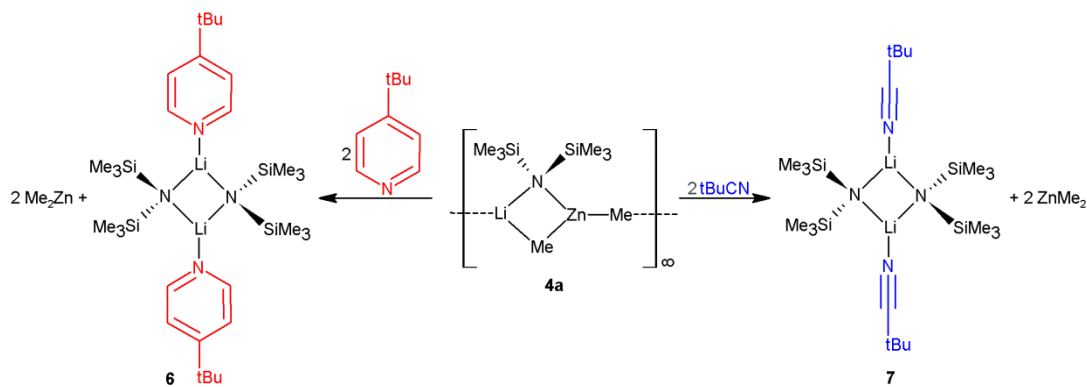


Figure 2.5 Modelled structures of **V** (in the absence of PMDETA) with terminal HMDS **Va*** (left) and bridging HMDS **Vb*** (right).

The combination of the hapticity and bulk of the PMDETA forces the HMDS into a terminal position, despite the electronic preference for the amide to bridge. In fact, when the amide does adopt a bridging function, as in model **Vb**, the tridentate PMDETA ligand coordinates to the lithium using only one of its N atoms, in a monodentate fashion (Figure 2.4, Table 2.3). The calculated value for Li-N4 in **Vb**, at 2.130 Å, is comparable to the average value of the Li-N_{PMDETA} contacts in **5** (2.147 Å), whereas the remaining distances (Li-N3: 3.711 Å and Li-N2: 5.035 Å) are too large to suggest any interaction. Hence, the inability of the PMDETA to coordinate in the preferred chelating manner may also contribute to the decreased stability of isomer **Vb** with respect to **Va**.

2.2.2 Monodentate Donors

Turning to the monodentate nitrogen ligands 4-*tert*-butylpyridine (*t*Bu-py) and *tert*-butylcyanide (*t*BuCN), in both cases the addition of a single equivalent to **4a** resulted in the isolation of colourless crystalline products. These were identified by ¹H NMR spectroscopy as the homometallic Lewis acid-base complexes [(*t*Bu-py)Li(HMDS)] **6** and [(*t*BuCN)Li(HMDS)] **7**; isolated in 72 % and 82 % yields, respectively (Scheme 2.7).



Scheme 2.7 Synthesis of homometallic [(^tBu-py)Li(HMDS)] **6** and [(^tBuCN)Li(HMDS)] **7** from **4a**.

Compound **7** has been previously prepared by the 1:1 reaction of LiHMDS with *tert*-butylcyanide, and its structure determined by X-ray crystallography (Figure 2.6).^[103] The molecular structure of **7** is a simple dimeric (LiN)₂ ring where the HMDS ligands span the two metals, and a terminal *tert*-butylcyanide molecule satisfies the coordination sphere of each lithium.^[103a] The ¹H NMR spectrum in C₆D₆ solution consists of two singlets at 0.71 and 0.49 ppm relating to the ^tBu and the HMDS protons respectively, and the ¹³C NMR spectrum shows three signals, relating to the ^tBu quaternary and methyl carbon atoms (27.2 and 27.1 ppm respectively) and those of the HMDS methyl groups (6.3 ppm). The inclusion of lithium is indicated by a resonance at 1.21 ppm in the ⁷Li NMR spectrum.

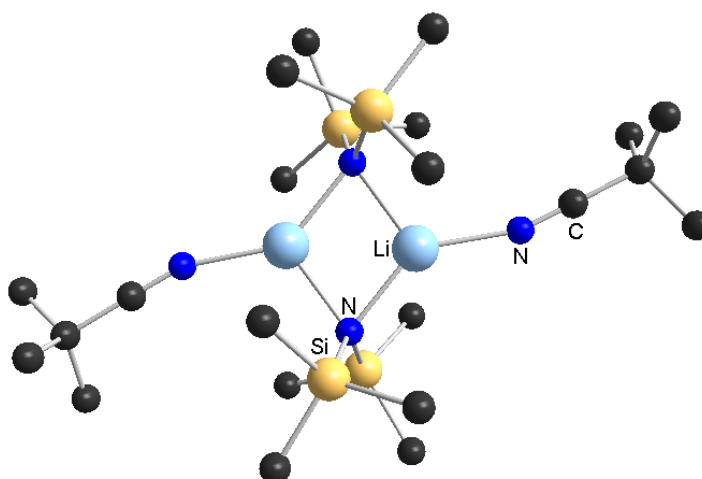


Figure 2.6 Molecular structure of [(^tBuCN)Li(HMDS)] **7** with H atoms omitted for clarity.

[^tBu-py)Li(HMDS)] **6** was characterised by ¹H, ¹³C and ⁷Li NMR spectroscopy. Thus, the ¹H NMR spectrum in C₆D₆ displayed signals corresponding to the aromatic protons of the ^tBu-py at 8.75 and 6.88 ppm, with the methyl protons of the ^tBu group resonating at 0.91 ppm. The remaining resonance at 0.53 ppm was assigned to the HMDS ligand, although it is significantly shifted with respect to non-solvated LiHMDS in the same solvent (0.12 ppm). A signal was observed at 2.75 ppm in the ⁷Li NMR spectrum, and the ¹³C NMR spectrum displays signals corresponding to the pyridine molecule (at 166.7, 149.7 and 121.6 ppm), with another signal at 6.6 ppm relating to the HMDS carbons. While the molecular structure of **6** was not determined crystallographically, it may reasonably be assumed to form a similar dimeric structure to that found in the unsubstituted pyridine analogue [{(Py)Li(HMDS)}₂] reported by Mulvey in 2001 (Figure 2.7).^[104]

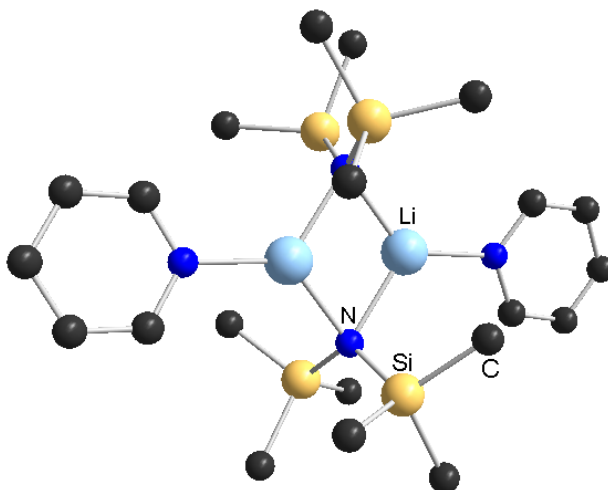
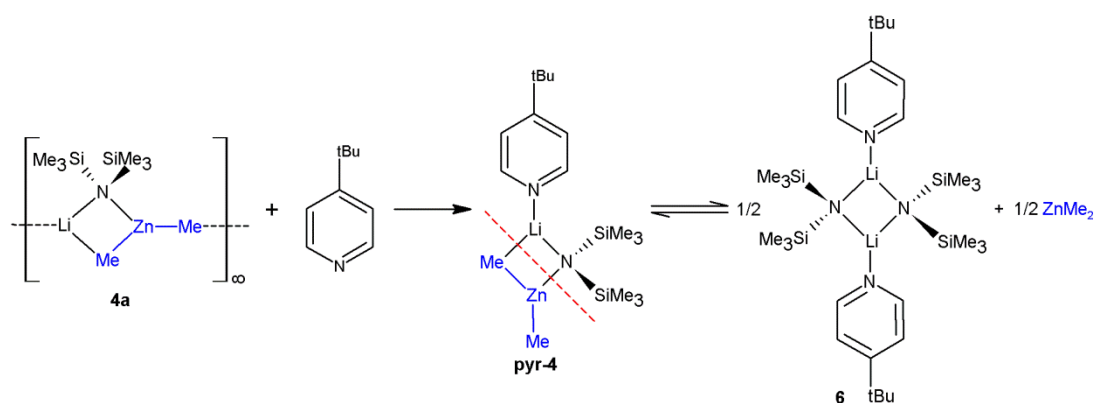


Figure 2.7 Molecular structure of [(Py)Li(HMDS)]₂ with H atoms omitted for clarity.

These findings suggest the disproportionation of **4a** into its homometallic constituent parts on the addition of these monodentate donors. The cleavage of other mixed-metal species under such conditions has been previously observed. For example, the pyridine complex [(Py)Li(HMDS)]₂ above was formed as a result of the addition of excess pyridine to the tris(amido)magnesiato [LiMg(HMDS)₃];^[104] with addition of the donor cleaving the magnesiato into the two monometallic species – [(Py)Li(HMDS)]₂ and the analogous magnesium complex [Mg(HMDS)₂(Py)₂]. The formation of the solvated magnesiato [LiMg(HMDS)₃Py], however, was

observed when pyridine was added stoichiometrically, in contrast to the zincate systems studied here, where only the disproportionation products arise, even without an excess of donor.

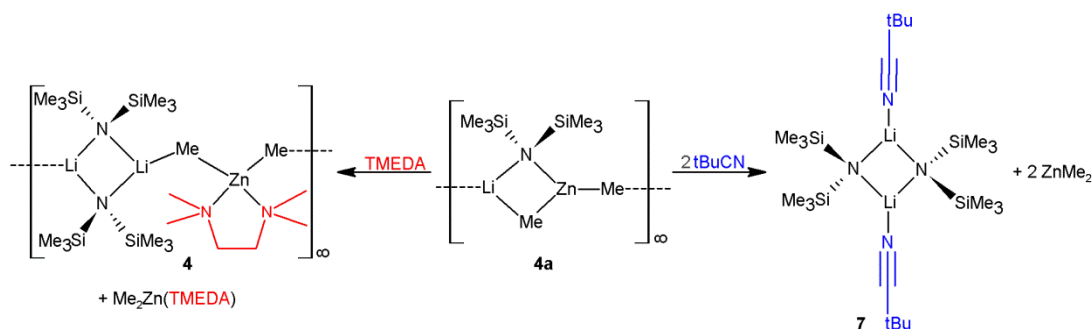
It is plausible that the initial solvation of **4a** would occur, fracturing the polymer into smaller aggregates, which might then disproportionate as shown in Scheme 2.8. The equilibrium shown favours the formation of the monometallic species, presumably due to the low solubility of [(*t*-Bu-py)Li(HMDS)] **6** in hexane solution. The same explanation can be employed for the *t*-BuCN system, and it is also noteworthy that although both *t*-butylcyanide and 4-*t*-butylpyridine are unsaturated molecules which are known to be susceptible to nucleophilic addition,^[2d] under the conditions used compound **4a** fails to react with either in this fashion.



Scheme 2.8 Plausible disproportionation pathway for the formation of **6**.

Unlike *t*-BuCN, 4-*t*-butylpyridine does form a complex with dimethylzinc; however, this donor displays a clear preference for lithium and thus no mixed metal complexes could be isolated. This is consistent with the formation of inverse zincate **4** from **4a**, where the effect of the donor is to split the bimetallic compound into its homometallic components, and rearrange to a structure forming {LiHMDS}₂ dimers flanked by a monodentate donor coordinated to each lithium atom. Whereas TMEDA favourably forms a complex with ZnMe₂ creating the Me₂Zn(TMEDA) donor in **4** – which uses both methyl groups to act in a bidentate fashion – these donors

preferentially bind to lithium. As such, discrete lithium dimers are formed and the formation of a bimetallic species is prevented (Scheme 2.9).



Scheme 2.9 The influence of mono- (^tBuCN) and bidentate (TMEDA) donors on [LiZn(HMDS)Me₂]_n

4a

2.3 Conclusions

The formation of unsolvated zincate **4a** has shown that the ability of a complex to aggregate has great influence over its formation. Unless the dialkylzinc species can breakdown the stable, aggregated state of the lithium amide, the mixed-metal species will not form. Theoretical and structural studies indicate that when co-complexation *is* favoured it is clearly dependent upon the ability of the new bimetallic species to aggregate, with the formation of a monomer of **4a** being unfavourable (endothermic), while dimer and trimer formation become increasingly exothermic.

The aggregation of **4a** is made possible by the partial negative charge on the methyl groups, but any intermolecular interaction between lithium and a neighbouring unit is readily sacrificed in preference for stronger interactions, such as those involving a Lewis basic solvent. Once the capacity for aggregation through the methyl carbon is removed – on solvation of the lithium atoms by a donor solvent – the stability of the mixed-metal species is compromised. Thus, the addition of a monodentate donor to **4a** will break the bimetallic compound down into its monometallic components, allowing the lithium amide to dimerise, as seen with **6** and **7**. In the unique case of **4**, the addition of bidentate TMEDA also causes the scission of the mixed-metal species

4a into single-metal compounds, yet in this instance the inclusion of dimethylzinc is favoured due to the ability of $\text{Me}_2\text{Zn}(\text{TMEDA})$ itself to act as a donor.

An exception to the above occurs when the tridentate donor PMDETA is employed, as in zincate **5**. Due to the greater steric bulk and higher denticity of this donor, the ability of the lithium amide to dimerise is reduced, and here it is the ability of the donor molecule to chelate to the alkali metal which is crucial. As there is no longer any significant gain from the collapse of the bimetallic species the mixed-metal complex remains intact and the lithium is simply solvated by the PMDETA donor. However, the same increase in denticity (and bulk) which prevents the complex from splitting also hinders the capacity of the larger amide ligand to bridge the two metals. This results in a switching of ligand function, whereby the amide, despite its superior bridging ability, is forced into a terminal position on the zinc in order to relieve steric strain, resulting instead in one of the methyl groups connecting the two metals.

Collectively, these findings establish that the stability (and therefore formation) of mixed lithium-zinc reagents is reliant on the ability of the resulting complex to aggregate. For the synthesis of an unsolvated species, it would appear that the capacity to polymerise, and form highly aggregated structures, is essential in order to thermodynamically drive the co-complexation process. The addition of neutral Lewis donors, however, has a dramatic effect on the constitution of such species, and it is evident that any interactions between the unsolvated bimetallic monomers are readily sacrificed in preference for any stronger donor-metal interactions. When the capacity for a zincate to polymerise is removed by solvation, the survival of the mixed-metal complex becomes dependent on the relative stabilities of its monometallic constituents: thus, monodentate donors favour the dimerisation of the lithium reagent over the inclusion of zinc, whereas the tridentate donor PMDETA is too bulky to allow effective aggregation and therefore results in the isolation of a mixed-metal complex. The bidentate donor TMEDA remains a peculiarity as, despite the bulk of the donor cleaving the bimetallic complex, the ability of the resulting $(\text{TMEDA})\text{ZnMe}_2$ to act as a donor to the accompanying $\text{Li}(\text{HMDS})$ also results in the eventual formation a mixed-metal complex.

Chapter 3 Donor-Dictated Co-Complexation Reactions: The Structures of New Methyl(NHDipp) Zincates

As already mentioned in Chapter 1, the reactivities and structures of dialkyl(amido)zincates are intimately related to the nature of the amide ligand.^[60] Until recently, the synthesis of dialkyl(amido)zincates had long been limited to the use of sterically demanding secondary amides such as HMDS,^[29c, 85, 101] TMP^[57, 59, 62, 75, 77] or DA.^[105] In light of this fact, the main focus of this chapter was to investigate the co-complexation reactions of dimethylzinc with the lithium amide LiNHDipp (Dipp = 2,6-diisopropylphenyl) – derived from a primary amine – in the presence of different Lewis donors.

It can be anticipated that the participation of a primary amide ligand will have a profound influence on the structure and reactivity of these compounds. The presence of hydrogen on the nitrogen atom is likely to diminish its efficiency as a metallating reagent, in comparison to the more basic, sterically demanding secondary amides such as DA and TMP. However, lithium primary amides are known to be versatile and valuable chemical intermediates, since they can behave as either amido (NHR^-) or imido (NR^{2-}) transfer agents.^[106] These new zincates could therefore be employed as precursors to prepare mixed-metal organoimido (NAr^{2-}) compounds by the removal of the remaining hydrogen on the nitrogen atom.^[107]

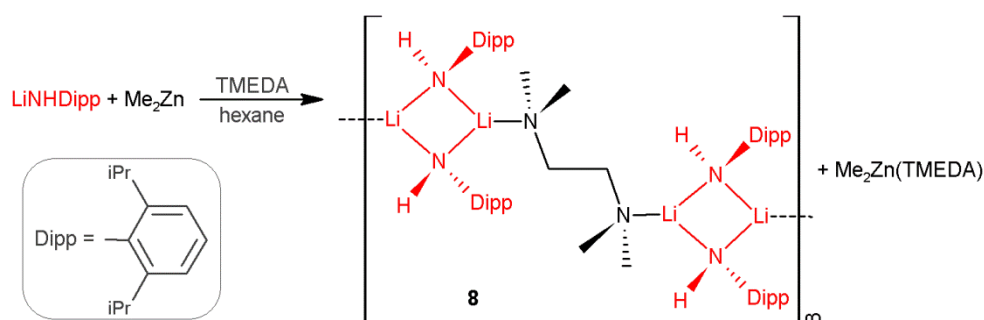
LiNHDipp was prepared by the deprotonation 2,6-diisopropylaniline with $^t\text{BuLi}$ in hexane; however, as previously noted for Zn^tBu_2 and LiTMP,^[29c, 75] no reaction between the primary lithium 2,6-diisopropylphenylamide and dimethylzinc was observed in the absence of a donor solvent.^[88] This is not unusual as alkali metal amides are known to exist as highly aggregated solution species^[108] which require a Lewis base to break them down into smaller, more reactive aggregates, thus favouring co-complexation with an organozinc reagent.^[95] The following novel heterobimetallic compounds were prepared using the aforementioned co-

complexation approach of combining the lithium anilide with dimethylzinc in the presence of Lewis bases of varying denticity.

3.1 The Effect of the Donor Solvent

3.1.1 TMEDA

The addition of one molar equivalent of the diamine TMEDA to an equimolar mixture of LiNHDipp and Me₂Zn resulted in dissolution of the lithium amide, affording a pale yellow solution, and seemingly indicating the formation of a mixed-metal complex (Scheme 3.1). A crop of colourless crystals were isolated from this solution and the ¹H, ¹³C and ⁷Li NMR data (in C₆D₆) obtained from them established the presence of lithium (as indicated by a resonance at 1.88 ppm in the ⁷Li NMR spectrum); however, the ¹H and ¹³C NMR spectra did not include any signal attributable to the methyl groups of ZnMe₂. Resonances corresponding to the amide ligand were observed; thus, in the ¹H NMR spectrum a doublet at 7.15 and a triplet at 6.71 ppm were present corresponding to the *meta* and *para* protons respectively, accompanied by a multiplet at 3.22 ppm indicating the CH of the isopropyl groups, a singlet at 2.84 ppm assigned to the remaining proton on nitrogen and another singlet denoting the methyl protons of the isopropyl groups at 1.36 ppm. Coordinated TMEDA was also detected, with singlets at 1.76 and 1.71 ppm for the methyl and methylene protons respectively.



Scheme 3.1 Reaction of LiNHDipp and Me₂Zn with TMEDA.

X-ray diffraction of the crystals confirmed the single-metal constitution of this compound $[\{\text{Li}_2(\text{NHDipp})_2\text{TMEDA}\}_\infty]$ **8** (Figure 3.1, Table 3.1), and ^1H NMR analysis of the filtrate revealed the formation of $\text{Me}_2\text{Zn}(\text{TMEDA})$, as evidenced by a singlet at -0.57 ppm in deuterated benzene.^[29c]

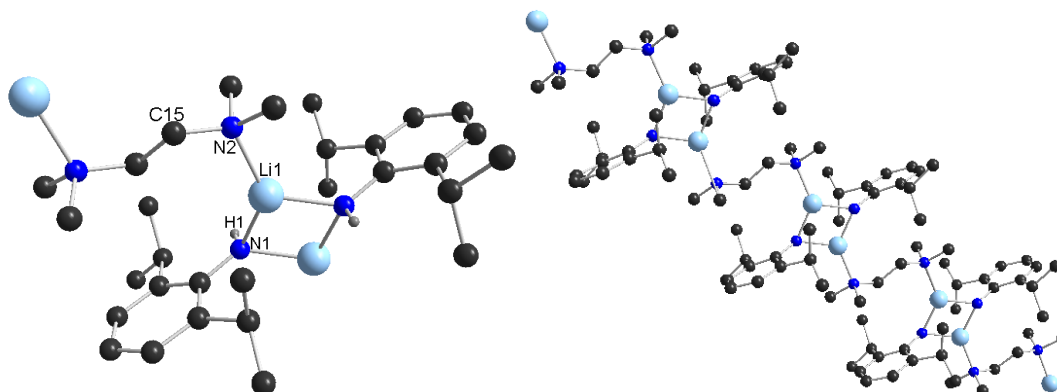


Figure 3.1 The repeating unit of $[\{\text{Li}_2(\text{NHDipp})_2\text{TMEDA}\}_\infty]$ **8** (left) and the extended polymeric chain (right) with H atoms (excluding NH) omitted for clarity.

Table 3.1 Selected bond lengths (Å) and angles (°) for **8**.

Li – N1	1.976(2)
	2.000(2)
Li – N2	2.080(2)
Li – N1 – Li	77.00(10)
N1 – Li – N1	103.00(10)

The structure of **8** consists of planar four-membered $(\text{LiN})_2$ rings (sum of the internal angles = 360°), linked via monodentate, bridging TMEDA molecules coordinated to two lithium atoms, affording a polymeric chain. The lithium atoms display a distorted trigonal planar geometry (sum of the bond angles about Li = 359.55°) bonding to three nitrogens – two from the anilido ligands (N1 in Figure 3.1) and one from the TMEDA (N2 in Figure 3.1). For each of the $(\text{LiN})_2$ dimers the hydrogen of the amido ligands (NH), and consequently the substituted aryl groups, lie transoid to

each other relative to the Li \cdots Li vector, in order to minimize steric repulsions within the small four-membered ring. The related TMEDA solvated lithium anilide [Li(NHAr)(TMEDA)] (Ar = 2,4,6-*t*Bu₃-C₆H₂) reported by Lappert,^[109] has a Li-N(H) distance of 1.895(8) Å, which is marginally shorter than the smallest corresponding contact in **8** (1.976(2) Å), although this is easily rationalised given the monomeric structure of this compound: such bonds are naturally elongated when the amido ligand adopts a bridging function. In contrast to the polymeric structure of **8**, however, this compound exhibits TMEDA chelation of the lithium rendering any further comparison futile.

The polymeric scaffold of **8** is analogous to the structure of the related lithium diisopropylamine TMEDA compound. The crystallisation of LDA from a hexane/TMEDA mixture results in a similar polymeric structure where cyclic dimers of (LDA)₂ are connected by a non-chelating TMEDA bridge.^[110] The bond distances in **8** are comparable to those of the LDA example; with lithium amide bonds of 2.071 Å *cf.* an average of 1.988 Å for **8**, and Li-N_{TMEDA} contacts of 2.163 Å, compared to 2.080(2) Å in **8**. The N1-Li-N1 angle however is marginally expanded (107.0 °) with respect to the 103.0 ° angle of **8**, presumably due to the greater bulk on the nitrogen in the case of the secondary (*versus* primary) amine.

Compound **8** can also be prepared via the reaction of lithium diisopropylaniline with TMEDA in the absence of dimethylzinc, and isolated in crystalline yields of up to 68 %. However, no mixed-metal compounds could be isolated from this system; although the addition of TMEDA to the unsolvated LiNHDipp collapses the polymeric structure (typical of lithium anilides),^[106, 111] forming the more soluble compound **8**, the degree of aggregation remains too high to favour the inclusion of zinc. Even when an excess of TMEDA is present no mixed-metal compounds were observed. Thus, it appears that the formation of the highly oligomerised lithium amide is more favoured than the co-complexation reaction with dimethylzinc, as this would involve the cleavage of the polymeric chain in order to generate a lithium zincate.

3.1.2 PMDETA

The tridentate ligand PMDETA was the next donor to be investigated. From the previous TMEDA example, it would appear that the degree of aggregation of the lithium amide after the addition of a donor solvent plays a pivotal role in determining whether a co-complexation reaction will occur.^[88] There is only one other reported lithium anilide structure containing PMDETA, that of $[(\text{PMDETA})_2\text{Li}_3(\text{NHPH})_3]$,^[112] which exhibits an unusual trinuclear structure displaying three-, four- and five-coordinated lithium centres (Figure 3.2), and since NH_2Dipp is significantly more sterically demanding than the unsubstituted aniline, it was anticipated that the relevant PMDETA solvated LiNHDipp would favour the formation of an even smaller oligomer. As such, when one molar equivalent of PMDETA was added to a suspension of LiNHDipp in hexane crystals of the solvated lithium anilide were isolated in a 79% yield (Scheme 3.2).

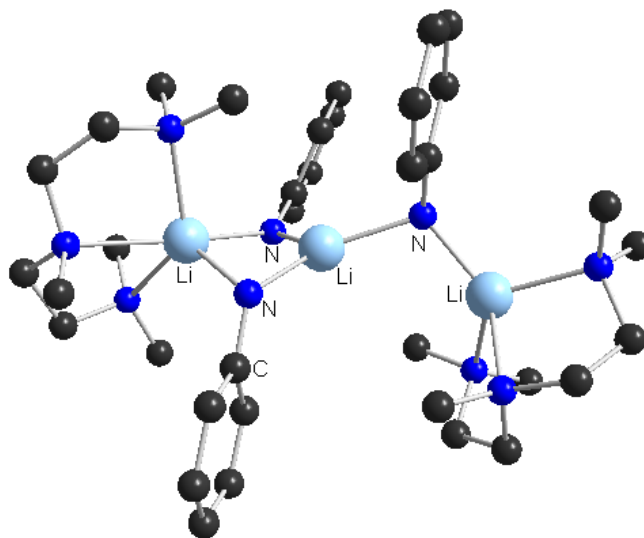
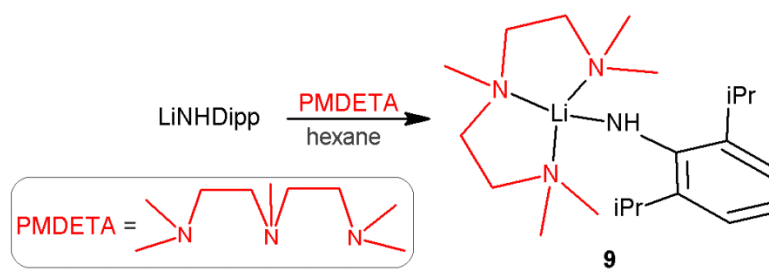


Figure 3.2 Molecular structure of $[(\text{PMDETA})_2\text{Li}_3(\text{NHPH})_3]$ with H atoms omitted for clarity.



Scheme 3.2 Complexation of LiNHDipp with PMDETA.

Multinuclear ^1H , ^{13}C and ^7Li NMR analysis identified these crystals as $[(\text{PMDETA})\text{Li}(\text{NHDipp})]$ **9**, with the ^1H NMR spectrum in C_6D_6 revealing a 1:1 ratio of PMDETA to $[\text{NHDipp}]^-$; thus two resonances were observed at 7.29 and 6.66 ppm corresponding to the aromatic *meta* and *para* protons of the amide ligand, along with a singlet at 3.09 ppm denoting the anilido proton, while a further multiplet at 3.34 ppm and doublet at 1.54 ppm indicate the CH and the CH_3 protons of the isopropyl groups respectively. PMDETA was also observed, with signals at 2.09 and 1.89 ppm corresponding to the two types of methyl proton and a broad singlet at 1.72 ppm indicating the methylene groups. The ^{13}C NMR spectrum showed ten resonances which range in chemical shift from 159.4 ppm for the *ipso* carbon of the anilide ring to 24.1 ppm for the methyl groups of the isopropyl groups, and a resonance at 1.47 ppm in the ^7Li NMR spectrum confirmed the presence of lithium (see 7.3 Synthesis of Numbered Compounds).

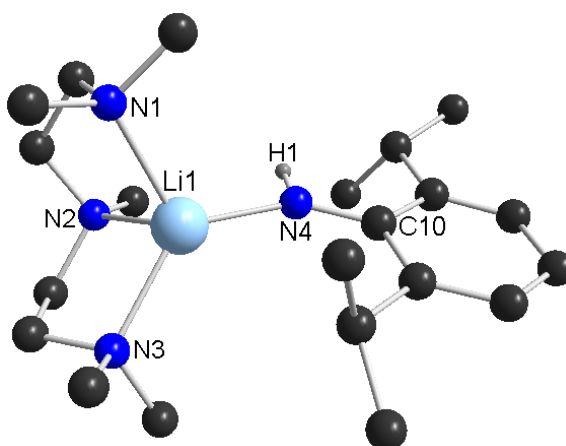


Figure 3.3 Molecular structure of $[(\text{PMDETA})\text{Li}(\text{NHDipp})]$ **9** with H atoms (excluding NH) omitted for clarity.

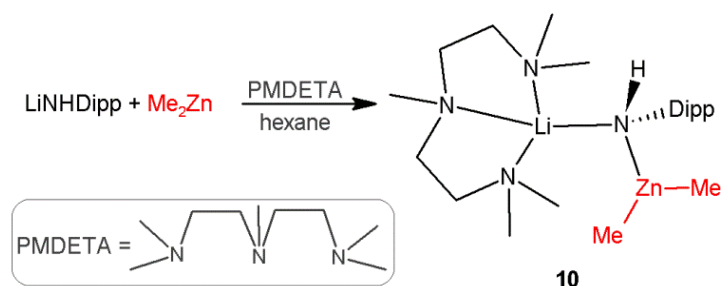
Table 3.2 Selected bond lengths (Å) and angles (°) for [(PMDETA)Li(NHDipp)] **9**.

Li-N1	2.230(5)	Li-N3	2.174(5)
Li-N2	2.170(5)	Li-N4	1.953(5)
N1-Li-N2	84.01(18)	N3-Li-N4	130.8(3)
N1-Li-N3	114.1(2)	N2-Li-N4	114.8(2)
N1-Li-N4	112.4(2)	Li-N4-C10	147.6(3)
N2-Li-N3	85.16(19)		

X-ray crystallography confirmed the monomeric structure of **9** (Figure 3.3, Table 3.2). In contrast to the polymeric structure of **8**, the monomeric arrangement of **9** consists of a distorted tetrahedral lithium centre (with N-Li-N angles ranging from 84.01(18)° to 130.8(3)°, and an average of 106.87°) bound to four nitrogen atoms – one amido nitrogen from NHDipp and three from the chelating PMDETA. The Li-N_{amide} bond length is significantly shorter than the dative Li-N_{PMDETA} bonds, at 1.953(5) Å, *versus* an average Li-N_{PMDETA} bond length of 2.191 Å. The Li-N_{amide} bond length is also slightly shorter than the corresponding bond length in the TMEDA polymer **8** (1.976(5) Å). As discussed above, the only precedent for a structurally defined monomeric lithium anilide is the TMEDA-solvate [Li(NHAr)(TMEDA)] (Ar = 2,4,6-*t*Bu₃-C₆H₂)^[109] where the lithium is tricoordinated in a distorted trigonal planar geometry, forming a shorter, and therefore stronger, bond to the nitrogen atom of the amide ligand (1.895(8) Å) as a consequence of its decreased coordination number with respect to that of **9**.

The reaction of **9** (prepared *in situ*) with a single equivalent of dimethylzinc afforded the heterobimetallic complex [(PMDETA)LiZn(NHDipp)Me₂] **10** as a crystalline solid in a yield of 65% (Scheme 3.3). Multinuclear ¹H, ¹³C and ⁷Li NMR analysis in C₆D₆ solution supported the mixed-metal constitution of **10**, with the ¹H NMR spectrum indicating the methyl groups at -0.32 ppm – a similar shift to that of free dimethylzinc in the same solvent (-0.52 ppm). A significant change in the chemical

shift of the signals corresponding to the NHDipp anion is also evident, in comparison to those of the homometallic PMDETA bound lithium amide **9** (Table 3.3). The ^{13}C NMR spectrum shows an upfield shift of the *ipso* carbon of the anilido ligand – from 159.4 ppm in **9** to 154.5 ppm in **10** – while the methyl carbons bound to zinc resonate at -8.1 ppm. Furthermore, the ^7Li NMR spectrum displays a singlet at 0.77 ppm, considerably different to that of the homometallic compound **9** (1.47 ppm).



Scheme 3.3 The co-complexation of LiNHDipp and Me_2Zn in the presence of PMDETA.

Table 3.3 Comparison of the ^1H NMR chemical shifts (ppm) of the anilido ligand of **9** and **10** in C_6D_6 .

	[(PMDETA)LiZn(NHDipp)Me ₂] 10	[(PMDETA)Li(NHDipp)] 9
H_{meta}	7.16	7.29
H_{para}	6.79	6.66
CHⁱPr	3.45	3.34
NH	2.84	3.09
CH₃ⁱPr	1.38	1.54

The molecular structure of **10** was established by X-ray crystallographic studies (Figure 3.4, Table 3.4) which disclosed an open contacted ion-pair motif where the two metals are bridged by the amide ligand (Li–N 2.055(3) Å, Zn–N 2.0869(13) Å, Figure 3.4) and the methyl groups both bond solely to the zinc (Zn–C2 1.999(2) Å, Zn–C1 1.984(2) Å). This is in contrast to the majority of previously structurally characterised dialkyl(amido)zincates, which involve a closed [LiN₂ZnC] ring.^[29c, 85] Therefore, the Zn–N1–Li angle of **10**, at 124.71(10) °, is substantially widened with

respect to the equivalent angle in TMP zincate **3** ($83.803(134)^\circ$) which exhibits a closed four-membered ring motif.

The lithium atom in **10** adopts a distorted tetrahedral geometry (angles subtended at Li range from $84.48(11)^\circ$ to $121.88(13)^\circ$, average 107.24°) by coordination to the tridentate PMDETA in an almost identical fashion to that seen in the homometallic complex **9**; however, the closest $\text{Li}\cdots\text{C}$ separation of $4.230(3) \text{ \AA}$ is too distant to suggest any significant interaction. Although the $\text{Li-N}_{\text{PMDETA}}$ interactions in **10**, at an average length of 2.173 \AA , are similar to those in **9**, the $\text{Li-N}_{\text{amide}}$ contact is remarkably longer ($\text{Li-N}_{\text{amide}} = 2.055(3) \text{ \AA}$ **10** versus $1.935(5) \text{ \AA}$ **9**). This can be rationalized by the increase in coordination number of the anilido nitrogen atom, which now acts as a bridge between both metals. Furthermore, this also affects the $\text{Li-N}_{\text{amide}}\text{-C}_{\text{ipso}}$ bond angle, which becomes substantially more acute on the inclusion of zinc: $147.6(3)^\circ$ for **9** versus $110.96(12)^\circ$ for **10**.

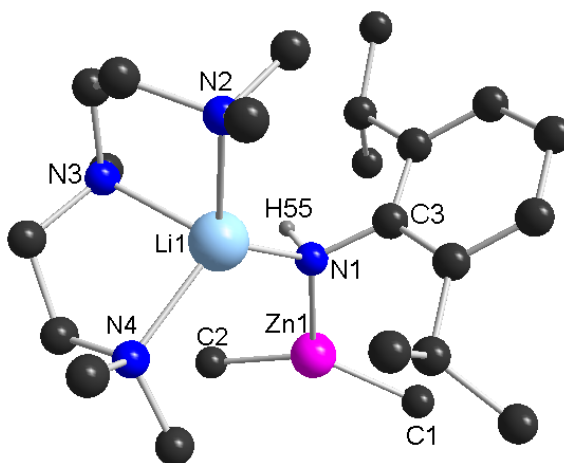


Figure 3.4 Molecular structure of $[(\text{PMDETA})\text{LiZn}(\text{NHDipp})\text{Me}_2]$ **10** with H atoms (excluding NH) omitted for clarity.

Table 3.4 Selected bond lengths (Å) and angles (°) for **10**.

Zn – C1	1.984(2)	Li – N2	2.220(3)
Zn – C2	1.999(2)	Li – N3	2.152(3)
Zn – N1	2.0869(13)	Li – N4	2.149(3)
Li – N1	2.055(3)	Li ⋯ C2	4.230(3)
C1 – Zn – C2	136.04(9)	N1 – Li – N4	118.23(13)
C1 – Zn – N1	114.55(7)	N2 – Li – N3	84.48(11)
C2 – Zn – N1	108.97(7)	N3 – Li – N4	87.72(11)
N1 – Li – N2	121.88(13)	N2 – Li – N4	116.94(12)
N1 – Li – N3	114.24(13)	Li – N1 – C3	110.96(12)

The unusual open structural motif displayed by **10** has already been discussed for the HMDS-lithium zincate [LiZn(HMDS)Me₂(PMDETA)] **5** (see Chapter 2.2.1 PMDETA)^[85] where a distance of 3.084(3) Å separates the lithium from the non-bridging methyl carbon (Figure 2.3). In this case the HMDS amido ligand adopts a terminal position in **5** as a consequence of the large steric bulk of the trimethylsilyl substituents, which overcomes the electronic preference for the amide to bridge the two metal centres. Contrastingly, in **10** the diisopropylanilide – being less sterically demanding than the HMDS – can adopt the preferred bridging function, although any long-range interaction between lithium and the alkyl ligands is still prevented (Li⋯C2 4.230(3) Å), presumably due to the tridentate coordination of PMDETA to Li, satisfying its coordination sphere. Due to the increased bulk of the anilide *cf.* the methyl bridging ligand, however, the structure of **10** is significantly more open than that of **5**, with Li⋯Zn separations of 3.6697(25) Å and 2.7895(22) Å, respectively.

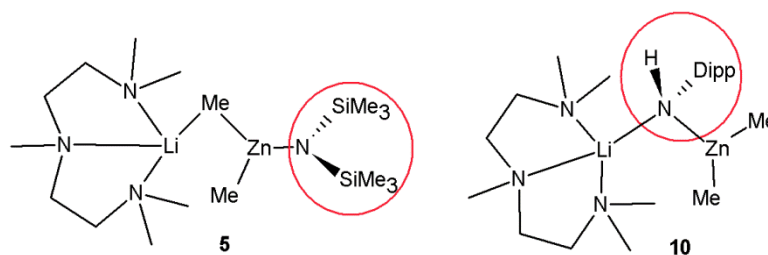
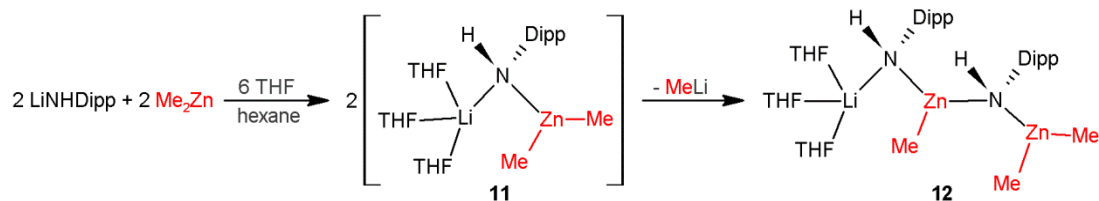


Figure 3.5 Comparison of the structures of $[\text{LiZn}(\text{HMDS})\text{Me}_2(\text{PMDETA})]$ **5** (terminal amide) and $[\text{LiZn}(\text{NHDipp})\text{Me}_2(\text{PMDETA})]$ **10** (bridging amide).

The terminal amide also results in a shorter Zn-N bond (1.9851(10) Å in **5**) in comparison to the contact with the bridging amido group of **10** at 2.0869(13) Å. This distance is more in keeping with the Zn-N bonds in the homometallic $[(\text{Me}_3\text{SiCH}_2)\text{Zn}(\text{NHDipp})]_2$ at an average of 2.044 Å, where the amido ligand acts as a bridge between two zinc atoms.^[113]

3.1.3 THF

We next investigated the co-complexation of ZnMe_2 and LiNHDipp in the presence of the monodentate donor THF (Scheme 3.4). The addition of four molar equivalents of THF to the $\text{LiNHDipp}/\text{ZnMe}_2$ mixture in hexane results in the formation of a solution which deposits crystals on cooling to -30°C . These crystals, which are extremely soluble at room temperature, were identified spectroscopically as $[(\text{THF})_3\text{LiZn}(\text{NHDipp})(\text{Me})_2]$ **11**. Thus a singlet was observed at -0.42 ppm in the ^1H NMR spectrum in C_6D_6 corresponding to the zinc bound methyl groups. The signals relating to the amido ligand were also present, with resonances at 7.14 and 6.75 ppm corresponding to the *meta* and *para* protons, a multiplet at 3.39 ppm for the CH and a singlet at 1.42 ppm for the CH_3 protons of the isopropyl groups, and a resonance for the NH at 2.86 ppm. Two multiplets at 3.28 and 1.30 ppm correspond to the THF donor, with the spectrum integrating to a ratio of three molecules of THF to two methyl groups and one amido ligand. A signal was also present in the ^7Li NMR spectrum at 1.01 ppm.



Scheme 3.4 Co-complexation of LiNHDipp and Me₂Zn in the presence of THF to form **11**, and its subsequent decomposition to **12**.

The monometallic [(THF)Li(NHDipp)] was prepared for comparison (Table 3.5) and ¹H NMR analysis in C₆D₆ shows that, although the two bimetallic compounds **10** and **11** display very similar chemical shifts for all of the amide protons, the monometallic system exhibits an upfield shift for most. Thus, the aromatic protons of **11**, at 7.14 and 6.75 ppm, are shifted to 6.17 and 6.61 ppm for the *meta* and *para* protons respectively, in the lithium-only system. The NH resonance is similarly shifted from 2.86 ppm in **11** to 2.79 ppm in the monometallic compound.

Table 3.5 Comparison of the ¹H NMR chemical shifts of the anilido ligand in **10** and **11** with the THF-solvated lithium anilide in C₆D₆.

	10	11	[(THF)Li(NHDipp)]
ArH _{<i>meta</i>}	7.16	7.14	6.17
ArH _{<i>para</i>}	6.79	6.75	6.61
CH ^{<i>i</i>} Pr	3.45	3.39	3.38
NH	2.84	2.86	2.79
CH ₃ ^{<i>i</i>} Pr	1.38	1.42	1.40

Multiple attempts at determining the solid state structure of **11** were unsuccessful, due to its high solubility in hexane. However, when a solution of **11** in hexane was left at room temperature for two weeks another crop of colourless crystals were deposited, with a much lower solubility than those formed in the freezer. These were identified crystallographically as the novel monolithium-dizinc trialkyl-

bis(amido)zincate $[(\text{THF})_3\text{LiZn}_2(\text{NHDipp})_2(\text{Me})_3]$ **12** (Figure 3.6, Table 3.6). The contacted ion-pair structure displays a trinuclear $\text{Li}\cdots\text{Zn}\cdots\text{Zn}$ arrangement where the metals are each linked via an amido bridge and the methyl groups bond terminally to the zinc centres, while three molecules of THF satisfy the coordination sphere of the lithium.

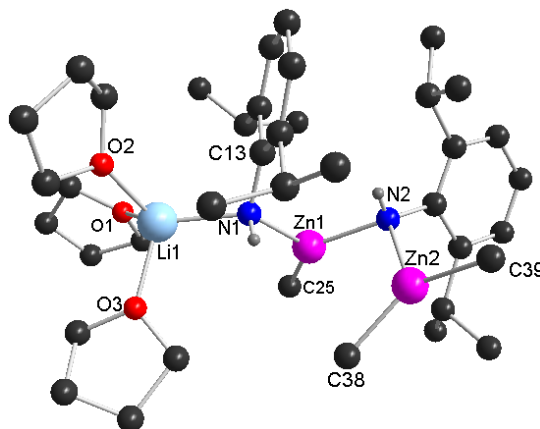


Figure 3.6 Molecular structure of $[(\text{THF})_3\text{LiZn}_2(\text{NHDipp})_2(\text{Me})_3]$ **12** with H atoms (excluding NH) omitted for clarity.

This structure is closely related to that of lithium-rich tetraorganozincates $[\text{Li}_2\text{ZnR}_4]$, which also display a similar trinuclear arrangement,^[29d] but the stoichiometry of this zinc-rich compound (1Li:2Zn:5R, R = monoanionic ligand) contrasts markedly with those found in previously reported synthetically useful tetraorganozincates^[23d] (2Li:1Zn:4R) and triorganozincates (1Li:1Zn:3R). Whereas tetraorganozincates, in general, exhibit a near linear $\text{Li}\cdots\text{Zn}\cdots\text{Li}$ arrangement – as with $[\text{Li}_2\text{ZnMe}_4]$ ($\text{Li}\cdots\text{Zn}\cdots\text{Li} = 162.48(17)^\circ$)^[29d] and $[(\text{TMEDA})_2\text{Li}_2\text{Zn}(\text{C}\equiv\text{CPh})_4]$ ($\text{Li}\cdots\text{Zn}\cdots\text{Li} = 146.70^\circ$)^[114] – with each anionic ligand acting as a bridge between two metal centres, the $\text{Li}\cdots\text{Zn}\cdots\text{Zn}$ angle ($115.7(2)^\circ$) displayed by **12** is significantly distorted from linearity. Each zinc centre in **12** presents a trigonal planar geometry (sum of the angles about Zn1 and Zn2 are 359.9 and 360.0° , respectively), while the distorted tetrahedral lithium lies almost coplanar with the N1-Zn1-N2 plane ($\text{Li1-N1-Zn1-N2} = 175.4(2)^\circ$) bound to the three THF molecules and the amide bridging to Zn1. There appears to be no interaction between lithium and Zn2. The Zn1-N bond lengths (Zn1-N1 $2.021(2)$ Å and Zn1-N2 $2.008(3)$ Å) are similar to those of the related

dimethyl(amido)zincate [(PMDETA)LiZn(NHDipp)(Me)₂] **10** (Zn-N 2.0869(13) Å) and the zinc alkyl amido compound [{(Me₃SiCH₂)Zn(NHDipp)}₂]^[113] (average Zn-N bond length 2.035 Å). However, the terminal zinc (Zn2), which lies almost perpendicular to the N1-Zn-N2 plane (N1-Zn1-N2-Zn2 78.72(12) °), shows an appreciably weaker interaction with the bridging amide, as shown by the elongation of the Zn2-N2 bond (2.139(3) Å).

Table 3.6 Selected bond lengths (Å) and angles (°) for [(THF)₃LiZn₂(NHDipp)₂(Me)₃] **12**.

Li-N1	2.074(6)	Zn2-C39	1.983(3)
Zn1-N1	2.021(2)	Li-O1	1.961(6)
Zn1-C25	1.969(3)	Li-O2	2.007(6)
Zn1-N2	2.008(3)	Li-O3	1.967(6)
Zn2-N2	2.139(3)	Li...C25	4.275(12)
Zn2-C38	1.989(3)		
Li-N1-Zn1	122.0(2)	Zn1-N2-Zn2	101.31(11)
N1-Zn1-C25	125.79(13)	C39-Zn2-C38	140.31(14)
C25-Zn1-N2	131.66(13)	C38-Zn2-N2	109.11(12)
N2-Zn1-N1	102.45(10)	C39-Zn2-N2	110.58(12)

In terms of stoichiometry, closer analogues from the literature are the cyclopentadienyl sodium zincate [{Na(THF)₆}⁺{Zn₂Cp₅}⁻]^[87] and the dipyritylamine (dpa) compounds [{M(THF)₆}⁺{Zn^tBu₂(dpa)Zn^tBu₂}⁻] (M = Na, K)^[89] which all exhibit solvent separated ion-pair structures (Figure 3.7, see 1.6 Structural Diversity in Organozincate Chemistry). The dimensions of the dpa structures are uncertain due to disorder in the crystallographic data; however, the zinc-carbon bonds of the cyclopentadienyl compound (ranging from 2.08 to 2.17 Å) are marginally longer than in **12** (1.969(3) to 1.989(3) Å). This is easily explained, however, by the fact that the cyclopentadienyl ligands are much bulkier than the methyl groups of **12**.

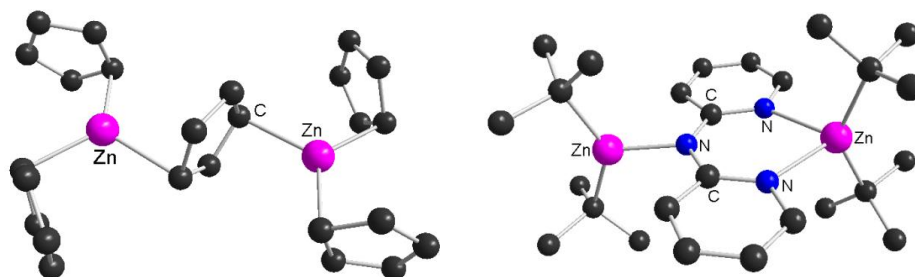


Figure 3.7 Molecular structures of the $\{Zn_2Cp_5\}^-$ anion^[87] (left) and the $\{Zn^tBu_2(dpa)Zn^tBu_2\}^-$ anion^[89] (right). H atoms have been omitted for clarity.

Another example is the bimetallic lithium bis(zinc) diamide $[(Et_2O)Li(\mu-L)Zn(\mu-L)Zn(LH)]$, where L is the bidentate 1,2-benzenebis(neopentylamido) ligand^[115] and each metal displays a distorted tetrahedral geometry (Figure 3.8). The CIP structure of this compound is more akin to that of **12**, and the Li-N contacts, at an average of 2.11 Å, are comparable to the analogous Li-N bond length in **12** (2.074(6) Å). The Zn1-N bond lengths, at an average of 2.056 Å, are again similar with respect to the Zn1-N bond lengths of **12** (average 2.015 Å), although the Zn2-N contacts (average 2.057 Å) are much shorter than the corresponding bond in **12** (2.139(3) Å). This is probably due to the terminal zinc of **12** being bonded to a single bridging amide, whereas both of the zinc atoms in $[(Et_2O)Li(\mu-L)Zn(\mu-L)Zn(LH)]$ are each bound to four nitrogen atoms.

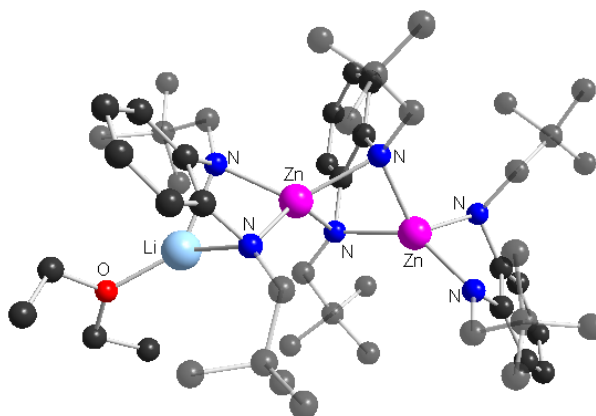
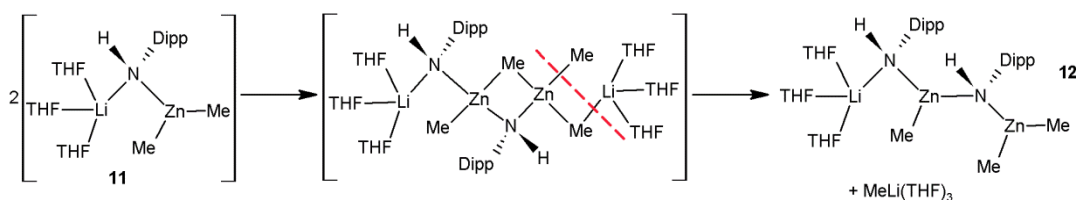


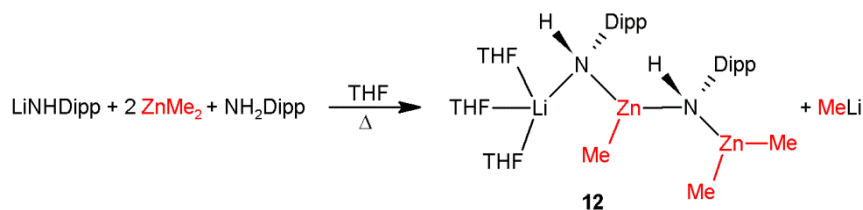
Figure 3.8 Molecular structure of $[(Et_2O)Li(\mu-L)Zn(\mu-L)Zn(LH)]$ ^[115] with H atoms excluded for clarity.

Considering the unexpected formation of **12**, it is reasonable to assume that the process involves partial redistribution of **11** in hexane solution, when stored at room temperature for extended periods of time. A plausible reaction pathway entails the formation of the thermodynamically more stable **12**, via the loss of methyl lithium from a dimer of the kinetic product **11** (Scheme 3.5). It has been previously shown that reducing the steric bulk of amido ligands can result in alkyl(amido)zincates with structures involving tetracoordinated zinc centres,^[29d] thus the putative intermediate shown below is plausible, given that NHDipp, being a primary amide, is far less sterically demanding than TMP or DA, for example.



Scheme 3.5 The proposed redistribution of zincate **11** in solution forming **12**.

¹H NMR analysis of the filtrate from which **12** was isolated showed that **11** remained the major species in solution, implying that the above disproportionation is only a minor process. It is however possible to synthesise **12** rationally, in good yield (58-64 %), by the reflux of LiNHDipp with two molar equivalents of ZnMe₂, one equivalent of the primary amine itself and three equivalents of THF in hexane solution (Scheme 3.6).

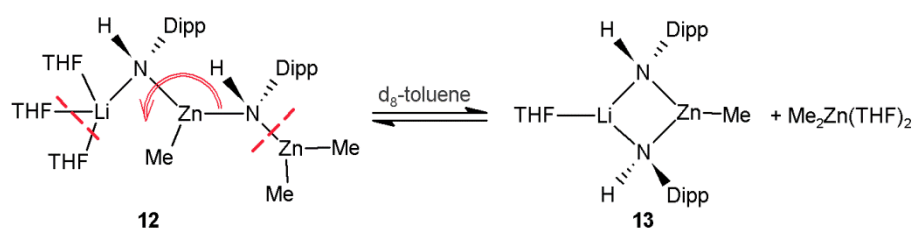


Scheme 3.6 Rational synthesis of [(THF)₃LiZn₂(NHDipp)₂(Me)₃] **12**.

¹H NMR analysis of **12** in C₆D₆ solution shows only a single resonance for the methyl groups (-0.43 ppm) and only one set of signals for the amido groups (7.12

ppm H_{meta}, 6.83 ppm H_{para}, 3.31 ppm CHⁱPr, 3.08 ppm NH and 1.35 ppm CH₃ⁱPr) the integration of which suggests a 3:2 methyl to NHDipp ratio. These signals are notably broader than in the spectra of related compounds, including those of **5** and **11**, which contain the same alkyl and amido ligands. Furthermore, broad signals in the ¹³C{¹H} NMR spectrum corresponding to the methyl groups (-9.09 ppm) and amido group carbons suggest that, unlike the solid state structure – which exhibits two distinct types of alkyl and amido group – the ligands undergo a dynamic exchange process in solution resulting in a single set of resonances for each.

The broad signals observed can be explained by an exchange process, where the weak (elongated) zinc-nitrogen bond continually breaks and reforms (Scheme 3.7). If this process is fast it would lead to a dynamic equilibrium between **12** and ZnMe₂ in solution, giving rise to a new species **13**.



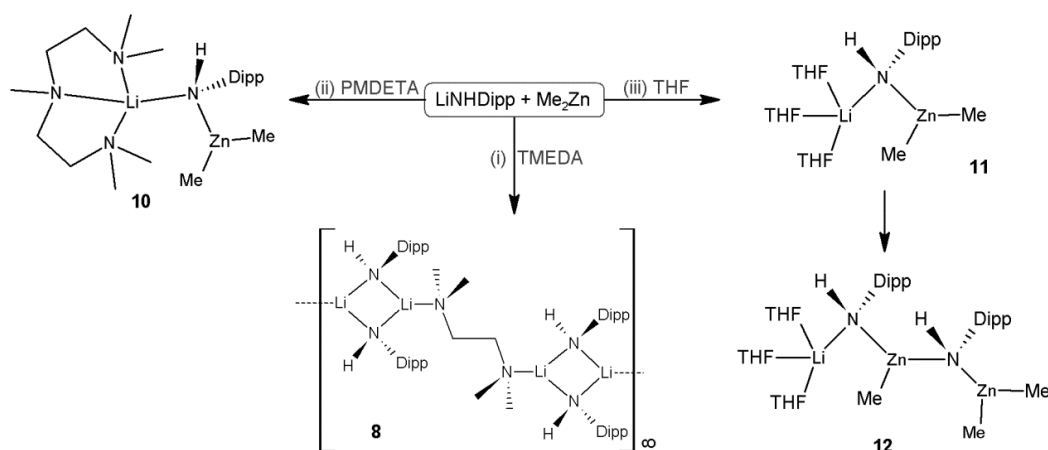
Scheme 3.7 Proposed dynamic equilibrium of **12** in solution with **13**.

Supporting this hypothesis, variable temperature ¹H NMR studies revealed that the relevant resonance for the methyl groups (-0.33 ppm at 300 K in deuterated toluene) splits into two singlets (0.15 and 0.05 ppm in a ratio of 2:1) when the temperature is decreased to 208 K. The hypothesis is further supported by the fact that ¹H NMR analysis of the solid residue obtained on dissolving crystals of **12** in toluene and removing the solvent under vacuum proved to be the monolithium-monozinc zincate [(THF)LiZn(NHDipp)₂Me] **13**. The ¹H NMR spectrum (in C₆D₆) shows a singlet at -0.38 ppm corresponding to the zinc-methyl group, which now integrates in a 1:2 ratio with respect to the anilido ligand, with a single molecule of THF present. A singlet appears in the ⁷Li NMR spectrum at 1.40 ppm. The formation of **13** can be explained by the high volatility of dimethylzinc, which results in it being lost under

vacuum at the same time as the solvent, consequently pushing the equilibrium to the right and favouring the formation of **13** (Scheme 3.7). Similar behaviour has also been observed in magnesium zincate chemistry, where $[(\text{THF})_6\text{Mg}_2\text{Cl}_3][\text{Zn}_2\text{Et}_5]$ exists in equilibrium with $[(\text{THF})_6\text{Mg}_2\text{Cl}_3][\text{ZnEt}_3]$ and free ZnEt_2 in THF solution.^[116] As with this system, removal of the volatile dialkylzinc under vacuum alters the position of the equilibrium.

3.2 Conclusions

From these results it can be inferred that the final outcome of the interlocking co-complexation reaction of dimethylzinc and the primary lithium anilide LiNHDipp is dictated by the donor ligand employed and the type of structure it forms on coordination of the lithium amide. With TMEDA the resulting structure is that of a polymer of such stable form it cannot react with dimethylzinc, precluding the formation of a mixed-metal complex (Scheme 3.8). In contrast, the tridentate ligand PMDETA results in the monomeric complex **9** when coordinated to LiNHDipp, which is now much more reactive towards ZnMe_2 and can successfully form zincate **10**, which displays an unusual open structure where both metals are connected by a single bridging amide ligand. This can be attributed to the coordinative saturation of lithium, on being solvated by the tridentate donor PMDETA.



Scheme 3.8 Co-complexation of LiNHDipp and Me₂Zn in the presence of (i) TMEDA, (ii) PMDETA and (iii) THF.

When a monodentate donor such as THF is employed the formation of an amido zincate **11** is again observed, with ^1H NMR information suggesting the solvation of lithium by three molecules of THF. The breakdown of zincate **11** to form the hitherto unprecedented zinc-rich zincate **12** (via the loss of methyllithium) has been shown to occur in hexane solution, although the rational synthesis of **12** has also been demonstrated in good yield. NMR studies in C_6D_6 solution reveal that **12** exists in equilibrium with dimethylzinc and a further zincate **13**, due to the dissociation of the more labile Zn-N bond. These equilibria illustrate the complex behaviour of such species in solution, and demonstrate the great influence which the donor solvent has on the probability of co-complexation. Thus, these results reflect the complicated nature of co-complexation reactions, and indicate that the switching of Lewis basic solvents can have a dramatic effect on the formation, and ultimately the constitution, of any bimetallic species formed.

Chapter 4 Arylation Studies of Electron-deficient *N*-Heterocycles

4.1 The Use and Reactivity of *N*-Heterocyclic Compounds

N-heterocyclic scaffolds are widely found in natural products and biologically active molecules and are therefore heavily utilised in pharmaceuticals.^[117] For example, the sodium-channel inhibitor (i)^[117b] and the NK₃ receptor antagonist (ii)^[117e] depicted in Figure 4.1, which both contain *N*-heterocyclic cores, are implicated in the treatment of neuropathic pain and psychiatric disorders (such as schizophrenia) respectively. In a recent survey of the synthesis of 128 drug candidate molecules from three pharma companies it was observed that more than 90 % of target molecules contained an aromatic ring, and a similar percentage contained at least one nitrogen atom, with “a strong preponderance of *N*-containing heterocycles” observed.^[118] Due to the significance of such compounds, selective, efficient methods of functionalising these molecules are highly sought after.

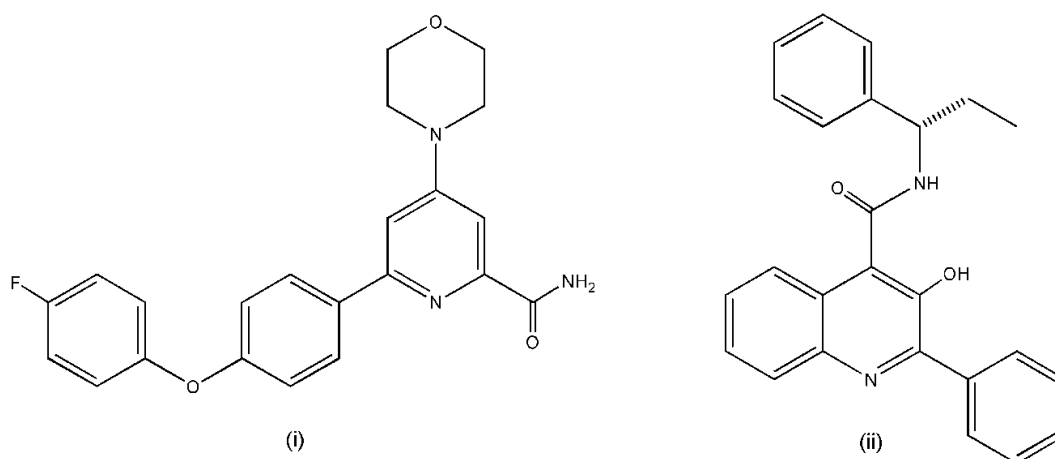
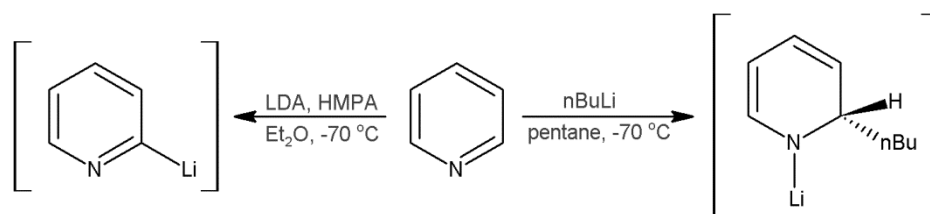


Figure 4.1 Examples of biologically active molecules containing *N*-heterocycles.

Arguably, deprotonative metallation,^[119] along with electrophilic substitution,^[120] constitute the most important synthetic methodologies for the regioselective

functionalisation of aromatic *N*-heterocyclic molecules. However, as the nitrogen content of a heterocycle increases, the aromatic stability decreases, and the molecule becomes increasingly electrophilic,^[121] making electron-deficient *N*-heterocycles notoriously difficult to elaborate via these methods.

The presence of nitrogen in an aromatic ring leads to a less highly conjugated *p*-orbital system, with respect to benzene.^[122] These nitrogen atoms are readily attacked by electrophiles and their presence in the ring reduces the reactivity of the carbon atoms towards electrophilic substitution.^[123] The result of this reduced aromaticity, coupled with the electron withdrawing effect of nitrogen – which decreases the energy of the LUMO further on inclusion of each successive heteroatom^[122] – is that these heterocycles are prone to nucleophilic attack. All of these factors mean that standard deprotonation reagents, such as butyllithium, are liable to react with such molecules via nucleophilic addition (Scheme 4.1, right).^[121] Indeed, this competing addition process is known to complicate deprotonation reactions, and although lithium amides can metallate these heterocycles in moderate yield, alkyllithium reagents react as alkylating reagents, preferentially undergoing nucleophilic addition.^[2d]



Scheme 4.1 Deprotonation with LDA^[124] (left) and nucleophilic addition of *n*BuLi^[125] (right) to pyridine.

Although only the strongest nucleophiles react with pyridine, increasing the nitrogen content of a ring makes the addition process easier, such that tri- and tetrazines are attacked even by weak nucleophiles.^[121] Similarly, the addition of a fused benzene ring decreases the loss of aromaticity inherent in the addition process, such that quinoline and acridine react more readily with nucleophiles than pyridine.^[121]

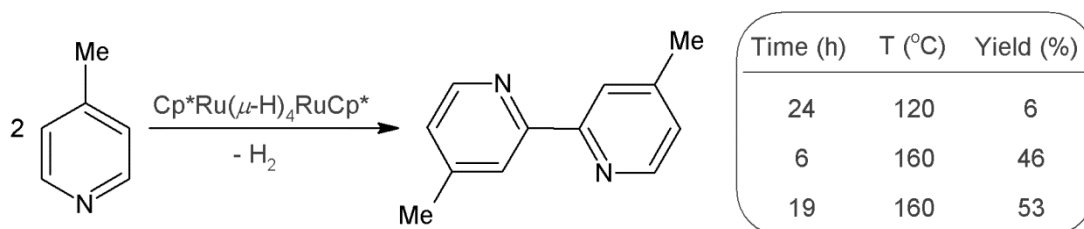
The α -protons of six-membered azines have been shown to be the least acidic ($pK_a \sim 35\text{--}40$)^[122] and, when metallated, the resulting carbanion tends to be very unstable due to the repulsion between the lone pair on nitrogen and the negative charge. This means the α -protons are more difficult to remove, and although the regiospecific deprotonation of these heterocycles can be achieved, the process is often problematic, frequently requiring the use of subambient temperatures and a large excess of the organometallic reagent.^[123] Indeed, Schlosser describes the metallation of pyridines as a tightrope walk, further commenting that “it requires skill and cleverly selected working conditions to manoeuvre successfully between the desired and undesired reaction modes.”^[119] Even when deprotonation can be favoured over nucleophilic addition – by using lithium TMP for example – the addition of the resulting lithiated species to any unreacted substrate may still cause problems^[2d] and, since such reactions proceed via equilibrium, an excess of base is often required to achieve reasonable yields.^[123] In some cases up to 12 equivalents of lithium amide can be required,^[123, 126] which is highly uneconomical, seriously limits any potential to scale up and complicates electrophilic quenching.

4.2 Direct C-H Arylation vs. Addition/Rearomatisation

Direct arylation of pyridine and other heteroaromatic compounds via C-H activation can be achieved through the use of transition metal catalysis.^[127] The coupling of heterocycles and arylhalides can be promoted by a variety of transition metals, although long reaction times and high temperatures are a standard requisite for this process, as the use of milder reaction conditions results in lower yields.^[128] There are a handful of examples of such direct C-H transformation of heterocycles known in the literature,^[129] although each reported method appears to be strongly substrate dependant, which significantly restricts the scope of these approaches.

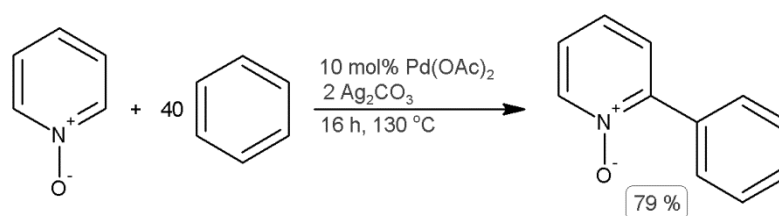
In some cases heterocycle activation is required,^[121] which is generally accomplished by its conversion to the relevant *N*-oxide^[130] or *N*-iminopyridinium ylide.^[128] However, even if this additional activation step can be avoided, several problems

remain. A variety of transition metal catalysts have been utilised for direct C-H arylation; from palladium^[128, 130b] and nickel^[131] to rhodium,^[132] ruthenium^[129a, 133] and rhenium.^[130c] All of these require high temperatures (ranging from a modest 80 °C^[131] to 190 °C)^[132a] and the rate of reaction is dependent on the specific methodology applied. For instance, the reaction time of the diruthenium promoted homocoupling of 4-substituted pyridines ranges from 6 to 24 hours depending on the substitution pattern of the pyridine and the specific catalyst employed (Scheme 4.2).^[133a] Similarly Ellman and Bergman described the rhodium catalysed arylation of pyridines and quinolines, reporting that the reaction time could be *reduced* to 24 hours on increasing the temperature to 190 °C.^[132a]



Scheme 4.2 Ruthenium catalysed homocoupling of 4-substituted pyridines.

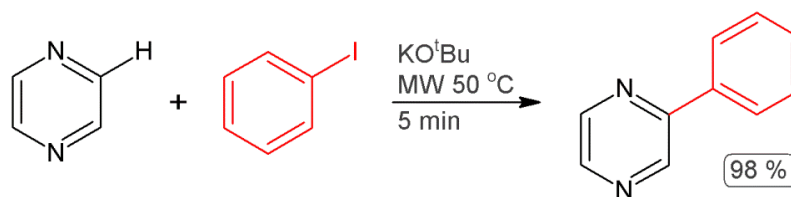
A frequent requirement amongst C-H activation methodologies is the need for an excess of one reactant. Indeed, the rhodium catalysed arylation method described above requires six molar equivalents of heterocycle to a single equivalent of arylhalide coupling partner.^[132a] Additionally, in the nickel catalysed arylation of pyridine the substrate is employed in vast excess as a solvent,^[131a] and the palladium catalysed arylation of pyridine *N*-oxides reported by Chang was a fortuitous side reaction in which the *N*-oxide was found to react with the benzene solvent (Scheme 4.3).^[130b]



Scheme 4.3 Pd-catalysed coupling of pyridine *N*-oxide and benzene.^[130b]

It has been noted that steric interference can complicate these coupling reactions; under certain circumstances the lack of a C2 substituent can prevent arylation,^[132a] and increasing substitution requires an excess of arylhalide coupling partner, whilst also lowering yields.^[128] Furthermore, it has been noted that these reactions are not always regioselective, with isomer mixtures resulting in several cases.^[130b, 131a] Consequently, all of these factors combined lead to moderate yields^[58] – usually ranging from 40 to 50 %.^[128-129, 130b, 130c, 131a, 132a, 133a]

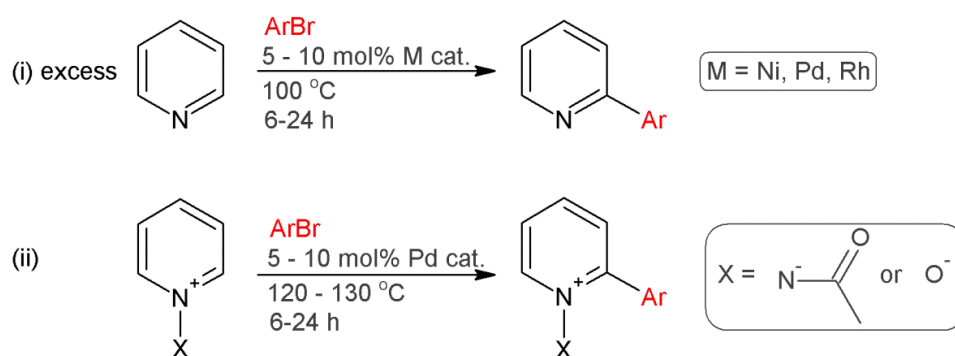
Related to these studies, Itami has recently reported a transition metal-free methodology, giving access to arylated *N*-heterocyclic molecules by employing an excess of the group 1 base potassium *t*-butoxide (Scheme 4.4).^[134] This discovery was made when a control reaction containing no iridium catalyst performed just as well as those with. As such it has been shown that the arylation of pyrazine may be carried out in 98 % yield in only 5 minutes under microwave irradiation. However, the reaction appears to be dependent on several factors, such as solvent and the nature of the arylhalide coupling partner, as the yields with other substrates were moderate at best.



Scheme 4.4 Microwave promoted KO^tBu catalysed biaryl coupling.

As discussed above, the reaction conditions for direct C-H arylation vary widely and mostly involve rigorous, prolonged heating.^[129b] The general points have been summarised in Scheme 4.5; however, it should be noted that these methods are far

from the norm in synthesis, and the most common methods for the arylation of heterocycles remain the Suzuki,^[135] Negishi^[8b] and Stille^[136] reactions.^[117f]



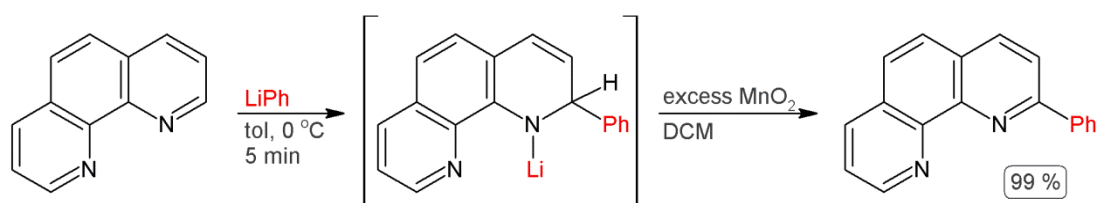
Scheme 4.5 General methodology for the direct C-H arylation of pyridine.

As an alternative approach, the regioselective functionalisation of pyridine and other related *N*-heterocycles can easily be achieved by the nucleophilic addition of organolithium or -magnesium reagents,^[2d, 121] the advantage of this method being selective 2- or 4-substitution^[137] and, in general, yields are better than those associated with the C-H arylation methods discussed above. Reaction times are also more convenient, taking minutes rather than hours.^[138] Another significant advantage of this procedure is that no catalysts or extra activation steps are required – indeed, the addition process cannot be avoided with certain reagents (Scheme 4.1, *vide supra*).^[2d]

However, as with many reactions involving these highly polar organometallic reagents, additions must be performed at low temperature as higher temperatures lead to side reactions and complex reaction mixtures.^[139] Steric interference may require temperatures be raised (albeit not above $-40\text{ }^\circ\text{C}$)^[140] but even so, such reactions are not always complete: a secondary rearomatisation step involving the use of an external oxidant (such as KMnO_4) may subsequently be required in order to furnish the desired product.^[137]

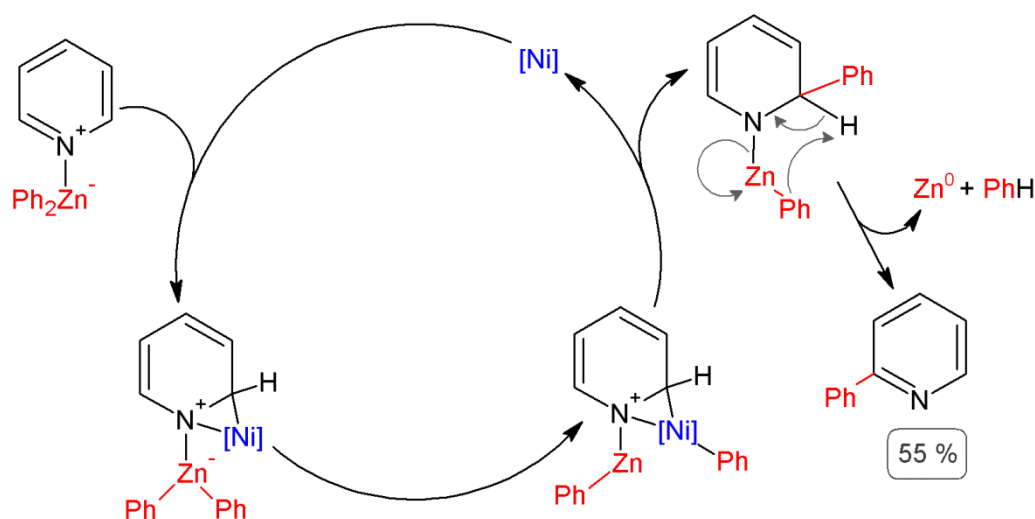
Traditional knowledge states that organolithium and -magnesium reagents react with pyridine (and its derivatives) via 1,2-addition, forming dihydro species (following

hydrolysis) which may then be oxidised to furnish 2- or 4-substituted heterocycles in moderate yields (see example with 1,10-phenanthroline, Scheme 4.6).^[141] Indeed, the *N*-lithio-2-*n*-butyl-1,2-dihydropyridine obtained on reaction of pyridine with butyllithium has been used to form a variety of 2,5-disubstituted pyridine derivatives.^[142]



Scheme 4.6 Alkylation of 1,10-phenanthroline via the 1,2-dihydropyridine intermediate.^[141c]

This overall process of addition and rearomatisation has been termed the oxidative nucleophilic substitution of hydrogen,^[143] and it has been proven that this mechanism can be applied to milder reagents such as arylzinc compounds.^[117a, 144] Although low polarity zinc reagents on their own cannot promote nucleophilic addition reactions, by employing nickel catalysis a variety of electron-deficient *N*-heterocycles have been successfully functionalised using this approach. Here the organozinc reagent plays an important role, coordinating to the substrate and activating it towards the arylation process.^[117a] This eliminates the need for prior activation steps such as *N*-oxide formation. A mechanism was proposed in which the nickel catalyst inserts into the π -system of the heterocycle, before abstracting a phenyl group from zinc. The reductive elimination of nickel then regenerates the catalyst and positions the phenyl group on the heterocycle, which can then rearomatise via elimination of benzene and the generation zinc metal (Scheme 4.7).



Scheme 4.7 Proposed catalytic cycle for the dearomatising arylation of pyridine.

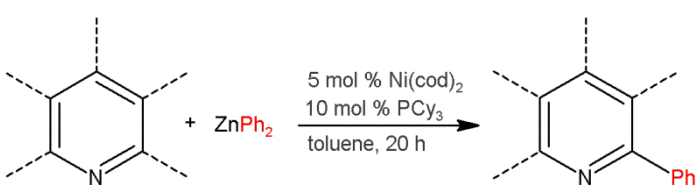
It was noted, however, that this reaction was sensitive to metal salt contamination of the organozinc reagent.^[144] Organozinc compounds are known to undergo homocoupling in the presence of certain metal salts, and this dimerisation process can be carried out catalytically in the presence of an oxidant such as *N*-chlorosuccinimide (NCS) or oxygen.^[145] This can complicate reactions in which zinc species are able to equilibrate and offers an explanation as to why the presence of halides from metal salts adversely affects yields in this case. However, this problem can be avoided if the arylzinc reagents are prepared by reaction of an appropriate arylboronic acid with diethylzinc.^[117a, 144] This allows a variety of functionalised aryl groups to be introduced to the 2-position of quinoline (Table 4.1).^[144]

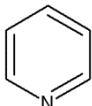
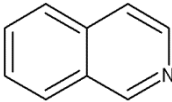
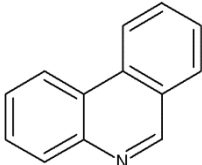
Table 4.1 Ni-catalysed arylation of quinoline with various arylzinc reagents.^[144]

Ar	Yield (%)
4-(MeO)C ₆ H ₄	97
4-(Me ₂ N)C ₆ H ₄	93
3-Cl-5-(MeO)C ₆ H ₃	51

Overall, this method displays good functional group tolerance and has been shown to be applicable to a range of substrates,^[117a, 144, 146] although the conditions required vary significantly depending on the specific heterocycle involved (20 hours at temperatures from 60 to 130 °C), and the corresponding yields are not always optimal. For instance, although phenanthridine can be converted to 6-phenylphenanthridine in greater than 99 % yield at 60 °C, the reaction with pyridine must be performed at 130 °C and yet only produces yields of 55 % (Table 4.2).^[144]

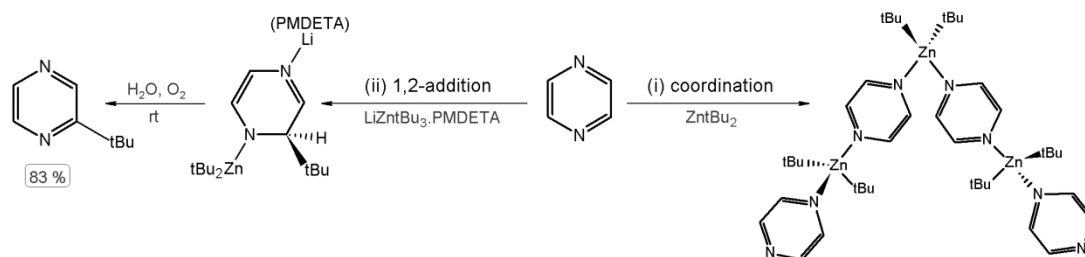
Table 4.2 Ni-catalysed arylation of various *N*-heterocycles.^[144]



Substrate	T (°C)	Yield (%)
	130	55
	100	90
	60	>99

By exploiting a related nucleophilic addition mechanism, which avoids the need for a transition metal catalyst, our group has recently shown that alkyllithium zincates can promote the regioselective alkylation of pyrazine under very mild conditions.^[147] Thus, when pyrazine is treated with the triorganozincate [(PMDTA)LiZn^tBu₃] **14** the chemoselective C-H alkylation of pyrazine can be accomplished efficiently at ambient temperature, affording 2-*tert*-butyl pyrazine in almost quantitative yield.

Trapping of the organometallic intermediate has established that it is the softer zinc centre which performs the nucleophilic addition; however, the presence of lithium and the zincate formation $[\text{Zn}^t\text{Bu}_3]^-$ are required in order to facilitate this process, as monometallic Zn^tBu_2 merely coordinates to the substrate forming the adduct $[(\text{C}_4\text{H}_4\text{N}_2)_6\text{Zn}_3^t\text{Bu}_6]$ (Scheme 4.8).



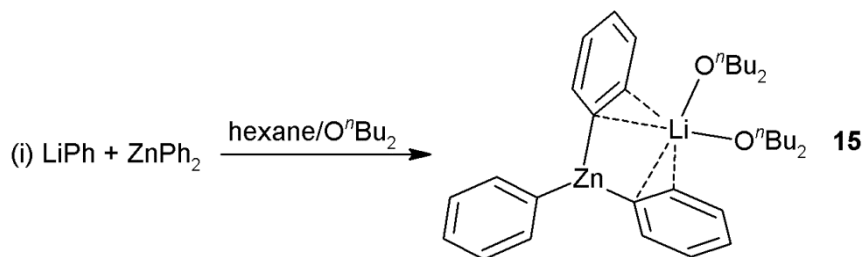
Scheme 4.8 Alkylation of pyrazine by zincate **14**.^[147]

Encouraged by these initial findings, we next endeavoured to apply this zincate mediated approach to the arylation of *N*-heterocyclic molecules. Thus, this chapter will focus on the design of a reagent capable of promoting the direct arylation of electron-deficient *N*-heterocycles without the need for a transition metal catalyst, and the development of a suitable methodology by which to do so.

4.3 Synthesis and Characterisation of Tri- and Tetraphenyl Lithium Zincates **15** and **16**

Building on our previous studies, we first investigated the synthesis of homoleptic zincate compounds based on aryl substituents. Thus, we explored the co-complexation reactions of varying amounts of phenyllithium and diphenylzinc, which led to the preparation of the tri- and tetraphenylzincates, $[\text{LiZnPh}_3]$ **15** and $[\text{Li}_2\text{ZnPh}_4]$ **16**. The one to one co-complexation of commercially available LiPh and ZnPh_2 (prepared according to literature methods^[148] and purified by sublimation) in hexane furnished the lithium zincate $[(\text{OBu}_2)_2\text{LiZnPh}_3]$ **15·OBu₂**, which incorporated

di-*n*-butylether (the commercial solvent for phenyllithium) in a 57 % crystalline yield (Scheme 4.9).



Scheme 4.9 Formation of zincate **15** in non-polar solvent.

This compound was fully characterised by multinuclear ^1H , ^{13}C and ^7Li NMR spectroscopy (Table 4.4, *vide infra*), and its molecular structure was determined by X-ray crystallography. These studies revealed that **15** displays a monomeric structural motif, solvated by two molecules of di-*n*-butylether (Figure 4.2, Table 4.3).

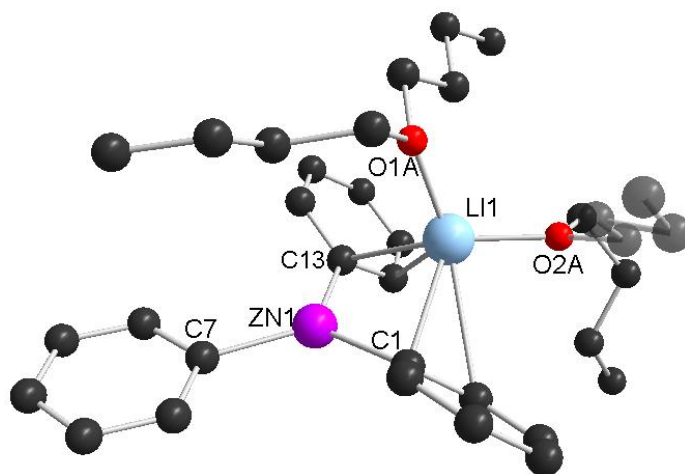


Figure 4.2 Molecular structure of $\text{Ph}_3\text{LiZn}(\text{O}^n\text{Bu}_2)_2$ **15**. Hydrogen atoms are omitted for clarity.

The structure is a contacted ion-pair in which the distorted trigonal planar zinc (sum of the angles about zinc = 359.99°) is sigma-bonded to three phenyl groups, whereas lithium adopts a perpendicular orientation, π -engaging with two of the phenyl rings via η^2 -interactions involving the *ipso* and one of the *ortho* carbons of each ring. The lithium itself displays a distorted tetrahedral geometry (angles ranging from

87.471(6) ° to 124.884(3) °, average angle = 109.1 °), completing its coordination sphere by bonding to two molecules of di-*n*-butylether. This combination of distinct bonding modes for each metal – Zn-C σ -bonds and M-C π -bonding – has been noted before in alkali metal zincate chemistry, for example, in [(TMEDA)Na(TMP)(*m*-C₆H₄-CF₃)Zn(^{*t*}Bu)], the product of the *meta* deprotonation of trifluoromethyl benzene by [(TMEDA)Na(TMP)Zn(^{*t*}Bu)₂],^[149] where a π -contact with the sodium centre stabilises the negative charge on the zincated *meta* carbon. Indeed, this is a signature feature of the arene products of alkali-metal-mediated-zincation,^[2i, 2j, 21] permitting the stabilisation of reaction intermediates.

Table 4.3 Selected bond lengths (Å) and angles (°) for **15**.

Zn1-C1	2.034(3)	Li1-C1	2.494(5)
Zn1-C7	1.991(2)	Li1-C6	2.786(5)
Zn1-C13	2.032(3)	Li1-C13	2.521(5)
		Li1-C18	2.8318(0)
C7-Zn1-C13	122.22(10)	O1-Li1-C1	113.9(2)
C7-Zn1-C1	120.77(11)	O1-Li1-C13	98.1(2)
C13-Zn1-C1	117.00(10)	O1-Li1-O2	112.8(3)

Inspection of the zinc-carbon bond distances in **15** shows that the average Zn-C contact of 2.019 Å is within the range found for other monomeric compounds of type {LiZnAr₃}; for example [(THF)LiZn(C₆H₄CH₂NMe₂-2)₃]^[150] and [Zn(μ -C₆H₄C(O)N^{*i*}Pr₂-2)₃Li·THF]^[94] which form contacted ion-pair structures via dative bonds between the lithium atom and their heteroatom functionalities, displaying average Zn-C_{aryl} bond lengths of 2.049 and 2.017 Å respectively (Figure 4.3).

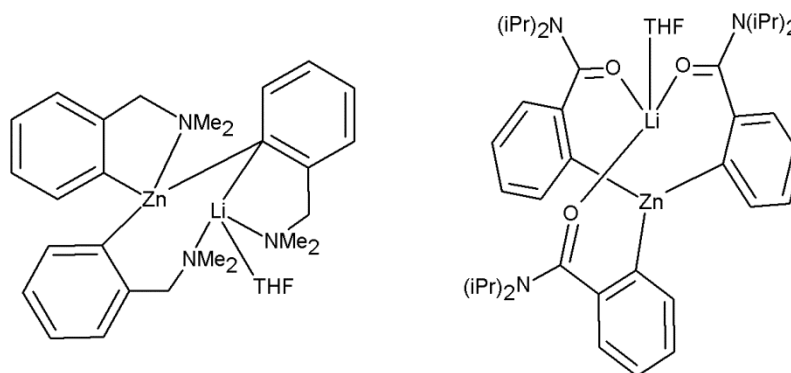


Figure 4.3 Chemdraw representations of $[(\text{THF})\text{LiZn}(\text{C}_6\text{H}_4\text{CH}_2\text{NMe}_2\text{-}2)_3]^{[150]}$ (left) and $[\text{Zn}(\mu\text{C}_6\text{H}_4\text{C}(\text{O})\text{N}^i\text{Pr}_2\text{-}2)_3\text{Li}\cdot\text{THF}]^{[94]}$ (right).

The structure of **15** can also be compared to that of diphenylzinc, which is dimeric in the solid state (Figure 4.4). Here, two phenyl groups bridge the two zinc centres via their *ipso* carbons, while the remaining phenyl groups adopt terminal positions.^[97] The trigonal planar zinc of **15** displays an almost identical Zn-C bond length to its terminal phenyl compared to those of $[\text{ZnPh}_2]_2$ (1.991(2) Å *versus* 1.946 Å), although the other two Zn-C distances, from the phenyl groups which also bind to Li (at an average of 2.033 Å), are noticeably shorter than in the monometallic compound (bridging phenyl groups Zn-C = 2.207 Å). The zinc anions of the related solvent separated magnesium triarylzincates $[\text{Mg}_2\text{Br}_3(\text{THF})_6][\text{ZnPh}_3]^{[151]}$ and $[\{\text{Mg}_2\text{Cl}_3(\text{THF})_6\}^+\{\text{Zn}(p\text{-Tol})_3\}^-]^{[48b]}$ also display a similar trigonal planar geometry to that of **15**. Although the rings of the phenyl compound are nearly perfectly coplanar, with an average Zn-C bond length of 2.007 Å, in the tolyl example only two of the toluene rings lie in the same plane as the zinc, resulting in a longer average Zn-C bond length of 2.022 Å. However, as both of these magnesium zincates exhibit solvent separated structures, no interaction between the cation metals and the aryl rings is observed.

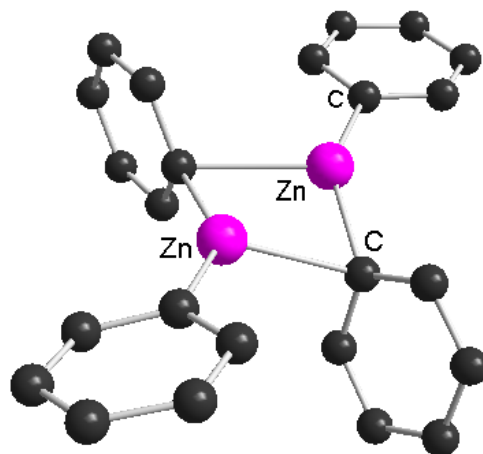


Figure 4.4 Molecular structure of $[\text{ZnPh}_2]_2$. H atoms are omitted for clarity.

In **15**, the two rings which coordinate to the lithium atom do so via η^2 π -interactions with the *ipso* and one of the *ortho* ring carbons, with Li-C distances ranging from 2.4940(5) Å to 2.8318(0) Å. The related phenyllithium structures $[(\text{PhLi}\cdot\text{OEt}_2)_4]^{[152]}$ and $[\text{PhLi}\cdot(-)\text{-sparteine}]_2^{[153]}$ exhibit Li-C sigma bridges with average values of 2.335 Å and 2.299 Å respectively, both significantly shorter than the π -contacts observed in **15** (2.494(5) Å at their shortest) and, of the two previous examples of $\{\text{LiZnAr}_3\}$ noted above (Figure 4.3),^[94, 150] neither display similar π -interactions between the lithium and the aromatic rings. Both of these examples possess heteroatom-functionalities with which the lithium preferentially interacts, resulting in only one structure, that of the *N,N*-dimethylbenzylamine compound $[(\text{THF})\text{LiZn}(\text{C}_6\text{H}_4\text{CH}_2\text{NMe}_2\text{-}2)_3]^{[150]}$ having a Li-C bond (2.414(6) Å), which is again shorter than the closest related interaction in **15** (Li1-C1 2.494(5) Å). The lithium-carbon contacts of **15** (η^2 average 2.66 Å) are however comparable to the η^6 Li-C π -interactions displayed by the unsolvated lithium aryl compound $[(\text{LiC}_6\text{H}_3\text{-}2,6\text{-Dipp}_2)_2]$ (Dipp = 2,6-diisopropylphenyl; average 2.448 Å),^[154] which exhibits a dimeric structure in the solid state (Figure 4.5), although this naturally displays shorter, stronger interactions due to the η^6 bonding mode of the alkali metal in this instance.

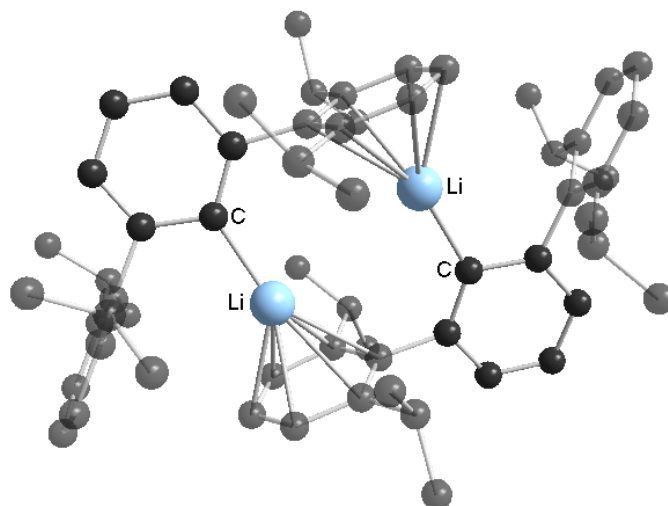


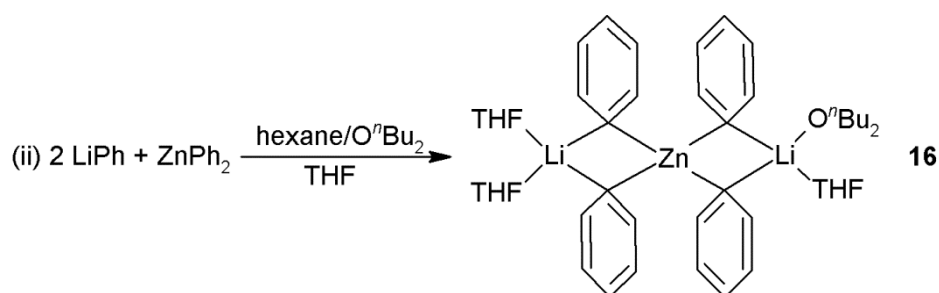
Figure 4.5 Molecular structure of $[(\text{LiC}_6\text{H}_3\text{-2,6-Dipp})_2]$. H atoms excluded for clarity.

The solubility of **15** in d_8 -THF enabled the solution constitution to be determined by ^1H , ^7Li and ^{13}C NMR spectroscopy (Table 4.4). Thus, the ^1H NMR spectrum displays a single set of resonances; a doublet at 7.84 ppm corresponding to the *ortho* protons, and multiplets at 6.98 and 6.87 ppm for the *meta* and *para* protons respectively. As there is only a single set of resonances it would appear that the exchange of phenyl groups occurs in solution, suggesting the formation of a solvent separated structure in which all phenyl groups are equivalent (*vide infra*). In the ^{13}C NMR spectrum the resonance of the *ipso* carbon of the phenyl rings (169.3 ppm) appears at a chemical shift intermediate to those observed for LiPh (187.5 ppm) and ZnPh_2 (156.8 ppm) although, being closer to that of the zinc species, this implies that **15** retains a significant proportion of zinc-character, in line with previously noted trends in lithium zincate chemistry.^[29c, 85, 91] Finally, the presence of lithium is confirmed by a sharp singlet at 1.09 ppm in the ^7Li NMR spectrum.

Table 4.4 NMR data corresponding to the starting materials and zincates **15** and **16** (ppm) in d_8 THF.*Values for zincates prepared *in situ* by salt metathesis of $x\text{LiPh}$ and ZnCl_2 ($x=3$, **15** and $x=4$, **16**).

Compound	$\delta^7\text{Li}$	$\delta^1\text{H}$	$\delta^{13}\text{C}$
PhLi	3.45	7.98 (<i>ortho</i>), 6.93 (<i>meta</i>), 6.83 (<i>para</i>)	187.5 (<i>ipso</i>), 144.2 (<i>ortho</i>), 125.0 (<i>meta</i>), 123.3 (<i>para</i>)
Ph₂Zn		7.55 (<i>ortho</i>), 7.09 (<i>meta</i>), 7.02 (<i>para</i>)	156.8 (<i>ipso</i>), 139.6 (<i>para</i>), 127.2 (<i>meta</i>), 126.1 (<i>ortho</i>)
LiZnPh₃ 15	1.09	7.84 (<i>ortho</i>), 6.98 (<i>meta</i>), 6.87 (<i>para</i>)	169.3 (<i>ipso</i>), 141.3 (<i>ortho</i>), 125.9 (<i>meta</i>), 124.0 (<i>para</i>)
Li₂ZnPh₄ 16	-0.13	7.89 (<i>ortho</i>), 6.97 (<i>meta</i>), 6.86 (<i>para</i>)	175.9 (<i>ipso</i>), 143.0 (<i>ortho</i>), 125.8 (<i>meta</i>), 123.9 (<i>para</i>)

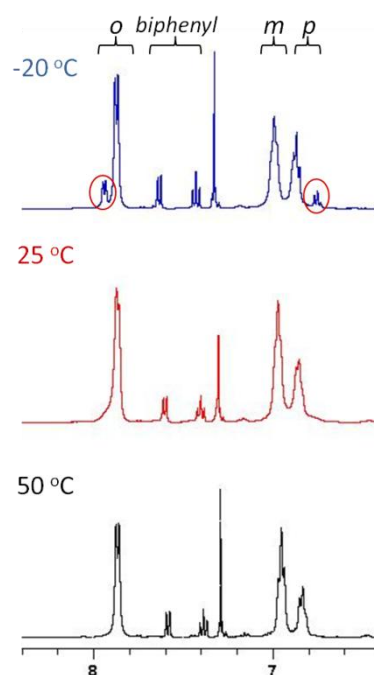
The tetraorganozincate $[\text{Li}_2\text{ZnPh}_4]$ **16** was also synthesised, being prepared in the same manner as **15**, from diphenylzinc and two equivalents of phenyllithium (Scheme 4.10). Although no crystalline material of **16** could be isolated, considering the structural similarities between alkali metal magnesiates and their zincate analogues,^[2], 21] it can be anticipated that **16** would adopt a linear Weiss motif comparable to that of the related magnesiate $[(\text{TMEDA})_2\text{Li}_2\text{MgPh}_4]$.^[155]

**Scheme 4.10** Formation of zincate **16** by co-complexation.

The composition of **16** in d_8 -THF solution was also determined spectroscopically by ^1H , ^{13}C and ^7Li NMR (see Table 4.4). Thus the ^1H NMR spectrum shows a single set of signals for the phenyl groups, with a doublet corresponding to the *ortho* protons at 7.89 ppm, and multiplets at 6.97 and 6.86 ppm corresponding to the *meta* and *para* protons respectively, once again indicating the equivalence of all phenyl groups in solution. Similarly to **15**, the *n*-butyl ether from the phenyllithium solution is present in the spectrum, integrating to a ratio of one ether molecule per $[\text{Li}_2\text{ZnPh}_4]$ fragment, with THF also present. The presence of lithium in **16** was confirmed by a resonance at -0.13 ppm in the ^7Li NMR spectrum and the resonance of the *ipso* carbon, although broad, can be seen at 175.9 ppm in the ^{13}C NMR spectrum, again occurring intermediate between that of both homometallic species. Reflecting the dianionic character of **16**, this chemical shift is significantly downfield in comparison to that of the tris(aryl)zincate **15** ($\Delta\delta^{13}\text{C}(\text{C}_{ipso}) = 6.6$ ppm).

The formation of mixed-metal species via the salt metathesis approach – where ZnCl_2 is reacted with varying amounts of a polar organometallic reagent such as an organolithium or Grignard reagent – is often complicated by the concurrent formation of inorganic salts (LiCl or MgCl_2) which, although commonly ignored, can sometimes have drastic effects on the reactivity and/or selectivity of the newly generated mixed-metal compound.^[35c] Indeed the inclusion of lithium chloride has been instrumental in the development of mixed-metal systems such as Knochel's turbo-Grignard reagents.^[156] Since such salt effects can be either positive or detrimental to the reactivity of these compounds, the synthesis of **15** and **16** via salt metathesis was performed in order to compare their reactivity with those of the salt-free species prepared by the co-complexation reactions described above. Thus, zincates **15** and **16** were also prepared *in situ* by reaction of zinc chloride with either three or four equivalents of phenyllithium in THF solution, forming $[\text{Ph}_3\text{LiZn}\cdot 2\text{LiCl}]$ **15**· LiCl and $[\text{Ph}_4\text{Li}_2\text{Zn}\cdot 2\text{LiCl}]$ **16**· LiCl respectively. These species could not be isolated in a crystalline form; however, spectroscopic analysis shows that they differ only from the LiCl free species in the shifts of the ^7Li NMR resonance (Table 4.4), which is consistent with the presence of lithium chloride in the reaction mixture.

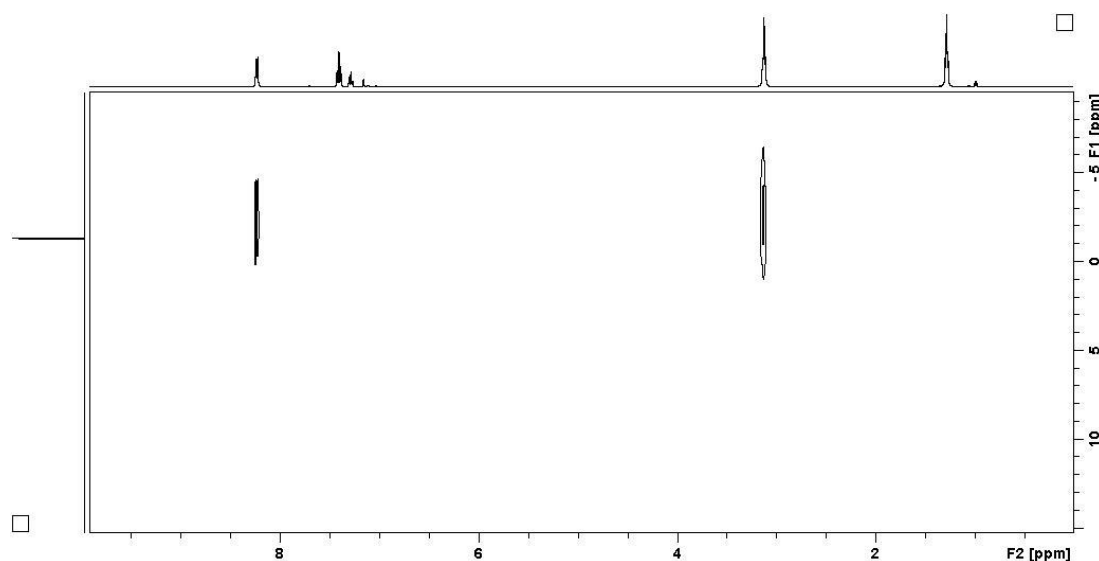
Variable temperature ^1H NMR studies on isolated crystals of **15** suggest that there is a minor solution equilibrium process in operation. Although the signals for the phenyl protons sharpen on heating, a second set of *ortho* (7.93 ppm) and *para* (6.75 ppm) resonances become visible below 0 °C (Spectrum 4.1). This may however be a consequence of thermal degradation of the sample, as a slight biphenyl contamination is also evident.



Spectrum 4.1 Aromatic region of the ^1H NMR spectra of **15** (in d_8 -THF) at 50 °C (bottom), 25 °C (centre) and -20 °C (top).

In order to gain some insight into the constitution of **15** in solution ^1H , ^7Li heteronuclear Overhauser effect spectroscopy (^1H , ^7Li -HOESY) experiments were also run. HOESY is a two dimensional spectroscopic technique which highlights the spatial proximity of two different nuclei – ^1H and ^7Li in this instance – by utilising the nuclear Overhauser effect (NOE), resulting from the through-space interactions of two magnetic nuclei which lie close to one another (within 2-4 Å), such that irradiation of one nucleus at its resonance frequency also results in the detection of the other nucleus.^[157] This experiment, when run in C_6D_6 solution, revealed an interaction between the ^7Li NMR resonance and that of the *ortho* protons, indicating

that lithium lies in close proximity to the *ortho* protons of the phenyl groups (Spectrum 4.2). This suggests that the structure of **15** remains intact in C₆D₆ solution, and therefore that the contacted ion-pair structure is retained.



Spectrum 4.2 ⁷Li-HOESY spectrum of **15** in C₆D₆ solution.

Conversely, however, the ¹H,⁷Li-HOESY spectrum of **15** in d₈-THF solution shows no interaction between the lithium centre and either the phenyl groups or the donor molecules, further supporting the formation of a solvent separated structure in this polar, Lewis basic solvent.

4.4 Reactivity of Zincates **15** and **16** towards Electron-deficient *N*-Heterocycles

4.4.1 Acridine

The tricyclic *N*-heterocycle acridine (Acr) was the first substrate to be investigated with these systems, as it exhibits important biological activities including anticancer,^[158] antibacterial^[159] and antifungal actions.^[160] Notably, the ability of the acridine scaffold to act as an intercalating ligand with DNA and related systems has earned this *N*-heterocycle a prominent place in the field of chemical biology.^[161]

Surprisingly, despite this synthetic relevance, the methods available for the efficient functionalisation of bare acridine are limited (Figure 4.6).^[146, 162] Thus, most of the approaches described in the literature rely heavily on the assembly of pre-functionalised ring systems.^[159, 163]

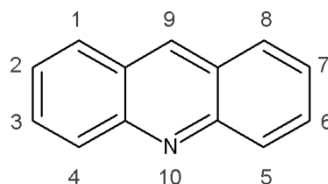
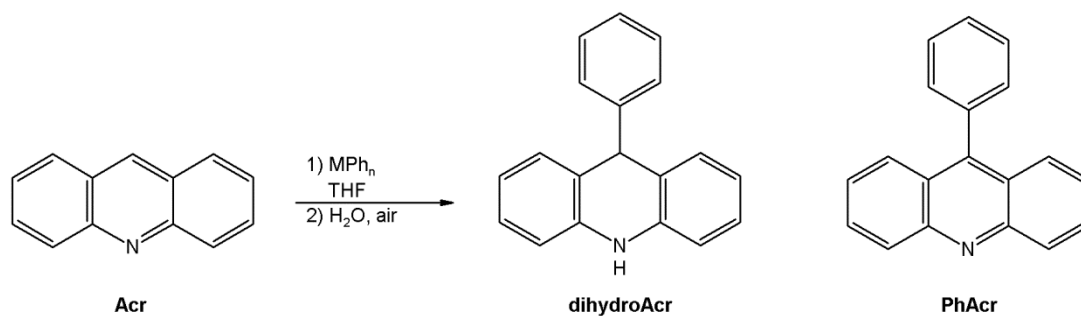


Figure 4.6 IUPAC numbering system for acridine.

The ability of zincates **15** and **16** to perform nucleophilic addition to acridine was therefore investigated. While the reaction of phenyllithium with acridine results in the formation of 9-phenyl-9,10-dihydroacridine, following hydrolysis, after 2 hours at room temperature (Table 4.5, entry 1, 95 % yield), the diphenylzinc does not react even after prolonged heating (entry 2). Furthermore, unlike the previously reported alkyl analogue [(PMDETA)LiZn^tBu₃] **14**,^[147] the phenyl zincates **15** and **16** display no reactivity at room temperature, which can be rationalised in terms of the weaker nucleophilic character of the phenyl ligand when compared to the *tert*-butyl group. Heating these reactions to reflux is sufficient to promote the addition of the phenyl group; however, even after 24 hours, complete conversion could not be achieved (Table 4.5; entries 4 and 5, 75 % and 78 % conversion respectively). It is also noteworthy that in the absence of a donor solvent the reactivity of zincate **15** shuts down (entry 3), suggesting that the reactive species is the SSIP structure found in THF solution (*vide supra*). The effect of LiCl was also investigated and it was observed that the presence of the lithium salt serves to increase levels of substrate conversion (Table 4.5; entries 6 and 7, 83 and 100 % conversion respectively), suggesting that the *in situ* prepared zincates **15**·LiCl and **16**·LiCl are more reactive; however, in all cases, oxidation was incomplete resulting in mixtures of the dihydro- and fully aromatic products.

Table 4.5 Reaction of acridine with various organometallic reagents.

	MPh_n	Time (hours)	T (°C)	Yield Acr (%) ^[a]	Yield dihydroAcr (%) ^[a]	Yield PhAcr (%) ^[a]
1	PhLi	2	18	1	95	0
2	Ph₂Zn	24	75	100	0	0
3 ^[b]	Ph₃LiZn 15	24	115	93	1	0
4		24	75	25	44	31
5	Ph₄Li₂Zn 16	24	75	22	78	0
6	Ph₃LiZn.2LiCl 15·LiCl	24	75	13	68	15
7	Ph₄Li₂Zn.2LiCl 16·LiCl	24	75	0	99	1

^[a] Yields determined by ¹H NMR using a ferrocene internal standard. ^[b] Toluene solvent.

Although heating seems to promote the aryl transfer process, extended reaction times were still required (24 hours). Thus, alternative conditions utilising microwave irradiation were investigated (125 °C, 10 minutes, Table 4.6). Control reactions show that even under these conditions $ZnPh_2$ itself is unable to perform nucleophilic addition (Table 4.6, entry 1) although, interestingly, the reaction of both **15** and **16** appeared to go to completion in only 10 minutes with microwave promotion, as determined by ¹H NMR spectroscopy using a ferrocene internal standard (Table 4.6; entries 2 and 6, 86 and 100 % conversion respectively). It was therefore decided to increase the substrate loading in order to assess if more than one phenyl group per zincate could be utilised in the reaction. Conversion of the full three equivalents was

not achieved in this time, with approximately 60 % and 20 % of the starting material remaining unreacted for **15** and **16** respectively (entries 4-5 and 8-10); however, heating the reaction in the microwave for excessive periods (up to 5 hours, entry 15) did not significantly improve yields.

Table 4.6 The reaction of acridine with zincates **15** and **16** under microwave conditions.

	MPh _n	Equivalents of Substrate	Time (min)	Equivalents of DDQ	Yield Acr (%) ^[a]	Yield dihydroAcr (%) ^[a]	Yield PhAcr (%) ^[a]
1	Ph ₂ Zn	1	10	0	84	0	0
2	Ph ₃ LiZn 15	1	10	0	10	67	19
3		1	10	1	6	28	58
4		3	10	0	60	16	24
5		3	10	1	61	2	35
6		Ph ₄ Li ₂ Zn 16	1	10	0	0	89
7	1		10	1	7	18	74
8	3		10	0	16	33	37
9	3		10	1	23	16	60
10	3		10	3	22	3	74
11	Ph ₃ LiZn.2LiCl	3	10	0	47	22	30
12	15 ·LiCl	3	10	1	37	13	45
13		3	10	3	51	2	46
14		Ph ₄ Li ₂ Zn.2LiCl	3	10	0	6	53
15	16 ·LiCl	3	300	0	5	52	44
16		3	10	1	17	22	52
17		3	10	3	8	12	71

^[a] Yields determined by ¹H NMR using a ferrocene internal standard.

The oxidant 2,3-dichloro-5,6-dicyano-1,4-benzoquinone (DDQ)^[117a, 162a] was next employed in attempt to rearomatise the 9-phenyl-9,10-dihydroacridine formed. When added prior to microwave irradiation the oxidant appeared to inhibit reaction, and although the yields of fully aromatic product were higher, the overall levels of substrate conversion dropped. A one-pot procedure for this reaction was therefore ruled out; however, the addition of DDQ after hydrolysis resulted in a satisfactory ratio of dihydro- to aromatic species whilst maintaining levels of substrate conversion (Table 4.6; entries 5 (2:35 %), 10 (3:74 %), 13 (2:46 %) and 17 (12:71 %)). Overall, it would appear that the presence of lithium chloride enhances the reactivity of the zincate towards nucleophilic addition (Table 4.6, entries 11 to 17), with the higher order tetraphenyl zincate **16**·LiCl being the most reactive (entry 17; 92 % conversion, 71 % PhAc).

Thus, these results show that under these optimised reaction conditions (microwave irradiation, THF and addition of an external oxidant) [Li₂ZnPh₄] **16** and **16**·LiCl can effectively promote the regioselective arylation of acridine in good yield (74 and 71 % respectively). These results are a little lower than the 85 % yield reported by Tobisu *et al*, on reaction of acridine with ZnPh₂ in the presence of a rhodium catalyst;^[144] however, this was only achieved after heating the reaction to 130 °C for 20 hours, in comparison to the 10 minutes required by the zincate methodology. Furthermore, the catalytic reaction is performed using a one to one ratio of acridine to arylzinc compound, a ratio which can be increased (3:1) by employing the higher order zincate **16**; thus the transition metal-free methodology offers increased atom efficiency in addition to significantly reduced reaction times.

With the apparent activation of up to three of its four phenyl groups, the microwave reaction of **16**·LiCl proved to be the most efficient, and it was therefore assumed that this reaction would provide the optimal conditions for the isolation of any reaction intermediate. Hence, the reaction of **16**·LiCl with three equivalents of acridine was

heated in the microwave for ten minutes before storage at $-70\text{ }^{\circ}\text{C}$. This resulted in the eventual isolation of crystals of lithium amide $[(\text{THF})_3\text{Li}(\text{NC}_{13}\text{H}_9\text{-9-Ph})]$ **17** in a 31 % yield (Figure 4.7, Table 4.7).

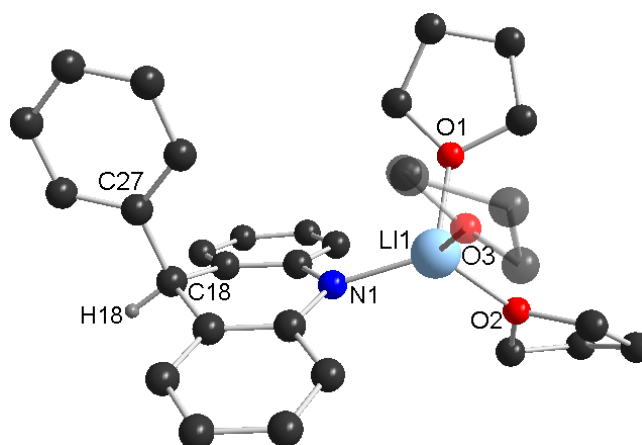


Figure 4.7 Molecular structure of $[(\text{THF})_3\text{Li}(\text{NC}_{13}\text{H}_9\text{-9-Ph})]$ **17** with H atoms (excluding H18) omitted for clarity.

Table 4.7 Selected bond lengths (\AA) and angles ($^{\circ}$) for **17**.

Li1-N1	1.989(4)	Li1-O2	1.930(4)
Li1-O1	1.974(4)	Li1-O3	2.014(4)
O1-Li1-O2	104.72(16)	C26-N1-Li1	125.65(16)
O1-Li1-O3	98.14(16)	C17-C18-H18	108.1(2)
O1-Li1-N1	109.36(16)	C17-C18-C19	109.6(2)
O2-Li1-O3	105.19(15)	C17-C18-C27	111.3(2)
O2-Li1-N1	120.64(19)	C19-C18-H18	108.1(2)
N1-Li1-O3	115.96(17)	C27-C18-H18	108.1(2)
C24-N1-C26	115.47(15)	C19-C18-C27	111.4(2)
C24-N1-Li1	118.42(16)		

The structure of **17** was determined crystallographically and found to contain only lithium. Displaying a monomeric motif, the distorted tetrahedral lithium (angles about Li1 range from $120.64(19)$ to $98.14(16)$ $^{\circ}$, average 109.0 $^{\circ}$) is bonded to the N atom of an anionic ligand, which results from the addition of the phenyl group to the

C9-position of acridine (C18 in Figure 4.7), forming a relatively short Li1-N1 bond (1.989(3) Å) by comparison to the related 1-lithio-4-hydropyridine structures [(Py)₂Li(NC₅H₆)]₂ (Figure 4.8 (left), average 2.098 Å)^[164] and [(THF)₂Li(2-Et-4-Bz-4-hydroPy)]₂ (Figure 4.8 (centre), average 2.076 Å)^[165] which were also prepared by the nucleophilic addition of an organolithium reagent (LiBu and LiBz, respectively). Both of these structures are dimeric, which would account for the elongated Li-N bond with respect to the monomeric **17**, which is closer to that of [(PMDETA)Li(2-(CHCH₃)-NC₅H₄)]^[165] at an average of 2.016 Å (Figure 4.8 (right)).

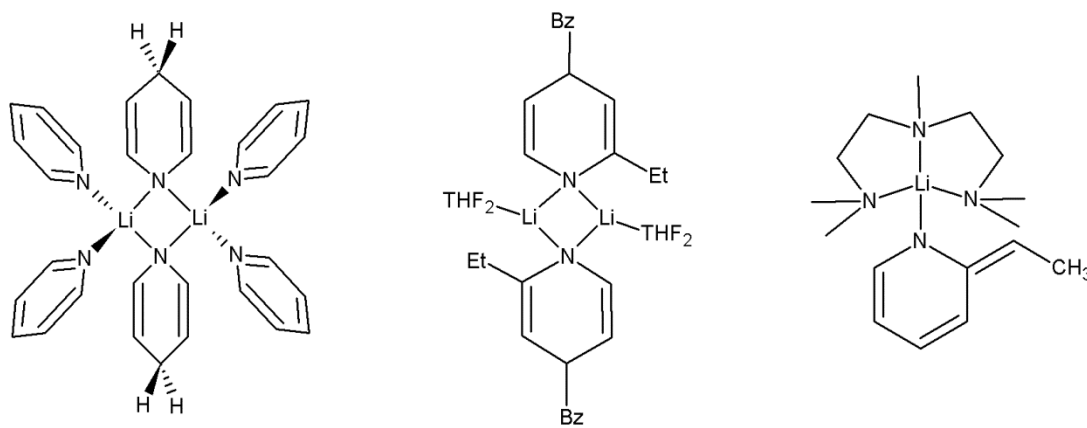
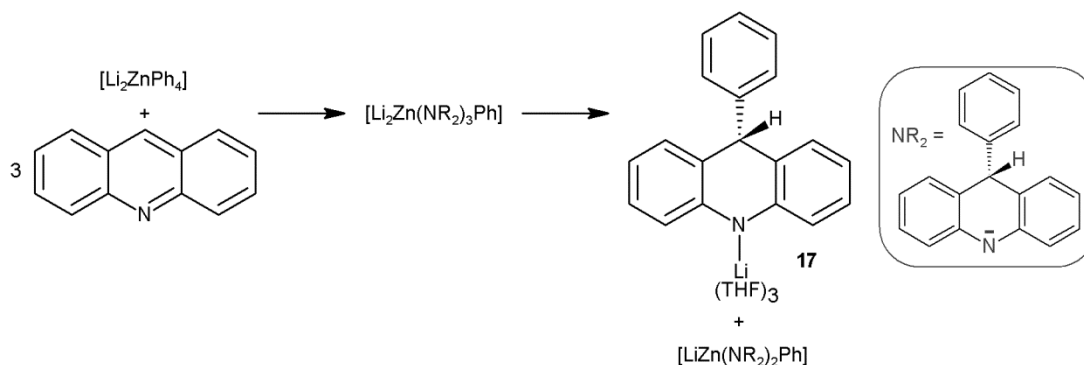


Figure 4.8 Chemdraw representations of [(Py)₂Li(NC₅H₆)]₂ (left), [(THF)₂Li(2-Et-4-Bz-4-hydroPy)]₂ (centre) and [(PMDETA)Li(2-(CHCH₃)-NC₅H₄)] (right).

Evidencing the nucleophilic addition, C18 displays a tetrahedral geometry resulting from the change of hybridisation, from sp² to sp³ (angles about C18 range from 111.4(2) ° to 108.1(2) °, average 109.44 °), and consequently lies 0.316 Å out of the plane defined by C17, C19, C24 and C26. This loss of aromaticity in the central ring results in the average C-C bond length across the entire acridine ring system (at 1.434 Å) being lengthened with respect to that of acridine itself (1.402 Å in **19**, *vide infra*).

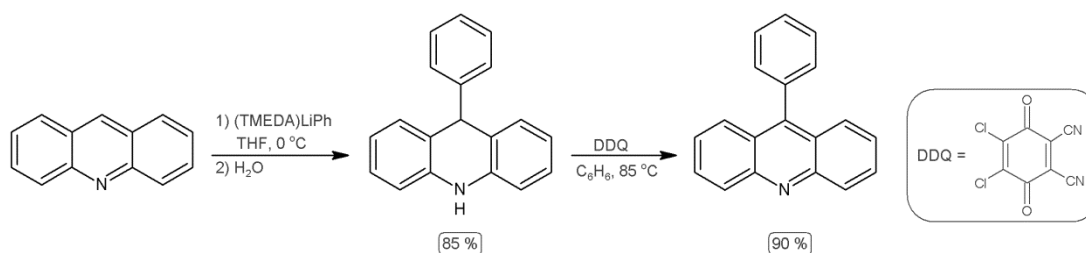
Compound **17** showed good solubility in d_8 -THF and was fully characterised by ^1H , ^{13}C and ^7Li NMR spectroscopy. The ^1H NMR spectrum displayed the protons of the phenyl group with a doublet at 7.06 ppm (*ortho*) a double doublet at 6.95 ppm and a triplet at 6.84 ppm (corresponding to the *meta* and *para* protons respectively). The aromatic protons of the acridine ligand were also evident with two doublets at 6.74 and 6.46 ppm (H1 and H4 respectively, according to the IUPAC numbering system in Figure 4.6, *vide supra*) and two triplets at 6.67 and 6.20 ppm (H3 and H2 respectively). The most diagnostic signal was a singlet at 5.00 ppm, which was assigned to the proton in the C9-position – a distinctly different chemical shift to the C9-proton of acridine in the same solvent (8.88 ppm). The loss of aromaticity is further demonstrated in the ^{13}C NMR spectrum where the resonance corresponding to C9 appears at 50.8 ppm, drastically upfield in comparison to the C9 resonance of acridine (136.3 ppm). The presence of lithium was confirmed by ^7Li NMR spectroscopy which displayed a singlet at 0.74 ppm.

The reactivity studies indicate that at least three of the four phenyl groups present in $[\text{Li}_2\text{ZnPh}_4]$ **16** are active towards the nucleophilic attack of acridine (see Table 4.6). Thus, it can be proposed that initially a higher order zincate $[\text{Li}_2\text{Zn}(\text{NR}_2)_3\text{Ph}]$ ($\text{NR}_2 = \text{NC}_{13}\text{H}_9\text{-9-Ph}$) is formed, which contains three amido ligands – resulting from the nucleophilic arylation of acridine – in addition to the remaining phenyl group. In solution, or under the crystallisation conditions imposed, this putative bimetallic intermediate may undergo a redistribution to give the lithium-only compound **17** (which has been isolated and structurally defined) and perhaps a lower order zincate $[\text{LiZn}(\text{NR}_2)_2\text{Ph}]$ (Scheme 4.11). Although the presence of this compound could not be demonstrated, the ^1H NMR spectrum of the reaction filtrate in d_8 -THF (despite presenting a very complex aromatic region) displayed a distinctive singlet at 5.28 ppm, which could be attributed to the C9-proton of the NR_2 ligand in the proposed zincate intermediate. The presence of lithium in the filtrate was also confirmed by a broad resonance in the ^7Li NMR spectrum at 2.16 ppm.



Scheme 4.11 Proposed mechanism for the formation of **17**.

The isolation of the monometallic **17** prompted us to examine the reaction of the parent compound phenyllithium towards acridine. Organic studies have shown that acridine can be converted to 9-phenyl-9,10-dihydroacridine in 85% yield with $\text{PhLi}(\text{TMEDA})$,^[162a] and this dihydro-species can then be rearomatised to 9-phenylacridine on treatment with the oxidising agent DDQ (Scheme 4.12). In order to gain better insight into the constitution of the organometallic intermediate involved in this reaction, acridine was treated with phenyllithium, without the additional hydrolysis and oxidation steps. This led to the formation of a deep purple solution which deposited purple crystals in a yield of 8% on storage at $-78\text{ }^\circ\text{C}$, although yields of isolated non-crystalline solid were considerably higher (42%).



Scheme 4.12 Reaction of $\text{PhLi}(\text{TMEDA})$ with acridine followed by hydrolysis and reduction to 9-phenylacridine.^[162a]

Although solution characterisation of this solid by ^1H NMR spectroscopy proved challenging due to a lack of solubility in C_6D_6 and $\text{d}_8\text{-THF}$, structural studies carried out by X-ray crystallography established its constitution as

$[\{(TMEDA)Li(THF)\}^+\{NC_{13}H_8-9-Ph\}^{\cdot-}]$ **18** (Figure 4.9, Table 4.8). This study confirmed that the phenyl group had been transferred to the C9-position of acridine; however, unlike **17**, the carbon which has undergone the addition displayed sp^2 hybridisation, with the sum of the angles about it totalling 359.96° (C7 in Figure 4.9). Furthermore, the lithium atom lies out of the plane of the acridine ring system (0.5506 \AA above the central ring) which, along with the lack of a C9-proton and the intense colour, suggests that the compound is a radical anion. Therefore, the poor quality of the NMR spectra may be due to the paramagnetic nature of the compound, in addition to the limited solubility of the crystals.

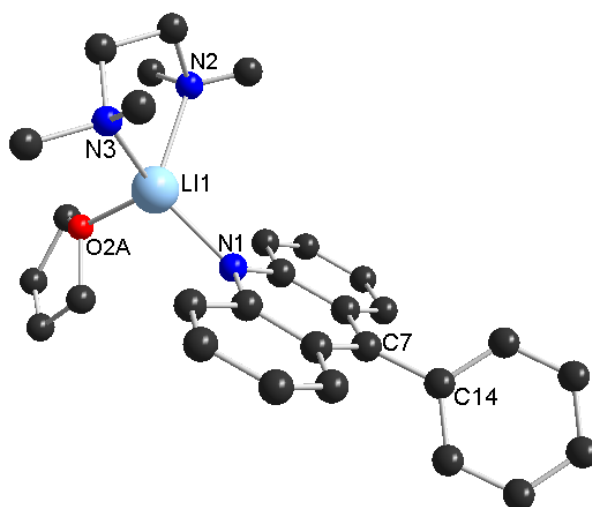


Figure 4.9 Molecular structure of $[\{(TMEDA)Li(THF)\}^+\{NC_{13}H_8-9-Ph\}^{\cdot-}]$ **18**. Hydrogen atoms have been omitted for clarity.

Table 4.8 Selected bond lengths (\AA) and angles ($^\circ$) for **18**.

N1-Li1	2.0702(3)	N3-Li1	2.1135(3)
N2-Li1	2.2823(2)	O1-Li1	1.9607(2)
Li1-N1-C1	118.712(10)	N1-Li1-O1	109.986(8)
Li1-N1-C13	122.089(12)	N2-Li1-N3	83.338(6)
N1-Li1-N2	117.795(6)	N2-Li1-O1	109.889(4)
N1-Li1-N3	124.070(6)	N3-Li1-O1	109.009(4)

The structure of **18** displays disorder due to the combination of Lewis bases which complete the coordination sphere of the lithium atom (approx. 73:27 Li(THF)₃ to Li(THF)(TMEDA)); nonetheless, the lithium atom sits in a distorted tetrahedral environment (angles about Li range from 124.070(6) to 83.338(6) °, average = 109.015 °) bonding to the nitrogen of the radical anion with a Li1-N1 distance of 2.0702(3) Å. This is marginally longer than the Li1-N1 contact of the non-radical species **17** (1.989(3) Å), and significantly shorter than the contacts to the donor nitrogen atoms in the structure (Figure 4.9, average Li1-N_{TMEDA} = 2.1979 Å). The average carbon-carbon distance in the acridine ring system is 1.406 Å across all three rings, consistent with delocalisation of the radical. Although structurally characterised lithium radical species are rare, these findings are in line with those reported for the lithium naphthalide radical anion [Li⁺(TMEDA)₂][C₁₀H₈^{•-}], which displays a solvent separated ion-pair structure,^[166] with a mean carbon-carbon distance practically identical to that of **18** at 1.408 Å. Furthermore, EPR analysis of **18** between 2 K and 70 K revealed an isotropic signal centred at $g = 2.006$, which remains almost unchanged over the temperature range. This is as expected for an unpaired electron centred on carbon.

A search of the literature confirmed that the three-ring fused structure of acridine is known to form radicals,^[167] including both cations^[168] and anions.^[169] The 9-phenylacridine radical anion itself has previously been formed by the alkali metal reduction of 9-phenylacridine, as reported by Bard in 1972.^[169b] In this communication it was suggested from the analysis of the ESR spectrum that the twist angle between that of the phenyl ring and the acridine ring system was approximately 65 ° due to steric restriction. Although the alkali metal counter ion was not specified in this instance, analysis of the lithium structure **18** supports this prediction, with the angle between the two planes in this instance being 62.653(97) °. The isolation of **18** suggest that LiPh reacts with acridine via a single electron transfer (SET) mechanism, which contrasts with the zincate-mediated arylation, where the isolation of **17** implies an anionic mechanism.

As discussed above, the elaboration of acridine by organozinc reagents was described by Tobisu *et al* in 2012^[146] and it was noted that the nucleophilic addition of ZnPh_2 to acridine can be achieved if refluxed in the presence of a rhodium catalyst (130 °C, 20 h). However, in accordance with these results, our control reactions confirm diphenylzinc does not react with acridine by itself; even after refluxing for 24 hours only starting materials were recovered, and microwave irradiation also failed to promote any reaction (Table 4.5 and Table 4.6, *vide supra*). In the absence of a catalyst, the donor complex $[\text{Ph}_2\text{Zn}(\text{NC}_{13}\text{H}_9)]$ **19** was isolated from hexane/toluene solution in a 29 % crystalline yield (Figure 4.10, Table 4.9). The molecular structure of **19** was determined by X-ray crystallography and found to be monomeric, with a single molecule of acridine coordinated to the distorted trigonal planar zinc (sum of the angles about Zn = 359.97 °), which is further bonded to the two phenyl groups at an average Zn-C bond length of 1.953 Å, near identical to the terminal Zn-C bonds of $[\text{ZnPh}_2]_2$ (1.946 Å).^[97] The Zn-N distance in **19**, at 2.1598(11) Å, is comparable to that previously reported for the related pyridine adduct $[\text{Ph}_2\text{Zn}(\text{C}_5\text{H}_5\text{N})_2]$ (average 2.1505(12) Å).^[170]

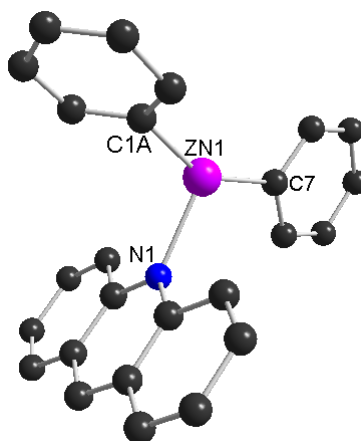
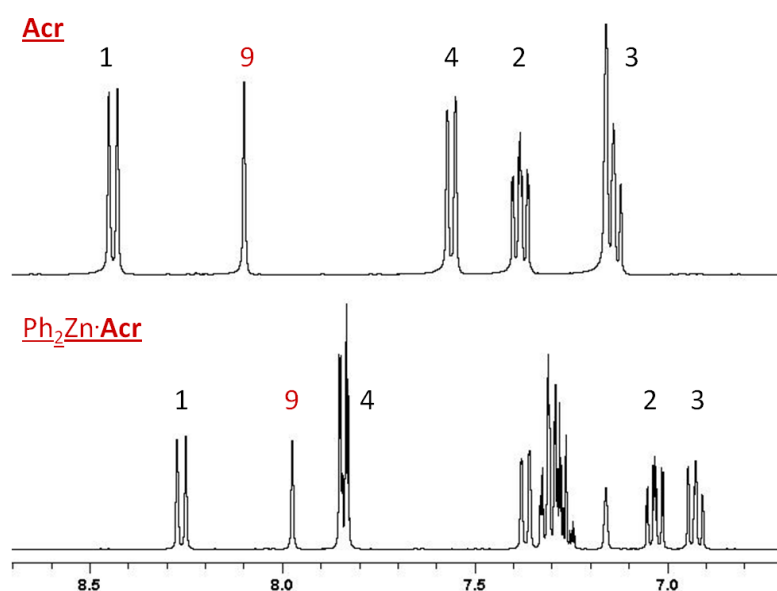


Figure 4.10 Molecular structure of $[\text{Ph}_2\text{Zn}(\text{NC}_{13}\text{H}_9)]$ **19**. Hydrogen atoms have been omitted for clarity.

Table 4.9 Selected bond lengths (Å) and angles (°) for **19**.

Zn1-C1	1.942(11)	Zn1-N1	2.1598(11)
Zn1-C7	1.9647(13)		
C1-Zn1-C7	146.9(5)	C1-Zn1-N1	104.1(5)
C7-Zn1-N1	108.97(5)		

NMR analysis of **19** in C_6D_6 solution shows that acridine remains coordinated to the diphenylzinc in solution. Thus, the 1H NMR spectrum of **19** shows that the relevant acridine resonances have been shifted upfield with respect to those observed for free acridine in the same solvent. The proton in the C9-position, for example, shifts from 8.10 ppm in the free heterocycle to 7.97 ppm for the $ZnPh_2$ complexed species **19** (Spectrum 4.3). A similar trend is observed for the ^{13}C NMR spectrum, although now the resonances for the coordinated acridine are significantly downfield with respect to those observed for free acridine (C9 = 84.5 ppm in acridine and 139.6 ppm in **19**). Moreover, in both 1H and ^{13}C NMR spectra the resonances due to the phenyl groups are also present despite free $ZnPh_2$ being largely insoluble in C_6D_6 . The most diagnostic of these signals is that of the $Zn-C_{ipso}$ resonance in the ^{13}C NMR spectrum which appears at 155.0 ppm.



Spectrum 4.3 Comparison of the ^1H NMR spectra of acridine (top) and $[\text{Ph}_2\text{Zn}(\text{acridine})]$ **19** (bottom) in C_6D_6 . The resonances of the acridine protons are labelled according to the IUPAC numbering system.

The isolation of **19** demonstrates that the coordination of ZnPh_2 to acridine does indeed occur in toluene solution. Therefore, assuming the rhodium catalysed arylation of acridine reported by Tobisu *et al*^[146] proceeds via the same mechanism suggested for the related nickel catalysed arylations (Scheme 4.7, *vide supra*),^[117a] **19** constitutes the first tangible evidence of any reaction intermediate, thus lending some credence to the proposed mechanism.

In their 2012 communication Tobisu *et al* also noted that, unlike diaryl reagents, diisopropylzinc was capable of performing an addition reaction in the absence of any catalyst when heated for prolonged periods in toluene.^[146] Intriguingly, only secondary alkyl groups were capable of the addition, with the primary alkyl reagents ZnMe_2 , ZnEt_2 and Zn^nBu_2 all failing to react under the same conditions. From our previous studies with pyrazine we have shown that the nucleophilic addition of an alkyl group to a heterocycle can be effected with the use of zincate reagents, although the addition of neutral Zn^tBu_2 was never observed.^[147] It was therefore decided to employ $\text{LiZnEt}_3(\text{TMEDA})_2$ **20** in order to investigate the addition of a primary alkyl group to acridine.

Previous reports by Richey have shown that triethyl lithium zincate LiZnEt_3 efficiently promotes ethyl transfer to aldehydes and ketones,^[53] and therefore we anticipated that a similar reaction would occur with acridine. $\text{LiZnEt}_3(\text{TMEDA})_2$ **20** was prepared by the co-complexation of equimolar amounts of ethyllithium and diethylzinc^[53, 171] in hexane solution in the presence of the chelating diamine TMEDA, yielding an oily solid. The constitution of **20** in d_8 -THF solution was studied in detail by multinuclear ^1H , ^{13}C and ^7Li NMR spectroscopy. Both ^1H and ^{13}C NMR spectra indicated a single set of resonances for the ethyl groups (Table 4.10),^[53] where the chemical shift of the methylene protons is intermediate to that of the constituent monometallic compounds (LiEt reacts with THF and could not be analysed in this solvent, however, it is expected that the shift of the methylene protons would be substantially upfield in comparison to that of the zinc species. The chemical shift in C_6D_6 is included for illustration only). This is consistent with the formation of a solvent separated ion-pair zincate species, although the presence of solution equilibria has not been ruled out.

Table 4.10 ^1H NMR data for $\text{ZnEt}_2(\text{TMEDA})$ and $\text{LiZnEt}_3(\text{TMEDA})_2$ **20** (ppm) in d_8 -THF.

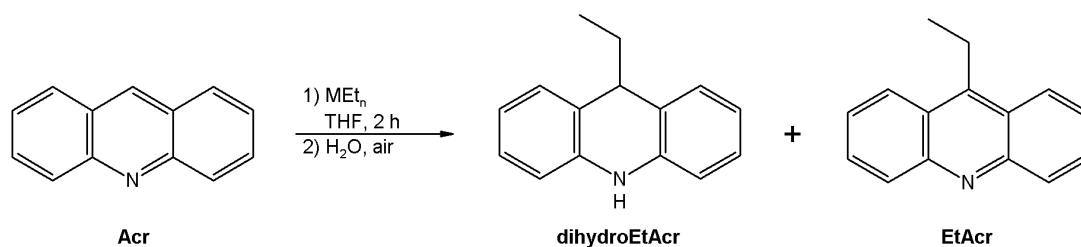
Compound	$\text{CH}_3\text{CH}_2\text{M}$	$\text{CH}_3\text{CH}_2\text{M}$	CH_3N	CH_2N
TMEDA			2.15	2.30
$\text{ZnEt}_2(\text{TMEDA})$	-0.15	1.19	2.27	2.43
LiEt^a	-0.97	1.24		
$\text{LiZnEt}_3(\text{TMEDA})_2$	-0.25	1.18	2.20	2.36
20				

^[a] NMR run in C_6D_6 .

Alkyl lithium reagents are known to perform nucleophilic addition to electron-deficient heterocycles,^[2d] and the addition of ethyllithium to acridine was confirmed by a control reaction in THF solution which produced 92% 9-ethyl-9,10-dihydroacridine after hydrolysis (Table 4.11, entry 1). Subsequently, $\text{LiZnEt}_3(\text{TMEDA})_2$ **20** was prepared *in situ* and reacted with acridine in a similar

fashion (Table 4.11, entry 2). This reaction again produced 9-ethyl-9,10-dihydroacridine (63 %), but significant levels of the fully rearomatised 9-ethylacridine were also observed (24 %), suggesting that some component of the zincate reagent is capable of acting as an oxidant. These results are consistent with previous reports that organozinc reagents can act in this capacity, with the ease of rearomatisation of the intermediate species evidently being the decisive factor.^[117a, 144, 146] However, this rearomatisation process is incomplete and a secondary oxidation step is required to obtain significant levels of 9-ethylacridine (Table 4.11, entry 3).

Table 4.11 The reaction of acridine with ethyllithium and LiZnEt₃ **20**.

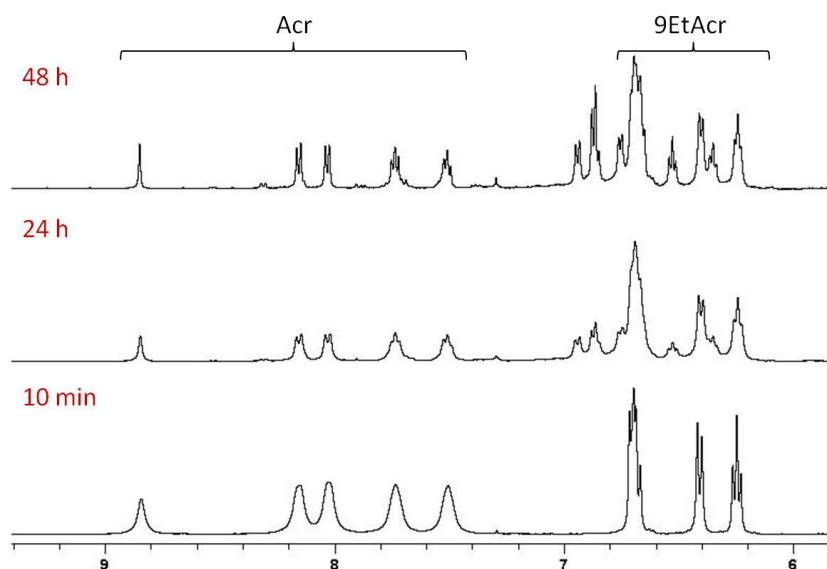


	MPh _n	Time (hours)	T (°C)	Yield Acr (%) ^[a]	Yield dihydroEtAcr (%) ^[a]	Yield EtAcr (%) ^[a]
1	LiEt	2	0	1	92	0
2	LiZnEt ₃ (TMEDA) ₂ 20	2	18	6	63	24
3 ^[b]	LiZnEt ₃ (TMEDA) ₂ 20	2	18	10	12	68

^[a] Yields determined by NMR with respect to a ferrocene internal standard. ^[b] 1 eq DDQ added following hydrolysis.

The same reaction was then performed in d₈-THF in a sealed NMR tube and the changes monitored over time. From these experiments it was apparent that the reaction was very rapid, with approximately 50 % conversion of acridine into a new product evident in the ¹H NMR spectrum 10 minutes after the addition of the substrate (Spectrum 4.4). Also apparent was the transformation of LiZnEt₃(TMEDA)₂ **20** into Et₂Zn(TMEDA), as evidenced by the change in chemical shift of Zn-CH₂ in the ¹H NMR spectrum, which moved from -0.25 ppm to -0.15

ppm (see Table 4.10). These findings suggest that although the zincate species is formed in solution, the addition product is a lithium species which develops accompanied by the concomitant formation of $\text{Et}_2\text{Zn}(\text{TMEDA})$.



Spectrum 4.4 Reaction of $\text{LiZnEt}_3(\text{TMEDA})_2$ **20** with acridine in $\text{d}_8\text{-THF}$.

This possibility was further supported by the isolation of $[(\text{TMEDA})(\text{THF})\text{Li}(\text{NC}_{13}\text{H}_9\text{-9-Et})]$ **21** from the reaction mixture (prior to hydrolysis) which could be isolated in a 20 % crystalline yield (Figure 4.11, Table 4.12). ^1H NMR spectroscopic analysis of the filtrate confirmed that $\text{Et}_2\text{Zn}(\text{TMEDA})$ remained in solution. Multinuclear ^1H , ^{13}C and ^7Li NMR analysis of **21** identified the addition of an ethyl group, indicated by resonances at 1.35 (methyl) and 0.68 ppm (methylene) in the ^1H NMR spectrum in $\text{d}_8\text{-THF}$ solution (35.0 and 11.7 ppm respectively in the ^{13}C NMR spectrum). The loss of aromaticity was evident due to the presence of a signal in the ^1H NMR spectrum corresponding to the proton in the C9-position which appears coincident to that of the α -protons of THF at 3.60 ppm; however, COSY and HSQC experiments confirm interactions with the CH_2 of the ethyl group and C9 (47.2 ppm in the ^{13}C NMR spectrum) respectively. Finally the presence of lithium was indicated by a signal at 2.57 ppm in the ^7Li NMR spectrum.

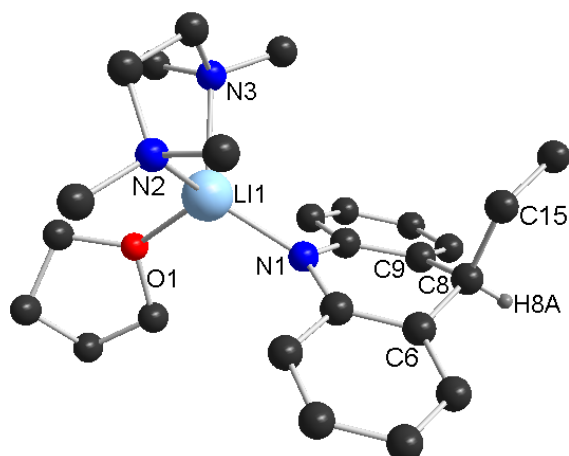


Figure 4.11 Molecular structure of [(TMEDA)(THF)Li(NC₁₃H₉-9-Et)] **21**. H atoms (excluding H8a) have been omitted for clarity.

Table 4.12 Selected bond lengths (Å) and angles (°) for **21**.

Li1-O1	1.967(8)	Li2-O2	2.020(9)
Li1-N1	1.991(9)	Li2-N4	2.021(9)
Li1-N2	2.149(9)	Li2-N5	2.168(9)
Li1-N3	2.189(9)	Li2-N6	2.129(10)
O1-Li1-N1	107.6(4)	C7-N1-C14	115.2(4)
O1-Li1-N2	111.0(4)	O2-Li2-N4	107.6(4)
O1-Li1-N3	110.4(4)	O2-Li2-N5	114.0(4)
N1-Li1-N2	121.6(4)	O2-Li2-N6	105.4(4)
N1-Li1-N3	119.0(4)	N4-Li2-N5	120.8(4)
N2-Li1-N3	85.9(3)	N4-Li2-N6	121.6(4)
Li1-N1-C7	126.4(4)	N5-Li2-N6	85.6(4)
Li1-N1-C14	118.0(4)		

X-ray crystallographic studies revealed the molecular structure of [(TMEDA)(THF)Li(NC₁₃H₉-9-Et)] **21**, which contains two independent molecules in its asymmetric unit. For brevity only one of these will be discussed. As was the case with [(THF)₃Li(NC₁₃H₉-9-Ph)] **17** (*vide supra*) compound **21** contains only lithium, and indeed the two compounds are essentially isostructural, with a distorted tetrahedral lithium centre (angles about Li range from 85.9(3) ° to 121.6(4) ° and an average angle of 109.3 ° for Li1 and 109.2 ° for Li2) bonding to the heterocyclic anion via a slightly longer Li-N bond (average of 2.006 Å) when compared to that found in **17** (1.989(3) Å). Similarly, the nitrogen atom sits in a trigonal planar environment (sum of angles about N1 359.6 °) while the loss of aromaticity in the central ring is evidenced by the sp³ hybridisation of C8 (angles about C8 range from 112.7(4) to 103(3) °, average 109.4 °; C27 113.0(4)-106(2) °, average 109.4 °) which drops 0.4394 Å out of the plane of the central ring (C7, C6, C9 and C14). The average C-C bond length across the acridine-based scaffold (at 1.431 Å) is also elongated with respect to the neutral aromatic acridine (1.402 Å in **19** *vide supra*).

As discussed above, Tobisu has previously reported that Zn^{*i*}Pr₂ can add across the C9-position of acridine without the aid of a transition metal catalyst; however, primary alkylzinc reagents do not react (Figure 4.12).^[146] Thus, no reaction with ZnEt₂ was expected, although it was anticipated that it would be possible to isolate a donor complex of the heterocycle and the zinc, similar to that reported on the reaction of pyrazine with di-*tert*-butylzinc.^[147]

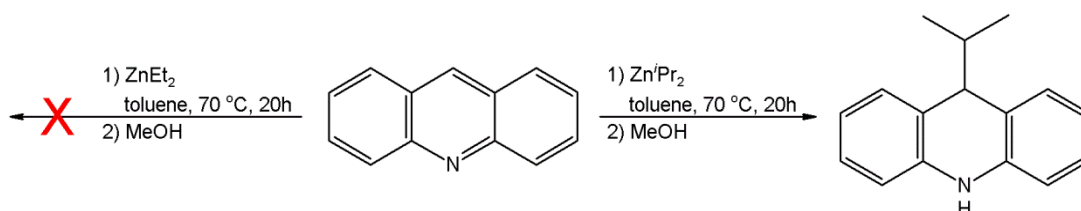


Figure 4.12 Addition of Zn^{*i*}Pr₂ to acridine.^[146]

The addition of ZnEt_2 to a solution of acridine resulted in a subtle colour change from yellow to orange, and the isolation of crystalline material was eventually realised; however, these crystals proved to be highly insoluble in all available deuterated solvents (C_6D_6 , d_8 -THF and d_6 -DMSO) and so could not be characterised by NMR spectroscopy. Surprisingly, X-ray crystallographic analysis revealed that this compound, far from being a coordination complex of diethylzinc and acridine, was in fact the centrosymmetric bis-acridan complex $[(\text{THF})_2\text{Zn}(\text{Et})_2]_2[\mu\text{-(NC}_{13}\text{H}_9\text{-C}_{13}\text{H}_9\text{N})]$ **22** shown in Figure 4.13 (Table 4.13). Each zinc atom is bound to a terminal ethyl group and two molecules of THF, while the two metal centres are connected by a bridging dianionic ligand resulting from the coupling of two acridine-based subunits at the C9-position. The Zn-N distance in **22**, at $1.946(2)$ Å, is shorter than that of the neutral zinc-acridine donor complex $[\text{Ph}_2\text{Zn}(\text{NC}_{13}\text{H}_9)]$ **19** ($2.1598(11)$ Å), being more in the range of zinc-amide bonds such as those of $\text{Zn}(\text{HMDS})_2$ (average 1.833 Å)^[92] and $[(\text{Li}\cdot 4\text{TEMPO})^+\{\text{Zn}(\text{HMDS})_3\}^-]$ (average 1.969 Å).^[172]

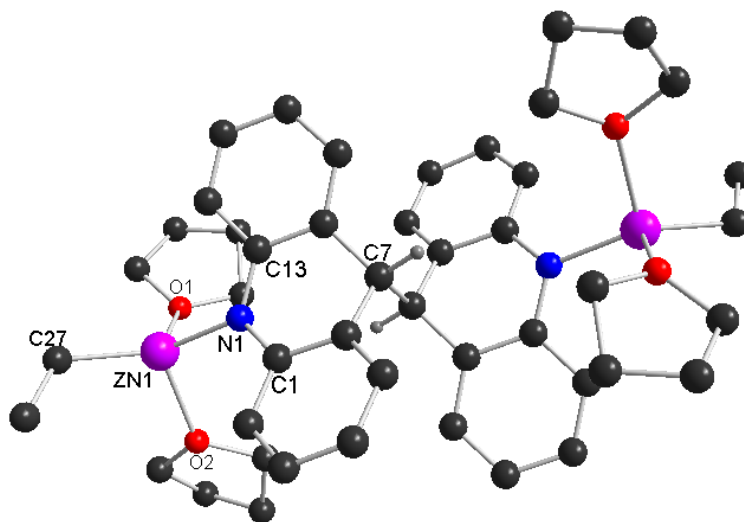


Figure 4.13 Molecular structure of $[(\text{THF})_2\text{Zn}(\text{Et})_2]_2[\mu\text{-(NC}_{13}\text{H}_9\text{-C}_{13}\text{H}_9\text{N})]$ **22**. Hydrogen atoms (excluding those on C7) have been omitted for clarity.

Table 4.13 Selected bond lengths (Å) and angles (°) for **22**.

Zn1-N1	1.946(2)	Zn1-O2	2.1463(18)
Zn1-C27	1.979(3)	C7-C7'	1.593(5)
Zn1-O1	2.1952(18)		
N1-Zn1-C27	141.80(11)	O1-Zn1-O2	88.17(7)
N1-Zn1-O1	100.41	C1-N1-C13	115.2(2)
N1-Zn1-O2	101.19(9)	C1-N1-Zn1	123.42(17)
C27-Zn1-O1	105.08(10)	C13-N1-Zn1	120.3(17)
C27-Zn1-O2	107.52(10)		

It should be noted that similar assemblies derived from the coupling of two acridine units have been previously reported. Indeed there are two known examples of a 9,9'-coupled acridine-based ligand supported by samarium; $[(\eta^5\text{-C}_5\text{Me}_5)_2\text{Sm}_2][\mu\text{-}\eta^3\text{-}\eta^3\text{-(C}_{13}\text{H}_9\text{N)}_2]$ ^[173] and $[(\text{C}_4\text{Me}_4\text{P})_2\text{Sm}]_2[\mu\text{-(NC}_{13}\text{H}_9\text{-C}_{13}\text{H}_9\text{N})]$ ^[174] (Figure 4.14).

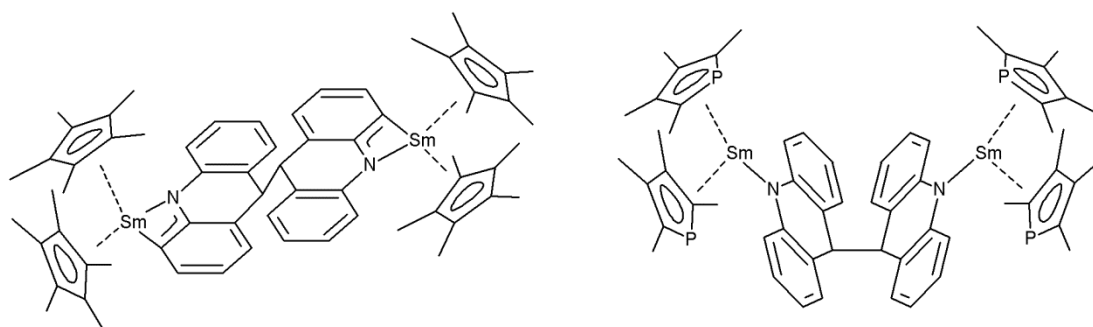
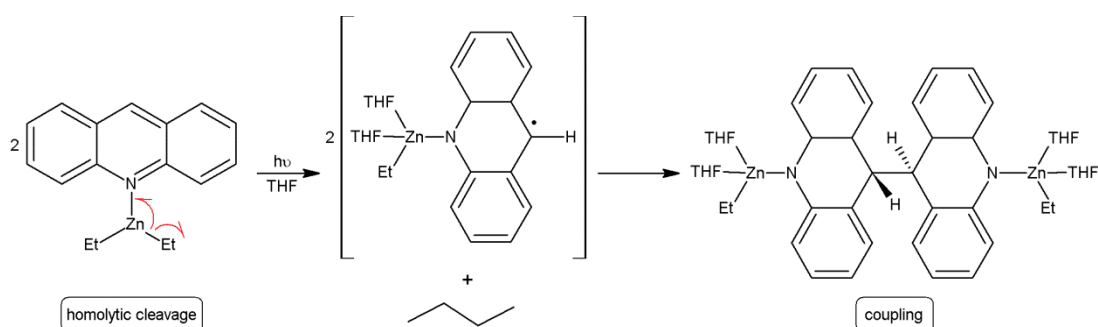


Figure 4.14 Chemdraw representations of $[(\text{Cp}^*)_2\text{Sm}]_2[\mu\text{-}\eta^3\text{-}\eta^3\text{-(C}_{13}\text{H}_9\text{N)}_2]$ ^[173] (left) and $[(\text{C}_4\text{Me}_4\text{P})_2\text{Sm}]_2[\mu\text{-(NC}_{13}\text{H}_9\text{-C}_{13}\text{H}_9\text{N})]$ ^[174] (right).

Although the acridine nitrogen of **22** remains almost perfectly trigonal planar (sum of the angles about N1 = 358.92 °) the loss of aromaticity in the central ring is evidenced by the sp^3 hybridisation of C7 (angles about C7 range from 108.3(2) to 111.5(2) °, average 109.5 °), which leaves it 0.4724(23) Å out of the plane of the central ring (defined by C1, C6, C8, C13). Of the two previous examples above, the best comparison is with the cyclopentadienyl samarium complex $[(\eta^5\text{-C}_5\text{Me}_5)_2\text{Sm}_2][\mu\text{-}\eta^3\text{-}\eta^3\text{-(C}_{13}\text{H}_9\text{N)}_2]$ ^[173] which displays the same *anti* conformation of

the acridine ring systems as that of **22** and that of the resulting 9,9',10,10'-tetrahydro-9,9'-bisacridine.^[175] Each of these display a N-C9-C9'-N' torsion angle of 180.00 °, and C9-C9' bond lengths of 1.59 Å, near identical to that of **22** (C7-C7' = 1.593(5) Å) and typical for a C-C single bond. These structures display more distortion of the acridine scaffold than in **22**, however; as although both have almost perfectly tetrahedral bridging carbon atoms (average angle subtended at C9 109.47 °), the nitrogen atoms display more pyramidal geometries, with the sum of the angles about N1 being 335.61 ° for the samarium complex and 350.48 ° for the tetrahydro-compound *versus* 358.92 ° for **22**.

These samarium complexes were both formed on addition of acridine to a solution of the relevant sandwich complex (Sm(C₅Me₅)₂ or Sm(C₄Me₄P)₂) in toluene, and DFT calculations have suggested that they form via a single electron transfer mechanism.^[174] Diethylzinc itself is known to undergo homolytic Zn-C cleavage at elevated temperatures^[16, 176] and a radical mechanism also seems likely for the formation of **22** (Scheme 4.13).



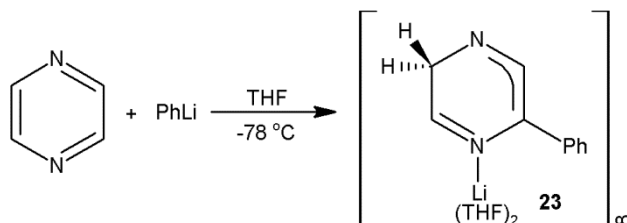
Scheme 4.13 Reaction of ZnEt₂ and acridine to form **22**.

Although these reactions were never heated, it became apparent through multiple failed attempts to repeat the coupling that such a reaction must have been initiated when the schlenk was left on the bench and exposed to natural light for a period of 21 days. Thus, subjecting a 1:1 molar ratio of acridine and ZnEt₂ in THF solution to UV irradiation successfully gave [(THF)₂Zn(Et)]₂[μ-(NC₁₃H₉-C₁₃H₉N)] **22** in up to an 18 % yield. Although the formation of **22** is clearly a minor side reaction – being

the major product of reaction of the coordination adduct – these results show the potential for the $[\text{Et}_2\text{Zn}(\text{Acr})]$ complex to undergo SET processes.

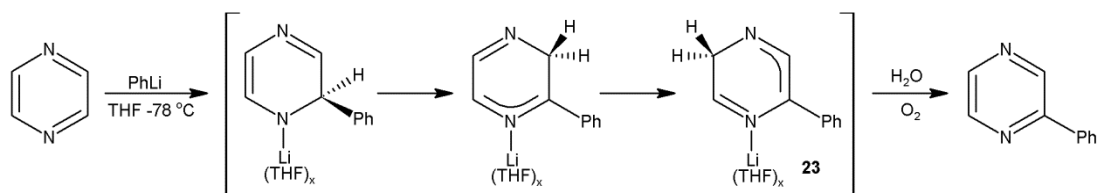
4.4.2 Pyrazine

Building on these acridine studies, we extended our arylation methodology to pyrazine, which had already proven to be a suitable substrate for functionalisation by the alkyllithium zincate $[\text{LiZn}(\text{tBu})_3(\text{PMDETA})]$ **14**.^[147] Firstly the reaction of pyrazine with the separate homometallic components of **15** and **16** was examined, and it was expected that these reactions would mirror those observed with acridine; where LiPh effects nucleophilic addition, while ZnPh_2 remains inert. Thus the reaction of phenyllithium and pyrazine was performed at -78°C and, upon storage at this temperature, the reaction intermediate **23** was subsequently isolated in a crystalline yield of 71 % (Scheme 4.14).



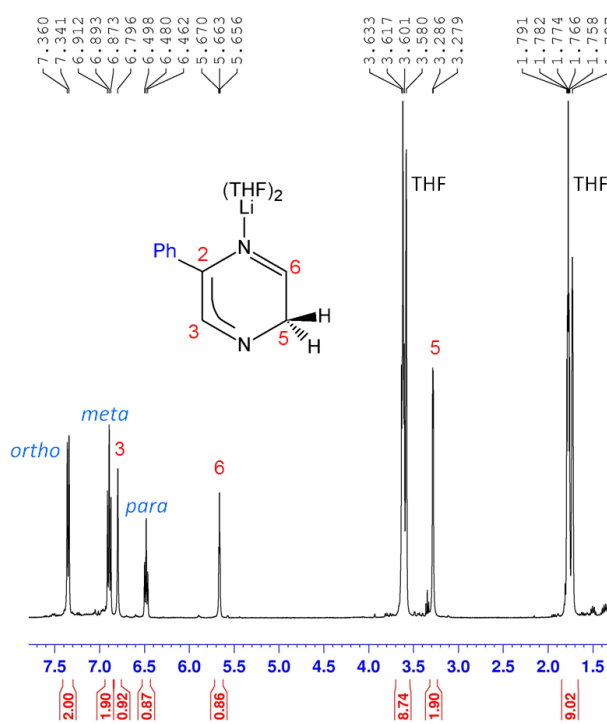
Scheme 4.14 The dearomatising arylation of pyrazine with phenyllithium.

^1H NMR analysis of these crystals in d_8 -THF solution indicated that the pyrazine had lost its aromaticity – with a resonance at 3.28 ppm evidencing the presence of a methylene group. This signal was assigned to the protons in the C5 position, suggesting that the addition occurs followed by a tautomerisation to $[(\text{THF})_2\text{Li}(\text{N}_2\text{C}_4\text{H}_4\text{-Ph})]_\infty$ **23** via a H-shift from the C2 to the C5 position (Scheme 4.15).



Scheme 4.15 Phenyllithium addition to pyrazine and the subsequent tautomerisation to **23**.

Thus, the ¹H NMR spectrum of **23** displays a singlet at 6.79 ppm and a triplet at 5.66 ppm, corresponding to the protons in the C3 and C6 positions respectively, and the doublet at 3.28 ppm was assigned to the remaining two protons in the C5 position (Spectrum 4.5). This spectrum is in stark contrast to the ¹H NMR spectrum of the free heterocycle in the same solvent which consists of a lone singlet at 8.55 ppm. The loss of aromaticity is also evident in the ¹³C NMR spectrum, where the resonance for C5 appears at 51.3 ppm, significantly upfield to that of the pyrazine starting material (146.1 ppm). Finally, the presence of lithium was confirmed by a resonance in the ⁷Li NMR spectrum at 0.19 ppm.



Spectrum 4.5 ¹H NMR spectrum of **23** in d₈-THF.

The structure of **23** was determined crystallographically, revealing an infinite polymeric chain arrangement, propagated via the interaction of each lithium atom with the pyridine-type nitrogen of a neighbouring heterocycle (Figure 4.15, Table 4.14).

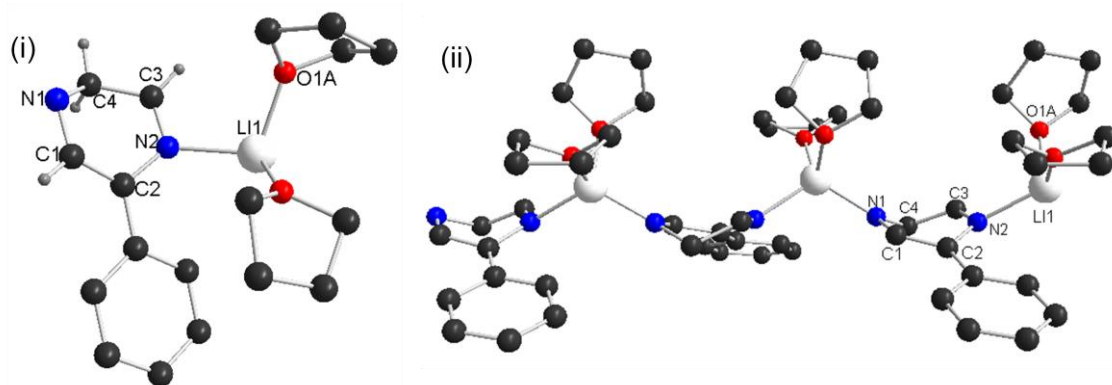


Figure 4.15 Structure of $[(\text{THF})_2\text{Li}(\text{N}_2\text{C}_4\text{H}_4\text{-Ph})]_\infty$ **23**; (i) asymmetric unit, and (ii) extended polymeric chain. Hydrogen atoms (excluding those of the heterocyclic ring in (i)) have been omitted for clarity.

Table 4.14 Selected bond lengths (Å) and angles (°) for 1-lithio-4-phenyl-2-hydroxypyridine **23**.

Li1–N1	1.974(6)	N1–C4	1.459(3)
Li1–N2	2.062(5)	N2–C3	1.285(3)
N1–C1	1.357(3)	N2–C2	1.400(3)
O2–Li1–O1	102.7(11)	O2–Li1–N2	117.0(6)
O2–Li1–N1	118.2(7)	O1–Li1–N2	105.1(7)
O1–Li1–N1	104.0(7)	N1–Li1–N2	114.6(2)

The asymmetric unit of **23** shows the addition of the phenyl group to the heterocycle with concurrent loss of aromaticity – as evidenced by the heterocyclic ring deviating from its planar aromatic geometry to a boat-type conformation. The C2 and C5 positions (C2 and C4 in Figure 4.15) are raised with respect to the other ring atoms;

this results in C2 being 0.2920 Å out of the plane defined by N2, C3 and N1, while C4 lies 0.6205 Å out of the same plane, and the angle between the plane of [C2, C1, N1, C4] and that of [C2, N2, C3, C4] is 42.624 ° through the C2-C4 axis. The C5 position is now sp³ hybridised with the bond angles subtended at C4 ranging from 107.8 ° to 110.2 °, with an average angle of 109.5 °. Furthermore, the N1-C4 and C4-C3 bonds are elongated (1.459(3) and 1.487(4) Å, respectively) with respect to those on the other side of the ring. These bonds average out at 1.386 Å, suggesting that one half of the pyrazine ring retains some level of conjugation; however, as a consequence of the restrictive cyclic structure, the lengthening of the bonds about C4 also results in the contraction of the N2-C3 bond (1.285(3) Å).

The distorted tetrahedral lithium (angles about Li1 range from 102.7(11) to 118.2(7) °, average 110.3 °) coordinates to the N2 atom (2.062(5) Å) of the heterocyclic ring and the second pyridine-type nitrogen (N1) of a neighbouring unit (1.974(6) Å), while two molecules of THF satisfy its coordination sphere. The related zincate compound [(PMDETA)Li(C₄N₂H₄-2-^tBu)Zn^tBu₂],^[147] which results from the addition of a *tert*-butyl group to pyrazine, has a similar Li-N contact (1.9811 Å) to the Li1-N1 distance of 1.974(6) Å found in **23**. A search of the CCDB revealed only four other examples of dearomatised pyrazine structures involving lithium,^[177] however, in each of these cases the compounds were obtained by deprotonation of a dihydropyrazine, and not via the addition of an aryllithium reagent (Figure 4.16). Nonetheless, their lithium-nitrogen distances range from 1.965 to 2.0869 Å,^[177b] in good agreement with those of **23** (1.974(6) Å and 2.062(5) Å).

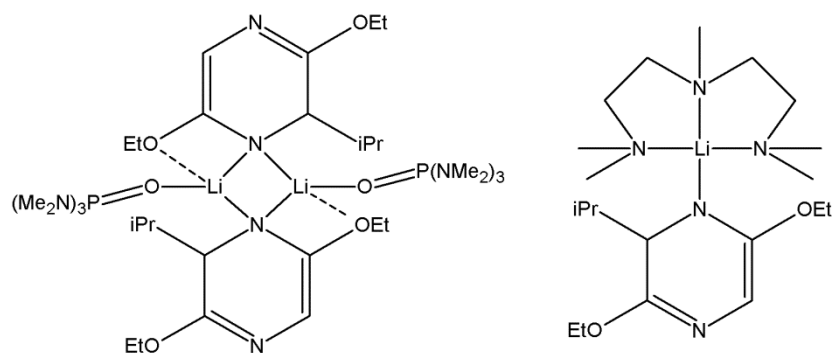
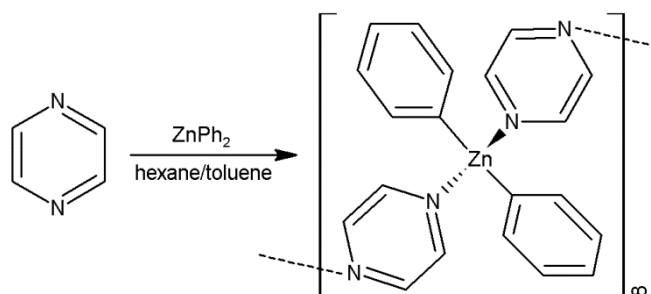


Figure 4.16 Lithiated Schöllkopf's bis[lactim ether] solvated by HMPA (left) and PMDETA (right).^[177b]

Next the reactivity of the homometallic diphenylzinc towards pyrazine was assessed. As with acridine, it was observed that diphenylzinc alone does not promote arylation of the heterocycle. Rather, the ZnPh_2 -pyrazine co-complex $[\text{Ph}_2\text{Zn}(\text{N}_2\text{C}_4\text{H}_4)_2]_\infty$ **24** was isolated from a hexane/toluene mixture in a 27 % crystalline yield (Scheme 4.16).



Scheme 4.16 Coordination of Ph_2Zn and pyrazine to form $[\text{Ph}_2\text{Zn}(\text{N}_2\text{C}_4\text{H}_4)_2]_\infty$ **24**.

The crystals of **24** were poorly soluble in C_6D_6 ; however, their solubility in d_8 -THF allowed for characterisation by ^1H and ^{13}C NMR spectroscopy. The ^1H NMR spectrum consists of a singlet at 8.60 ppm corresponding to the pyrazine protons, a doublet at 7.56 ppm and two multiplets at 7.10 and 7.05 ppm, corresponding to the *ortho*, *meta* and *para* protons of the phenyl groups, respectively. These values are indicative of both free species suggesting that **24** is broken down in THF solution, in the presence of the stronger oxygen donor.

The structure of **24** was determined by X-ray crystallography (Figure 4.17, Table 4.15), and found to consist of a zigzag chain of zinc atoms connected via coordination with the nitrogen atoms of two pyrazine molecules.

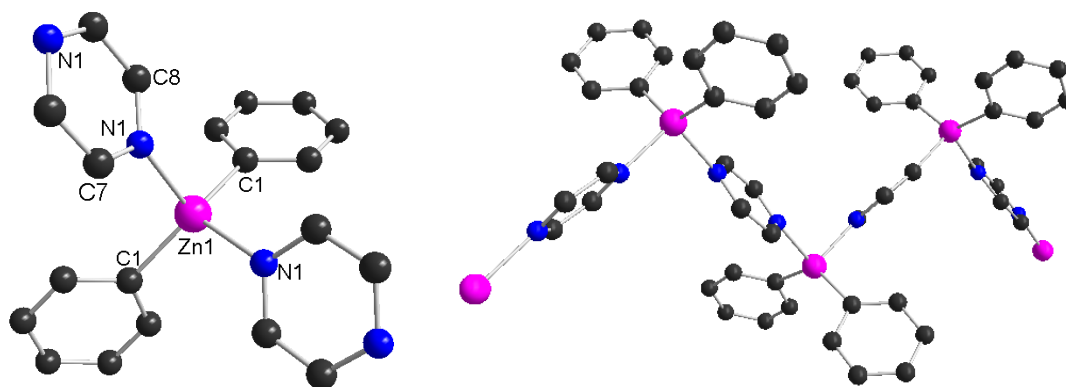


Figure 4.17 Polymeric structure of $[\text{Ph}_2\text{Zn}(\text{pyrazine})]_\infty$ **24**; repeating unit (left) and the extended polymeric chain (right). Hydrogen atoms have been omitted for clarity.

Table 4.15 Selected bond lengths (Å) and angles (°) for $[\text{Ph}_2\text{Zn}(\text{Pyrazine})]_\infty$ **24**.

Zn1-C1	2.0111(17)	Zn1-N1	2.1780(14)
C1-Zn1-C1'	130.17(9)	C1-Zn1-N1	106.10(6)
C1-Zn1-N1'	105.78(6)	N1-Zn1-N1'	98.62(7)

Each zinc atom lies in a distorted tetrahedral environment (bond angles subtended at Zn ranging from 130.17(9) to 98.62(7) °, average = 108.76 °), bonding to the pyrazine rings via Zn-N contacts of 2.1780(14) Å. The structure of **24** is akin to that of the Zn^tBu_2 compound $[\{\text{Zn}^t\text{Bu}_2\}_3\{\text{C}_4\text{H}_4\text{N}_2\}_4]^{[147]}$ (Figure 4.18); however, the steric bulk of the *tert*-butyl group prevents aggregation beyond an open zinc trimer, whereas the planar nature of the phenyl group allows for infinite aggregation. The increased size of the *tert*-butyl group also results in longer Zn-N bonds (2.289 Å)

with respect to those of **24** (2.1780(14) Å), which are more consistent with the Zn-N contacts observed in the monomeric pyridine structure [Ph₂Zn(Py)₂]^[170] (2.1505(12) Å).

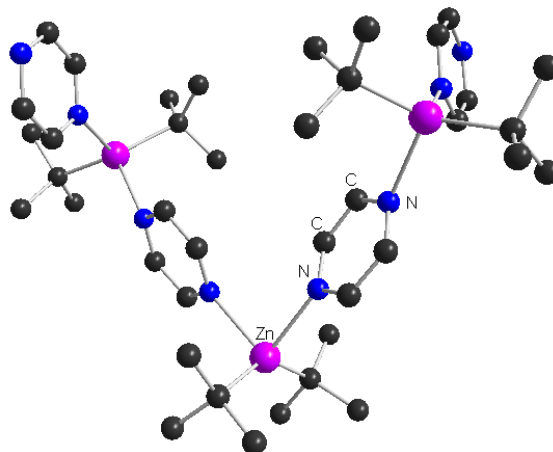
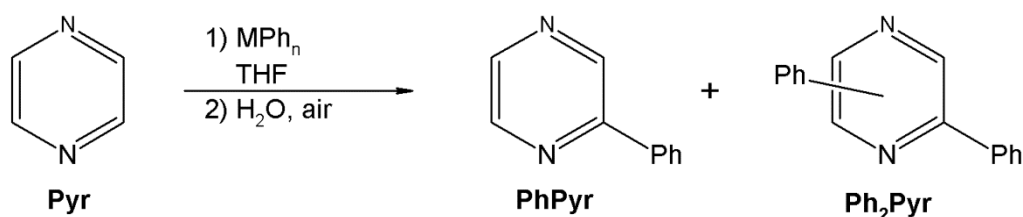


Figure 4.18 Molecular structure of [$\{\text{Zn}^t\text{Bu}_2\}_3\{\text{C}_4\text{H}_4\text{N}_2\}_4$]. Hydrogen atoms have been omitted for clarity.

Having established the contrasting reactivities of the monometallic constituents towards pyrazine, the bimetallic reagents **15** and **16** were then employed. Whereas the lithiation of pyrazine with phenyllithium in THF results in the isolation of 2-phenylpyrazine after two hours at room temperature, following hydrolysis (Table 4.16, entry 1), no reaction with ZnPh₂ was observed even after 24 hours at reflux (entry 2). As with acridine (see section 4.4.1 Acridine), it was noted that neither **15** or **16** react with pyrazine at room temperature, and so the reactions were refluxed for 24 hours before hydrolysis. Again, it was observed that it is possible to promote the arylation process by heating, although in this case only moderate conversion could be achieved, with the higher order zincates **16** and **16·LiCl** again proving to be most effective (Table 4.16, entries 4 (24 %) and 7 (37 %)).

Table 4.16 Reaction of pyrazine with various organometallic reagents.

	MPh_n	Time (hours)	T (°C)	Yield Pyr (%)^{[a][b]}	Yield PhPyr (%)^[a]	Yield Ph₂Pyr (%)^[a]
1	PhLi	2	-78	2	87	0
2	Ph₂Zn	24	75	0	0	0
3	Ph₃LiZn 15	24	75	0	12	2
4	Ph₄Li₂Zn 16	24	75	0	12	24
5	Ph₃LiZn.2LiCl	24	75	0	22	2
6 ^[c]	15•LiCl	24 min	125	0	2	4
7	Ph₄Li₂Zn.2LiCl	24	75	0	7	36
8 ^[c]	16•LiCl	24 min	125	0	0	14

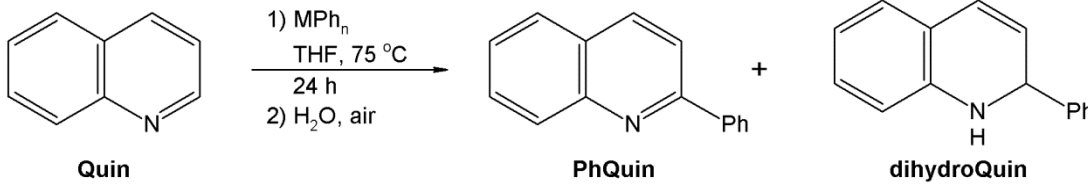
^[a] Yields determined by NMR with respect to a ferrocene internal standard. ^[b] Due to the high volatility of pyrazine, all remaining starting material was lost on work up. ^[c] Reaction performed under microwave irradiation.

The rearomatisation of this substrate occurs spontaneously; however, product mixtures were again obtained due to both mono- and diarylation of the heterocycle. Diarylation was found to predominate with the higher order zincates **16** and **16•LiCl** (Table 4.16, entries 4 and 7). By ¹H and ¹³C NMR the diphenyl isomer formed appears consistent with 2,5-diphenylpyrazine.^[178] Due to their similar polarities the 2-phenyl- and the diphenylpyrazine could not be separated cleanly (by column chromatography or recrystallisation), and the exact identity of the isomer could not be confirmed; however, the 2,5- isomer is expected to be the most stable due to the lack of steric restriction in comparison to the 2,3- or 2,6-diphenyl isomers.

Since microwave irradiation was found to successfully promote the arylation of acridine, the most efficient pyrazine reactions were repeated under microwave conditions (Table 4.16, entries 6 and 8). In contrast to the acridine systems, however, microwave irradiation of the reactions of **16** and **16·LiCl** with pyrazine appeared to inhibit the arylation process and no further optimisation of the microwave methodology was attempted.

4.4.3 Quinoline

As pyrazine appeared to be relatively resistant to nucleophilic addition, it was decided to attempt the arylation of a benzo-fused analogue, on the assumption that the ease of nucleophilic addition to a bicyclic substrate would be intermediate to that of pyrazine and acridine. Thus, quinoline was chosen as the next substrate and the reaction of both homometallic reagents were first examined. The reaction of phenyllithium with quinoline (THF, -78 °C, followed by hydrolysis) leads to a 35 % yield of 2-phenylquinoline and 65 % of 2-phenyl-1,2-dihydroquinoline at room temperature, as determined by ¹H NMR spectroscopy with respect to a hexamethylbenzene internal standard (Table 4.17, entry 1). When attempting to purify this mixture by column chromatography, however, it was found that the dihydro-species oxidised to 2-phenylquinoline on silica, resulting in much higher yields of the fully aromatic product (approximately 70 %).

Table 4.17 Reaction of quinoline with various organometallic reagents.


	MPh_n	Time (hours)	T (°C)	Yield Quin (%) ^[a]	Yield PhQuin (%) ^[a]	Yield DihydroQuin (%) ^[a]
1	PhLi	2	18	0	35	65
2	Ph₂Zn	24	75	97	0	0
3	Ph₃LiZn 15	24	75	17	50	26
4	Ph₄Li₂Zn 16	24	75	0	64	36
5	Ph₃LiZn.2LiCl 15·LiCl	24	75	12	57	2
6	Ph₄Li₂Zn.2LiCl 16·LiCl	24	75	6	70	9

^[a] Yields determined by NMR with respect to a hexamethylbenzene internal standard.

Again, zincates **15** and **16** were found not to promote arylation at room temperature; however, refluxing the reaction afforded 2-phenylquinoline following aqueous work up - 50 % for **15** and 64 % for **16** (Table 4.17, entries 3 and 4 respectively). The presence of the dihydro species indicates incomplete oxidation; however, unlike the acridine studies rearomatisation occurs on column during purification, and therefore the use of an external oxidant, such as DDQ, would likely not be required with this substrate. In contrast to the trend observed with the previous heterocycles, however, it appears from these results that the presence of lithium chloride in the reaction mixture does not notably improve the efficiency of the reaction (entries 5 and 6).

No addition was observed using diphenylzinc, even under forcing conditions (Table 4.17, entry 2); however, all attempts to isolate crystals of the putative donor complex

resulted in the isolation of the oxygen insertion product $[(\text{Quin})\text{Zn}(\text{OPh})\text{Ph}]_2$ **25** (Figure 4.19).

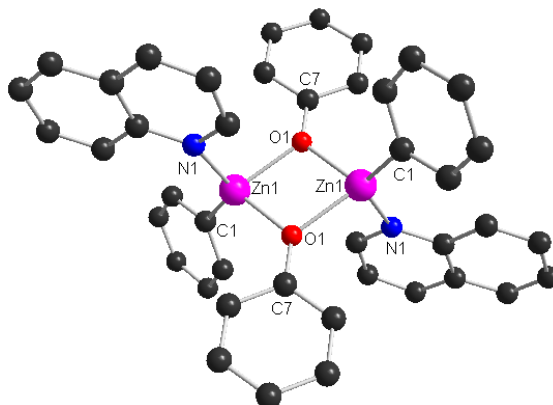


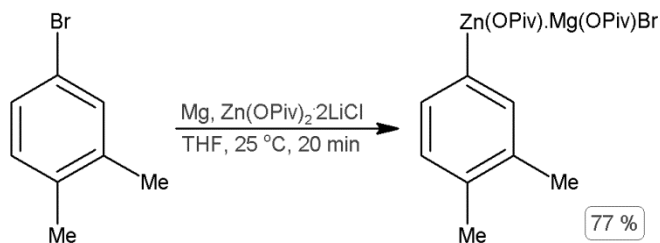
Figure 4.19 Molecular structure of $[(\text{Quin})\text{Zn}(\text{OPh})\text{Ph}]_2$ **25**. H atoms have been omitted for clarity.

The structure of **25** is dimeric, with the heterocycle coordinating to the zinc, as in the donor complexes with acridine and pyrazine (**19** and **24**, respectively). Here, however, the two zinc atoms are bridged by phenoxide ligands, which result from the insertion of oxygen into the Zn-Ph bonds. The remaining phenyl groups bond terminally to the zinc atoms, in a manner reminiscent to that of $[\text{ZnPh}_2]_2$. This oxygen insertion product was isolated multiple times, and due to the sensitivity of this system no lithium quinoline-based structures could be isolated.

4.5 Zinc Pivalates as Arylating Reagents

Recently, Knochel reported that the incorporation of pivalate salts into organozinc reagents increases not only their reactivity, but also their stability towards air and moisture.^[179] These reagents, of type $\text{RZn}(\text{OPiv})\cdot\text{Mg}(\text{OPiv})\text{X}\cdot n\text{LiCl}$ (where OPiv = pivalate, R = aryl, X = Cl, Br, I), were synthesised by transmetalation of the relevant magnesium reagent with the zinc pivalate compound $\text{Zn}(\text{OPiv})_2\cdot 2\text{LiCl}$, and boast only 5 % degradation after exposure to air for 5 minutes (Scheme 4.17).^[179a] As this synthesis was relatively straightforward, it was decided to attempt the arylation of

some of the above heterocycles using these pivalate reagents, anticipating that their enhanced air-stability might aid in the isolation of any reaction intermediates.



Scheme 4.17 Reported synthesis of the air-stable arylzinc pivalate reagents.^[179a]

Thus $\text{Zn(OPiv)}_2\cdot 2\text{LiCl}$ was prepared according to literature methods – by the deprotonation of pivalic acid by methyllithium, followed by transmetalation with ZnCl_2 .^[179a] The pivalate reagent was then reacted with a commercial solution of phenylmagnesium chloride, before the introduction of the *N*-heterocyclic substrate pyrazine. It was found that these mixtures did not promote the arylation of any of the heterocycles used under these conditions; in the absence of a transition metal catalyst, even refluxing for 24 hours was insufficient to promote reaction, resulting only in the recovery of the pyrazine starting material and significant levels of biphenyl as a side product. However, attempts to crystallise organometallic intermediates from this system lead to the isolation of an unprecedented monometallic 16 magnesium cluster $[(\text{THF})_6\text{Mg}_{16}(\text{OPiv})_{12}(\text{O}_2)_4(\text{OH})_{12}]$ **26**, incorporating 12 pivalate anions and, most significantly, 12 hydroxyl groups and four peroxide anions at its core (Figure 4.20).

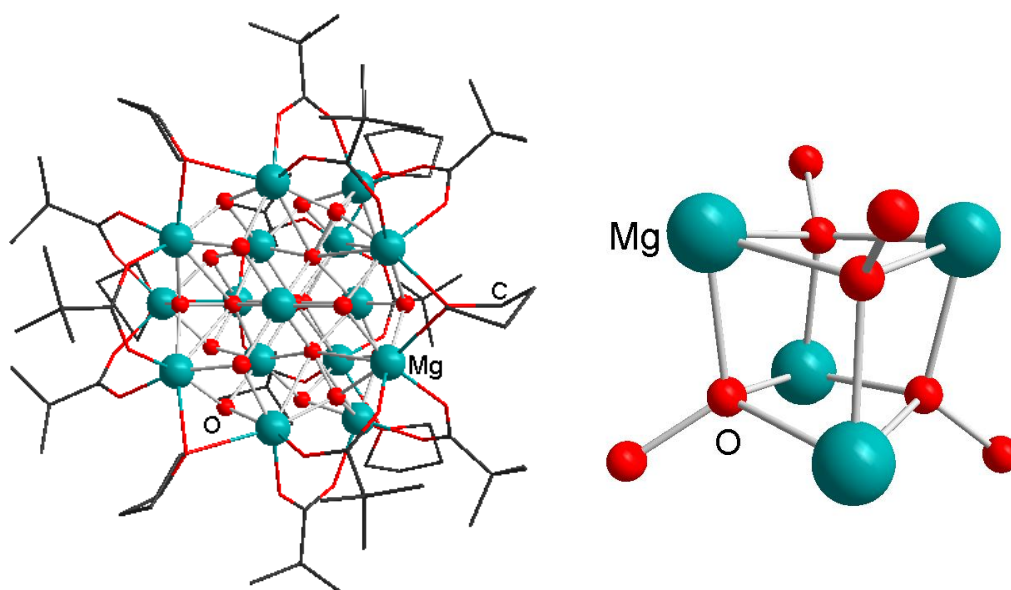


Figure 4.20 Molecular structure of $[(\text{THF})_6\text{Mg}_{16}(\text{OPiv})_{12}(\text{O}_2)_4(\text{OH})_{12}]$ **26** (left), and its peroxide core (right). H atoms have been omitted for clarity.

The lack of phenyl ligands suggests complete transmetalation from $\text{Zn}(\text{OPiv})_2 \cdot 2\text{LiCl}$ to PhMgCl , resulting in the formation of the magnesium pivalate structure **26** (Scheme 4.18, *vide infra*). Furthermore, the assimilation of hydroxyl and peroxide ions into the cluster seems to imply that magnesium pivalate can act as a scavenger, trapping any oxygen and/or moisture contamination present, thus protecting the organozinc from degradation and providing the reported enhanced air-stability. This idea was supported by the isolation of further magnesium clusters (also containing hydroxyl and oxo ions, Figure 4.21) when attempting to prepare samples of the contaminant free $\text{Mg}(\text{OPiv})_2$.^[180]

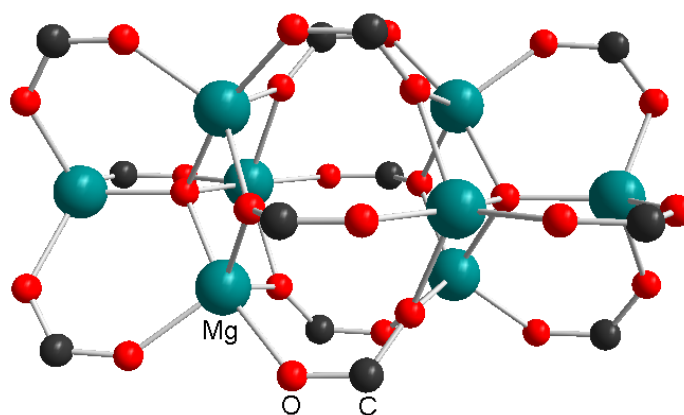


Figure 4.21 Molecular structure of $[\{Mg_6(OPiv)_{12}\}(MgO_2)] \cdot C_7H_8$. H atoms and t Bu groups have been omitted for clarity.

The synthesis of this cluster was found to be reproducible, as all attempts to synthesise $Mg(OPiv)_2$ directly from pivalic acid were hampered by its moisture scavenging ability. In order to prevent any contamination the synthesis had to be performed using carefully dried pivalic acid and $Mg(CH_2SiMe_3)_2$, which had to be prepared and then purified by sublimation.^[180]

As all of the isolated clusters contained only pivalate groups, and no zinc, it would appear that the transmetallation process described for the synthesis of these pivalate reagents does indeed go beyond the monopivalate $Mg(OPiv)X$ constitution of $RZn(OPiv) \cdot Mg(OPiv)X \cdot nLiCl$, instead forming the bispivalate product $Mg(OPiv)_2$ (Scheme 4.18).



Scheme 4.18 Transmetallation of $Zn(OPiv)_2 \cdot 2LiCl$ and Grignard reagents.

Thus, the preparation of both monometallic pivalate compounds was undertaken for comparison. As described, the synthesis of $Mg(OPiv)_2$ had to be performed under strictly controlled conditions to prevent oxygen contamination; however, crystals of $Zn(OPiv)_2 \cdot 2LiCl$ **27** were obtained on recrystallisation from THF, and the molecular structure was determined by X-ray crystallography (Figure 4.22, Table 4.18).

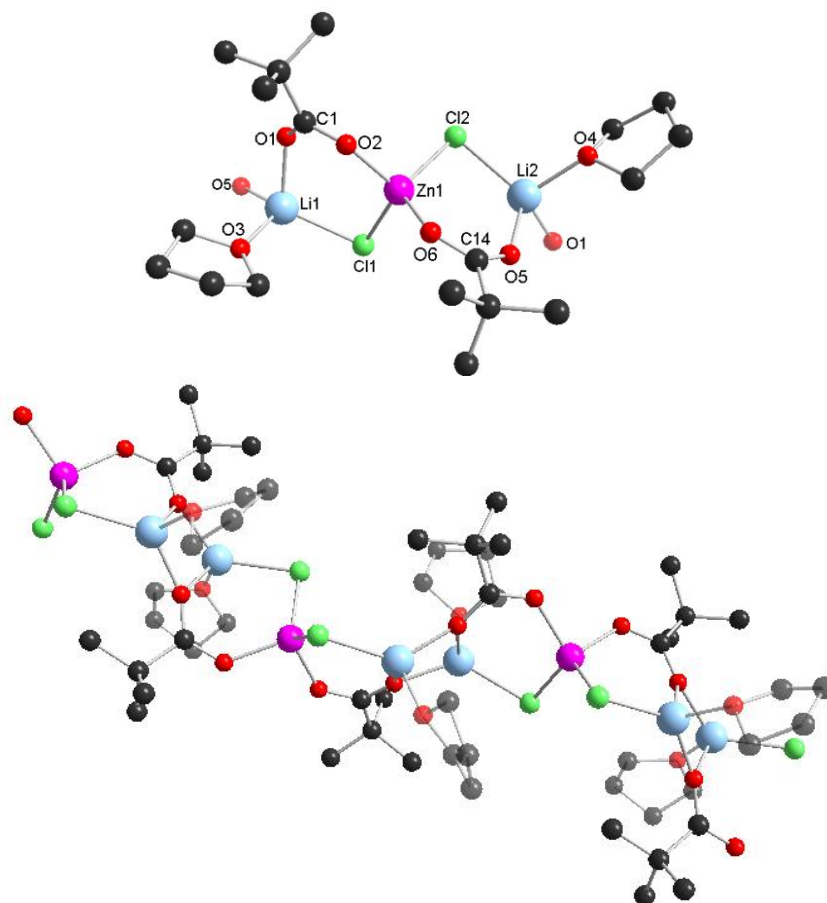


Figure 4.22 Supramolecular structure of $\text{Zn(OPiv)}_2 \cdot 2\text{LiCl}$ **27** with H atoms omitted for clarity. Asymmetric unit (top) and extended polymer chain (bottom).

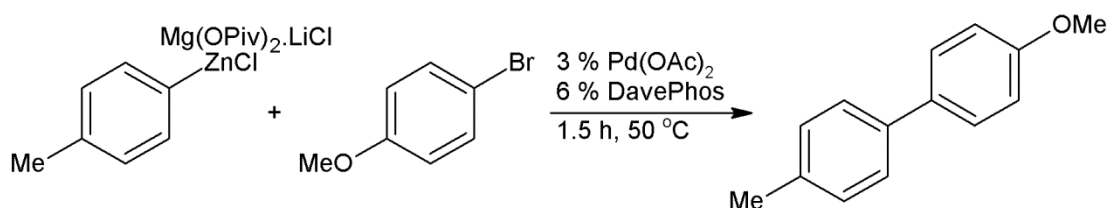
Table 4.18 Selected bond lengths (Å) and angles (°) for $\text{Zn(OPiv)}_2 \cdot 2\text{LiCl}$ **27**.

Zn1-O2	1.9499(16)	Li1-Cl1	2.3744(45)	Li2-Cl2	2.3738(44)
Zn1-O6	1.9531(17)	Li1-O1	1.9647(40)	Li2-O4	1.9430(43)
Zn1-Cl1	2.2549(7)	Li1-O3	1.9156(41)	Li2-O5	1.9430(43)
Zn1-Cl2	2.2476(8)	Li1-O5	1.9452(44)	Li2-O1	1.9308(43)
O2-Zn1-Cl1	114.038(55)	Cl1-Li1-O1	109.929(181)	Cl2-Li2-O4	106.907(195)
O2-Zn1-Cl2	107.453(56)	Cl1-Li1-O3	106.119(185)	Cl2-Li2-O5	113.131(179)
O6-Zn1-Cl2	113.203(60)	O3-Li1-O1	106.356(186)	Cl2-Li2-O1	131.919(210)
O6-Zn1-Cl1	108.272(52)	O3-Li1-O5	110.490(194)	O4-Li2-O5	110.410(191)
O6-Zn1-O2	98.357(68)	O5-Li1-O1	91.092(169)	O4-Li2-O1	100.664(178)
Cl1-Zn1-Cl2	114.482(28)	O5-Li1-Cl1	130.086(219)	O5-Li2-O1	92.184(173)

The lithium chloride solubilises $\text{Zn}(\text{OPiv})_2$ by coordination to both the pivalate and the zinc, satisfying their coordination spheres and forming a trinuclear unit. Thus, the distorted tetrahedral zinc (angles about Zn1 range from 98.357 to 114.482 °, average 106.0 °) bonds to two pivalate groups, at an average bond length of 1.9515 Å, and to the chloride ion of two LiCl units (average Zn-Cl distance = 2.2513 Å). The distorted tetrahedral lithium centres (angles about Li range from 91.092 to 131.919 °, averages 109.0 and 109.2 ° for Li1 and Li2 respectively) bond to their chloride partners (average Li-Cl 2.374 Å) and a single molecule of THF, in addition to the carbonyl oxygen of two $\text{Zn}(\text{OPiv})_2$ units (average Li- O_{Piv} 1.9459 Å), thereby propagating a polymeric arrangement.

Once both contaminant-free compounds were obtained for comparison, the transmetallation process was studied in detail by NMR spectroscopy, and ESI-MS studies were also carried out in collaboration with Kozinowski. These investigations identified a variety of organozincate species in solution, with no $\text{Zn}(\text{OPiv})_2$ being observed, thus confirming the complete transmetallation of $\text{Zn}(\text{OPiv})_2$ to $\text{Mg}(\text{OPiv})_2$ (Scheme 4.18, *vide supra*).^[180]

Further research carried out in collaboration with the Knochel group confirmed the air-stability imparted by the pivalate compounds, with Negishi cross-couplings carried out both in air and under inert atmosphere displaying similar reactivities (Table 4.19).

Table 4.19 Cross-coupling of zinc reagents under inert atmosphere *versus* in air.

Solvent	Reaction Conditions	Yield (%)
THF	Under argon	82
THF	In air	88
EtOAc	Under argon	85
EtOAc	In air	81

In summary, this work has shown for the first time that magnesium pivalates can act as scavengers which help to protect the sensitive organozinc reagents from decomposition in air, allowing short manipulations to be carried out without a significant loss in reactivity, breaking new ground towards the synthesis of new polar organometallic reagents which can be used in the presence of air.^[180]

4.6 Conclusions

In summary, it has been shown that the phenylzincates **15** and **16** are capable of the arylation of several electron deficient *N*-heterocycles via nucleophilic addition without the need for transition metal catalysis. Due to the limited nucleophilicity of the phenyl groups, this methodology requires some heating (75-125 °C), with microwave irradiation proving to be particularly efficient in the case of acridine. It is also apparent from the acridine studies that the activation of multiple phenyl ligands is possible, allowing for the sub-stoichiometric use of both zincates. The presence of lithium chloride (**15**·LiCl and **16**·LiCl) does not appear to be detrimental to their reactivity, although the higher order zincate **16** proved to be the most reactive of all

the mixed-metal reagents studied. The activation of all four of its aryl groups was not achieved; however, it appears that up to three phenyl groups may be transferred in total.

Despite the successful arylation of acridine, the limited nucleophilicity of these zincates restricts their reactivity towards more stable heterocycles such as pyrazine. In this instance, even microwave irradiation is insufficient to promote satisfactory levels of substrate conversion. Quinoline, however, can be converted to 2-phenylquinoline in good yield on reflux (75 °C). Although this substrate has not yet been studied under microwave conditions, it is expected that this would significantly reduce the required reaction time. The potential to increase the substrate to zincate ratio has also yet to be fully investigated; however, initial results appear promising.

New insights have been gained into the the constitution of the organometallic intermediates involved in these reactions. The isolation of the lithium radical anion species **18** and the anionic lithium species **17** suggests that the bimetallic reactions proceed via a different mechanism to that of the monometallic reagent phenyllithium. Thus, although no mixed-metal reaction intermediates were isolated from these systems, it would appear that the zincates remain intact in solution. Similarly, the reaction of LiZnEt_3 **20** with acridine also produces a homometallic lithium species, $[(\text{TMEDA})(\text{THF})\text{Li}(\text{NC}_{15}\text{H}_{14})]$ **21**, alongside $\text{Et}_2\text{Zn}(\text{TMEDA})$. Furthermore, the isolation of the diphenylzinc donor complexes **19** and **24** provide the first structural evidence of any intermediates in the transition metal catalysed arylation reactions described by Hyodo and Tobisu.^[117a, 144, 146]

Thus, zincates **15** and **16** provide a useful alternative for the arylation of several electron-deficient *N*-heterocycles, avoiding the use of expensive transition metal catalysts, and with the aid of microwave irradiation, significantly reducing reaction times. Due to the reduced polarity of the mixed-metal reagents, this bimetallic approach offers a milder arylation technique than the addition reactions of their organolithium precursors, which in turn should provide a greater functional group

tolerance. As such, the use of functionalised heterocycles and functionalised aryl groups would offer a logical extension to the current methodology.

Chapter 5 Synthesis of Zincates Containing Bulky Bis(amido)silyl Ligands

Ligands

5.1 Zinc-Zinc Bonding and the use of Bulky ligands

In 2004 Carmona *et al* reported the synthesis of the first stable Zn(I) compound, decamethyldizincocene $[\text{Zn}_2(\eta^5\text{-C}_5\text{Me}_5)]$, containing a hitherto unprecedented zinc-zinc bond.^[181] This situation was made possible by the kinetic stabilisation provided by the bulky cyclopentadienyl ligands employed.^[182] Since this pioneering discovery there have been numerous instances of Zn-Zn bonds reported in the literature, reaching a total of 25 compounds in 2012,^[183] all of which are supported by sterically demanding, often chelating ligands such as β -diketiminates, substituted arenes or cyclopentadienes, or bis(amido)silyl ligands (Figure.5.1).^[182-184]

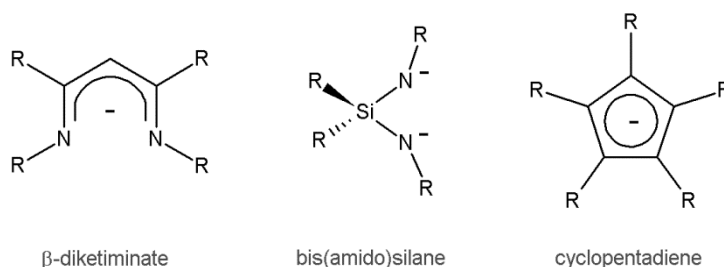
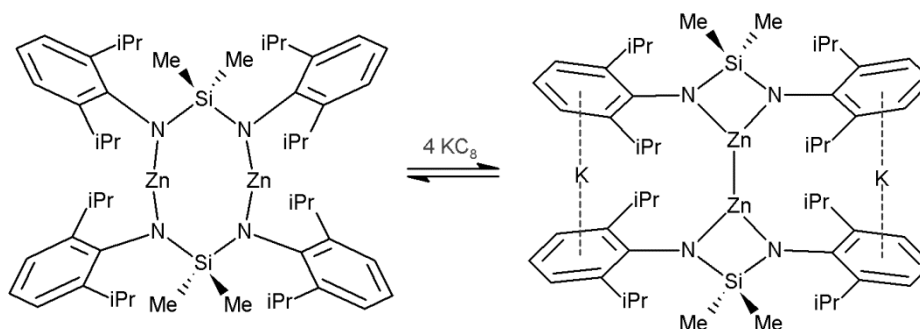


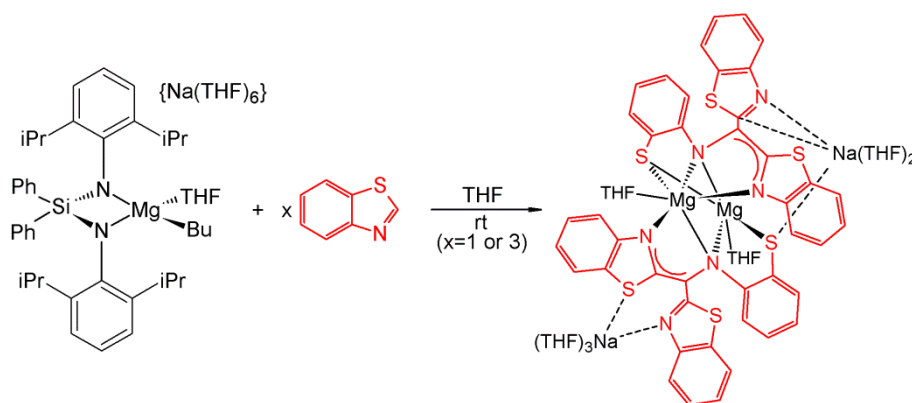
Figure.5.1 Sterically demanding ligands.

Following previous success in stabilising Mo-Mo quadruple bonds with bis(amido)silyl ligands, Tsai and co-workers reported the synthesis of the dizinc anion $[(\eta^2\text{-Me}_2\text{Si}(\text{NDipp})_2)\text{ZnZn}(\eta^2\text{-Me}_2\text{Si}(\text{NDipp})_2)]^{2-}$ by the reduction of a neutral zinc complex with potassium graphite (Scheme.5.1).^[185]



Scheme.5.1 Synthesis of $K_2[\{Me_2Si(NDipp)_2\}_2Zn_2]$.

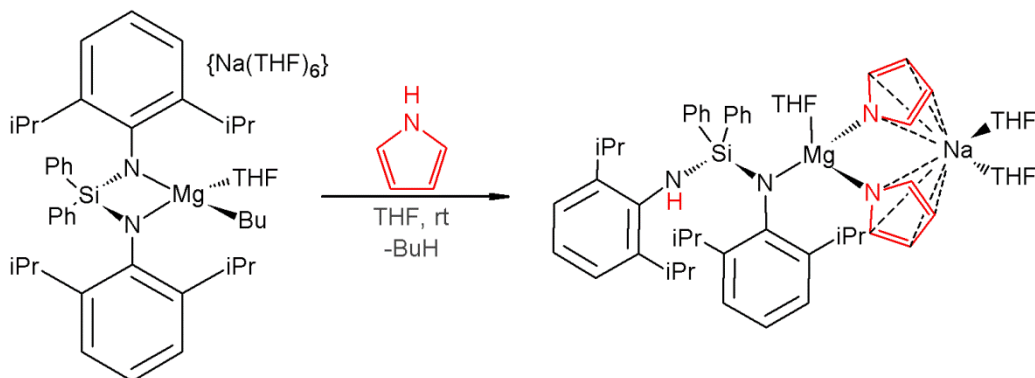
Such bis(amido)silyl ligands are well known in main group chemistry,^[186] for example in magnesium chemistry, where the tetraaryl $[Ph_2Si(NDipp)_2]^{2-}$ ligand has been found to assist in the room temperature ring-opening cascade reaction of benzothiazole (Scheme.5.2).^[187] Our group has shown that sodium magnesiate $[\{Na(THF)_6\}^+\{(Ph_2Si(NDipp)_2)MgBu(THF)\}^-]$ **28** not only ring-opens benzothiazole, but that this ring-opened substrate then couples to two further intact benzothiazole molecules creating a novel trianionic ligand. The formation of this complex ligand contrasts to the reactivity observed when Hauser bases^[188] or Grignard reagents are used,^[3, 156d] which results simply in the deprotonation of the substrate at the C2 position.



Scheme.5.2 Ring-opening of benzothiazole.

Despite the widespread use of such bulky ligands to provide steric stabilisation of metal complexes, there are a limited number of reports assessing their effect on the

reactivity of the resulting compounds. Thus, intrigued by the remarkable activity observed with benzothiazole, the reactivity of this sodium magnesiate towards other substrates was also investigated.^[189]



Scheme 5.3 Deprotonation of pyrrole with $[\{\text{Na}(\text{THF})_6\}^+\{(\text{Ph}_2\text{Si}(\text{NDipp})_2)\text{MgBu}(\text{THF})\}^-]$ **28**.

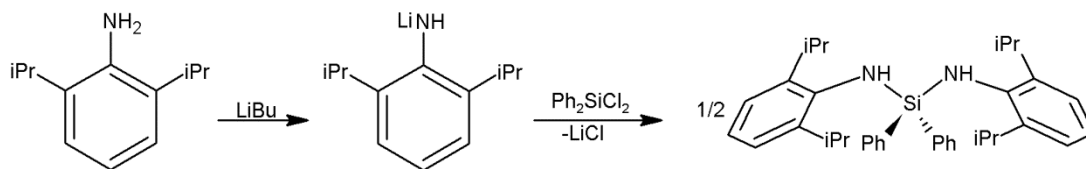
These studies confirmed the polybasicity of the magnesiate reagent and demonstrated the ability to selectively magnesiate substrates such as *N*-methylbenzimidazole and pyrrole (Scheme 5.3). Given the intriguing reactivity displayed by $[\{\text{Na}(\text{THF})_6\}^+\{(\text{Ph}_2\text{Si}(\text{NDipp})_2)\text{MgBu}(\text{THF})\}^-]$ **28**, an investigation into the synthesis and reactivity of related sodium zincates supported by the bulky bis(amido)silyl ligand $[\text{Ph}_2\text{Si}(\text{NDipp})_2]^{2-}$ was carried out.

5.2 Synthesis of Sodium Zincates based on $\text{Ph}_2\text{Si}(\text{NHDipp})_2$

5.2.1 Synthesis of $\text{Ph}_2\text{Si}(\text{NHDipp})_2$

As discussed above, the bisamide $[\text{Ph}_2\text{Si}(\text{NHDipp})_2]^{2-}$ has been previously employed as a bulky ligand and the resulting magnesiate compound $[\{\text{Na}(\text{THF})_6\}^+\{(\text{Ph}_2\text{Si}(\text{NDipp})_2)\text{MgBu}(\text{THF})\}^-]$ **28** has been shown to promote the ring-opening cascade reaction of benzothiazole.^[187] The ligand precursor $\text{Ph}_2\text{Si}(\text{NHDipp})_2$ was prepared according to the literature procedure described by Murugavel in 2003 (Scheme 5.4).^[186b] Thus, the deprotonation of DippNH_2 with

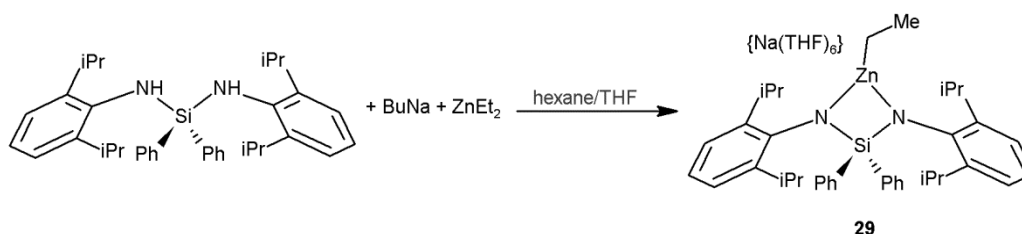
butyllithium was followed by reaction with Ph_2SiCl_2 . Following the removal of lithium chloride, storing the resulting solution at $-27\text{ }^\circ\text{C}$ resulted in the formation of colourless crystals of $\text{Ph}_2\text{Si}(\text{NHDipp})_2$. These crystals were isolated and used in the synthesis of the two zincate bases described below.



Scheme 5.4 Synthesis of $\text{Ph}_2\text{Si}(\text{NHDipp})_2$.

5.2.2 Synthesis of $[\{\text{Na}(\text{THF})_6\}^+\{(\text{Ph}_2\text{Si}(\text{NDipp})_2)\text{ZnEt}\}^-] \mathbf{29}$

The sodium magnesiate $[\{\text{Na}(\text{THF})_6\}^+\{(\text{Ph}_2\text{Si}(\text{NDipp})_2)\text{MgBu}(\text{THF})\}^-] \mathbf{28}$ was prepared by reaction of the diphenyl(diamino)silane $\text{Ph}_2\text{Si}(\text{NHDipp})_2$ (above) with the homoleptic magnesiate $[\text{NaMgBu}_3]$ and a similar procedure was employed to synthesise the zincate analogue $[\{\text{Na}(\text{THF})_6\}^+\{(\text{Ph}_2\text{Si}(\text{NDipp})_2)\text{ZnEt}\}^-] \mathbf{29}$. Thus, the trialkylzincate $[\text{NaZnBuEt}_2]$ was prepared *in situ* by the addition of diethylzinc to a suspension of butylsodium in hexane. The reaction of this zincate with a single equivalent of the silane, followed by the addition of THF, resulted in the formation of a colourless oil which forms crystals of **29** on storage at $-27\text{ }^\circ\text{C}$ (65 % yield, Scheme 5.5).



Scheme 5.5 Synthesis of $[\{\text{Na}(\text{THF})_6\}^+\{(\text{Ph}_2\text{Si}(\text{NDipp})_2)\text{ZnEt}\}^-] \mathbf{29}$.

Multinuclear ^1H and ^{13}C NMR analysis of these crystals confirmed the presence of the amido ligand and the ethyl group in a one to one ratio; with multiplets in the ^1H NMR spectrum in C_6D_6 corresponding to the phenyl groups, at 7.53 and 7.09 ppm (*ortho* and *meta/para* respectively), and those corresponding to the Dipp groups at 7.18 and 6.98 ppm (*meta* and *para* respectively). The double deprotonation of the bisamine was implied by the lack of amido protons, which resonate at 3.52 ppm in the ^1H NMR spectrum of the free amine in the same solvent. The isopropyl substituents were evidenced by a singlet at 1.14 ppm and a septet at 4.27 ppm, the latter being significantly downfield with respect to the same resonance in the free amine (3.39 ppm). The methylene protons of the ethyl group appear at 0.45 ppm, in a similar range to the resonance displayed by that of $[(\text{TMEDA})\text{LiZn}(\textit{cis}\text{-DMP})\text{Et}_2]$ (0.39 ppm).^[190]

The ^{13}C NMR spectrum displays the relevant signals for the amido ligand, and those of the ethyl group appear at 13.0 ppm (methyl) and 9.0 ppm (methylene). THF is also evident, appearing in both the ^1H and ^{13}C NMR spectra, integrating to a ratio of three THF molecules per ligand. The molecular structure of **29** was determined by single crystal X-ray diffraction studies (Figure 5.2, Table 5.1), which show that this bimetallic compound exhibits an SSIP structure similar to that established for the magnesium species $[\{\text{Na}(\text{THF})_6\}^+\{\text{(Ph}_2\text{Si}(\text{NDipp})_2\text{)MgBu}(\text{THF})\}^-]$ **28**.

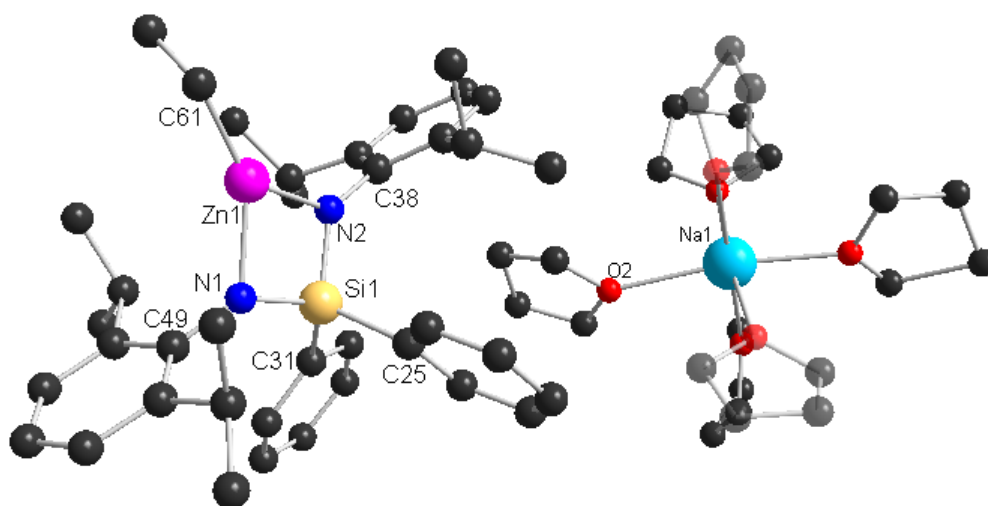


Figure 5.2 Molecular structure of $[\{\text{Na}(\text{THF})_6\}^+\{\text{(Ph}_2\text{Si}(\text{NDipp})_2\text{)ZnEt}\}^-]$ **29**. H atoms have been omitted for clarity.

Table 5.1 Selected bond lengths (Å) and angles (°) for **29**.

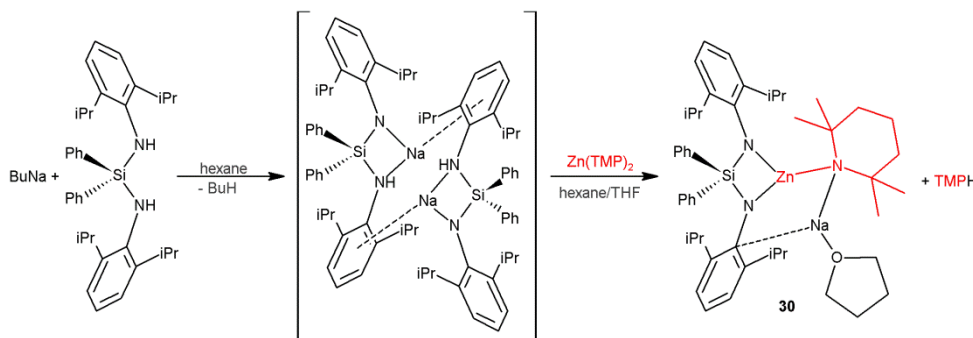
Zn1-N1	2.0106(16)	Si1-N1	1.6927(16)
Zn1-N2	1.9707(15)	Si1-N2	1.7020(16)
Zn1-C61	1.968(2)		
C61-Zn1-N2	141.36(10)	Si1-N1-Zn1	90.58(7)
C61-Zn1-N1	138.39(10)	C38-N2-Si1	134.97(13)
N2-Zn1-N1	79.64(6)	C38-N2-Zn1	132.86(12)
C49-N1-Si1	134.36(14)	Si1-N2-Zn1	91.67(7)
C49-N1-Zn1	128.32(13)		

29 is composed of the same $\{\text{Na}(\text{THF})_6\}^+$ cation as **28** (in which the sodium atom is solvated by six THF molecules) and a zincate anion. The distorted trigonal planar zinc (angles about zinc range from 79.64(6) to 141.36(10) °, sum = 359.39 °) is bound to the bis(amido)silyl ligand by the chelation of the two nitrogen atoms (N1-Zn1-N2 = 79.64 °). These both display a trigonal planar geometry (sum of the angles about N1 = 353.26 ° and N2 = 359.5 °), although the geometry imposed by the chelating ligand results in some distortion due to the bulk of the aryl substituents. The zinc-nitrogen bond lengths (2.0106(16) Å to N1 and 1.9707(15) Å to N2) show marginally unequal bonding, which can again be attributed to the bulk of the amido ligand; these contacts are similar to the Zn-N bonds of the related bis(silyl)amido zinc complex $\text{K}_2\{[\text{Me}_2\text{Si}(\text{NHDipp})_2]_2\text{Zn}_2\}$ which also displays chelation of the zinc atoms (2.025 and 1.992 Å, Scheme.5.1, *vide supra*).^[185] The shorter Zn1-N1 interaction (1.9707(15) Å) is comparable to the 1.9851 Å bonding found in the terminal zinc-amide bond of $[(\text{PMDETA})\text{LiZn}(\text{HMDS})\text{Me}_2]$ **5**,^[29d] whereas the longer interaction is more in the range of a bridging amide bond, such as that of $[(\text{PMDETA})\text{LiZn}(\text{NHDipp})\text{Me}_2]$ **10**,^[88] which also contains the bulky Dipp group (Zn-N = 2.0869 Å), or the zinc amidinate complex $[\{\text{MeC}(\text{N}^i\text{Pr})_2\}\text{ZnMe}]_2$ which displays an average Zn-N bond length of 2.039 Å.^[191] The Zn1-C61 bond length (1.968(2) Å) is also typical of a bond to a terminal alkyl group, for instance those

found in $[\text{Li}(\text{TMP})\text{ZnEt}_2]$ (2.0137(14) Å),^[94] and $[(\text{TMEDA})\text{ZnMe}_2]$ (average 1.982 Å).^[192]

5.2.3 Synthesis of $[(\text{Ph}_2\text{Si}(\text{NDipp})_2)\text{Zn}(\text{TMP})\text{Na}(\text{THF})]$ **30**

The related homoleptic trisamidozincate $[(\text{Ph}_2\text{Si}(\text{NDipp})_2)\text{Zn}(\text{TMP})\text{Na}(\text{THF})]$ **30** was prepared by the monodeprotonation of $\text{Ph}_2\text{Si}(\text{NHDipp})_2$ by butylsodium, followed by reaction with $\text{Zn}(\text{TMP})_2$ (Scheme 5.6). The addition of THF led to the formation of a colourless solution which deposited crystals on standing at room temperature (75 % yield).



Scheme 5.6 Synthesis of $[(\text{Ph}_2\text{Si}(\text{NDipp})_2)\text{Zn}(\text{TMP})\text{Na}(\text{THF})]$ **30**.

These were identified crystallographically as $[(\text{Ph}_2\text{Si}(\text{NDipp})_2)\text{Zn}(\text{TMP})\text{Na}(\text{THF})]$ **30**, and found to display a contacted ion-pair structure in which the sodium and zinc atoms are linked via the bridging TMP ligand (Figure 5.3, Table 5.2). A secondary electrostatic interaction between the sodium and the *ipso* carbon of one the Dipp groups serves to complete a central five-membered $[\text{NaNZnNC}]$ ring. This structural motif is in sharp contrast to that observed for the related magnesium derivative $[\{\text{Na}(\text{THF})_3\}^+\{(\text{Ph}_2\text{Si}(\text{NDipp})_2)\text{Mg}(\text{TMP})\}^-]$ which exhibits an SSIP structure in the solid state,^[193] although it is reminiscent of other zincates containing the TMP anion, such as $[(\text{TMEDA})\text{Na}(\mu\text{-Ph})(\mu\text{-TMP})\text{Zn}(\text{tBu})]$,^[75] in which the TMP ligand connects the sodium and the zinc, and the alkali metal π -engages with the phenyl group giving rise to a four membered $[\text{NaNZnC}]$ ring.

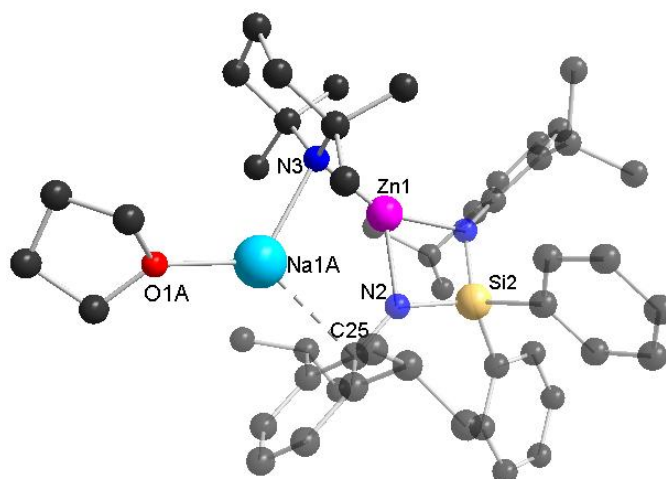


Figure 5.3 Molecular structure of $[(\text{Ph}_2\text{Si}(\text{NDipp})_2)\text{Zn}(\text{TMP})\text{Na}(\text{THF})]$ **30**. H atoms have been omitted for clarity.

Table 5.2 Selected bond lengths (Å) and angles (°) for **30**.

Zn1 – N1	1.922(3)	Na1 – O1A	2.184 (8)
Zn1 – N2	2.042(3)	Na1 – N3	2.453(4)
Zn1 – N3	1.938(3)	Na1 – C25	2.712(5)
N1 – Zn1 – N3	154.77(12)	O1A – Na1 – N3	121.9(3)
N1 Zn1 N2	80.16(12)	O1A – Na1 – C25	130.9(3)
N2 – Zn1 – N3	120.87(13)	N3 – Na1 – C25	105.62(15)

Similarly to **29**, zinc is bound to three anionic ligands; however, due to the bulk of the TMP group in addition to that of the bis(amido)silyl ligand, a slightly pyramidal geometry results (sum of the angles subtended at Zn1 = 355.8 °). Zinc bonds to the TMP with a Zn1-N3 contact of 1.9838(3) Å, which is intermediate to that of the related bisalkyl zincate $[(\text{TMEDA})\text{Na}(\text{TMP})\text{Zn}(\text{tBu})_2]$ **2** (Zn-N = 2.033 Å)^[75] and the parent amide $\text{Zn}(\text{TMP})_2$ (average Zn-N = 1.820 Å).^[194] The two nitrogen atoms of the bis(amido)silyl ligand chelate to the zinc with a bite angle of 80.16(12) ° (N1-Zn1-N2 angle of **29** = 79.64(6) °), and again the bonding is unequal, with Zn-N distances of 1.922(3) and 2.042(3) Å. This uneven Zn-N bonding is more

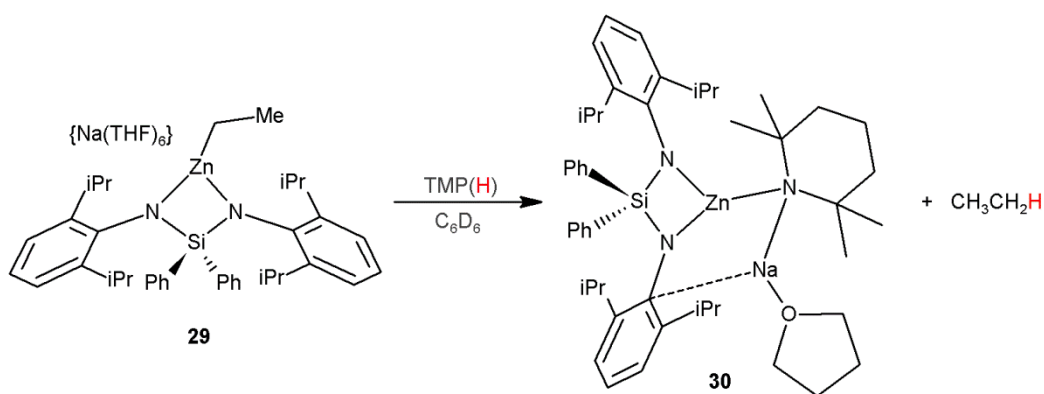
pronounced than in the ethyl zincate **29**, (Zn-N bonds of 1.9707(15) and 2.0106(16) Å) due to accommodating the added bulk of the TMP and the sodium atom. The sodium itself adopts an almost perfectly trigonal planar geometry (sum of the angles about Na1A = 358.42 °), bridging to the zinc via a Na1-N3 bond length of 2.453(4) Å and closing the [NaNZnNC] ring via an electrostatic interaction with the *ipso* carbon of the nearest Dipp group (Na1A-C25 = 2.712(5) Å), as steric restrictions prevent interaction with the amide nitrogen (Na1A-N2 = 3.005(4) Å). These distances are comparable to those observed in [(TMEDA)Na(μ -Ph)(μ -TMP)Zn(^tBu)], which displays a Na-N bond of 2.412 Å and a Na-C distance of 2.706 Å.^[75]

Compound **30** was also fully characterised by ¹H and ¹³C NMR spectroscopy. Thus, the ¹H NMR spectrum in C₆D₆ solution shows the phenyl groups resonating at 7.56 and 7.11 ppm (for the *ortho* and *meta/para* protons respectively), and the aromatic protons of the Dipp groups at 7.18 and 6.95 ppm. These chemical shifts are near identical to the ethyl analogue **29** (*vide supra*); however, the most diagnostic signal – that of the CH of the isopropyl groups – is shifted downfield, from 4.27 ppm in ethyl zincate **29** to 4.37 ppm in TMP zincate **30**. The inclusion of the TMP anion is indicated by a multiplet at 1.47 ppm and a singlet at 1.27 ppm corresponding to the γ - and methyl protons respectively. The β -protons, however, are coincident to the methyl protons of the Dipp groups, which appear as a broad singlet between 0.97 and 1.18 ppm; this is presumably a result of the restricted rotation of the isopropyl groups, suggesting that the contacted structure remains intact in benzene solution. These assignments were confirmed by HSQC experiments, which showed this broad singlet to correspond to two resonances in the ¹³C NMR spectrum – that of the β -carbon of the TMP anion at 40.9 ppm, and the methyl carbon of the isopropyl groups at 25.3 ppm. As with the ¹H NMR spectra, the resonances of the bis(amido)silyl ligand in the ¹³C NMR spectra of both **29** and **30** are essentially identical (Table 5.3).

Table 5.3 Comparison of the ^1H NMR chemical shifts (ppm) of the protons of the bis(amido)silyl ligand in **26** and **27**. The most diagnostic signals are highlighted in red.

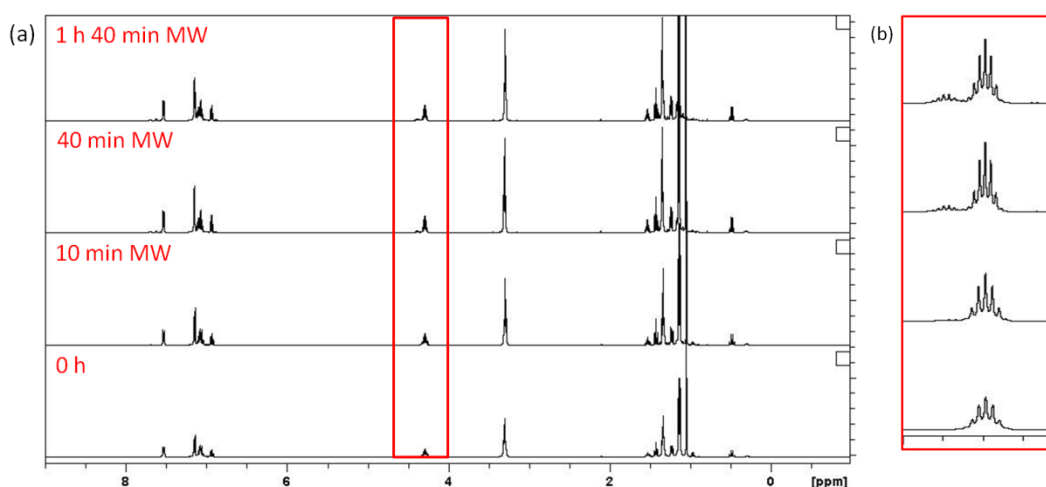
	$[\{\text{Na}(\text{THF})_6\}^+\{(\text{Ph}_2\text{Si}(\text{NDipp})_2)\text{ZnEt}\}^-]$	$[(\text{Ph}_2\text{Si}(\text{NDipp})_2)\text{Zn}(\text{TMP})\text{Na}(\text{THF})]$
	29	30
Ph_{ortho}	7.53	7.56
$\text{Ph}_{meta/para}$	7.09	7.11
Dipp_{meta}	7.18	7.18
Dipp_{para}	6.98	6.95
$i\text{Pr CH}_3$	1.14	1.08
$i\text{Pr CH}$	4.27	4.37

It should be noted that compound **30** was obtained by the stepwise metallation of the bisamine $\text{Ph}_2\text{Si}(\text{NHDipp})_2$, first with NaBu to generate $[\text{Ph}_2\text{Si}(\text{NHDipp})(\text{NDipp})\text{Na}]_2^{[193]}$ *in situ*, which in turn undergoes a second deprotonation on treatment with $\text{Zn}(\text{TMP})_2$. Thus, the reaction of alkyl derivative **29** with a single equivalent of $\text{TMP}(\text{H})$ was studied as an alternative route to **30** (Scheme 5.7).

**Scheme 5.7** Conversion of $[\{\text{Na}(\text{THF})_6\}^+\{(\text{Ph}_2\text{Si}(\text{NDipp})_2)\text{ZnEt}\}^-]$ **29** to $[(\text{Ph}_2\text{Si}(\text{NDipp})_2)\text{Zn}(\text{TMP})\text{Na}(\text{THF})]$ **30**.

Accordingly, isolated crystals of $[\{\text{Na}(\text{THF})_6\}^+\{(\text{Ph}_2\text{Si}(\text{NDipp})_2)\text{ZnEt}\}^-]$ **29** were dissolved in C_6D_6 and a single equivalent of $\text{TMP}(\text{H})$ was introduced. The reaction was monitored over time by ^1H NMR spectroscopy and, although no conversion was

observed on refluxing the reaction for several hours, it was noted that, after extended microwave irradiation, a second isopropyl resonance appeared (Spectrum 5.1). As discussed above, the resonance of the CH of the isopropyl groups in the ^1H NMR spectrum is the most distinctive (see Table 5.3) – whilst the shifts corresponding to the other protons of the bis(amido)silyl ligand are only slightly affected by the substitution of an ethyl ligand for TMP, the CH is shifted marginally downfield from 4.27 ppm (zincate **29**) to 4.37 ppm (zincate **30**).



Spectrum 5.1 (a) ^1H NMR spectra of the reaction of $[\{\text{Na}(\text{THF})_6\}^+\{(\text{Ph}_2\text{Si}(\text{NDipp})_2)\text{ZnEt}\}^-]$ **29** with TMP(H) under microwave irradiation and (b) expansion of the highlighted region.

As can be seen in the expanded portion of the ^1H NMR spectra (Spectrum 5.1(b)), a new isopropyl CH resonance gradually appears alongside that of zincate **29**. This new resonance, at 4.37 ppm, is consistent with that of TMP zincate **30**, although clearly **29** (4.27 ppm) remains the major species in solution. There are no obvious changes in the aliphatic region which would indicate the deprotonation of TMP(H); however, this is most likely due to the low concentration of zincate **30** with respect to the free amine. Based on this evidence it would seem that it is possible to convert **29** to **30**, but the level of conversion is so low, even under such forcing conditions, that this particular method would not be a viable synthesis for **30**. The efficiency of the reaction might conceivably be improved by the use of an alternative solvent with

different dielectric properties, which may enhance effective microwave heating and promote conversion.^[195] Switching to the more polar solvent THF may show improvement, as this particular solvent has already proven useful in the microwave synthesis of functionalised heterocycles (see Chapter 4).

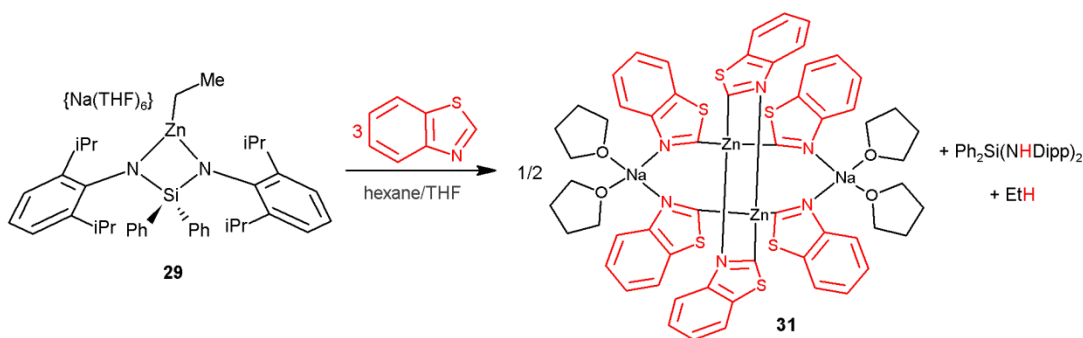
5.3 Reactivity Studies Assessing the Metallating Ability of Zincates **29** and **30**

Alkali metal zincates have an extensive track record of selectively deprotonating a variety of substrates.^[2i, 2j, 21] The isolation and structural characterisation of numerous reaction intermediates stand as evidence that these reactions are performed by the less polar metal, with the alkali metal acting to enhance the reactivity of the zinc and then to stabilise the metallated substrate. This synergic cooperation, observed when two metals are contained within the same reagent, has led to such reactions being termed alkali-metal-mediated-zincations (AMMZn, see Chapter 1). Given the utility of other zincate reagents an investigation of the reactivities of $[\{\text{Na}(\text{THF})_6\}^+\{\text{(Ph}_2\text{Si}(\text{NDipp})_2\text{)ZnEt}\}^-]$ **29** and $[(\text{Ph}_2\text{Si}(\text{NDipp})_2\text{)Zn}(\text{TMP})\text{Na}(\text{THF})]$ **30** was then conducted.

5.3.1 Reaction with Benzothiazole

As the analogous magnesiate $[\{\text{Na}(\text{THF})_6\}^+\{\text{(Ph}_2\text{Si}(\text{NDipp})_2\text{)MgBu}(\text{THF})\}^-]$ **28** displays a novel reactivity towards benzothiazole (Btz), performing the ring-opening and coupling cascade reaction described above,^[187] this heterocycle was chosen as the first substrate to test the metallating ability of zincates **29** and **30**. Benzothiazole is readily deprotonated at the most acidic C2 position (calculated *pKa* of 27.3)^[122] by Grignard and organolithium reagents, although there are no examples in the literature of the metallation of this heterocycle with a single metal organozinc reagent.

Consequently, benzothiazole was added to a solution of $[\{\text{Na}(\text{THF})_6\}^+\{(\text{Ph}_2\text{Si}(\text{NDipp})_2)\text{ZnEt}\}^-]$ **29** in a mixture of hexane and THF, resulting in an instant change from colourless to bright red. This dramatic colour change was accompanied by the precipitation of a highly insoluble solid, which once formed could not be re-dissolved. The solid, once isolated, was poorly soluble in d_8 -THF making spectroscopic analysis difficult. Thus, unable to determine the composition of this product, the reaction was repeated by layering a THF solution of benzothiazole on the surface of a dilute solution of zincate **29** (Scheme 5.8).



Scheme 5.8 Deprotonation of benzothiazole by zincate **29**.

The slow diffusion of the substrate through solution inhibited the reaction rate enough to allow the growth of crystals of suitable quality for X-ray analysis, and the product was subsequently identified as the novel sodium zincate $[\text{Na}(\text{THF})_2\text{Zn}(\text{Btz}^*)_3]_2$ **31** (Figure 5.4, Table 5.4).

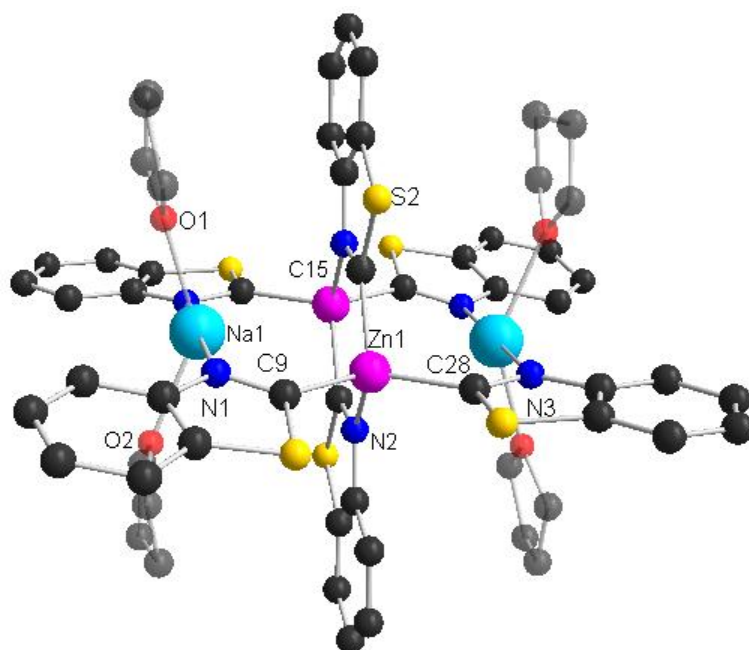


Figure 5.4 Molecular structure of $[\text{Na}(\text{THF})_2\text{Zn}(\text{NSC}_7\text{H}_4)_3]_2$ **31**. H atoms have been omitted for clarity.

Table 5.4 Selected bond lengths (Å) and angles (°) for **31**.

Zn1-N2	2.069(4)	Na1-N1	2.445(5)
Zn1-C9	2.017(6)	Na1-N3	2.442(5)
Zn1-C15	2.037(5)	Na1-O1	2.349(5)
Zn1-C28	2.027(6)	Na1-O2	2.369(5)
C9-Zn1-C28	118.9(2)	O- Na1-O2	138.1(2)
C9-Zn1-C15	108.8(2)	O1-Na1-N3	89.73(16)
C28-Zn1-C15	108.7(2)	O2-Na1-N3	90.68(17)
C9-Zn1-N2	107.83(19)	O1-Na1-N1	93.70(17)
C28-Zn1-N2	107.9(2)	O2-Na1-N1	87.65(17)
C15-Zn1-N2	103.67(18)	N3-Na1-N1	176.32(19)

The structure of **31** shows that no bis(amido)silyl ligand is present; instead, three equivalents of benzothiazole have been deprotonated at the C2 position. The structure is dimeric, consisting of two near perpendicular rings – a 12-membered $[\text{NaNcZnCN}]_2$ ring and a smaller 6-membered $[\text{ZnNC}]_2$ ring (angle between the rings = 88.06°). Each tetrahedral zinc atom (angles about Zn range from $103.67(18)$

to 118.9(2) °, average 109.3 °) bonds to four benzothiazolyl units; three resulting from zincation at the C2 position (C9, C15 and C28 in Figure 5.4, average Zn-C bond length = 2.027 Å), and one via a Zn-N interaction (2.069(4) Å) to a further benzothiazolyl unit (C2 metallated by the other zinc centre), which serves as bridge between the two zinc atoms. The distorted tetrahedral sodium atoms (angles about Na range from 87.65(17) to 176.32(19) °, average 112.29 °) are incorporated into the structure by an interaction with the remaining benzothiazolyl nitrogen atoms. These benzothiazolyl units orientate themselves in such a manner as to enable this chelation, in an almost perfectly linear fashion (N1-Na1-N3 = 176.32(19) °), again forming a bridge between the two zinc atoms.

A search of the CCDB shows that there are no known structures of C2-zincated benzothiazole, and the closest comparative structure is that of the magnesium β -diketiminate compound $[\{\text{DippNC}(\text{Me})\text{CHC}(\text{Me})\text{NDipp}\}_2\text{Mg}_2\{\text{NSC}_7\text{H}_4\}_2]$ ^[196] which also dimerises through interaction of the ring nitrogen to the second metal centre.

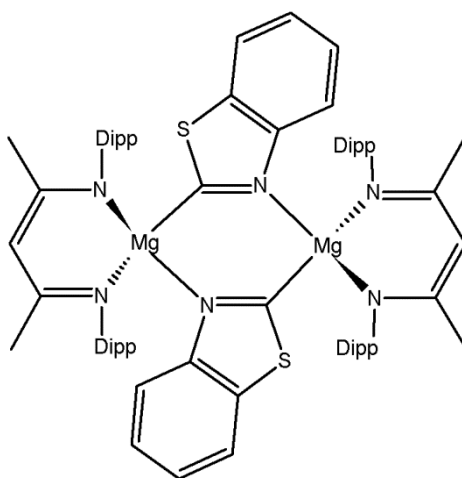


Figure 5.5 Chemdraw representation of $[\{\text{DippNC}(\text{Me})\text{CHC}(\text{Me})\text{NDipp}\}_2\text{Mg}_2\{\text{NSC}_7\text{H}_4\}_2]$ ^[196]

Although zincate **29** does not promote the ring-opening of benzothiazole, as observed with the magnesium analogue **28**,^[187] it can be seen from the molecular structure of **31** that all three of the anionic arms of the zincate have been utilised for deprotonation of the substrate, demonstrating the same polybasicity observed in the

magnesiates systems.^[189] Repetition of this reaction with three equivalents of benzothiazole increases the yield of **31**; however, accurate figures cannot be quoted due to the difficulties of purifying the solids obtained as, although **31** was insoluble in d_8 -THF, ^1H NMR analysis of the solids obtained indicated the presence of unreacted benzothiazole and $\text{Ph}_2\text{Si}(\text{NHDipp})_2$ even after thorough washing.

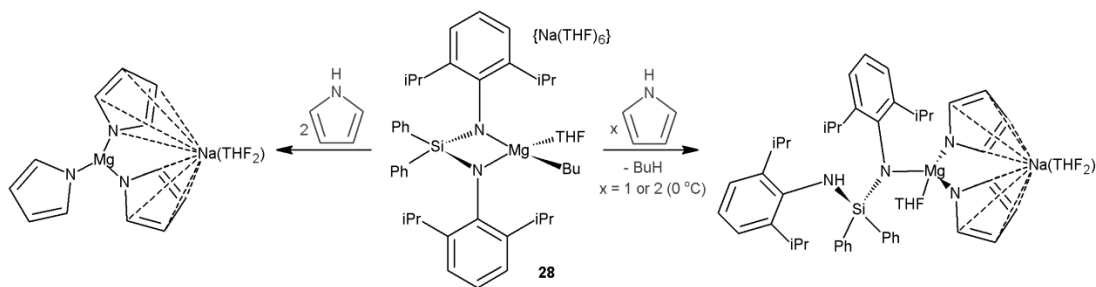
A similar reaction was found to occur between benzothiazole and $[(\text{Ph}_2\text{Si}(\text{NDipp})_2)\text{Zn}(\text{TMP})\text{Na}(\text{THF})]$ **30**. However, this reaction occurred much faster than that with **29** and no crystalline material could be obtained. Due to the limited solubility of the precipitate, the product could not be conclusively identified; however, ^1H NMR analysis of the filtrate suggested the formation of the free $\text{Ph}_2\text{Si}(\text{NHDipp})_2$ ligand and $\text{TMP}(\text{H})$, implying that all three of the anionic ligands had performed a deprotonation. As discussed above, zincate **30** was predicted to be a stronger base than zincate **29**, as such it may be reasonably assumed that both are capable of the deprotonation of benzothiazole and that the same compound, $[\text{Na}(\text{THF})_2\text{Zn}(\text{Btz}^*)_3]_2$ **31**, would be formed in both instances. The ring-opening of the benzothiazole substrate, as observed with the related magnesiate $[\{\text{Na}(\text{THF})_6\}^+\{(\text{Ph}_2\text{Si}(\text{NDipp})_2)\text{MgBu}(\text{THF})\}^-]$ **28**, is unlikely as mixed lithium-zinc systems have not been observed to promote ring-opening of this substrate following deprotonation.^[197]

5.3.2 Reaction with Pyrrole

The five-membered *N*-heterocycle pyrrole was the next substrate to be employed. The deprotonation of this particular substrate by sodium tri-*n*-butylzincate has already been studied in depth,^[90] and it was determined that the structure of the resulting pyrrolylzincate was dependent on the Lewis basic solvent employed, with both lower and higher order zincates isolated.

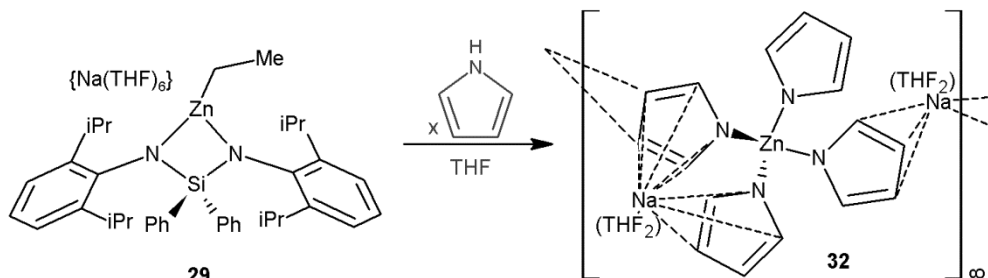
The bis(amido)silyl magnesiate **28** has also demonstrated the ability to deprotonate three equivalents pyrrole,^[189] and it was found that this magnesiate reacted with two

equivalents of pyrrole even when the two compounds were mixed in an equimolar ratio (Scheme 5.9).



Scheme 5.9 Magnesiumation of pyrrole by $[\{\text{Na}(\text{THF})_6\}^+\{(\text{Ph}_2\text{Si}(\text{NDipp})_2)\text{MgBu}(\text{THF})\}^-]$ **28**.^[189]

When two equivalents of the substrate were employed in attempt to boost the yield of the bis(pyrrolyl) compound only the tris(pyrrolyl)magnesiato was isolated, unless the reaction was performed at low temperature. Given the polybasicity of zincate **29** towards benzothiazole, a similar reaction with this substrate was anticipated, and the reaction with pyrrole resulted in the isolation of the novel higher order zincate $[\text{Na}_2(\text{THF})_4\text{Zn}(\text{NC}_4\text{H}_4)_4]_\infty$ **32** (Scheme 5.10).



Scheme 5.10 Deprotonation of pyrrole with **29**.

When pyrrole was added to a solution of **29** in a mixture of hexane and THF the solution began to bubble. This was very brief and as no obvious temperature change was detected it was assumed to be due to the evolution of ethane from the loss of the ethyl group. Cooling the resulting solution to $-27\text{ }^\circ\text{C}$ for 24 hours resulted in the isolation of colourless crystals of **32** in a 20 % yield (80 % with respect to pyrrole). The reaction with pyrrole was initially performed in a one to one ratio; however,

zincate **32** was the sole product crystallised, regardless of the stoichiometry employed. The crystalline yield increased to 41 % (82 % with respect to pyrrole) when the reaction was performed using a molar ratio of two pyrrole to one zincate (Scheme 5.10).

The crystals of **32** were poorly soluble in benzene, but dissolution in d_8 -THF enabled ^1H and ^{13}C NMR analysis. It is clear from the ^1H NMR spectrum that only the pyrrolyl anion – indicated by two triplets at 6.93 and 6.05 ppm – and THF (3.62 and 1.78 ppm) were present in compound **32**, integrating to a ratio of four to one, with no resonances corresponding to the bis(amido)silyl ligand present. Likewise, the ^{13}C NMR spectrum also consisted of only four signals – 127.2 and 106.6 ppm for the pyrrolyl α - and β -carbons respectively, and 68.3 and 26.4 ppm for the α - and β -carbons of the THF. These chemical shifts are marginally downfield with respect to the corresponding resonances of the free heterocycle in the same solvent (at 6.65/117.9 ppm and 6.03/108.0 ppm for α - and β -positions respectively); however, the spectra are identical to those of the previously reported tris(pyrrolyl)zincate $[\{(\text{THF})_2\text{NaZn}(\text{THF})(\text{NC}_4\text{H}_4)_3\}_\infty]$ **33**,^[90] which is not surprising since an excess of the donor solvent THF is required to effect dissolution, most likely resulting in a solvent separated structure in solution.

Single crystal X-ray analysis of the crystals confirmed that a disproportionation reaction had occurred, resulting in the formation of the higher order zincate **32** (2 Na: 1 Zn, Figure 5.7, Table 5.5). The distorted tetrahedral zinc (angles about Zn1 range from 99.26(13) to 113.72(14) °, average 108.33 °) forms four sigma bonds to the pyrrolyl ligands at an average Zn-N bond length of 1.995 Å, practically identical to that of the other higher order pyrrolyl zincates $[\{(\text{PMDETA})\text{Na}\}_2\text{Zn}(\text{NC}_4\text{H}_4)_4]$ (1.996 Å, Figure 5.6 (left)) and $[\{(\text{TMEDA})\text{Na}\}_2\text{Zn}(\text{NC}_4\text{H}_4)_4]$ (1.984 Å, Figure 5.6 (right)).^[90]

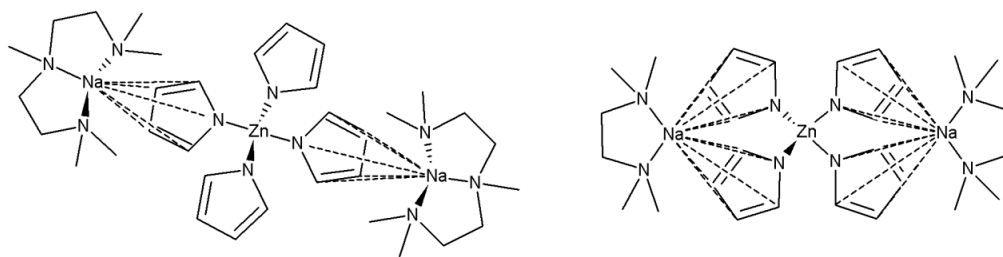


Figure 5.6 Chemdraw representations of zincates $[\{(PMDETA)Na\}_2Zn(NC_4H_4)_4]$ (left) and $[\{(TMEDA)Na\}_2Zn(NC_4H_4)_4]$ (right).^[90]

Like both of these compounds, the sodium atoms are incorporated into the structure through π -contacts with the pyrrolyl rings; however, the uniform η^5 -coordination observed in both of these structures is totally different to the η^5/η^3 - and η^3/η^2 -coordination displayed by Na1 and Na2 respectively in **32**.

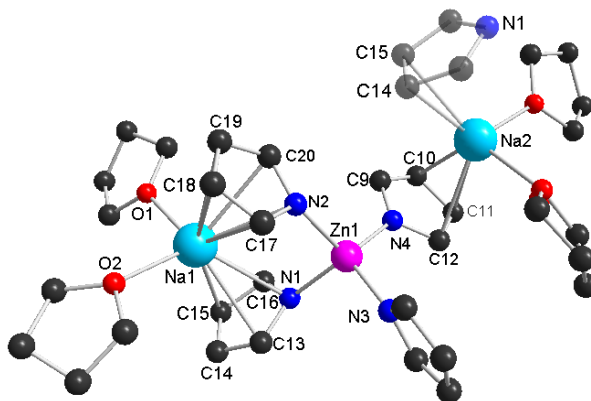


Figure 5.7 Asymmetric unit of $[Na_2(THF)_4Zn(NC_4H_4)_4]_\infty$ **32**. H atoms have been omitted for clarity.

Table 5.5 Selected bond lengths (Å) and angles (°) for **32**.

Zn1-N1	2.024(3)	Na1-C15	2.881(5)	Na2-O5	2.405(13)
Zn1-N2	2.010(3)	Na1-C17	2.778(5)	Na2-O6	2.314(4)
Zn1-N3	1.972(3)	Na1-C18	2.816(5)	Na2-C10	2.860(6)
Zn1-N4	1.974(3)	Na1-C19	2.832(5)	Na2-C11	2.790(6)
Na1-O1	2.300(4)	Na1-C20	2.813(4)	Na2-C12	2.838(5)
Na1-O2	2.344(6)	Na1-N1	2.778(4)	Na2-C14	2.757(6)
Na1-C13	2.869(5)	Na1-N2	2.804(3)	Na2-C15	2.793(5)
<hr/>					
N2-Zn1-N1	99.26(13)	N4-Zn1-N1	108.79(14)	N3-Zn1-N2	109.79(14)
N3-Zn1-N1	108.65(13)	N3-Zn1-N2	109.79(14)	N3-Zn1-N4	113.72(14)

In contrast to these higher order pyrrolyl zincates, the structure of **32** is polymeric, forming an infinite chain propagated via the Na- π interactions (Figure 5.8). In this respect the polymeric arrangement of **32** is strikingly similar to that of the lower order tris(pyrrolyl)zincate $[\{(THF)_2NaZn(THF)(NC_4H_4)_3\}_\infty]$ **33**.^[90] As in **33**, there is a single pyrrolyl ring in **32** which does not interact with either sodium atom; this results in the Zn1-N3 bond being shorter and stronger than those to the rings which bridge between the two metals (1.972(3) Å vs. 2.024(3) and 2.010(3) Å for Zn1-N1 and Zn1-N2 respectively). Similar to the sodium atom in **33**, which displays an η^5/η^2 -coordination to two of the rings, the Na2 of **32** binds in a η^3/η^2 -fashion and remains towards the back edge of both pyrrole rings. Na2 lies closest to the C11-C12 bond of the N4 ring (Na2-C11 = 2.790(6) Å, Na2-C12 = 2.838(5) Å), and the C14-C15 bond of the N1 ring (Na2-C14 = 2.757(6) Å and Na2-C15 = 2.793(5) Å). Contrastingly, the Na1 atom bonds more strongly to the nitrogen atoms of the N1 and N2 rings (Na1-N1 = 2.778(4) Å and Na1-N2 = 2.804(3) Å) and lies in the V-shaped π -pocket closer to the front of the ring, as seen in the higher order zincate $[\{(TMEDA)Na\}_2Zn(NC_4H_4)_4]$.^[90]

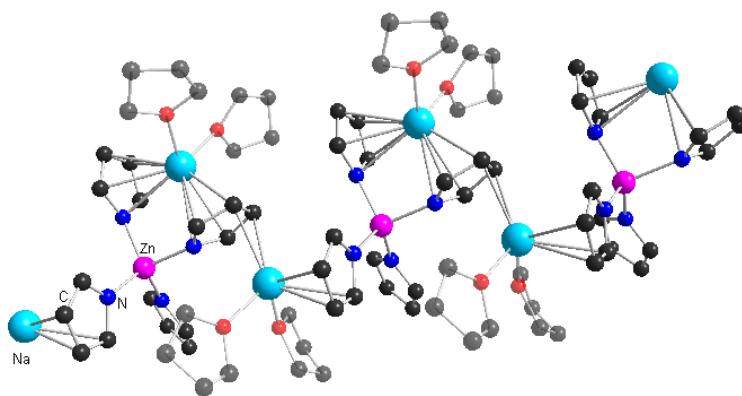
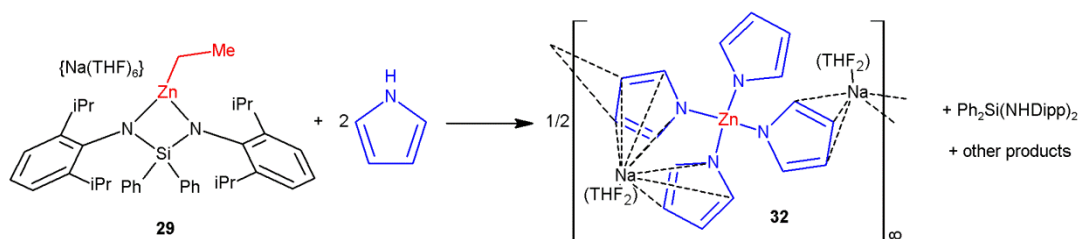


Figure 5.8 Extended polymeric chain of **32**.

The pyrrole polymer **32** clearly forms as the result of a disproportionation, and as such another zinc species must also have been formed (Scheme 5.11). The free amide $Ph_2Si(NHDipp)_2$ was detected in the filtrate and, as no other Dipp species were observed, the remaining products were assumed to be either diethylzinc or metallic

zinc (as the evolution of ethane gas was suspected, *vide supra*). The reaction of **29** with pyrrole was repeated in a sealed NMR tube and monitored over time by ^1H NMR spectroscopy, in attempt to identify the disproportionation products; however, no signals which could be attributed to the methylene protons of diethylzinc were observed, and the region of the spectrum where ethane appears (0.85 ppm in $\text{d}_8\text{-THF}$)^[198] was obscured by the methyl protons of the Dipp groups (0.97 ppm). A grey precipitate had been previously noted on prolonged storage of this reaction, and as diethylzinc is known to decompose via β -hydride elimination,^[176] zinc hydride was also considered as a possible product. However, this process generally requires excessive heating, and as there was no evidence of the ethene which would be formed via this mechanism, the identity of any other disproportionation products remains uncertain at this time.



Scheme 5.11 Disproportionation reaction to form **32**.

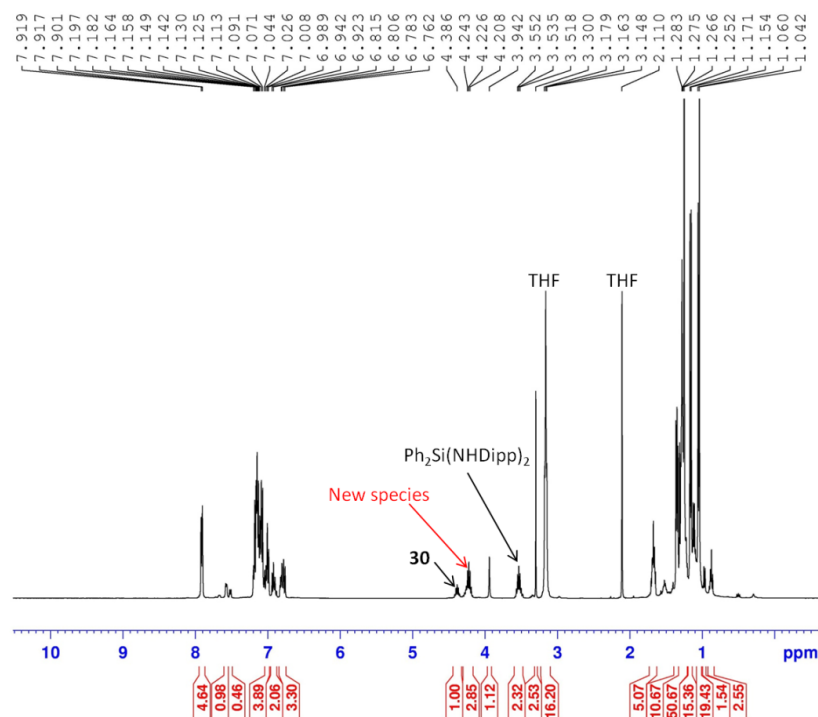
The reaction of the TMP base **30** with pyrrole again resulted in the formation of **32** in similar yields. The determination of any disproportionation products in this instance has yet to be attempted.

5.3.3 Reaction with Anisole

As both ethyl base **29** and TMP base **30** displayed similar reactivities towards the two previous substrates it was decided to employ a molecule with less acidic protons in order to determine if this would highlight the differences in their reactivity. Thus, anisole (a benchmark molecule for DoM) was chosen as the next substrate^[199] and a

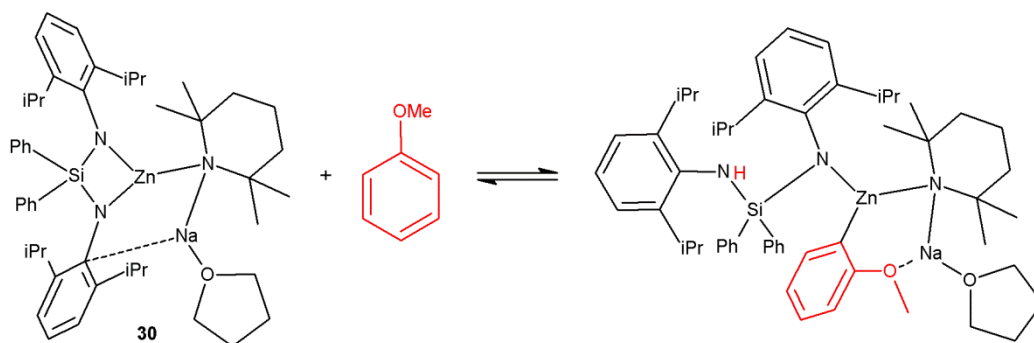
single molar equivalent was introduced to a solution of **29** in hexane/THF solution. The reaction was stirred at room temperature for 60 minutes and no discernible changes were noted during this time. ^1H NMR analysis of the reaction mixture confirmed no reaction had taken place, with only the signals corresponding to **29** and to free anisole being present. Another ^1H NMR spectrum, run after the reaction was left to stir overnight, again showed only the starting materials; however, the formation of a grey powder (suspected to be zinc metal) in the reaction vessel suggested that the base had begun to decompose and the reaction was abandoned.

Building on previous studies in zinc chemistry, which show that zinc amides are more powerful metallating reagents than alkylzinc compounds (on the basis of their enhanced kinetic reactivity), the TMP zincate **30** was next reacted with anisole. Thus, a single molar equivalent of anisole was added to a solution of **30** in hexane/THF, and the reaction was left to stir for one hour before an aliquot was removed for NMR analysis. The ^1H NMR spectrum of the reaction mixture showed mainly free anisole; however, some free $\text{Ph}_2\text{Si}(\text{NHDipp})_2$ was observed, suggesting that some reaction had occurred (Spectrum 5.2).



Spectrum 5.2 Reaction of **30** with anisole after one hour.

The resonance at 1.68 ppm, identified as corresponding to TMP γ -protons, does not correspond to either **30** or free TMP(H), and a third isopropyl-containing species was also evident at 4.22 ppm. The THF protons appear at 3.16 and 2.11 ppm for the α - and β -protons respectively, significantly different chemical shifts to that of the free solvent (3.57 and 1.40 ppm in C_6D_6),^[198] suggesting the coordination of THF to an organometallic species. As these results proved promising the reaction was left to stir over night and the 1H NMR spectrum was repeated, at which point only the two starting materials were visible. Thus, it would appear that the deprotonation of anisole does occur; however, this reaction appears to be reversible resulting in the reappearance of the starting base **30** (Scheme 5.12).



Scheme 5.12 Possible equilibrium on the deprotonation of anisole by **30**.

The intermediate species were not isolated and as such their identity remains uncertain; however, as **30** has displayed polybasicity towards other substrates, it is anticipated that repeating this reaction with two or three equivalents of anisole might force this apparent equilibrium to the right, allowing these products to be isolated. Nonetheless, despite being unable to positively identify the intermediate, the spectroscopic evidence of its formation supports the notion that **30** is the stronger base, as the ethyl analogue **29** did not react with this substrate.

5.4 Conclusions

The bulky chelating bis(amido)silyl ligand $[\text{Ph}_2\text{Si}(\text{NDipp})_2]^{2-}$ has been successfully incorporated into two zincate bases, $[\{\text{Na}(\text{THF})_6\}^+\{(\text{Ph}_2\text{Si}(\text{NDipp})_2)\text{ZnEt}\}^-]$ **29** and $[(\text{Ph}_2\text{Si}(\text{NDipp})_2)\text{Zn}(\text{TMP})\text{Na}(\text{THF})]$ **30**. The conversion of the ethyl zincate **29** to the TMP analogue **30** on microwave heating has also been demonstrated; however, at present this represents an unfeasible synthesis, with the stepwise reaction of $\text{Ph}_2\text{Si}(\text{NHDipp})_2$ by butylsodium and then by $\text{Zn}(\text{TMP})_2$ being much more efficient. The ability of both zincates to deprotonate substrates which contain a relatively acidic proton has been established, resulting in the isolation of a novel tris(benzothiazolyl)zincate $[\text{Na}(\text{THF})_2\text{Zn}(\text{Btz})_3]_2$ **31**, which exhibits a highly symmetrical bicyclic structure. The novel higher order pyrrolyl zincate $[\text{Na}_2(\text{THF})_4\text{Zn}(\text{NC}_4\text{H}_4)_4]_\infty$ **32** has also been fully characterised. Exhibiting a polymeric structure in the solid state this zincate serves to complete the set of higher and lower order pyrrolyl zincates published in 2011.^[90] The difference in reactivity between the two zincates has been highlighted by the reaction of **30** towards anisole, a substrate which remains untouched by the ethyl zincate **29**. The work on these compounds is still in its infancy; however, these results show a tendency towards polybasicity which could potentially provide an atom economical route to the functionalisation of a variety of organic substrates, or be used to trap sensitive anions by exploiting their steric bulk.

Chapter 6 Conclusions and Future Work

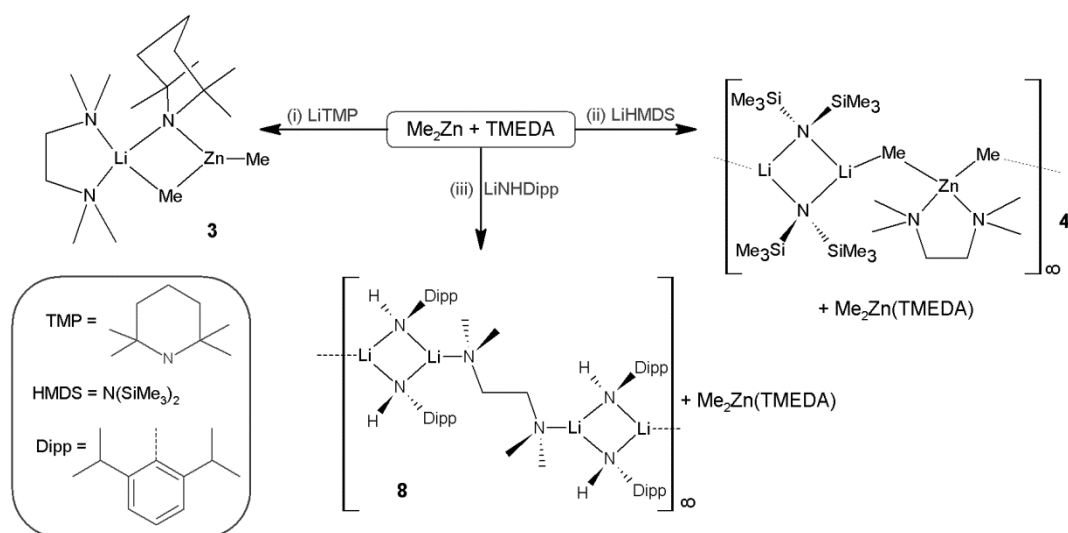
Our studies and structural authentication of heteroleptic dialkyl(amido)zincates shed new light on the prominent role that the donor ligands and amido groups play in the formation of these heterobimetallic compounds. Thus, in a non-polar medium, and in the absence of a Lewis base, co-complexation relies on the ability of the alkylzinc reagent to breakdown the aggregation of the lithium amide. The stability of such a non-solvated species is in turn dictated by its ability to aggregate: thus, unless the newly formed mixed-metal complex can oligomerise, it is likely that it will preferentially remain as a mixture of both monometallic components.

This has been shown by the formation of **4a** which relies on the ability of the methyl group to coordinate to an adjacent bimetallic subunit via $\text{Li}\cdots\text{CH}_3$ interactions, propagating a polymeric chain and stabilising the mixed-metal species with respect to a mixture of its monometallic constituents. The compact size and high charge density of the single carbon of a methyl group is ideally suited for this purpose, in the absence of any other donor. However, as the size of the alkyl group increases the charge becomes more diffuse. This, coupled with the increase in motion expected of a larger alkyl ligand, may explain why certain mixed-metal systems – such as $[\text{Li}(\text{TMP})\text{Zn}^t\text{Bu}_2]$ and $[\text{Na}(\text{TMP})\text{Zn}^t\text{Bu}_2]$ – do not form in the absence of a Lewis base.^[29c]

In systems where co-complexation is not observed, the formation of a mixed-metal species is dependent on the ability of a donor to breakdown the high aggregation of the lithium amide to the extent where reaction with the alkylzinc becomes feasible. When TMEDA is added to a mixture of LiNHDipp and dimethylzinc, for example, the polymeric structure of the lithium amide is deaggregated to $[\text{LiNHDipp}]_2$ dimers. TMEDA then coordinates to these dimers as a bridging ligand, giving rise to another polymeric structure **9** – which appears to be too stable an arrangement to be broken apart by the dimethylzinc. Hence, the ability to breakdown a large oligomer is not alone sufficient to ensure the formation of a mixed-metal species, rather the ability of

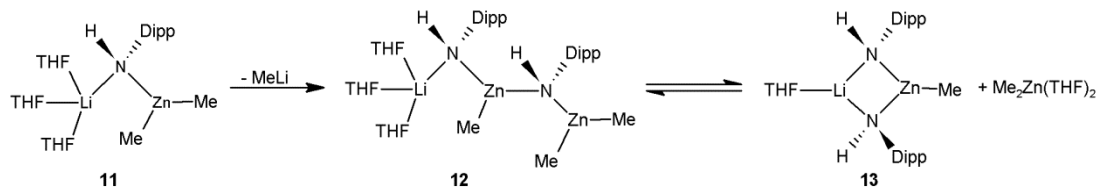
said mixed-metal species *itself* to aggregate is also required. As such, there does not appear to be any obvious relationship between the denticity of the donor solvent used and the formation of a mixed-metal species.

Furthermore, the formation of a dialkyl(amido)zincate appears to be dependent on the nature of both the homometallic constituents; the alkyl substituent on the zinc and the solution structure of the lithium amide. Switching from LiTMP, to LiHMDS, to LiNHDipp results in the formation of three distinctly different structures when combined with dimethylzinc and TMEDA (Scheme 6.1), illustrating that the formation of a mixed-metal species is not always obvious and cannot be easily predicted.



Scheme 6.1 Formation of various structures from the reaction of ZnMe₂, TMEDA and (i) LiTMP, (ii) LiHMDS and (iii) LiNHDipp.

In addition, complex solution equilibria exist which allow the formation of unusual stoichiometries, as observed in the novel lithium dizincate [(THF)₃LiZn₂(NHDipp)₂(Me)₃] **12**. This compound results from the elimination of methyl lithium from [(THF)₃LiZn(NHDipp)(Me)₂] **11**, yet due to the labile nature of the interaction between the terminal zinc and the bridging anilido nitrogen of **12**, it is subject to a further equilibrium in which its ZnMe₂ extremity continually dissociates and recombines (Scheme 6.2).

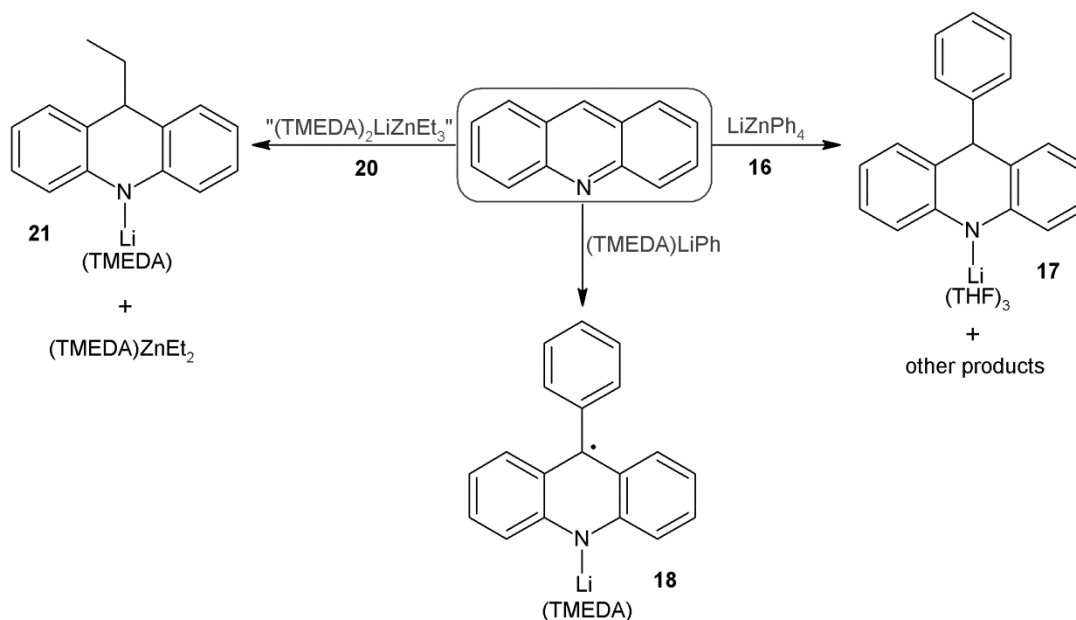


Scheme 6.2 Solution processes on reaction of LiNHDipp and ZnMe₂ in the presence of THF.

Therefore, the formation of a lithium dialkyl(amido)zincate would seem to be dependent on the combination of each of its three components: the nature of the alkyl ligand, the nature of the amido ligand and the ability of the donor solvent to break down the aggregation state of the lithium amide all play an important role in determining the constitution of the resulting compound. Due to the immense variety of possible alkyl, amido and donor ligands there are an infinite number of potential combinations. Given the added complication of underlying solution equilibria, even when it *is* possible to form a mixed-metal complex, said species may not always result from the straightforward combination of the monometallic species. Thus, as no obvious trends have revealed themselves, each possible system must be assessed individually.

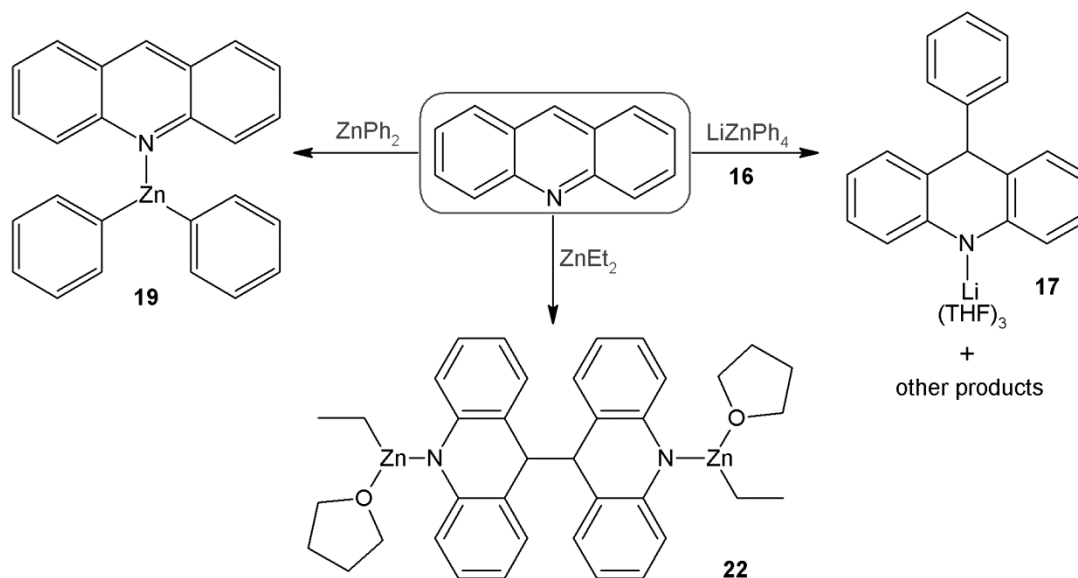
The nucleophilic addition of organolithium reagents to heterocycles is often a complicating factor when these polar species are employed as metallating reagents; however, this process can be utilised for their functionalisation in its own right. The addition of phenyllithium to acridine has been used to synthesise 9-phenylacridine in excellent yield,^[162a] and through our investigations into this process the radical lithium anion intermediate $[(\text{TMEDA})\text{Li}(\text{THF})]^+\{\text{NC}_{19}\text{H}_{13}\}^{\cdot-}$ **18** has been structurally characterised for the first time. This structure substantiates earlier predictions of the angle between the phenyl group and the acridine rings, and reconfirms that the mechanism of this reaction is a single electron process. In contrast, the isolation of the ionic species $[(\text{THF})_3\text{Li}(\text{NC}_{19}\text{H}_{14})]$ **17** from the reaction with tetraphenyl lithium zincate $[\text{Li}_2\text{ZnPh}_4]$ **16**, implies a different mechanism entirely (Scheme 6.3). Similarly, the reaction of acridine and LiZnEt_3 **20** also

produces monometallic intermediates, resulting in the isolation of $[(\text{TMEDA})(\text{THF})\text{Li}(\text{NC}_{15}\text{H}_{14})]$ **21** accompanied by the concomitant formation of $(\text{TMEDA})\text{ZnEt}_2$.



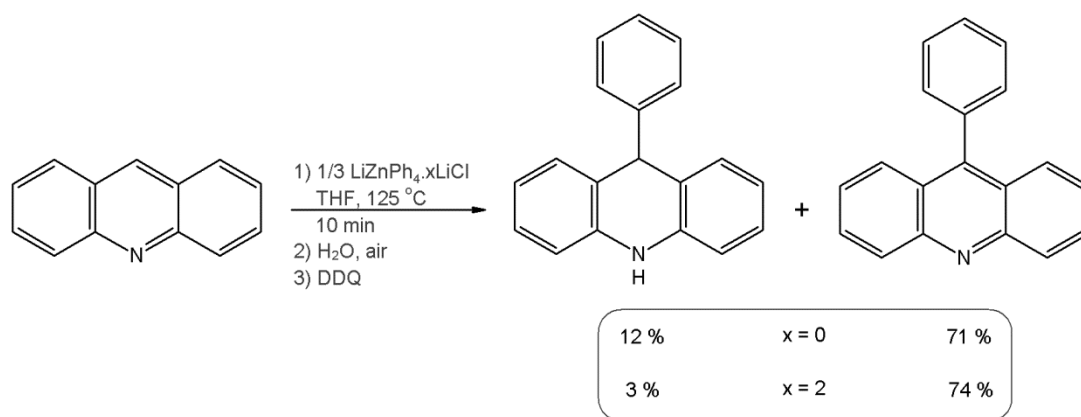
Scheme 6.3 Reaction of acridine with various organometallic species.

Both of these organolithium reagents (ethyl- and phenyllithium) are reactive towards electron-deficient heterocycles, giving rise to the ethylacridine species $[(\text{TMEDA})(\text{THF})\text{Li}(\text{NC}_{15}\text{H}_{14})]$ **21**, the radical anion $[(\text{TMEDA})\text{Li}(\text{THF})]^+\{\text{NC}_{19}\text{H}_{13}\}^-$ **18** and the 2-phenylpyrazine polymer $[(\text{THF})_2\text{Li}(\text{N}_2\text{C}_4\text{H}_4\text{-Ph})]_\infty$ **23** respectively. Organozinc reagents, however, are much less reactive, resulting in only the coordination of ZnPh_2 with acridine and pyrazine (forming $[\text{Ph}_2\text{Zn}(\text{C}_{13}\text{H}_9\text{N})]$ **19** and $[\text{Ph}_2\text{Zn}(\text{N}_2\text{C}_4\text{H}_4)_2]_\infty$ **24**, respectively). ZnEt_2 however can prove reactive enough to perform nucleophilic addition to acridine, if irradiated with ultra-violet light. This results in the 9,9'-coupling of two acridine fragments $[(\text{THF})_2\text{Zn}(\text{Et})_2][\mu\text{-}(\text{NC}_{13}\text{H}_9\text{-C}_{13}\text{H}_9\text{N})]$ **22**; however, yields indicate that this is only a minor product (Scheme 6.4).



Scheme 6.4 Reaction of acridine with various zinc reagents.

The salt-free lithium zincates $[\text{LiZnPh}_3]$ **15** and $[\text{Li}_2\text{ZnPh}_4]$ **16**, and their lithium chloride containing analogues, have been proven to be active toward the nucleophilic addition of electron-deficient *N*-heterocycles, such as acridine and pyrazine, provided they are employed in the donor solvent THF, resulting in the solvent separated, active form. The reduced nucleophilicity of the aryl ligand, with respect to alkyl groups, necessitates that these reactions be performed at high temperature; however, the use of microwave irradiation enables the reaction to be performed in only ten minutes. Furthermore, the activation of three of the four phenyl groups in **16** allows for the arylation of three equivalents of acridine in 70 % yield after oxidation (Scheme 6.5).



Scheme 6.5 The arylation of three equivalents of acridine by LiZnPh_4 **16**.

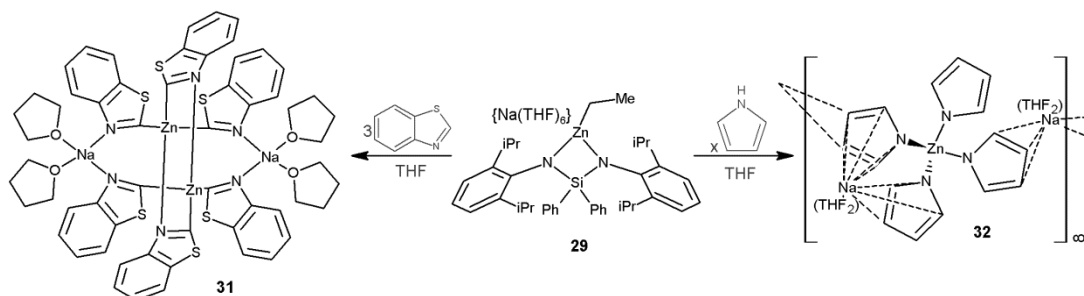
The arylation of other heterocycles has also been demonstrated – with pyrazine and quinoline both proving to be suitable substrates. Although pyrazine fails to react under microwave irradiation due to its aromatic stability, it is anticipated that the reaction with quinoline would be significantly enhanced by microwave heating. As the reaction with acridine shows (Scheme 6.5), these zincates can be used substoichiometrically and it is also probable that multiple equivalents of quinoline could be transformed simultaneously in this manner. Thus, the functionalisation of a variety of *N*-heterocyclic molecules could be carried out in an atom economical manner without the additional complication of a transition metal catalyst.

The generality of this microwave arylation methodology has yet to be assessed; however, these initial studies suggest that elaboration of benzo-fused *N*-heterocycles would certainly be possible. The functional group tolerance of these reactions also remains to be investigated but the use of pre-functionalised heterocyclic substrates and functionalised aryl groups would widen the scope of these reactions immensely, providing an efficient and cost-effective route to countless scaffolds which might otherwise be difficult to obtain.

The combination of PhMgCl and $[\text{Zn}(\text{OPiv})_2 \cdot 2\text{LiCl}]$ **27** proved to be ineffectual for promoting the arylation of acridine, with ESI-MS and NMR studies suggesting that complete transmetallation occurs in such mixtures, resulting in the formation of magnesium pivalate and organozinc compounds. Furthermore, isolation of the

magnesium clusters $[(\text{THF})_6\text{Mg}_{16}(\text{OPiv})_{12}(\text{O}_2)_4(\text{OH})_{12}]$ **26** and $[\{\text{Mg}_6(\text{OPiv})_{12}\}(\text{MgO}_2)]\cdot\text{C}_7\text{H}_8$ implies that these magnesium pivalates are capable of acting as scavengers, serving to protect the organozinc reagent from decomposition when briefly handled in air, thus affording the first generation of "air-stable" organozinc reagents. If the stabilising power of magnesium pivalates could be extended to other organometallic reagents, it would provide significant advantages – limiting the requirement for specialist equipment and often time-consuming inert atmosphere techniques. However, much more research would need to be performed in order to achieve such a goal.

The bulky bis(amido) silyl ligand $[\text{Ph}_2\text{Si}(\text{NDipp})_2]^{2-}$ has been successfully incorporated into two heteroleptic zincates $[\{\text{Na}(\text{THF})_6\}^+\{(\text{Ph}_2\text{Si}(\text{NDipp})_2)\text{ZnEt}\}^-]$ **29** and $[(\text{Ph}_2\text{Si}(\text{NDipp})_2)\text{Zn}(\text{TMP})\text{Na}(\text{THF})]$ **30** which have been fully characterised both in solution and the solid state. Initial studies into the reactivity of these reagents reveal that they are capable of the deprotonation of multiple equivalents of heterocycle simultaneously producing the novel homoleptic zincates $[\text{Na}(\text{THF})_2\text{Zn}(\text{Btz})_3]_2$ **31** and $[\text{Na}_2(\text{THF})_4\text{Zn}(\text{NC}_4\text{H}_4)_4]_\infty$ **32** under very mild conditions (Scheme 6.6).



Scheme 6.6 Reaction of $[\{\text{Na}(\text{THF})_6\}^+\{(\text{Ph}_2\text{Si}(\text{NDipp})_2)\text{ZnEt}\}^-]$ **29** with benzothiazole and pyrrole.

The ring-opening of benzothiazole was not observed with either of these species, as it was with the related magnesiate $[\{\text{Na}(\text{THF})_6\}^+\{(\text{Ph}_2\text{Si}(\text{NDipp})_2)\text{MgBu}(\text{THF})\}^-]$ **28**,^[187] which is consistent with the formation of more stable (less polarised) metal-carbon bonds in the zinc-based systems. However, the different relative reactivities of **29** and **30** has been implied by the deprotonation of anisole. While **29** does not

appear to react with this substrate, the deprotonation of anisole by **30** has been observed by ^1H NMR spectroscopy – although this reaction proved to be reversible and no intermediates have been identified as yet. These investigations are in their infancy; however, these preliminary results are promising and it is hoped that by increasing the ratio of anisole to **30** it will be possible to fully characterise the reaction intermediate. The extension of this methodology to other substrates is also required in order to properly gauge the relative reactivities of both bases.

Collectively, all of these findings highlight the complexity surrounding the formation, structure and reactivity of alkali metal zincates, as well as indicating new synthetic applications for these intriguing reagents; with progress being made towards new bimetallic protocols for the chemoselective functionalisation of heteroaromatic substrates via nucleophilic addition and deprotonative metallation.

Chapter 7 Experimental Procedures

7.1 General Experimental Techniques

7.1.1 Schlenk Techniques

Unless otherwise stated, all reactions were performed under a protective argon atmosphere using standard Schlenk techniques. Due to the highly air and moisture sensitive nature of the organometallic reagents employed, specialist Schlenk lines and glassware were required to ensure a dry, inert atmosphere under which to perform manipulations (Figure 7.1).

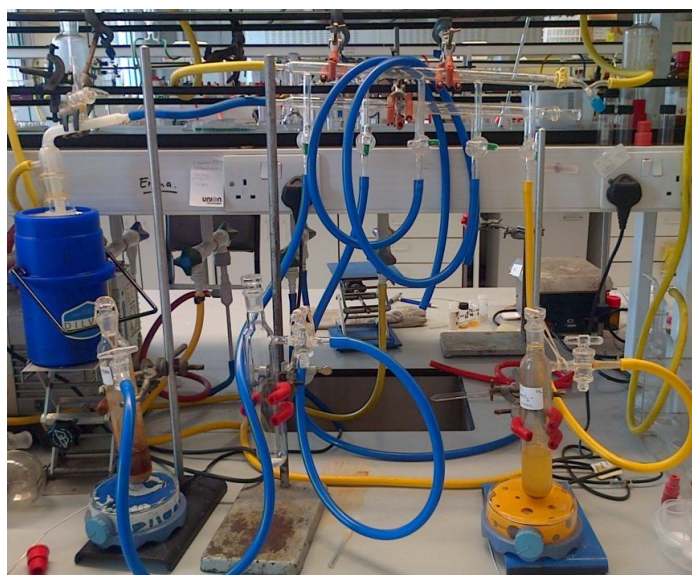


Figure 7.1 Schlenk Line.

A Schlenk line is a double manifold system consisting of two independent paths; one providing high vacuum and the other a flow of dry, oxygen-free argon gas. A series of two-way taps allow any apparatus attached to the line to be isolated, or placed under either vacuum or argon as required (Figure 7.1). A series of Dreschel bottles are attached to monitor the flow of argon through the manifold – these also serve as to prevent any over-pressure of the equipment. The other half of the manifold is attached to a vacuum pump, via a solvent trap, which is cooled with liquid nitrogen,

in order to condense any volatiles before they reach the pump itself. All taps and joints were lubricated with high vacuum grease to ensure a tight seal.

Reactions were performed in Schlenk tubes, which attach to the Schlenk line via rubber tubing (see Figure 7.1). These vessels can be evacuated, by applying vacuum from the Schlenk line, and then charged with argon as required. In order to ensure an inert atmosphere this procedure of evacuation and re-filling was routinely performed three times prior to commencing any reaction. Furthermore, any addition of solvent, or reagent to the reaction vessel was performed under a positive pressure of argon, to prevent any air from entering the system.

7.1.2 Glove Box

The manipulation of air-sensitive solids required the use of a glove box (or dry box, Figure 7.2). This apparatus provides an inert atmosphere within a sealed system, the main body of which has a plastic window above neoprene gloves allowing the user to perform activities such as the weighing of reactants or products and the preparation of samples for NMR spectroscopy or microanalysis. Items are introduced to (or removed from) the main chamber of the glove box via an antechamber on one side, which can be isolated, evacuated and charged with dry argon. In order to establish an air-free atmosphere within the antechamber, it was purged three times before opening the port into the main argon-filled chamber. This is a standard procedure, the same as is used to purge glassware on the Schlenk line, and is performed to minimise oxygen contamination of the argon atmosphere inside the glove box.



Figure 7.2 Ronnie the glovebox.

The gas inside the glove box is continually circulated over a catalyst and molecular sieves, which serve to remove any traces of oxygen and water present within the system. The levels of O₂ and moisture (ppm) are monitored by sensors within the glove box and displayed on the panel above the antechamber. Regular regeneration was performed (typically every 3 months) to ensure that these levels remain low; this involves heating the molecular sieves under vacuum to remove water, and passing forming gas through the catalyst.

7.1.3 Purification of Solvents and Reagents

Hexane, diethylether, tetrahydrofuran (THF), and toluene were dried by heating to reflux over sodium and benzophenone, and distilled under nitrogen prior to use. In the absence of moisture, the reaction of sodium with benzophenone produces the intensely blue coloured sodium ketyl radical, thus acting as a visual indication that the solvents are free of moisture.

Deuterated solvents were purified by drying over molecular sieves, and then degassed using a freeze-pump-thaw procedure to remove dissolved gases. The purified solvents were then stored under argon in an ampoule in the glove box.

Hygroscopic reagents, such as 2,6-diisopropylaniline, were purified prior to use by distillation over calcium hydride, collected into an oven-dried argon-filled flask and stored over 4 Å molecular sieves.

Diphenylzinc was purified by sublimation by heating to 120 – 140 °C under vacuum, and the resulting solid was stored in the glove box.

7.1.4 Standardisation of Organometallic Reagents

As the concentration of a solution of an organometallic reagent can change over time – due to evaporation or degradation caused by air entering the bottle – these solutions were standardised before use. Organolithium reagents were titrated against (L)-menthol, using 1,10-phenanthroline as an indicator.^[200] In THF solution these compounds are colourless; however, gradual addition of an organolithium reagent produces first a yellow colour – on the deprotonation of the alcohol – and finally a red colour, indicating the complete consumption of the menthol. Organozinc and -magnesium reagents were standardised using iodine and a THF solution of LiCl,^[201] the end point being indicated by the loss of colour from the iodine in solution.

7.1.5 Instrumentation

NMR spectra were recorded on a Bruker AV400 MHz spectrometer, operating at 400.13 MHz for ¹H, 150.32 MHz for ⁷Li and 100.62 MHz for ¹³C. All ¹³C spectra were proton decoupled and the shifts quoted are relative to TMS at 0.0 ppm. The ⁷Li spectra are referenced against LiCl in D₂O. The abbreviations used are as follows: s (singlet), d (doublet), t (triplet), q (quartet), m (multiplet), b (broad).

Elemental analyses were carried out on a Perkin-Elmer 2400 elemental analyzer. Samples for microanalysis were prepared in an argon-filled glove box and sealed inside a gas-tight box, under an argon atmosphere, before removal from the glove

box. Despite these measures, the significant air- and moisture-sensitivity of the compounds synthesised meant that achieving reliable results was not always possible.

Crystallographic data were collected on Brüker SMART and Nonius KappaCCD diffractometers at 150 K, or Oxford Diffraction Xcalibur or Gemini diffractometers at 123 K with Mo-K α or Cu-K α radiation ($\lambda = 0.71073$ and 1.54180 Å respectively). The structures were refined by full-matrix least-squares using all unique F^2 values with programs of the SHELX family.

Microwave experiments were performed using a CEM Discover SP microwave reactor. All reactions were heated to 125 °C for ten minutes, unless otherwise stated.

EPR spectra were recorded between 2 K and 70 K with sweep width of 200 G and with a center field of 3357.2 G. Resolution was 1024 points. Frequency of microwave radiation was 9.42 GHz and the power used was 0.1001 mW.

7.2 Synthesis of Common Starting Materials

7.2.1 Preparation of ZnPh₂

Ph₂Zn was prepared according to literature methods.^[148] Thus, a solution of PhMgCl (40 mL of a 2 M in THF, 40 mmol) was added to a solution of ZnCl₂ (2.72 g, 20 mmol) in THF (40 mL) at 0 °C, and the resulting solution was stirred at room temperature for 3 hours. Crystals of the magnesium salt were isolated following 12 hours at -40 °C, and the remaining solution was dried then purified by sublimation (see 7.1.3 Purification of Solvents and Reagents) to afford the purified Ph₂Zn in 40 – 50 % yields.

¹H NMR (400.13 MHz, 298 K d₈-THF) δ ppm: 7.55 (dd, 2H, H_{meta}), 7.09 (t, 2H, H_{ortho}), 7.02 (tt, 1H, H_{para}).

^{13}C { ^1H } NMR (100.62 MHz, 298 K, d_8 -THF) δ ppm: 156.8 (C_{ipso}), 139.6 (C_{para}), 127.2 (C_{meta}), 126.1 (C_{ortho}).

7.2.2 Synthesis of BuNa

A suspension of NaO^tBu (1.92 g, 20 mmol) in hexane (20 mL) was cooled to 0 °C before the addition of butyllithium (13.3 mL of a 1.5 M solution in hexane, 20 mmol). The resulting suspension was wrapped in black plastic and left to stir overnight at room temperature. The butylsodium was filtered and washed three times with 10 mL of hexane until the washings ran clear, and dried under vacuum. Typical yields of 80% were obtained.

7.2.3 Synthesis of $[\text{Ph}_2\text{Si}(\text{NHDipp})_2]$

Butyllithium (18.75 mL of a 1.6 M solution in hexane, 30 mmol) was added to a solution of DippNH_2 (5.8 mL, 30 mmol) in diethylether (40 mL) at 0 °C and the reaction allowed to warm to room temperature. The solution was again cooled to 0 °C, Ph_2SiCl_2 (3.15 mL, 15 mmol) was added and the reaction left to stir overnight. The precipitated LiCl was removed by filtration through celite and the filtrate concentrated under vacuum until a precipitate appeared. The solid was redissolved by briefly refluxing and the reaction stored at -27 °C until a crop of colourless crystals were obtained. Typical yields of 80 - 90% were achieved.

^1H NMR (400.13 MHz, 298 K d_8 -THF) δ ppm: 7.69 - 7.74 (m, 4 H, H_{ortho} phenyl) 7.09 - 7.14 (m, 6 H, $\text{H}_{\text{meta/para}}$ phenyl) 7.03 - 7.08 (m, 6 H, $\text{H}_{\text{meta/para}}$ Dipp) 3.52 (s, 2 H, NH) 3.39 (septet, $J=6.80$ Hz, 4 H, CH^iPr) 0.97 (d, $J=6.78$ Hz, 24 H, CH_3^iPr).

^{13}C { ^1H } NMR (100.62 MHz, 298 K, d_8 -THF) δ ppm: 143.1 (s) 139.7 (s) 136.3 (q?) 135.8 (s) 130.4 (s) 124.2 (s) 124.1 (q?) 29.4 (CH^iPr) 23.9 (CH_3^iPr)

7.2.4 Synthesis of Zn(TMP)₂

A solution of TMP(H) (6.8 mL, 40 mmol) in hexane (40 mL) was cooled to 0°C and butyllithium (27 mL of a 1.48 M solution in hexane, 40 mmol) added and the solution stirred at room temperature for one hour. The hexane was removed *in vacuo* and replaced with 40 mL of diethylether and ZnCl₂ (2.72 g, 20 mmol) was added. The resulting yellow suspension was stirred at room temperature for 72 hours, before removal of the ether and the addition of 80 mL of hexane. The precipitated LiCl was removed by filtration through celite and washed with copious amounts of hexane, until the washings ran colourless. The remaining yellow filtrate was concentrated *in vacuo* until a viscous orange oil was obtained. Storage of this oil at -27°C resulted in the isolation of an orange solid in 76% yield.

7.3 Synthesis of Numbered Compounds

Synthesis of [LiZn(HMDS)Me₂] 4a

Li(HMDS) was prepared *in situ* by reaction of BuLi (2.5 mL of a 1.6 M solution in hexane, 4 mmol) and HMDS(H) (0.84 mL, 4 mmol) in hexane. Me₂Zn (2 mL of a 2 M solution in toluene) was then introduced. A white precipitate is formed immediately. At this stage 5 mL of toluene were added and the mixture was gently heated until all of the white solid dissolved affording a transparent colourless solution. Allowing this solution to cool slowly to room temperature produced a crop of colourless crystals (0.85 g, 81%).

¹H NMR(400 MHz, 298K, C₆D₆): δ 0.14 (s, 18H, HMDS), -0.67 (s, Zn-CH₃, Me).

¹³C{¹H} NMR (100.63 MHz, 298K, C₆D₆): δ 5.51 (HMDS), -6.67 (Zn-CH₃, Me).

⁷Li NMR (155.50 MHz, 298K, C₆D₆, reference LiCl in D₂O at 0.00 ppm): δ 0.46.

Synthesis of [(PMDETA)Li(μ -Me)Zn(HMDS)Me] **5**

To a suspension of **4a** (4 mmol) in hexane, prepared *in situ* as previously described, was added PMDETA (0.84 mL, 4 mmol). The resulting colourless solution was concentrated by removal of some solvent *in vacuo* and placed in the freezer at -26 °C. A crop of colourless crystals was deposited after 48 h (1.60 g, 92%).

^1H NMR (400 MHz, 298K, C_6D_6): δ 1.87 (s, 12H, CH_3 , PMDETA), 1.85 (s, 3H, CH_3 , PMDETA), 1.72 (br s, 8H, CH_2 , PMDETA), 0.50 (s, 18H, HMDS), -0.53 (s, Zn- CH_3 , Me).

$^{13}\text{C}\{^1\text{H}\}$ NMR (100.63 MHz, 298K, C_6D_6): δ 56.85 (CH_2 , PMDETA), 53.97 (CH_2 , PMDETA), 45.85 (CH_3 , PMDETA), 6.69 (HMDS), -6.99 (Zn- CH_3 , Me).

^7Li NMR (155.50 MHz, 298K, C_6D_6 , reference LiCl in D_2O at 0.00 ppm): δ 0.67.

Synthesis of [$^t\text{Bu-py}$ Li(HMDS)] **6**

To a suspension of **4a** (4 mmol) in hexane, prepared *in situ* as previously described, was added *tert*-butylpyridine (0.59 mL, 4 mmol). The resulting colourless solution was concentrated by removal of some solvent *in vacuo* until it became slightly cloudy. The solution was briefly heated to ensure complete dissolution of the precipitate. A pale yellow solution was obtained. This solution was slowly cooled by leaving it in a Dewar flask filled with hot water. On reaching ambient temperature, colourless crystals of **6** were obtained (0.88 g, 72%).

^1H NMR (400 MHz, 298K, C_6D_6): δ 8.75 (d, 2H, Ha, $^t\text{Bu-py}$), 6.88 (d, 2H, Hb, $^t\text{Bu-py}$), 0.91 (s, 9H, CH_3 , $^t\text{Bu-py}$), 0.53 (s, 18H, HMDS).

$^{13}\text{C}\{^1\text{H}\}$ NMR (100.63 MHz, 298K, C_6D_6): δ 161.66 (Ca, $^t\text{Bu-py}$), 149.74 (Cb, $^t\text{Bu-py}$), 121.59 (Cc, $^t\text{Bu-py}$), 34.61 ($\text{C}(\text{CH}_3)_3$, $^t\text{Bu-py}$), 30.08 ($\text{C}(\text{CH}_3)_3$, $^t\text{Bu-py}$), 6.64 (HMDS).

^7Li NMR (155.50 MHz, 298K, C_6D_6 , reference LiCl in D_2O at 0.00 ppm): δ 2.75.

Synthesis of [^tBuCN)Li(HMDS)] 7

To a suspension of **4a** (4 mmol) in hexane, prepared *in situ* as previously described, was added *tert*-butylcyanide (0.44 mL, 4 mmol). The resulting colourless solution was concentrated by removal of some solvent *in vacuo* and placed in the freezer at $-26\text{ }^{\circ}\text{C}$. A crop of colourless crystals was deposited after 48 h (0.83 g, 83%).

¹H NMR (400 MHz, 298K, C₆D₆): δ 0.71 (s, 9H, CH₃, ^tBuCN), 0.49 (s, 18H, HMDS).

¹³C{¹H} NMR (100.63 MHz, 298K, C₆D₆): δ 27.20 (C(CH₃)₃, ^tBuCN), 27.16 (C(CH₃)₃, ^tBuCN), 6.25 (HMDS).

⁷Li NMR (155.50 MHz, 298K, C₆D₆, reference LiCl in D₂O at 0.00 ppm): δ 1.21.

Synthesis of [{Li₂(NHDipp)₂(TMEDA)}_∞] 8

To a solution of hexane (5 mL) and 2,6-diisopropylaniline (0.35 mL, 2 mmol) was added ⁿBuLi (1.6M in hexane, 1.25 mL, 2 mmol), and the resulting suspension was stirred for 1 h. TMEDA (0.3 mL, 2 mmol) was then added, followed by toluene (7 mL) and gentle heating to afford a pale yellow solution. At this stage ZnMe₂ (2 mL of a 1 M solution in heptane, 2 mmol) was introduced. The resulting solution was left to cool overnight in a Dewar with hot water. Small colourless crystals were isolated (0.309 g, yield 64%).

¹H NMR (400.13 MHz, 298 K, C₆D₆): δ 7.15 (4H, d, H_{meta}), 6.71 (2H, t, H_{para}), 3.22 (4H, m, CH, ⁱPr), 2.84 (2H, s, NH), 1.76 (12H, s, CH₃, TMEDA), 1.71 (4H, s, CH₂, TMEDA), 1.36 (24H, d, CH₃, ⁱPr).

⁷Li NMR (298K, C₆D₆, reference LiCl in D₂O at 0.00 ppm): δ 1.88.

^1H NMR (400.13 MHz, 298 K, d_8 -THF): δ 6.68 (4H, d, H_{meta}), 6.03 (2H, t, H_{para}), 3.22 (4H, m, CH, $i\text{Pr}$), 2.68 (2H, s, NH), 2.32 (4H, s, CH_2 , TMEDA), 2.16 (12H, s, CH_3 , TMEDA), 1.20 (24H, d, CH_3 , $i\text{Pr}$).

$^{13}\text{C}\{^1\text{H}\}$ NMR (100.62 MHz, 298 K, d_8 -THF): δ 158.2 (Cipso), 131.5 (Cortho), 122.2 (Cmeta), 109.4 (Cpara), 58.8 (CH_2 , TMEDA), 46.2 (CH_3 , TMEDA), 28.4 (CH, $i\text{Pr}$), 23.9 (CH_3 , $i\text{Pr}$).

^7Li NMR (298 K, d_8 -THF, reference LiCl in D_2O at 0.00 ppm): δ -0.62.

Elemental analysis calcd (%) for $\text{C}_{30}\text{H}_{52}\text{Li}_2\text{N}_4$: C 74.65, H 10.85, N 11.60; **found:** C 74.11, H 11.03, N 11.39.

Synthesis of [(PMDETA)Li(NHDipp)] 9

To a solution of hexane (5 mL) and 2,6-diisopropylaniline (0.35 mL, 2 mmol) was added $n\text{BuLi}$ (1.6 M in hexane, 1.25 mL, 2 mmol), and the resulting suspension was stirred for 10 min. PMDETA (0.42 mL, 2 mmol) was then added affording a pale yellow solution which deposited colourless crystals when placed in the freezer (-20°C) and left overnight (0.564 g, yield 79%).

^1H NMR (400.13 MHz, 298 K, C_6D_6): δ 7.29 (2H, d, H_{meta}), 6.66 (1H, t, H_{para}), 3.34 (2H, m, CH, $i\text{Pr}$), 3.09 (1H, s, NH), 2.09 (3H, s, NCH_3 , PMDETA), 1.89 (12H, bs, CH_3 PMDETA), 1.72 (8H, bs, CH_+ , PMDETA), 1.54 (12H, d, CH_3 , $i\text{Pr}$).

$^{13}\text{C}\{^1\text{H}\}$ NMR (100.62 MHz, 298 K, C_6D_6): δ 159.4 (Cipso), 131.3 (Cortho), 122.3 (Cmeta), 105.9 (Cpara), 57.2, 53.4 (CH_2 , PMDETA), 45.7 ($\text{N}(\text{CH}_3)_2$, PMDETA), 44.2 ($\text{N}(\text{CH}_3)$, PMDETA), 29.0 (CH, $i\text{Pr}$), 24.1 (CH_3 , $i\text{Pr}$).

^7Li NMR (298K, C_6D_6 , reference LiCl in D_2O at 0.00 ppm): δ 1.47.

Elemental analysis calcd (%) for $\text{C}_{21}\text{H}_{41}\text{LiN}_4$: C 70.75, H 11.59, N 15.72; **found:** C 70.21, H 11.64, N 15.10.

Synthesis of [(PMDETA)LiZn(NHDipp)(Me)₂] 10

To a solution of hexane (5 mL) and 2,6-diisopropylaniline (0.35 mL, 2 mmol) was added *n*BuLi (1.6 M in hexane, 1.25 mL, 2 mmol), and the resulting suspension was stirred for 10 min. Me₂Zn (2 mL of a 1 M solution in heptane, 2 mmol) was then added, and the reaction mixture stirred for 30 min, followed by the addition of PMDETA (0.42 mL, 2 mmol). After stirring for 2 h the precipitate was still present. Addition of toluene (6 mL) and gentle heating afforded a yellow solution, which was placed in the fridge (0 °C) and left overnight. Small colourless crystals were isolated (0.550 g, yield 61%).

¹H NMR (400.13 MHz, 298 K, C₆D₆): δ 7.15 (2H, d, H_{meta}), 6.79 (1H, t, H_{para}), 3.45 (2H, m, CH, ⁱPr), 2.84 (1H, s, NH), 2.14 (3H, s, NCH₃, PMDETA), 1.72 (20H, bs, CH₃ and CH₂, PMDETA), 1.38 (12H, d, CH₃, ⁱPr), -0.32 (6H, s, Zn-(CH₃)₂).

¹³C{¹H} NMR (100.62 MHz, 298 K, C₆D₆): δ 154.5 (C_{ipso}), 134.1 (C_{ortho}), 122.8 (C_{meta}), 114.2 (C_{para}), 57.1, 53.2 (CH₂, PMDETA), 45.7 (N(CH₃)₂, PMDETA), 44.7 (N(CH₃), PMDETA), 27.9 (CH, ⁱPr), 24.5 (CH₃, ⁱPr), -8.1 (Zn(CH₃)₂).

⁷Li NMR (298K, C₆D₆, reference LiCl in D₂O at 0.00 ppm): δ 0.77.

Elemental analysis calcd (%) for C₂₃H₄₇LiN₄Zn: C 61.12, H 10.48, N 12.40;
found: C 61.41, H 10.80, N 12.33.

Synthesis of [(THF)₃LiZn(NHDipp)(Me)₂] 11

To a solution of hexane (5 mL) and 2,6-diisopropylaniline (0.35 mL, 2 mmol) was added *n*BuLi (1.6 M in hexane, 1.25 mL, 2 mmol), and the resulting suspension was stirred for 10 min. ZnMe₂ (2 mL of a 1 M solution in heptane, 2 mmol) was then added, and the reaction mixture stirred for 30 min, followed by the addition of THF (0.49 mL, 6 mmol), to give an oil, which remained even after addition of toluene (1 mL) and gentle heating. The Schlenk tube was placed in the freezer (-20 °C) and left for several days. A batch of colourless crystals was isolated (0.43 g, yield 43%).

^1H NMR (400.13 MHz, 298 K, C_6D_6): δ 7.14 (2H, d, H_{meta}), 6.75 (1H, t, H_{para}), 3.39 (2H, m, CH, ^iPr), 3.38 (12H, m, OCH_2 , THF), 2.86 (1H, s, NH), 1.42 (12H, d, CH_3 , ^iPr), 1.39 (12H, m, CH_2 , THF), -0.42 (6H, s, $\text{Zn}(\text{CH}_3)_2$).

$^{13}\text{C}\{^1\text{H}\}$ NMR (100.62 MHz, 298 K, C_6D_6): δ 154.2 (Cipso), 134.8 (Cortho), 123.3 (Cmeta), 116.2 (Cpara), 68.1 (OCH_2 , THF), 28.5 (CH, ^iPr), 25.4 (CH_2 , THF), 24.2 (CH_3 , ^iPr), -9.0 ($\text{Zn}(\text{CH}_3)_2$).

^7Li NMR (298K, C_6D_6 , reference LiCl in D_2O at 0.00 ppm): δ 1.01.

Satisfactory elemental analysis of this compound could not be obtained because of its highly air and moisture sensitive nature.

Synthesis of $[(\text{THF})_3\text{LiZn}_2(\text{Me})_3(\text{NHDipp})_2]$ **12**

To a solution of hexane (8 mL) and 2,6-diisopropylaniline (0.35 mL, 2 mmol) was added *n*BuLi (1.6M in hexane, 1.25 mL, 2 mmol), and the resulting suspension was stirred for 10 min. Me_2Zn (4mL of a 1 M solution in heptane, 4 mmol) was then added, and the reaction mixture stirred for 20 min. A second equivalent of 2,6-diisopropylaniline (0.35 mL, 2 mmol) was added, and the suspension stirred for a further 20 min, followed by the addition of THF (0.49 mL, 6 mmol) to give a white precipitate. The reaction mixture was then refluxed for 2 h to give a colourless solution, which on cooling to room temperature gave an oil. The Schlenk tube was placed in the freezer (-20 °C) and left overnight. A white microcrystalline solid was isolated (0.856 g, yield 57%).

^1H NMR (400.13 MHz, 298 K, C_6D_6): δ 7.12 (4H, d, H_{meta}), 6.83 (2H, t, H_{para}), 3.31 (4H, m, CH, ^iPr), 3.29 (12H, m, OCH_2 , THF), 3.08 (2H, bs, NH), 1.35 (24H, d, CH_3 , ^iPr), 1.26 (12H, m, CH_2 , THF), -0.43 (9H, s, $\text{Zn}(\text{CH}_3)_2$).

$^{13}\text{C}\{^1\text{H}\}$ NMR (100.62 MHz, 298 K, C_6D_6): δ 154.5 (Cipso), 134.8 (Cortho), 123.3 (Cmeta), 116.6 (Cpara), 68.1 (OCH_2 , THF), 28.5 (CH, ^iPr), 25.4 (CH_2 , THF), 24.3 (CH_3 , ^iPr), -9.1 ($\text{Zn}(\text{CH}_3)_2$).

^7Li NMR (298K, C_6D_6 , reference LiCl in D_2O at 0.00 ppm): δ 1.07.

Elemental analysis calcd (%) for $C_{39}H_{69}LiN_2O_3Zn_2$: C 62.31, H 9.25, N 3.72;
found: C 62.28, H 9.60, N 3.91.

Synthesis of [(THF)LiZn(NHDipp)₂Me] **13**

Isolated crystals of [(THF)₃LiZn₂(Me)₃(NHDipp)₂] **12** (0.751 g, 1 mmol) were dissolved in toluene (10 mL) affording a colourless solution which was stirred at room temperature for 10 min. Volatiles were removed under vacuum affording a colourless oil which was characterized by multinuclear NMR (¹H, ¹³C and ⁷Li) spectroscopy.

¹H NMR (400.13 MHz, 298 K, C₆D₆): δ 7.06 (4H, d, H_{meta}), 6.84 (2H, t, H_{para}), 3.35 (4H, bs, CH, ⁱPr), 3.18 (2H, bs, NH), 2.85 (4H, m, OCH₂, THF), 1.32 (24H, bs, CH₃, ⁱPr), 0.98 (4H, m, CH₂, THF), -0.38 (3H, s, Zn(CH₃)₂).

¹³C{¹H} NMR (100.62 MHz, 298 K, C₆D₆): δ 1.49.5 (C_{ipso}), 135.4 (C_{ortho}), 123.5 (C_{meta}), 118.0 (C_{para}), 68.2 (OCH₂, THF), 28.9 (CH, ⁱPr), 25.0 (CH₃, ⁱPr), 24.1 (CH₂, THF), -12.7 (Zn(CH₃)₂).

⁷Li NMR (298K, C₆D₆, reference LiCl in D₂O at 0.00 ppm): δ 1.40.

Synthesis of Ph₃LiZn(THF)₃ **15**·THF₃

a) To a suspension of Ph₂Zn (0.11 g, 0.5 mmol) in hexane (2 mL) was added LiPh (0.28 mL of a 1.8 M solution in dibutyl ether, 0.5 mmol). THF (5 mL) was added to achieve dissolution and the resulting solution was stirred at room temperature for 10 minutes. A crop of colourless crystals were isolated at -68 °C (1.48 g, 57 %).

b) Alternatively, **15**·LiCl was prepared *in situ* from ZnCl₂ (0.07 g, 0.5 mmol) in THF (2 mL), to which was added LiPh (0.84 mL, 1.5 mmol).

^1H NMR (400.13 MHz, 298 K $\text{d}_8\text{-THF}$) δ ppm: 7.84 (d, $J=6.32$ Hz, 6H, H_{ortho}), 6.99 (t, $J=7.07$ Hz, 6H, H_{meta}), 6.87 (t, $J=7.07$ Hz, 3H, H_{para}), 3.61 (tt, $J=6.57$, 2.78 Hz, 12H, $\text{H}_{\alpha}\text{-THF}$), 1.78 (tt, $J=6.57$, 3.28 Hz, 12H, $\text{H}_{\beta}\text{-THF}$).

^{13}C { ^1H } NMR (100.62 MHz, 298 K, $\text{d}_8\text{-THF}$) δ ppm: 169.3 (C_{ipso}), 141.3 (C_{ortho}), 125.9 (C_{meta}), 124.0 (C_{para}), 68.2 ($\text{C}_{\alpha}\text{-THF}$), 26.3 ($\text{C}_{\beta}\text{-THF}$).

^7Li NMR (298 K, $\text{d}_8\text{-THF}$, reference LiCl in D_2O at 0.00 ppm) δ ppm: 1.09 or 1.87 (LiCl).

Calculated; C (69.30%), H (7.56%). Observed; (70.15%), H (7.31%).

Synthesis of $\text{Ph}_4\text{Li}_2\text{Zn}(\text{THF})_3(\text{O}^i\text{Bu}_2)$ 16

a) To a suspension of Ph_2Zn (0.11 g, 0.5 mmol) in THF (0.5 mL) was added PhLi (0.56 mL of a 0.8 M solution in dibutyl ether, 1 mmol). The resulting solution was stirred at room temperature for 10 minutes. No crystalline material was ever isolated, but oils were formed in quantitative yields.

b) Alternatively, $16\cdot\text{LiCl}$ was prepared *in situ* from ZnCl_2 (0.07 g, 0.5 mmol) in THF (2 mL), to which was added PhLi (1.12 mL, 2 mmol).

^1H NMR (400.13 MHz, 298 K $\text{d}_8\text{-THF}$) δ ppm: 7.89 (d, $J=6.32$ Hz, 8H, H_{ortho}), 6.97 (t, $J=7.07$ Hz, 8H, H_{meta}), 6.86 (t, $J=7.33$ Hz, 4H, H_{para}), 3.62 (t, $J=6.32$ Hz, 12H, $\text{H}_{\alpha}\text{-THF}$), 3.36 (t, $J=6.32$ Hz, 4H, $\text{OCH}_2\text{-butyl}$), 1.78 (dt, $J=6.38$, 3.25 Hz, 12H, $\text{H}_{\beta}\text{-THF}$), 1.51 (m, 4H, $\text{OCH}_2\text{CH}_2\text{-butyl}$), 1.38 (m, 4H, $\text{CH}_2\text{CH}_3\text{-butyl}$), 0.92 (t, $J=7.33$ Hz, 6H, $\text{CH}_3\text{-butyl}$).

^{13}C { ^1H } NMR (100.62 MHz, 298 K, $\text{d}_8\text{-THF}$) δ ppm: 143.0 (C_{ortho}), 125.8 (C_{meta}), 123.9 ($\text{C}_{\text{para-phenyl}}$), 71.1 ($\text{OCH}_2\text{-butyl}$), 68.2 ($\text{C}_{\alpha}\text{-THF}$), 32.9 ($\text{OCH}_2\text{CH}_2\text{-butyl}$), 26.3 ($\text{C}_{\beta}\text{-THF}$), 20.3 ($\text{CH}_2\text{CH}_3\text{-butyl}$), 14.3 ($\text{CH}_3\text{-butyl}$).

^7Li NMR (298 K, $\text{d}_8\text{-THF}$, reference LiCl in D_2O at 0.00 ppm) δ ppm: -0.13 or 0.14 (LiCl).

Synthesis of 9, 10-dihydro-9-phenylacridine

Acridine (1.5 mL of a 1 M solution in THF, 1.5 mmol) was added to a THF solution of zincate **15** or **16** (0.5 mmol) prepared *in situ* as above. This reaction mixture was then microwaved (125 °C) for 10 minutes, before being quenched with air and water. The mixture was extracted three times with ethyl acetate and the organic layer was purified by silica flash chromatography.

¹H NMR (400.13 MHz, 298 K, CDCl₃) δ ppm: 7.18 - 7.26 (m, 3H, H_{meta} and H_{para} overlapping), 7.04 - 7.18 (m, 5H, H_{ortho}, H₁ and H₂ overlapping), 6.84 (td, *J*=7.45, 1.26 Hz, 2H, H₃), 6.77 (dd, *J*=7.83, 1.01 Hz, 2H, H₄), 6.12 (br. s., 1H, NH), 5.31 (s, 1H, H₉).

¹³C {¹H} NMR (100.62 MHz, 298 K, CDCl₃) δ ppm: 147.1 (C_{ipso}), 138.9 (C₅), 129.6 (C₂), 128.6 (C_{meta}), 127.8 (C_{para}), 127.3 (C₁), 126.3 (C_{ortho}), 123.6 (C₆), 120.9 (C₃), 113.8 (C₄), 47.5 (C₉).

Synthesis of 9-phenylacridine

Acridine (1.5 mL of a 1 M solution in THF, 1.5 mmol) was added to a THF solution of zincate **15** or **16** (0.5 mmol) prepared *in situ* as above. This mixture was then microwaved (125 °C) for 10 minutes, before being quenched with oxygen and water. DDQ (0.5 mL of a 1 M solution in THF, 0.5 mmol) was added and the mixture left to stir for one hour before being extracted three times with ethyl acetate. The organic layer was purified by silica flash chromatography.

¹H NMR (400.13 MHz, 298 K, CDCl₃) δ ppm: 8.29 (d, *J*=8.78 Hz, 2H, H₁-acridine), 7.78 (m, 2H, H₂-acridine), 7.72 (d, *J*=8.78 Hz, 2H, H₄-acridine), 7.59 - 7.66 (m, 3H, H_{meta} and H_{para} overlapping), 7.41 - 7.48 (m, 4H, H₃-acridine and H_{ortho} overlapping).

^{13}C $\{^1\text{H}\}$ NMR (100.62 MHz, 298 K, CDCl_3) δ ppm: 148.9 ($\text{C}_{\text{quaternary}}$), 130.4 (C4), 129.9 (C3), 129.6 (C_{meta}), 128.4 (C_{ortho}), 128.3 ($\text{C}_{\text{quaternary}}$), 126.9 (C2), 125.6 (C1), 125.2 ($\text{C}_{\text{quaternary}}$). Consistent with published data.^[146]

Synthesis of $[(\text{THF})_3\text{Li}(\text{NC}_{13}\text{H}_9\text{-9-Ph})]$ **17**

Acridine (1 mL of a 1 M solution in THF, 1 mmol) was added to a THF solution of zincate **16** (0.5 mmol) prepared *in situ* as above. This mixture was then microwaved (125 °C) for 10 minutes. Crystals of **17** were isolated in a 31 % yield (with respect to acridine) after storage at -70 °C.

^1H NMR (400.13 MHz, 298 K $\text{d}_8\text{-THF}$) δ ppm: 7.06 (d, $J=7.60$ Hz, 2 H, H_{ortho}), 6.95 (t, $J=7.33$ Hz, 2 H, H_{meta}), 6.84 (t, $J=6.82$ Hz, 1 H, H_{para}), 6.74 (d, $J=7.33$ Hz, 2 H, $\text{H}_1\text{-acridine}$), 6.67 (t, $J=7.20$ Hz, 2 H, $\text{H}_3\text{-acridine}$), 6.46 (d, $J=7.83$ Hz, 2 H, $\text{H}_4\text{-acridine}$), 6.20 (t, $J=7.07$ Hz, 2 H, $\text{H}_2\text{-acridine}$), 5.00 (s, 1 H, $\text{H}_9\text{-acridine}$), 3.54 - 3.62 (m, 12 H, $\text{H}_\alpha\text{-THF}$), 1.68 - 1.77 (m, 12 H, $\text{H}_\beta\text{-THF}$).

^{13}C $\{^1\text{H}\}$ NMR (100.62 MHz, 298 K, $\text{d}_8\text{-THF}$) δ ppm: 153.9 ($\text{C}_{\text{quaternary}}$), 151.7 ($\text{C}_{\text{quaternary}}$), 141.2 (C_{ipso}), 129.3 (C1), 128.4 (C_{ortho}), 128.1 (C_{meta}), 126.3 (C3), 125.3 (C_{para}), 118.8 (C4), 114.2 (C2), 68.3 ($\text{C}_\alpha\text{-THF}$), 50.8 (C9), 33.0 ($\text{C}_\beta\text{-THF}$).

^7Li NMR (298 K, $\text{d}_8\text{-THF}$, reference LiCl in D_2O at 0.00 ppm) δ ppm: 0.74 ppm. Calculated; C (77.64%), H (7.99%), N (2.92%). Observed; C (76.46%), H (8.06%), N (3.11%).

Synthesis of $\{[(\text{TMEDA})\text{Li}(\text{THF})]^+\{\text{NC}_{13}\text{H}_8\text{-9-Ph}\}^-\}$ **18**

To a solution of acridine (0.18 g, 1 mmol) in THF (5 mL) was added TMEDA (0.45 mL, 3 mmol). The solution was cooled to 0 °C and PhLi (1.12 mL of a 0.8 M solution in dibutyl ether, 1 mmol) was added dropwise, and the reaction stirred for 2 hours before being warmed to room temperature. The solution deposited deep purple crystals in 8% yield on standing at room temperature.

Calculated; C (77.13%), H (8.48%), N (9.33%). Observed; C (75.43%), H (8.18%), N (9.10%).

Synthesis of $[\text{Ph}_2\text{Zn}(\text{NC}_{13}\text{H}_9)]$ 19

To a suspension of Ph_2Zn (0.22 g, 1 mmol) in hexane (10 mL) was added acridine (0.18 g, 1 mmol). 30 mL of hot toluene was added giving a yellow solution which was cooled to room temperature slowly in a hot water bath resulting in the deposition of crystals in a 29% yield.

^1H NMR (400.13 MHz, 298 K, C_6D_6) δ ppm: 8.26 (dd, $J=8.84, 0.76$ Hz, 2 H, H_1 -acridine), 7.97 (s, 1 H, H_9 -acridine), 7.82 - 7.86 (m, 4 H, H_{ortho}), 7.37 (dt, $J=8.40, 0.73$ Hz, 2 H, H_{para}), 7.32 - 7.26 (m, 6 H, H_{meta} and H_4 -acridine overlapping), 7.03 (ddd, $J=8.65, 6.76, 1.52$ Hz, 2 H, H_2 -acridine), 6.90 - 6.96 (m, 2 H, H_3 -acridine).

^{13}C $\{^1\text{H}\}$ NMR (101.69 MHz, 298 K, C_6D_6) δ ppm: 155.0 ($\text{C}_{\text{quaternary}}$), 147.7 ($\text{C}_{\text{quaternary}}$), 139.6 (C_9 and C_{ortho}), 132.7 (C_2), 128.8 (C_{para}), 127.7 (C_{meta}), 127.4 (C_4), 126.7 ($\text{C}_{\text{quaternary}}$), 126.2 (C_3), 125.9 (C_1).

^1H NMR (400.13 MHz, 298 K d_8 -THF) δ ppm: 8.87 (s, 1 H, H_9 -acridine) 8.18 (dd, $J=8.08, 0.76$ Hz, 2 H, H_1 -acridine) 8.05 (br. dd, $J=9.30, 8.60$ Hz, 2 H, H_4 -acridine) 7.75 (ddd, $J=8.65, 6.76, 1.52$ Hz, 2 H, H_2 -acridine) 7.55 - 7.59 (m, 4 H, H_{ortho}) 7.52 (ddd, $J=8.15, 6.76, 1.01$ Hz, 2 H, H_3 -acridine) 7.11 (br. dt, $J=7.80, 7.10, 7.10$ Hz, 4 H, H_{meta}) 7.04 (tt, $J=7.33, 2.53$ Hz, 2 H, H_{para}).

^{13}C $\{^1\text{H}\}$ NMR (100.62 MHz, 298 K, d_8 -THF) δ ppm: 156.8 ($\text{C}_{\text{quaternary}}$), 150.2 ($\text{C}_{\text{quaternary}}$), 139.6 (C_{ortho}), 136.3 (C_9) 130.6, (C_3 and C_4), 129.0 ($\text{C}_{\text{quaternary}}$), 127.6 (C_1), 127.2 (C_2), 126.3 (C_{meta}), 126.1 (C_{para}).

Calculated; C (75.29%), H (4.80%), N (3.51%). Observed; C (74.24%), H (4.79%), N (4.03%).

Synthesis of [(TMEDA)₂LiZnEt₃] 20

To a solution of ethyllithium (2 mL of a 0.5 M solution in hexane/benzene, 1 mmol) in hexane was added diethylzinc (1 mL of a 1 M solution in heptane, 1 mmol) followed by TMEDA (0.30 mL, 2 mmol).

¹H NMR (400.13 MHz, 298 K d₈-THF) δ ppm: 2.36 (s, 8 H, CH₂-N TMEDA), 2.20 (s, 24 H, CH₃-N TMEDA), 1.18 (t, *J*=8.08 Hz, 12 H, CH₃ ethyl), -0.25 (q, *J*=8.08 Hz, 6 H, CH₂ ethyl).

¹³C {¹H} NMR (100.62 MHz, 298 K, d₈-THF) δ ppm: 58.5 (CH₂-TMEDA), 46.7 (CH₃-TMEDA), 15.3 (CH₃ ethyl), 3.9 (CH₂ ethyl).

⁷Li NMR (298 K, d₈-THF, reference LiCl in D₂O at 0.00 ppm) δ ppm: 1.49.

Synthesis of 9-ethylacridine

To a solution of **20** in hexane, prepared *in situ* as above, was added acridine (0.1 ml of a 1M solution in THF, 1 mmol). The resulting solution stirred at room temperature for 2 hours before being quenched with oxygen and water. The mixture was extracted three times with ethyl acetate and the organic layer was purified by silica flash chromatography.

¹H NMR (400.13 MHz, 298 K CDCl₃) δ ppm: 8.41 (d, *J*=8.78 Hz, 2 H, H₁-acridine) 8.35 (d, *J*=8.53 Hz, 2 H, H₄-acridine) 7.91 (ddd, *J*=8.72, 6.59, 1.25 Hz, 2 H, H₂-acridine) 7.68 (ddd, *J*=8.91, 6.65, 1.00 Hz, 2 H, H₃-acridine) 3.75 (q, *J*=7.78 Hz, 2 H, CH₂-ethyl) 1.53 (t, *J*=7.65 Hz, 3 H, CH₃-ethyl). **¹³C {¹H} NMR (100.62 MHz, 298 K, CDCl₃)** δ ppm: 144.9 (C_{quaternary}), 132.3 (C₂), 131.1 (C_{quaternary}), 127.0 (C₁), 126.5 (C₃), 124.4 (C₄), 21.6 (CH₂-ethyl), 15.6 (CH₃-ethyl).

Synthesis of [(TMEDA)(THF)Li(NC₁₃H₉-9-Et)] 21

To a solution of **20** – prepared *in situ* as above – was added acridine (0.18g, 1 mmol) followed by 1 mL of THF. The resulting solution was stirred at room temperature for one hour, before flash freezing in liquid nitrogen. Crystals of **21** were isolated in a 20 % yield after 48 hours storage at -27 °C.

¹H NMR (400.13 MHz, 298 K d₈-THF) δ ppm: 6.69 (m, 4 H, H₁ and H₄-acridine), 6.41 (br. s., 2 H, H₃-acridine), 6.23 (br. s., 2 H, H₂-acridine), 3.61 (m, 5 H, H₂-acridine and H_α-THF), 2.32 (s, 4 H, CH₂-TMEDA), 2.16 (s, 12 H, CH₃-TMEDA), 1.77 (m, 4 H, H_β-THF), 1.37 (s, 2 H, CH₂-ethyl), 0.68 (t, *J*=7.33 Hz, 3 H, CH₃-ethyl).
¹³C {¹H} NMR (100.62 MHz, 298 K, d₈-THF) δ ppm: 154.3 (C_{quaternary}), 128.6 (C1), 126.0 (C4), 118.1 (C3), 113.8 (C2), 68.4 (C_α-THF), 59.0 (CH₂-TMEDA), 47.1 (C9), 46.5 (CH₃-TMEDA), 34.2 (CH₂-ethyl), 26.5 (C_β-THF), 11.1 (CH₃-ethyl).

⁷Li NMR (298 K, d₈-THF, reference LiCl in D₂O at 0.00 ppm) δ ppm: 2.57.

Synthesis of [(THF)₂Zn(Et)]₂[μ-(NC₁₃H₉-C₁₃H₉N)] 22

To a solution of acridine (0.18g, 1 mmol) in THF (2 mL) was added diethylzinc (1 mL, 1 mmol) and the resulting solution was left under a UV lamp for 4 hours, resulting in the crystallisation of **22** in an 18 % yield. Due to the highly insoluble nature of this compound no useful NMR data could be obtained.

Calculated; C (66.10%), H (7.24%), N (3.35%). Observed; C (%), H (%), N (%).

Synthesis of [(THF)₂Li(N₂C₄H₄-2-Ph)]_∞ 23

To a solution of pyrazine (0.08g, 1mmol) in THF (2 mL) cooled to -78 °C was added PhLi (0.56 mL of a 0.8 M solution in dibutyl ether, 1 mmol). The reaction was stirred for 5 minutes at -78 °C before being placed in the freezer (-30 °C) still in the -78 °C cooling bath. A crop of orange crystals were isolated in a 71% yield.

¹H NMR (400.13 MHz, 298 K d₈-THF) δ ppm: 7.35 (d, *J*=7.58 Hz, 2H, H_{ortho}), 6.89 (t, *J*=7.71 Hz, 4H, H_{meta}), 6.80 (s, 1H, H₃-pyrazine), 6.48 (t, *J*=7.20 Hz, 1H, H_{para}), 5.66 (t, *J*=2.65 Hz, 1H, H₆-pyrazine), 3.62 (t, *J*=6.57 Hz, 8H, H_α-THF), 3.28 (d, *J*=2.53 Hz, 2H, H₅-pyrazine), 1.69 - 1.83 (m, 8H, H_β-THF).

¹³C {¹H} NMR (100.62 MHz, 298 K, d₈-THF) δ ppm: 145.0 (C₂), 142.8 (C₃), 128.1 (C_{meta}), 124.4 (C_{ipso}), 119.4 (C_{ortho}), 118.9 (C_{para}), 115.4 (C₆), 68.2 (C_α-THF), 51.3 (C₅), 26.54 (C_β-THF).

⁷Li NMR (298 K, d₈-THF, reference LiCl in D₂O at 0.00 ppm) δ ppm: 0.19.

Synthesis of [Ph₂Zn(Pyr)₂]_∞ **24**

To a suspension of ZnPh₂ (0.22 g, 1 mmol) in hexane (10 mL) was added 1,4-pyrazine (0.08 g, 1 mmol), giving a thick yellow suspension which was stirred at room temperature for 2 hours. The precipitate was dissolved on the addition of hot toluene (60 mL) and the resulting solution left to cool slowly to room temperature. A crop of yellow crystals were isolated (0.08 g, 27 %).

¹H NMR (400.13 MHz, 298 K d₈-THF) δ ppm: 8.60 (s, 4H, H-pyrazine), 7.56 (dd, 4H, H_{ortho}), 7.11 (t, 4H, H_{meta}), 7.01 (tt, 2H, H_{para}).

¹³C {¹H} NMR (100.62 MHz, 298 K, d₈-THF) δ ppm: 157.1 (C_{ipso}), 146.1 (pyrazine-CH), 139.7 (C_{ortho}), 127.3 (C_{meta}), 126.0 (C_{para}).

Synthesis of 2-Phenylpyrazine

Pyrazine (0.08 g, 1 mmol) was added to a THF solution of zincate **15** or **16** prepared *in situ* as above. This reaction mixture was then refluxed (75 °C) for 24 hours, before being quenched with air and water. The mixture was extracted three times with ethyl acetate and the organic layer was purified by silica flash chromatography.

¹H NMR (400.13 MHz, 298 K, CDCl₃) δ ppm: 9.02 (s, 1H, H₃-pyrazine), 8.62 (d, 1H, H₆-pyrazine), 8.50 (d 1H, H₅-pyrazine), 8.01 (dd, 2H, H_{ortho}), 7.50 (m, 3H, H_{meta} and H_{para} overlapping).

¹³C {¹H} NMR (100.62 MHz, 298 K, CDCl₃) δ ppm: 152.8 (C₂), 144.1 (C₃), 142.9 (C₆), 142.2 (C₅), 136.3 (C_{ipso}), 129.9 (C_{meta}), 129.0 (C_{para}), 126.9 (C_{ortho}). Consistent with published data.^[144144]

Synthesis of 2,5-Diphenylpyrazine

Pyrazine (0.08 g, 1 mmol) was added to a THF solution of zincate **15** or **16** prepared *in situ* as above. This reaction mixture was then refluxed (75 °C) for 24 hours, before being quenched with air and water. The mixture was extracted three times with ethyl acetate and the organic layer was purified by silica flash chromatography.

¹H NMR (400.13 MHz, 298 K, CDCl₃) δ ppm: 9.04 (s, 2H, H-pyrazine), 8.23 (dd, 4H, H_{ortho}), 7.60-7.48 (m, 6H, H_{meta} and H_{para} overlapping).

¹³C {¹H} NMR (100.62 MHz, 298 K, CDCl₃) δ ppm: 151.5 (C₂), 142.2 (C-pyrazine), 136.5 (C_{ipso}), 128.9 (C_{meta}), 126.9 (C_{ortho}).

Synthesis of 2-Phenylquinoline

Quinoline (0.12 mL, 1 mmol) was added to a THF solution of zincate **15** or **16** prepared *in situ* as above. This reaction mixture was then refluxed (75 °C) for 24 hours, before being quenched with air and water. The mixture was extracted three times with ethyl acetate and the organic layer was purified by silica flash chromatography.

¹H NMR (400.13 MHz, 298 K, CDCl₃) δ ppm: 8.25 (d, *J*=8.59 Hz, 1H, H₄-quinoline), 8.18 (m, 3H, H₆-quinoline and H_{ortho} overlapping), 7.89 (d, *J*=8.59 Hz, 1H, H₅-quinoline), 7.84 (d, *J*=8.08 Hz, 1H, H₃-quinoline), 7.74 (t, *J*=8.08 Hz, 1H,

H₇-quinoline), 7.55 (m, 3H, H₈-quinoline and H_{meta} overlapping), 7.48 (tt, $J=7.33$, 2.02 Hz, 1H, H_{para}).

¹³C {¹H} NMR (100.62 MHz, 298 K, CDCl₃) δ ppm: 157.4 (C_{quarternary}), 150.4 (C_{quarternary}), 148.3 (C_{quarternary}), 139.7 (C_{quarternary}), 136.8 (C₄), 129.7 (C₇), 129.4 (C₅), 129.2 (C_{para}), 128.7 (C_{meta}), 127.7 (C_{ortho}), 127.5 (C₆), 126.4 (C₈), 119.0 (C₃).

Synthesis of $[\{\text{Na}(\text{THF})_6\}^+\{\text{Ph}_2\text{Si}(\text{NDipp})_2\text{ZnEt}\}^-]$ **29**

To a suspension of butylsodium (0.08 g, 1 mmol) in hexane (2 mL) was added a solution of diethylzinc (1.0 mL of a 1 M solution in heptane, 1 mmol). The resulting colourless solution was stirred at room temperature for 20 minutes before the addition of Ph₂Si(NHDipp)₂ (0.53 g, 1 mmol) and the resulting white suspension left to stir at room temperature for 40 minutes. THF (2 mL) was then added to dissolve the precipitate, resulting in the formation of a colourless oil which was frozen in liquid nitrogen and stored at -27°C for 24 hours, resulting in the isolation of colourless crystals in a 60% yield.

¹H NMR (400.13 MHz, 298 K, C₆D₆) δ ppm: 7.49 - 7.56 (m, 4 H, H_{ortho} phenyl) 7.18 (s, 4 H, H_{meta} Dipp) 7.02 - 7.15 (m, 6 H, H_{meta} and H_{para} phenyl) 6.94 - 7.01 (m, 2 H, H_{para} Dipp) 4.27 (septet, $J=13.60$ Hz, 4 H, CH ⁱPr) 3.28 - 3.41 (m, 12 H, H_α-THF) 1.42 (t, $J=7.96$ Hz, 3 H, CH₃ ethyl) 1.29 - 1.38 (m, 12 H, H_β-THF) 1.14 (d, $J=6.82$ Hz, 24 H, CH₃ ⁱPr) 0.45 (q, $J=8.08$ Hz, 2 H, CH₂ ethyl).

¹³C {¹H} NMR (101.69 MHz, 298 K, C₆D₆) δ ppm: 150.8 (quaternary phenyl) 144.5 (quaternary Dipp) 144.2 (quaternary Dipp) 135.3 (C_{ortho} phenyl) 126.9 (C_{meta} and C_{para} phenyl) 123.6 (C_{meta} Dipp) 119.5 (C_{para} Dipp) 68.2 (C_α THF) 28.2 (CH ⁱPr) 25.5 (C_β THF) 24.6 (CH₃ ⁱPr) 13.0 (CH₃ ethyl) 0.9 (CH₂ ethyl).

Synthesis of $[\text{Ph}_2\text{Si}(\text{NHDipp})_2\text{Zn}(\text{TMP})\text{Na}(\text{THF})]$ **30**

To a suspension of butylsodium (0.08 g, 1 mmol) in hexane (2 mL) was added Ph₂Si(NHDipp)₂ (0.53 g, 1 mmol) and the resulting suspension stirred for one hour.

THF (~ 0.5 mL) was added dropwise until a clear solution was obtained and Zn(TMP)₂ (0.35 g, 1 mmol) was added and left to stir for 2 hours. Storage at - 27 °C resulted in a crop of colourless crystals in a 75 % yield.

¹H NMR (400.13 MHz, 298 K, C₆D₆) δ ppm: 7.56 (d, *J*=3.03 Hz, 4 H, H_{ortho} phenyl) 7.18 (s, 4 H, H_{meta} Dipp) 7.11 (br. s., 6 H, H_{meta} and H_{para} phenyl) 6.95 (t, *J*=7.83 Hz, 2 H, H_{para} Dipp) 4.37 (septet, *J*=13.50 Hz, 4 H, CH ^{*i*}Pr) 3.18 (m, 4 H, H_α THF) 1.47 (m, 2 H, H_γ TMP) 1.27 (s, 12 H, CH₃ TMP) 1.22 (br. s., 4 H, H_β THF) 0.97 - 1.18 (m, 28 H, CH₃ ^{*i*}Pr and H_β TMP).

¹³C {¹H} NMR (101.69 MHz, 298 K, C₆D₆) δ ppm: 149.6 (Q_{uaternary} phenyl) 145.0 (Q_{uaternary} Dipp) 135.7 (C_{ortho} phenyl) 126.9 (C_{meta/para} phenyl) 123.9 (C_{meta} Dipp) 119.8 (C_{para} Dipp) 68.1 (C_α THF) 52.8 (C_α TMP) 40.9 (C_β TMP) 37.0 (CH₃ TMP) 28.0 (CH ^{*i*}Pr) 25.4 (C_β THF) 25.3 (CH₃ ^{*i*}Pr) 18.7 (C_γ TMP).

Synthesis of [Na(THF)₂Zn(NSC₇H₄)₃]₂ **31**

To a solution of either [$\{\text{Na}(\text{THF})_6\}^+\{(\text{Ph}_2\text{Si}(\text{NDipp})_2)\text{ZnEt}\}^-]$ **29** or $[(\text{Ph}_2\text{Si}(\text{NDipp})_2)\text{Zn}(\text{TMP})\text{Na}(\text{THF})]$ **30** (1 mmol) in a 1:1 mixture of hexane and THF, prepared *in situ* as above, was layered a solution of benzothiazole (0.33 mL, 3 mmol) in THF (2 mL) and the two solutions allowed to slowly diffuse. This resulted in the formation of a yellow solid which was isolated in batches of up to 250 mg. The product was poorly soluble in d₈-THF; however, the spectra obtained confirmed that the compound was not pure.

Synthesis of [Na₂(THF)₄Zn(NC₄H₄)₄]_∞ **32**

To a solution of either [$\{\text{Na}(\text{THF})_6\}^+\{(\text{Ph}_2\text{Si}(\text{NDipp})_2)\text{ZnEt}\}^-]$ **29** or $[(\text{Ph}_2\text{Si}(\text{NDipp})_2)\text{Zn}(\text{TMP})\text{Na}(\text{THF})]$ **30** (1 mmol) in a 1:1 mixture of hexane and THF, prepared *in situ* as above, was added 2 equivalents of pyrrole (0.14 mL, 2 mmol) and the solution was stirred at room temperature for 60 minutes. Storage at - 27 °C for 24 hours resulted in the isolation of colourless crystals in a 41% yield.

¹H NMR (400.13 MHz, 298 K, THF) δ ppm: 6.93 (t, $J=1.41$ Hz, 8 H, α -CH pyrrole), 6.05 (t, $J=1.57$ Hz, 8 H, β -CH pyrrole), 3.59 - 3.65 (m, 4 H, H_{α} THF), 1.75 - 1.81 (m, 4 H, H_{β} THF).

¹³C NMR (101.69 MHz, 298 K, THF) δ ppm: 127.2 (α -C pyrrole), 106.6 (β -C pyrrole), 68.3 (C_{α} THF), 26.4 (H_{β} THF).

Bibliography

- [1] D. B. Collum, *Acc. Chem. Res.* **1993**, *26*, 227-234.
- [2] a) P. Beak, V. Snieckus, *Acc. Chem. Res.* **1982**, *15*, 306-312; b) P. Beak, A. I. Meyers, *Acc. Chem. Res.* **1986**, *19*, 356-363; c) V. Snieckus, *Chem. Rev.* **1990**, *90*, 879-933; d) J. Clayden, *Organolithiums: Selectivity for Synthesis*, Vol. 23, Pergamon, Oxford, **2002**; e) M. Schlosser, *Angew. Chem., Int. Ed. Engl.* **2005**, *44*, 376-393; f) R. Chinchilla, C. Nájera, M. Yus, *Chem. Rev.* **2004**, *104*, 2667-2722; g) M. C. Whisler, S. MacNeil, V. Snieckus, P. Beak, *Angew. Chem., Int. Ed. Engl.* **2004**, *43*, 2206-2225; h) G. Wu, M. Huang, *Chem. Rev.* **2006**, *106*, 2596-2616; i) R. E. Mulvey, F. Mongin, M. Uchiyama, Y. Kondo, *Angew. Chem., Int. Ed. Engl.* **2007**, *46*, 3802-3824; j) R. E. Mulvey, *Acc. Chem. Res.* **2009**, *42*, 743-755.
- [3] M. Schlosser, Second ed., John Wiley & Sons, Chichester, **2004**.
- [4] a) W. E. Parham, Y. A. Sayed, *J. Org. Chem.* **1974**, *39*, 2053-2056; b) C. J. Upton, P. Beak, *J. Org. Chem.* **1975**, *40*, 1094-1098; c) W. E. Parham, L. D. Jones, *J. Org. Chem.* **1976**, *41*, 2704-2706; d) P. Stanetty, M. D. Mihovilovic, *J. Org. Chem.* **1997**, *62*, 1514-1515.
- [5] B. Haag, M. Mosrin, H. Ila, V. Malakhov, P. Knochel, *Angew. Chem., Int. Ed. Engl.* **2011**, *50*, 9794-9825.
- [6] P. Knochel, W. Dohle, N. Gommermann, F. F. Kneisel, F. Kopp, T. Korn, I. Sapountzis, V. A. Vu, *Angew. Chem., Int. Ed. Engl.* **2003**, *42*, 4302-4320.
- [7] a) S. Reformatsky, *Ber. Dtsch. Chem. Ges.* **1887**, *20*, 1210-1211; b) P. G. Cozzi, A. Mignogna, L. Zoli, *Pure Appl. Chem.* **2008**, *80*, 891-901.
- [8] a) E.-I. Negishi, A. O. King, N. Okukado, *J. Org. Chem.* **1977**, *42*, 1821-1823; b) A. O. King, N. Okukado, E.-I. Negishi, *J. Chem. Soc., Chem. Commun.* **1977**, 683-684; c) A. O. King, E.-I. Negishi, F. J. Villani Jr., A. Silveira Jr., *J. Org. Chem.* **1978**, *43*, 358-360.
- [9] a) H. E. Simmons, R. D. Smith, *J. Am. Chem. Soc.* **1958**, *80*, 5323-5324; b) H. E. Simmons, R. D. Smith, *J. Am. Chem. Soc.* **1959**, *81*, 4256-4264.
- [10] E. Frankland, *Justus Liebigs Ann.* **1849**, *71*, 171.

- [11] a) P. Knochel, P. Jones, *Organozinc Reagents a Practical Approach*, Oxford University Press, **1999**; b) R. D. Rieke, *Acc. Chem. Res.* **1977**, *10*, 301-306; c) Z. Rappoport, I. Marek, in *Patai Series; The Chemistry of Functional Groups, Vol. Part 1* (Ed.: Z. Rappoport), John Wiley & Sons, Chichester, **2006**.
- [12] a) R. D. Rieke, S. J. Uhm, P. M. Hudnall, *J. Chem. Soc., Chem. Commun.* **1973**, 269-270; b) R. D. Rieke, S. J. Uhm, *Synthesis* **1975**, *7*, 452.
- [13] R. D. Smith, H. E. Simmons, *Org. Synth.* **1961**, *41*, 72.
- [14] a) A. Vaupel, P. Knochel, *J. Org. Chem.* **1996**, *61*, 5743-5753; b) K. Kanai, H. Wakabayashi, T. Honda, *Org. Lett.* **2000**, *2*, 2549-2551; c) J. C. Adrian, M. L. Snapper, *J. Org. Chem.* **2003**, *68*, 2143-2150.
- [15] a) J. Furukawa, N. Kawabata, J. Nishimura, *Tetrahedron Lett.* **1966**, 3353-3354; b) J. Furukawa, N. Kawabata, J. Nishimura, *Tetrahedron* **1968**, *24*, 53-58.
- [16] D. Seyferth, *Organometallics* **2001**, *20*, 2940-2955.
- [17] M. Hatano, S. Suzuki, K. Ishihara, *J. Am. Chem. Soc.* **2006**, *128*, 9998-9999.
- [18] a) J. A. Wanklyn, *Justus Liebigs Ann. Chem.* **1858**, *107*, 125; b) J. A. Wanklyn, *Proceedings of the Royal Society of London* **1858**, *9*, 341-345.
- [19] D. T. Hurd, *J. Org. Chem.* **1948**, *13*, 711-713.
- [20] G. Wittig, F. J. Meyer, G. Lange, *Justus Liebigs Ann. Chem.* **1951**, *571*, 167.
- [21] R. E. Mulvey, *Organometallics* **2006**, *25*, 1060-1075.
- [22] F. F. Kneisel, M. Dochnahl, P. Knochel, *Angew. Chem., Int. Ed. Engl.* **2004**, *43*, 1017-1021.
- [23] a) M. Uchiyama, M. Koike, M. Kameda, Y. Kondo, T. Sakamoto, *J. Am. Chem. Soc.* **1996**, *118*, 8733-8734; b) M. Uchiyama, M. Kameda, O. Mishima, N. Yokoyama, M. Koike, Y. Kondo, T. Sakamoto, *J. Am. Chem. Soc.* **1998**, *120*, 4934-4946; c) M. Uchiyama, T. Furuyama, M. Kobayashi, Y. Matsumoto, K. Tanaka, *J. Am. Chem. Soc.* **2006**, *128*, 8404; d) T. Furuyama, M. Yonehara, S. Arimoto, M. Kobayashi, Y. Matsumoto, M. Uchiyama, *Chem. Eur. J.* **2008**, *14*, 10348-10356.
- [24] a) M. Uchiyama, S. Furumoto, M. Saito, Y. Kondo, T. Sakamoto, *J. Am. Chem. Soc.* **1997**, *119*, 11425-11433; b) M. Uchiyama, S. Nakamura, T.

- Ohwada, M. Nakamura, E. Nakamura, *J. Am. Chem. Soc.* **2004**, *126*, 10897-10903.
- [25] W. Clegg, G. C. Forbes, A. R. Kennedy, R. E. Mulvey, S. T. Liddle, *Chem. Commun.* **2003**, 406-407.
- [26] P. C. Andrikopoulos, D. R. Armstrong, D. V. Graham, E. Hevia, A. R. Kennedy, R. E. Mulvey, C. T. O'Hara, C. Talmard, *Angew. Chem., Int. Ed.* **2005**, *44*, 3459-3462.
- [27] D. R. Armstrong, W. Clegg, S. H. Dale, E. Hevia, L. M. Hogg, G. W. Honeyman, R. E. Mulvey, *Angew. Chem., Int. Ed. Engl.* **2006**, *45*, 3775-3778.
- [28] A. R. Kennedy, J. Klett, R. E. Mulvey, D. S. Wright, *Science* **2009**, *326*, 706-708.
- [29] a) G. C. Forbes, A. R. Kennedy, R. E. Mulvey, B. A. Roberts, R. B. Rowlings, *Organometallics* **2002**, *21*, 5115-5121; b) A. E. H. Wheatley, *New J. Chem.* **2004**, *28*, 435-443; c) D. V. Graham, E. Hevia, A. R. Kennedy, R. E. Mulvey, *Organometallics* **2006**, *25*, 3297-3300; d) D. R. Armstrong, C. Dougan, D. V. Graham, E. Hevia, A. R. Kennedy, *Organometallics* **2008**, *27*, 6063-6070.
- [30] C. Lambert, P. von Ragué Schleyer, *Angew. Chem., Int. Ed. Engl.* **1994**, *33*, 1129-1140.
- [31] S. Merkel, D. Stern, J. Henn, D. Stalke, *Angew. Chem., Int. Ed.* **2009**, *48*, 6350-6353.
- [32] S. Nakamura, C.-Y. Liu, A. Muranaka, M. Uchiyama, *Chem. Eur. J.* **2009**, *15*, 5686-5694.
- [33] T. A. Mobley, S. Berger, *Angew. Chem., Int. Ed. Engl.* **1999**, *38*, 3070-3072.
- [34] E. Weiss, R. Wolfrum, *Chem. Ber.* **1968**, *101*, 35.
- [35] a) A. Metzger, S. Bernhardt, G. Manolikakes, P. Knochel, *Angew. Chem., Int. Ed. Engl.* **2010**, *49*, 4665-4668; b) D. R. Armstrong, W. Clegg, P. Garcia-Álvarez, A. R. Kennedy, M. D. McCall, L. Russo, E. Hevia, *Chem. Eur. J.* **2011**, *17*, 8333-8341; c) E. Hevia, R. E. Mulvey, *Angew. Chem., Int. Ed. Engl.* **2011**, *50*, 6448-6450.
- [36] A. P. Purdy, C. F. George, *Organometallics* **1992**, *11*, 1955-1959.

- [37] a) D. Seyferth, *Organometallics* **2006**, *25*, 2-24; b) D. Seyferth, *Organometallics* **2009**, *28*, 2-33.
- [38] H. Gilman, R. G. Jones, *J. Am. Chem. Soc.* **1941**, *63*, 1441-1443.
- [39] W. Langham, R. Q. Brewster, H. Gilman, *J. Am. Chem. Soc.* **1941**, *63*, 545-549.
- [40] H. Gilman, R. D. Gorsich, *J. Am. Chem. Soc.* **1956**, *78*, 2217-2222.
- [41] a) J. Clayden, S. A. Yasin, *New J. Chem.* **2002**, *26*, 191-192; b) A. R. Kennedy, J. Klett, R. E. Mulvey, D. S. Wright, *Science (Washington, DC, U. S.)* **2009**, *326*, 706-708.
- [42] a) S. Vettel, A. Vaupel, P. Knochel, *J. Org. Chem.* **1996**, *61*, 7473-7481; b) A. Lemire, A. Côté, M. K. Janes, A. B. Charette, *Aldrichimica Acta* **2009**, *42*, 71-83.
- [43] D. Tilly, F. Chevallier, F. Mongin, P. C. Gros, *Chem. Rev.* **2013**, *114*, 1207-1257.
- [44] T. Harada, K. Hattori, T. Katsuhira, A. Oku, *Tetrahedron Lett.* **1989**, *30*, 6035-6038.
- [45] a) T. Harada, T. Katsuhira, A. Oku, *J. Org. Chem.* **1992**, *57*, 5805-5807; b) T. Harada, T. Katsuhira, K. Hattori, A. Oku, *J. Org. Chem.* **1993**, *58*, 2958-2965.
- [46] Y. Kondo, N. Takazawa, C. Yamazaki, T. Sakamoto, *J. Org. Chem.* **1994**, *59*, 4717-4718.
- [47] L. Micouin, P. Knochel, *Synlett* **1997**, 327.
- [48] a) M. D. McCall, Doctoral Thesis thesis, University of Strathclyde (Glasgow), **2011**; b) E. Hevia, J. Z. Chua, P. García-Álvarez, A. R. Kennedy, M. D. McCall, *PNAS* **2010**, *107*, 5294-5299.
- [49] Y. Kondo, T. Komine, M. Fujinami, M. Uchiyama, T. Sakamoto, *J. Comb. Chem.* **1999**, *1*, 123-126.
- [50] M. Isobe, S. Kondo, N. Nagasawa, C. Goto, *Chem. Lett.* **1977**, 679-682.
- [51] a) R. A. Watson, R. A. Kjonaas, *Tetrahedron Lett.* **1986**, *27*, 1437-1440; b) W. Tuckmantel, K. Oshima, N. Hozaki, *Chem. Ber.* **1986**, *119*, 1581; c) R. A. Kjonaas, R. K. Hoffer, *J. Org. Chem.* **1988**, *53*, 4133-4135; d) A. B. Smith III, T. A. Rano, N. Chida, G. A. Sulikowski, *J. Org. Chem.* **1990**, *55*, 1136-

- 1138; e) N. Shida, T. Uyehara, Y. Yamamoto, *J. Org. Chem.* **1992**, *57*, 5049-5051; f) A. Vaughn, R. D. Singer, *Tetrahedron Lett.* **1995**, *36*, 5683-5686; g) I. Fleming, D. Lee, *Tetrahedron Lett.* **1996**, *37*, 6929-6930; h) I. Fleming, D. Lee, *J. Chem. Soc., Perkin Trans. 1* **1998**, 2701-2709; i) T. Kajiwara, T. Terabayashi, M. Yamashita, K. Nozaki, *Angew. Chem., Int. Ed.* **2008**, *47*, 6606-6610.
- [52] A. G. M. Barrett, J. Head, M. L. Smith, N. S. Stock, A. J. P. White, D. J. Williams, *J. Org. Chem.* **1999**, *64*, 6005-6018.
- [53] C. A. Musser, H. J. Richey Jr., *J. Org. Chem.* **2000**, *65*, 7750-7756.
- [54] H. J. Reich, *Chem. Rev.* **2013**, *113*, 7130-7178.
- [55] T. Katsuhira, T. Harada, K. Maejima, A. Osada, A. Oku, *J. Org. Chem.* **1993**, *58*, 6166-6168.
- [56] T. Harada, T. Katsuhira, A. Osada, K. Iwazaki, K. Maejima, A. Oku, *J. Am. Chem. Soc.* **1996**, *118*, 11377-11390.
- [57] Y. Kondo, M. Shilai, M. Uchiyama, T. Sakamoto, *J. Am. Chem. Soc.* **1999**, *121*, 3539-3540.
- [58] F. Mongin, G. Quéguiner, *Tetrahedron* **2001**, *57*, 4059-4090.
- [59] M. Uchiyama, Y. Matsumoto, D. Nobuto, T. Furuyama, K. Yamaguchi, K. Morokuma, *J. Am. Chem. Soc.* **2006**, *128*, 8748-8750.
- [60] T. Imahori, M. Uchiyama, T. Sakamoto, Y. Kondo, *Chem. Commun.* **2001**, 2450-2451.
- [61] M. Uchiyama, T. Miyoshi, Y. Kajihara, T. Sakamoto, Y. Otani, T. Ohwada, Y. Kondo, *J. Am. Chem. Soc.* **2002**, *124*, 8514-8515.
- [62] W. Clegg, S. H. Dale, E. Hevia, G. W. Honeyman, R. E. Mulvey, *Angew. Chem., Int. Ed. Engl.* **2006**, *45*, 2370-2374.
- [63] K. W. Klinkhammer, *Chem. Eur. J.* **1997**, *3*, 1418-1431.
- [64] M. Uchiyama, C. Wang, *Top. Organomet. Chem.* **2014**, DOI 10.1007/3418_2013_1072.
- [65] W. Clegg, S. H. Dale, A. M. Drummond, E. Hevia, G. W. Honeyman, R. E. Mulvey, *J. Am. Chem. Soc.* **2006**, *128*, 7434-7435.
- [66] a) H. Gilman, R. L. Bebb, *J. Am. Chem. Soc.* **1939**, *61*, 109-112; b) G. Wittig, G. Fuhrman, *Chem. Ber.* **1940**, *73*, 1197.

- [67] W. Bauer, P. von Ragué Schleyer, *J. Am. Chem. Soc.* **1989**, *111*, 7191-7198.
- [68] J. M. Saá, P. M. Deyá, G. A. Suñer, A. Frontera, *J. Am. Chem. Soc.* **1992**, *114*, 9093-9100.
- [69] M. Stratakis, *J. Org. Chem.* **1997**, *62*, 3024-3025.
- [70] a) R. A. Rennels, A. J. Maliakal, D. B. Collum, *J. Am. Chem. Soc.* **1998**, *120*, 421-422; b) S. T. Chadwick, R. A. Rennels, J. L. Rutherford, D. B. Collum, *J. Am. Chem. Soc.* **2000**, *122*, 8640-8647.
- [71] M. Uchiyama, Y. Matsumoto, S. Usui, Y. Hashimoto, K. Morokuma, *Angew. Chem., Int. Ed. Engl.* **2007**, *46*, 926-929.
- [72] M. Uchiyama, S. Nakamura, T. Furuyama, E. Nakamura, K. Morokuma, *J. Am. Chem. Soc.* **2007**, *129*, 13360-13361.
- [73] D. Nobuto, M. Uchiyama, *J. Org. Chem.* **2008**, *73*, 1117-1120.
- [74] W. Clegg, B. Conway, E. Hevia, M. D. McCall, L. Russo, R. E. Mulvey, *J. Am. Chem. Soc.* **2009**, *131*, 2375-2384.
- [75] P. C. Andrikopoulos, D. R. Armstrong, H. R. L. Barley, W. Clegg, S. H. Dale, E. Hevia, G. W. Honeyman, A. R. Kennedy, R. E. Mulvey, *J. Am. Chem. Soc.* **2005**, *127*, 6184-6185.
- [76] D. R. Armstrong, W. Clegg, S. H. Dale, D. V. Graham, E. Hevia, L. M. Hogg, G. W. Honeyman, A. R. Kennedy, R. E. Mulvey, *Chem. Commun.* **2007**, 598-600.
- [77] W. Clegg, S. H. Dale, E. Hevia, L. M. Hogg, G. W. Honeyman, R. E. Mulvey, C. T. O'Hara, *Angew. Chem., Int. Ed. Engl.* **2006**, *45*, 6548-6550.
- [78] D. R. Armstrong, J. García-Álvarez, D. V. Graham, G. W. Honeyman, E. Hevia, A. R. Kennedy, R. E. Mulvey, *Chem. Eur. J.* **2009**, *15*, 3800-3807.
- [79] L. Balloch, A. R. Kennedy, R. E. Mulvey, T. Rantanen, S. D. Robertson, V. Snieckus, *Organometallics* **2011**, *30*, 145-152.
- [80] W. Clegg, S. H. Dale, R. W. Harrington, E. Hevia, G. W. Honeyman, R. E. Mulvey, *Angew. Chem., Int. Ed. Engl.* **2006**, *45*, 2374-2377.
- [81] L. Balloch, A. R. Kennedy, J. Klett, R. E. Mulvey, C. T. O'Hara, *Chem. Commun.* **2010**, *46*, 2319-2321.
- [82] B. Conway, E. Hevia, A. R. Kennedy, R. E. Mulvey, *Chem. Commun.* **2007**, 2864-2866.

- [83] E. Weiss, *Angew. Chem., Int. Ed. Engl.* **1993**, *32*, 1501-1523.
- [84] D. R. Armstrong, H. S. Emerson, A. Hernán-Gómez, A. R. Kennedy, E. Hevia, *Dalton Trans.* **2014**, DOI 10.1039/c1034dt01131g.
- [85] D. R. Armstrong, E. Herd, D. V. Graham, E. Hevia, A. R. Kennedy, W. Clegg, L. Russo, *Dalton Trans.* **2008**, 1323-1330.
- [86] L. Balloch, J. A. Garden, A. R. Kennedy, T. Rantanen, S. D. Robertson, V. Snieckus, *Angew. Chem., Int. Ed.* **2012**, *51*, 6934-6937.
- [87] E. Alvarez, A. Grirrane, I. Resa, D. del Río, Rodríguez, E. Carmona, *Angew. Chem., Int. Ed. Engl.* **2007**, *46*, 1296-1299.
- [88] W. Clegg, D. V. Graham, E. Herd, E. Hevia, A. R. Kennedy, M. D. McCall, L. Russo, *Inorg. Chem.* **2009**, *48*, 5320.
- [89] D. R. Armstrong, J. A. Garden, A. R. Kennedy, R. E. Mulvey, S. D. Robertson, *Angew. Chem., Int. Ed.* **2013**, *52*, 7190-7193.
- [90] J. A. Garden, A. R. Kennedy, R. E. Mulvey, S. D. Robertson, *Dalton Trans.* **2011**, *40*, 11945-11954.
- [91] H. R. L. Barley, W. Clegg, S. H. Dale, E. Hevia, G. W. Honeyman, A. R. Kennedy, R. E. Mulvey, *Angew. Chem., Int. Ed. Engl.* **2005**, *44*, 6018-6021.
- [92] G. Margraf, H.-W. Lemer, M. Bolte, M. Wagner, *Z. Anorg. Allg. Chem.* **2004**, *630*, 217-218.
- [93] G. C. Forbes, A. R. Kennedy, R. E. Mulvey, R. B. Rowling, W. Clegg, S. T. Liddle, C. C. Wilson, *Chem. Commun.* **2000**, 1759-1760.
- [94] Y. Kondo, J. V. Morey, J. C. Morgan, H. Naka, D. Nobuto, P. R. Raithby, M. Uchiyama, A. E. H. Wheatley, *J. Am. Chem. Soc.* **2007**, *129*, 12734-12738.
- [95] M. Westerhausen, B. Rademacher, W. Schwarz, *Z. Anorg. Allg. Chem.* **1993**, *619*, 675.
- [96] D. Mootz, A. Zinnius, B. Böttcher, *Angew. Chem., Int. Ed. Engl.* **1969**, *8*, 378-379.
- [97] P. R. Markies, G. Schat, O. S. Akkerman, F. Bickelhaupt, W. J. J. Smeets, A. L. Spek, *Organometallics* **1990**, *9*, 2243-2247.
- [98] A. R. Kennedy, R. E. Mulvey, R. B. Rowlings, *J. Am. Chem. Soc.* **1998**, *120*, 7816-7824.

- [99] P. C. Andrikopoulos, D. R. Armstrong, A. R. Kennedy, R. E. Mulvey, C. T. O'Hara, R. B. Rowling, S. Weatherstone, *Inorg. Chim. Acta* **2007**, *360*, 1370-1375.
- [100] C. A. Ogle, B. K. Huckabee, H. C. J. IV, P. F. Sims, S. D. Winslow, *Organometallics* **1993**, *12*, 1960-1963.
- [101] M. Westerhausen, B. Rademacher, W. Schwarz, *Z. Naturforsch., B: Chem. Sci* **1994**, *49*, 199.
- [102] S. E. Baillie, W. Clegg, P. Garcia-Álvarez, E. Hevia, A. R. Kennedy, J. Klett, L. Russo, *Organometallics* **2012**, *31*, 5131-5142.
- [103] a) G. Boche, I. Langholtz, M. Marsch, K. Harms, G. Frenking, *Angew. Chem., Int. Ed. Engl.* **1993**, *32*, 1171-1173; b) M. P. Coles, D. C. Swenson, R. F. Jordan, V. G. Young Jr, *Organometallics* **1997**, *16*, 5183-5194.
- [104] G. C. Forbes, A. R. Kennedy, R. E. Mulvey, P. A. Rodgers, R. E. Rowlings, *Dalton Trans.* **2001**, 1477-1484.
- [105] a) D. R. Armstrong, W. Clegg, S. H. Dale, J. García-Álvarez, R. W. Harrington, E. Hevia, G. W. Honeyman, A. R. Kennedy, R. E. Mulvey, C. T. O'Hara, *Chem. Commun.* **2008**, 187-189; b) W. Clegg, J. García-Álvarez, P. Garcia-Álvarez, D. V. Graham, R. W. Harrington, E. Hevia, A. R. Kennedy, R. E. Mulvey, L. Russo, *Organometallics* **2008**, *27*, 2654-2663.
- [106] W. Clegg, S. T. Liddle, R. E. Mulvey, A. Robertson, *Chem. Commun.* **2000**, 223-224.
- [107] R. E. Allan, M. A. Beswick, N. Feeder, M. Kranz, M. E. G. Mosquera, P. R. Raithby, A. E. H. Wheatley, D. S. Wright, *Inorg. Chem.* **1998**, *37*, 2602.
- [108] a) N. D. R. Barnett, R. E. Mulvey, W. Clegg, P. O'Neil, *J. Am. Chem. Soc.* **1991**, *113*, 8187-8188; b) B. Gehrhus, P. B. Hitchcock, A. R. Kennedy, M. F. Lappert, R. E. Mulvey, P. J. A. Rodger, *J. Organomet. Chem.* **1999**, *587*, 88-92.
- [109] T. Fjeldberg, P. B. Hitchcock, M. F. Lappert, A. J. Thorne, *J. Chem. Soc., Chem. Commun.* **1984**, 822-824.
- [110] M. P. Bernstein, F. E. Romesberg, D. J. Fuller, A. T. Harrison, D. B. Collum, Q.-Y. Liu, P. G. Williard, *J. Am. Chem. Soc.* **1992**, *114*, 5100-5110.

- [111] a) W. Clegg, L. Horsburgh, F. M. Mackenzie, R. E. Mulvey, *J. Chem. Soc., Chem. Commun.* **1995**, 2011-2012; b) W. Clegg, L. Horsburgh, S. T. Liddle, F. M. Mackenzie, R. E. Mulvey, A. Robertson, *Journal of the Chemical Society, Dalton Transactions* **2000**, 1225-1231.
- [112] D. Barr, W. Clegg, L. Cowton, L. Horsburgh, F. M. Mackenzie, R. E. Mulvey, *J. Chem. Soc., Chem. Commun.* **1995**, 891-892.
- [113] M. M. Olmstead, W. J. Grigsby, D. R. Chacon, T. Hascall, P. P. Power, *Inorg. Chim. Acta* **1996**, 251, 273-284.
- [114] A. J. Edwards, A. Fallaize, P. R. Raithby, M.-A. Rennie, A. Steiner, K. L. Verhorevoot, D. S. Wright, *Dalton Trans.* **1996**, 133-137.
- [115] P. B. Hitchcock, M. F. Lappert, X.-H. Wei, *Dalton Trans.* **2006**, 1181-1187.
- [116] D. R. Armstrong, W. Clegg, P. Garcia-Álvarez, M. D. McCall, L. Nuttall, A. R. Kennedy, L. Russo, E. Hevia, *Chem. Eur. J.* **2011**, 17, 4470-4479.
- [117] a) I. Hyodo, M. Tobisu, N. Chatani, *Chem. Asian. J.* **2012**, 7, 1357-1365; b) B. Shao, S. Victory, V. I. Ilyin, R. R. Goehring, Q. Sun, D. Hogenkamp, D. D. Hodges, K. Islam, D. Sha, C. Zhang, P. Nguyen, S. Robledo, G. Sakellaropoulos, R. B. Carter, *J. Mater. Chem.* **2004**, 47, 4277-4285; c) R. W. Friesen, C. Brideau, C. C. Chan, S. Charleson, D. Deschênes, D. Dubé, D. Ethier, R. Fortin, J. Y. Gauthier, Y. Girard, R. Gordon, G. M. Greig, D. Riendeau, C. Savoie, Z. Wang, E. Wong, D. Visco, L. J. Xu, R. N. Young, *Bioorg. Med. Chem. Lett.* **1998**, 8, 2777-2782; d) F. Buron, N. Plé, A. Turck, G. Quéguiner, *J. Org. Chem.* **2005**, 70, 2616-2621; e) P. W. Smith, P. A. Wyman, P. Lovell, C. Goodacre, H. T. Serafinowska, A. Vong, F. Harrington, S. Flynn, D. M. Bradley, R. Porter, S. Coggon, G. Murkitt, K. Searle, D. R. Thomas, J. M. Watson, W. Martin, Z. Wu, L. A. Dawson, *Bioorg. Med. Chem. Lett.* **2009**, 19, 837-840; f) L.-C. Campeau, K. Fagnou, *Chem. Soc. Rev.* **2007**, 36, 1058-1068.
- [118] J. S. Carey, D. Laffan, C. Thomson, M. T. Williams, *Org. Biomol. Chem.* **2006**, 4, 2337-2347.
- [119] M. Schlosser, F. Mongin, *Chem. Soc. Rev.* **2007**, 36, 1161-1172.
- [120] B. Liégault, D. Lapointe, L. Caron, A. Vlassova, K. Fagnou, *J. Org. Chem.* **2009**, 74, 1826-1834.

- [121] A. R. Katritzky, *Handbook of Heterocyclic Chemistry*, 1st ed., Pergamon, New York, **1985**.
- [122] K. Shen, Y. Fu, J.-N. Li, L. Liu, Q.-X. Guo, *Tetrahedron* **2007**, *63*, 1568-1576.
- [123] F. Chevallier, F. Mongin, *Chem. Soc. Rev.* **2008**, *37*, 595-609.
- [124] A. J. Clarke, S. McNamara, O. Meth-Cohn, *Tetrahedron Lett.* **1974**, *15*, 2373-2376.
- [125] R. F. Francis, C. D. Crews, B. S. Scott, *J. Org. Chem.* **1978**, *43*, 3227-3230.
- [126] C. Y. Zhang, J. M. Tour, *J. Am. Chem. Soc.* **1999**, *121*, 8783-8790.
- [127] D. Alberico, M. E. Scott, M. Lautens, *Chem. Rev.* **2007**, *107*, 174-238.
- [128] A. Larivée, J. J. Mousseau, A. B. Charette, *J. Am. Chem. Soc.* **2008**, *130*, 52-54.
- [129] a) M. Murakami, S. Hori, *J. Am. Chem. Soc.* **2003**, *125*, 4720-4721; b) I. Seregin, V. Gevorgyan, *Chem. Soc. Rev.* **2007**, *36*, 1173-1193.
- [130] a) L.-C. Campeau, S. Rousseaux, K. Fagnou, *J. Am. Chem. Soc.* **2005**, *127*, 18020-18021; b) S. H. Cho, S. J. Hwang, S. Chang, *J. Am. Chem. Soc.* **2008**, *130*, 9254-9256; c) L.-C. Campeau, D. R. Stuart, J.-P. Leclerc, M. Bertrand-Laperle, E. Villemure, H.-Y. Sun, S. Lasserre, N. Guimond, M. Lecavallier, K. Fagnou, *J. Am. Chem. Soc.* **2009**, *131*, 3291-3306; d) J.-P. Leclerc, K. Fagnou, *Angew. Chem., Int. Ed.* **2006**, *45*, 7781-7786.
- [131] a) O. Kobayashi, D. Uraguchi, T. Yamakawa, *Org. Lett.* **2009**, *11*, 2679-2682; b) Y. Nakao, K. S. Kanyiva, T. Hiyama, *J. Am. Chem. Soc.* **2008**, *130*, 2448-2449.
- [132] a) A. M. Berman, J. C. Lewis, R. G. Bergman, J. A. Ellman, *J. Am. Chem. Soc.* **2008**, *130*, 14926-14927; b) J. C. Lewis, R. G. Bergman, J. A. Ellman, *J. Am. Chem. Soc.* **2007**, *129*, 5332-5333.
- [133] a) T. Kawashima, T. Takao, H. Suzuki, *J. Am. Chem. Soc.* **2007**, *129*, 11006-11007; b) E. J. Moore, W. R. Pretzer, T. J. O'Connell, J. Harris, L. LaBounty, L. Chou, S. S. Grimmer, *J. Am. Chem. Soc.* **1992**, *114*, 5888-5890.
- [134] S. Yanagisawa, K. Ueda, T. Taniguchi, K. Itami, *Org. Lett.* **2008**, *10*, 4673-4676.

- [135] a) N. Miyaura, K. Yamada, A. Suzuki, *Tetrahedron Lett.* **1979**, *20*, 3437-3440; b) N. Miyaura, A. Suzuki, *Chem. Commun.* **1979**, 866-867.
- [136] D. Milstein, J. K. Stille, *J. Am. Chem. Soc.* **1978**, *100*, 3636-3638.
- [137] J. C. W. Evans, C. F. H. Allen, *Org. Synth.* **1938**, *18*.
- [138] a) A. V. Askenov, A. V. Sarapy, *Chem. Heterocycl. Compd. (N. Y., NY, U. S.)* **2001**, *37*, 261-262; b) A. V. Askenov, O. N. Nadein, *Chem. Heterocycl. Compd. (N. Y., NY, U. S.)* **2000**, *36*, 1314-1318.
- [139] E. V. Panteleeva, V. D. Shteingarts, J. Grobe, B. Krebs, M. U. Triller, H. Rabeneck, *Z. Anorg. Allg. Chem.* **2003**, *629*, 71-82.
- [140] C. Cochenec, P. Rocca, F. Marsais, A. Godard, G. Quéguiner, *J. Chem. Soc., Perkin Trans. 1* **1995**, 979-984.
- [141] a) P. J. Pijper, H. van der Goot, H. Timmerman, W. T. Nauta, *Eur. J. Med. Chem.* **1984**, *19*, 399-404; b) S. W. Goldstein, P. J. Dambek, *Synthesis* **1989**, 221-222; c) S. Jakobsen, M. Tilset, *Tetrahedron Lett.* **2011**, *52*, 3072-3074.
- [142] a) R. Levine, W. M. Kadunce, *J. Chem. Soc. D* **1970**, 921-922; b) C. S. Giam, J. L. Stout, *J. Chem. Soc. D* **1970**, 478.
- [143] M. Mąkosza, *Chem. Soc. Rev.* **2010**, *39*, 2855-2868.
- [144] M. Tobisu, I. Hyodo, N. Chatani, *J. Am. Chem. Soc.* **2009**, *131*, 12070-12071.
- [145] K. M. Hossain, T. Kameyama, T. Shibata, K. Takagi, *Bull. Chem. Soc. Jpn.* **2001**, *74*, 2415-2420.
- [146] I. Hyodo, M. Tobisu, N. Chatani, *Chem. Commun.* **2012**, *48*, 308-310.
- [147] S. E. Baillie, V. L. Blair, D. C. Blakemore, D. Hay, A. R. Kennedy, D. C. Pryde, E. Hevia, *Chem. Commun.* **2012**, *48*, 1985-1987.
- [148] a) K. Kojima, M. Kimura, S. Ueda, Y. Tamaru, *Tetrahedron* **2006**, *62*, 7512-7520; b) D. G. Yakhvarov, Y. S. Ganushevich, O. G. Sinyashin, *Mendeleev Commun.* **2007**, *17*, 197-198.
- [149] D. R. Armstrong, V. L. Blair, W. Clegg, S. H. Dale, J. García-Álvarez, G. W. Honeyman, E. Hevia, R. E. Mulvey, L. Russo, *J. Am. Chem. Soc.* **2010**, *132*, 9480-9487.
- [150] E. Rijnberg, J. T. B. H. Jastrzebski, J. Boersma, H. Kooijman, N. Veldman, A. L. Spek, G. van Koten, *Organometallics* **1997**, *16*, 2239-2245.

- [151] M. Krieger, G. Geisler, K. Harms, J. Merle, W. Massa, K. Dehnicke, Z. *Anorg. Allg. Chem.* **1998**, 624, 1387-1388.
- [152] H. Hope, P. P. Power, *J. Am. Chem. Soc.* **1983**, 105, 5320-5324.
- [153] C. Strohmann, S. Dilsky, K. Strohfeltdt, *Organometallics* **2006**, 25, 41-44.
- [154] B. Schiemenz, P. P. Power, *Angew. Chem., Int. Ed. Engl.* **1996**, 35, 2150-2152.
- [155] D. Thoennes, E. Weiss, *Chem. Ber.* **1978**, 111, 3726-3731.
- [156] a) A. Krasovskiy, P. Knochel, *Angew. Chem., Int. Ed. Engl.* **2004**, 43, 3333-3336; b) H. Ren, A. Krasovskiy, P. Knochel, *Org. Lett.* **2004**, 6, 4215-4217; c) H. Ren, A. Krasovskiy, P. Knochel, *Chem. Commun.* **2005**, 543-545; d) A. Krasovskiy, V. Krasovskaya, P. Knochel, *Angew. Chem., Int. Ed. Engl.* **2006**, 45, 2958-2961.
- [157] D. H. Williams, I. Fleming, *Spectroscopic Methods in Organic Chemistry*, Fifth Edition ed., McGraw-Hill, London, **1995**.
- [158] a) L. A. Graham, J. Suryadi, T. K. West, G. L. Kucera, U. Bierbach, *J. Med. Chem.* **2012**, 55, 7817-7827; b) S. Ding, X. Qiao, G. L. Kucera, U. Bierbach, *J. Med. Chem.* **2012**, 55, 10198-10203.
- [159] R. M. Acheson, *Acridines*, Interscience Publishers Ltd, London, **1956**.
- [160] B. Jiang, X. Wang, M.-Y. Li, Q. Wu, Q. Ye, H.-W. Xu, S.-J. Tu, *Org. Biomol. Chem.* **2012**, 10, 8533-8538.
- [161] a) H. T. Nguyen Thi, C.-Y. Lee, K. Teruya, W.-Y. Ong, K. Doh-ura, M.-L. Go, *Bioorg. Med. Chem.* **2008**, 16, 6737-6746; b) G. W. Collie, S. Sparapani, G. N. Parkinson, S. Neidle, *J. Am. Chem. Soc.* **2011**, 133, 2721-2728; c) K. Zelenka, L. Borsig, R. Alberto, *Bioconjugate Chem.* **2011**, 22, 958-967; d) T. Nguyen, Y. Sakasegawa, K. Doh-ura, M.-L. Go, *Eur. J. Med. Chem.* **2011**, 46, 2917-2929; e) M. Tonelli, G. Vettoretti, B. Tasso, F. Novelli, V. Boido, F. Sparatore, B. Busonera, A. Ouhtit, P. Farci, S. Blois, G. Giliberti, P. La Colla, *Antiviral Res.* **2011**, 91, 133-141; f) L. Janovec, M. Kožurková, D. Sabolová, J. Ungvarský, H. Paulíková, J. Plšíková, Z. Vantová, J. Imrich, *Bioorg. Med. Chem.* **2011**, 19, 1790-1801; g) X. Luan, C. Gao, N. Zhang, Y. Chen, Q. Sun, C. Tan, H. Liu, Y. Jin, Y. Jiang, *Bioorg. Med. Chem.* **2011**, 19, 3312-3319.

- [162] a) B. Dutta, G. K. Kar, J. K. Ray, *Tetrahedron Lett.* **2003**, *44*, 8641-8643; b) J. Kwak, M. Kim, S. Chang, *J. Am. Chem. Soc.* **2011**, *133*, 3780-3783.
- [163] a) K. Yoon, S. M. Ha, K. Kim, *J. Org. Chem.* **2005**, *70*, 5741-5744; b) D. C. Rogness, R. C. Larock, *J. Org. Chem.* **2010**, *75*, 2289-2295; c) D. Tselikhovsky, S. L. Buchwald, *J. Am. Chem. Soc.* **2010**, *132*, 14048-14051; d) Z. Huang, Y. Yang, Q. Xiao, Y. Zhang, J. Wang, *Eur. J. Org. Chem.* **2012**, 6586-6593; e) G. Cholewiński, K. Dzierzbicka, A. M. Kołodziejczyk, *Pharmacol. Rep.* **2011**, *63*, 305-336; f) Y. Lian, J. R. Hummel, R. G. Bergman, J. A. Ellman, *J. Am. Chem. Soc.* **2013**, *135*, 12548-12551.
- [164] W. Clegg, L. Dunbar, L. Horsburgh, R. E. Mulvey, *Angew. Chem., Int. Ed. Engl.* **1996**, *35*, 753-755.
- [165] T. Wilklund, S. Olsson, A. Lennartson, *Monatsh. Chem.* **2011**, *142*, 813-819.
- [166] C. Melero, A. Guijarro, M. Yus, *Dalton Trans.* **2009**, 1286-1289.
- [167] a) B. Tamamushi, H. Akiyama, *Trans. Faraday Soc.* **1939**, *35*, 491-494; b) R. Noyori, M. Katô, M. Kawanisi, H. Nozaki, *Tetrahedron* **1969**, *25*, 1125-1136.
- [168] a) K. L. Handoo, J.-P. Cheng, V. D. Parker, *J. Chem. Soc., Perkin Trans. 2* **2001**, 1476-1480; b) N. Mackiewicz, J. A. Delaire, A. W. Rutherford, E. Doris, C. Mioskowski, *Chem. Eur. J.* **2009**, *15*, 3882-3888.
- [169] a) J. Chaudhuri, S. Kume, J. Jagur-Grodzinski, M. Szwarc, *J. Am. Chem. Soc.* **1968**, *90*, 6421-6425; b) A. Lomax, L. S. Marcoux, A. J. Bard, *J. Phys. Chem.* **1972**, *76*, 3958-3960; c) M. Ishikawa, S. Fukuzumi, *J. Am. Chem. Soc.* **1990**, *112*, 8864-8870; d) J. S. Jaworski, M. Cembor, *Tetrahedron Lett.* **2000**, *41*, 7267-7270; e) M. Taguchi, M. Moriyama, H. Namba, H. Hiratsuka, *Radiat. Phys. Chem.* **2002**, *64*, 115-122; f) S. Fukuzumi, J. Yuasa, N. Satoh, T. Suenobu, *J. Am. Chem. Soc.* **2004**, *126*, 7585-7594.
- [170] A. Lennartson, M. Håkansson, *Acta Crystallogr., Sect. C: Cryst. Struct. Commun.* **2009**, m205-m207.
- [171] W. Schlenk, J. Holz, *Ber. Dtsch. Chem. Ges.* **1917**, *50*, 262-274.
- [172] G. C. Forbes, A. R. Kennedy, R. E. Mulvey, P. J. A. Rodger, *Chem. Commun.* **2001**, 1400-1401.

- [173] W. J. Evans, S. L. Gonzales, J. W. Ziller, *J. Am. Chem. Soc.* **1994**, *116*, 2600-2608.
- [174] S. Labouille, F. Nief, X.-F. Le Goff, L. Maron, D. R. Kindra, H. L. Houghton, J. W. Ziller, W. J. Evans, *Organometallics* **2012**.
- [175] A. Sattler, G. Zhu, G. Parkin, *J. Am. Chem. Soc.* **2009**, *131*, 7828-7838.
- [176] Y. S. Kim, Y. S. Won, H. Hagelin-Weaver, N. Omenetto, T. Anderson, *J. Phys. Chem. A* **2008**, *112*, 4246-4253.
- [177] a) D. Seebach, W. Bauer, J. Hansen, T. Laube, W. B. Schweizer, J. D. Dunitz, *J. Chem. Soc., Chem. Commun.* **1984**, 853-854; b) P. C. Andrews, M. Maguire, E. Pombo-Villar, *Helv. Chim. Acta* **2002**, *85*, 3516-3524; c) P. C. Andrews, M. Maguire, E. Pombo-Villar, *Eur. J. Inorg. Chem.* **2003**, 3305-3308.
- [178] M. Chaignaud, I. Gillaizeau, N. Ouhamou, G. Coudert, *Tetrahedron* **2008**, *64*, 8059-8066.
- [179] a) S. Bernhardt, G. Manolikakes, T. Kunz, P. Knochel, *Angew. Chem., Int. Ed.* **2011**, *50*, 9205-9209; b) C. I. Stathakis, S. Bernhardt, V. Quint, P. Knochel, *Angew. Chem., Int. Ed.* **2012**, *51*, 9428-9432; c) C. I. Stathakis, S. M. Manolikakes, P. Knochel, *Org. Lett.* **2013**, *15*, 1302-1305.
- [180] A. Hernán-Gómez, E. Herd, E. Hevia, A. R. Kennedy, P. Knochel, K. Koszinowski, S. M. Manolikakes, R. E. Mulvey, C. Schnegelsberg, *Angew. Chem., Int. Ed.* **2014**, *126*, 2744-2748.
- [181] I. Resa, E. Carmona, E. Gutierrez-Puebla, A. Monge, *Science (Washington, DC, U. S.)* **2004**, *305*, 1136-1138.
- [182] S. Schulz, *Chem. Eur. J.* **2010**, *16*, 6416-6428.
- [183] T. Li, S. Schulz, P. W. Roesky, *Chem. Soc. Rev.* **2012**, *41*, 3759-3771.
- [184] E. Carmona, A. Galindo, *Angew. Chem., Int. Ed.* **2008**, *47*, 6526-6536.
- [185] Y.-C. Tsai, D.-Y. Lu, Y.-M. Lin, J.-K. Hwang, J.-S. K. Yu, *Chem. Commun.* **2007**, 4125-4127.
- [186] a) M. Veith, *Chem. Rev.* **1990**, *90*, 3-16; b) R. Murugavel, N. Palanisami, R. J. Butcher, *J. Organomet. Chem.* **2003**, *675*, 65-71.
- [187] V. L. Blair, W. Clegg, A. R. Kennedy, Z. Livingstone, L. Russo, E. Hevia, *Angew. Chem., Int. Ed.* **2011**, *50*, 9857-9860.

- [188] M. Shilai, Y. Kondo, T. Sakamoto, *J. Chem. Soc., Perkin Trans. 1* **2001**, 442-444.
- [189] D. R. Armstrong, W. Clegg, A. Hernán-Gómez, A. R. Kennedy, Z. Livingstone, S. D. Robertson, L. Russo, E. Hevia, *Dalton Trans.* **2014**, 43, 4361-4369.
- [190] D. R. Armstrong, J. A. Garden, A. R. Kennedy, S. M. Leenhouts, R. E. Mulvey, P. O'Keefe, C. T. O'Hara, A. Steven, *Chem. Eur. J.* **2013**, 19, 13492-13503.
- [191] S. Schmidt, S. Schulz, D. Bläser, R. Boese, M. Bolte, *Organometallics* **2010**, 29, 6097-6103.
- [192] P. C. Andrews, C. L. Raston, B. W. Skelton, A. H. White, *Organometallics* **1998**, 17, 779-782.
- [193] Z. Livingstone, University of Strathclyde (Glasgow), **2012**.
- [194] W. S. Rees, O. Just, H. Schumann, R. Weimann, *Polyhedron* **1998**, 17, 1001-1004.
- [195] C. O. Kappe, *Angew. Chem., Int. Ed.* **2004**, 43, 6250-6284.
- [196] S. E. Baillie, V. L. Blair, T. D. Bradley, W. Clegg, J. Cowan, R. W. Harrington, A. Hernán-Gómez, A. R. Kennedy, Z. Livingstone, E. Hevia, *Chem. Sci.* **2013**, 4, 1895-1905.
- [197] J.-M. L'Helgoual'ch, A. Seggio, F. Chevallier, M. Yonehara, E. Jeanneau, M. Uchiyama, F. Mongin, *J. Org. Chem.* **2008**, 73, 177-183.
- [198] G. R. Fulmer, A. J. M. Miller, N. H. Sherden, H. E. Gottlieb, A. Nudelman, B. M. Stoltz, J. E. Bercaw, K. I. Goldberg, *Organometallics* **2010**, 29, 2176-2179.
- [199] A. Streitwieser, A. Facchetti, L. Xie, X. Zhang, E. C. Wu, *J. Org. Chem.* **2012**, 77, 985-990.
- [200] S. C. Watson, J. F. Eastham, *J. Organomet. Chem.* **1967**, 9, 165-168.
- [201] A. Krasovicky, P. Knochel, *Synthesis* **2006**, 5, 890-891.

Appendix of Crystallographic Data

compound	4a	5	8
formula	C ₈ H ₂₄ LiNSi ₂ Zn	C ₁₇ H ₄₇ LiN ₄ Si ₂ Zn	C ₃₀ H ₅₂ Li ₂ N ₄
form wt	262.77	436.08	482.6
cryst system	Monoclinic	monoclinic	Triclinic
space group	<i>P2₁/n</i>	<i>P2₁/c</i>	<i>P1</i>
<i>a</i> , Å	6.7840(3)	9.616(3)	8.4634(5)
<i>b</i> , Å	13.9936(7)	13.522(4)	9.1374(10)
<i>c</i> , Å	15.8133(7)	20.444(6)	10.9932(7)
<i>α</i> , deg	90	90	10.9932(7)
<i>β</i> , deg	97.650(2)	100.676(4)	87.935(6)
<i>γ</i> , deg	90	90	72.640(7)
<i>V</i> , Å ³	1487.84(12)	2612.2(12)	784.49(11)
<i>Z</i>	4	4	1
<i>D</i> _{calcd} , mg m ⁻³	1.173	1.109	1.022
<i>μ</i> , mm ⁻¹	1.777		0.059
<i>T</i> , K	123(2)	150	150
cryst size, mm	0.40 x 0.08 x 0.05	---	0.37 x 0.34 x 0.29
reflns measd	17703	22855	8844
unique reflns	3239	6301	2709
<i>R</i> _{int}	0.069	0.0185	0.029
no of params	141		173
<i>R</i> (<i>F</i> , <i>F</i> ² > 2σ)	0.0655	0.0227	0.043
<i>R</i> _w (<i>F</i> ² , all data)	0.1347	0.0642	0.110
goodness of fit	1.239	1.036	1.08
max, min Δρ, e Å ⁻³	0.772, -0.515	±0.344	0.20, -0.17

compound	9	10	12
formula	C ₂₁ H ₄₁ LiN ₄	C ₂₃ H ₄₇ LiN ₄ Zn _{0.5} C ₇ H ₈	C ₃₉ H ₆₉ LiN ₂ O ₃ Z n ₂
form wt	356.5	498.0	751.6
cryst system	Orthorhombic	Triclinic	Orthorhombic
space group	<i>P2₁2₁2₁</i>	<i>P1</i>	<i>Pbca</i>
<i>a</i> , Å	10.0117(11)	9.6061(10)	18.1783(1)
<i>b</i> , Å	14.6223(17)	9.8717(7)	18.6099(2)
<i>c</i> , Å	15.682(2)	16.5903(17)	24.4975(2)
<i>α</i> , deg	90	91.976(7)	90
<i>β</i> , deg	90	101.641(8)	90
<i>γ</i> , deg	90	104.928(7)	90
<i>V</i> , Å ³	2295.7(5)	1482.6(2)	8287.42(12)
<i>Z</i>	4	2	8
<i>D</i> _{calcd} , mg m ⁻³	1.031	1.116	1.205
<i>μ</i> , mm ⁻¹	0.061	0.847	1.192
<i>T</i> , K	150	150	123
cryst size, mm	0.82 x 0.48 x 0.32	0.61 x 0.48 x 0.39	0.32 x 0.08 x 0.08
reflns measd	8017	21036	17290
unique reflns	2249	5171	9026
<i>R</i> _{int}	0.030	0.033	0.024
no of params	248	323	439
<i>R</i> (<i>F</i> , <i>F</i> ² > 2σ)	0.047	0.028	0.045
<i>R</i> _w (<i>F</i> ² , all data)	0.145	0.074	0.121
goodness of fit	0.99	1.05	1.09
max, min Δρ, e Å ⁻³	0.44, -0.23	0.35, -0.21	0.99, -0.39

compound	15	17	18
formula	C ₃₄ H ₅₁ LiO ₂ Zn	C ₃₁ H ₃₈ LiNO ₃	C ₃₀ H ₃₇ Li N ₃ O ₂
form wt	564.06	479.56	471.00
cryst system	Monoclinic	Monoclinic	Monoclinic
space group	P2 ₁ /c	C 2/c	P2 ₁ /n
<i>a</i> , Å	10.0754(2)	23.5458(17)	11.2576(14)
<i>b</i> , Å	15.4637(2)	12.2928(6)	13.2749(15)
<i>c</i> , Å	21.0465(3)	22.9569(15)	20.827(4)
<i>α</i> , deg	90	90	90
<i>β</i> , deg	93.894(2)	119.215(9)	121.455(11)
<i>γ</i> , deg	90	90	90
<i>V</i> , Å ³	3271.54(9)	5799.5(8)	2655.1(7)
<i>Z</i>	4	8	4
<i>D</i> _{calcd} , mg m ⁻³	1.145	1.098	1.178
<i>μ</i> , mm ⁻¹	1.222	0.069	0.570
<i>T</i> , K	123(2)	123(2)	123(2)
cryst size, mm	0.20 x 0.15 x 0.10	---	0.35 x 0.2 x 0.1
reflns measd	12765	16246	10151
unique reflns	6351	6308	4981
<i>R</i> _{int}	0.0220	0.0698	0.0333
no of params	406	325	378
<i>R</i> (<i>F</i> , <i>F</i> ² > 2σ)	0.0519	0.0602	0.0749
<i>R</i> _w (<i>F</i> ² , all data)	0.0589	0.1759	0.2531
goodness of fit	1.069	0.993	1.024
max, min Δρ, e Å ⁻³	1.249, -0.602	0.354 and -0.268	0.365 and -0.262

compound	19	21	22
formula	C ₂₅ H ₁₉ NZn	C ₂₇ H ₄₂ LiN ₃ O _{1.5}	C ₄₆ H ₆₀ N ₂ O ₄ Zn ₂
form wt	398.78	439.57	835.70
cryst system	Monoclinic	Monoclinic	Monoclinic
space group	P2 ₁ /c	C 2/c	P2 ₁ /c
<i>a</i> , Å	15.3642(4)	19.2908(4)	14.5403(6)
<i>b</i> , Å	10.9499(2)	16.9267(4)	9.8708(3)
<i>c</i> , Å	11.3094(3)	15.7419(4)	14.2643(6)
<i>α</i> , deg	90	90	90
<i>β</i> , deg	92.602(3)	90	97.879(4)
<i>γ</i> , deg	90	90	90
<i>V</i> , Å ³	1900.69(8)	5140.2(2)	2027.95(13)
<i>Z</i>	4	8	2
<i>D</i> _{calcd} , mg m ⁻³	1.394	1.136	1.369
<i>μ</i> , mm ⁻¹	1.300	0.069	1.806
<i>T</i> , K	123(2)	123(2)	123(2)
cryst size, mm	0.25 x 0.25 x 0.1	---	0.20 x 0.15 x 0.10
reflns measd	13723	16876	11235
unique reflns	4715	9173	11237
<i>R</i> _{int}	0.0183	0.0348	0.0000
no of params	251	614	246
<i>R</i> (<i>F</i> , <i>F</i> ² > 2σ)	0.0256	0.0622	0.0603
<i>R</i> _w (<i>F</i> ² , all data)	0.0680	0.1652	0.1945
goodness of fit	1.061	1.028	1.048
max, min Δρ, e Å ⁻³	0.357 and -0.291	0.654 and -0.356	0.958 and -0.398

compound	23	24	29
formula	C ₁₈ H ₂₅ LiN ₂ O ₂	C ₁₆ H ₁₄ N ₂ Zn	C ₆₂ H ₉₇ N ₂ NaO ₆ SiZn
form wt	308.34	299.66	1082.86
cryst system	Orthorhombic	Monoclinic	Monoclinic
space group	Pca2 ₁	Cc	P 2 ₁ /c
<i>a</i> , Å	17.9002(13)	20.1307(5)	18.0178(5)
<i>b</i> , Å	8.0757(7)	6.09820(10)	13.6705(4)
<i>c</i> , Å	12.1516(10)	11.2722(3)	25.3898(7)
<i>α</i> , deg	90	90	90
<i>β</i> , deg	90	96.616(2)	95.675(2)
<i>γ</i> , deg	90	90	90
<i>V</i> , Å ³	1756.6(2)	1374.57(5)	6223.2(3)
<i>Z</i>	4	4	4
<i>D</i> _{calcd} , mg m ⁻³	1.166	1.448	1.156
<i>μ</i> , mm ⁻¹	0.591	2.352	0.469
<i>T</i> , K	123(2)	123(2)	123(2)
cryst size, mm	0.40 x 0.35 x 0.30	0.25 x 0.20 x 0.10	---
reflns measd	5320	4352	60658
unique reflns	2698	1360	16103
<i>R</i> _{int}	0.0308	0.0250	0.0462
no of params	241	87	715
<i>R</i> (<i>F</i> , <i>F</i> ² > 2σ)	0.0601	0.0267	0.0484
<i>R</i> _w (<i>F</i> ² , all data)	0.0611	0.0270	0.1256
goodness of fit	1.041	1.078	1.033
max, min Δρ, e Å ⁻³	0.264, -0.234	0.399, -0.263	0.586 and -0.397

compound	30	31	32
formula	C ₄₉ H ₇₀ N ₃ NaOSiZn	C ₅₈ H ₅₆ N ₆ Na ₂ O ₄ S ₆ Zn ₂	C ₃₂ H ₄₈ N ₄ Na ₂ O ₄ Zn
form wt	833.53	1270.17	664.09
cryst system	Orthorhombic	Triclinic	Monoclinic
space group	P 2c -2n	P $\bar{1}$	Cc
<i>a</i> , Å	17.2893(3)	9.8371(4)	23.6422(12)
<i>b</i> , Å	21.3819(4)	11.4768(6)	8.1652(3)
<i>c</i> , Å	12.5798(3)	13.7537(7)	19.3302(10)
α , deg	90	91.026(5)	90
β , deg	90	108.304(4)	113.312(6)
γ , deg	90	99.002(4)	90
<i>V</i> , Å ³	4650.48(16)	1452.32(12)	3426.9(3)
<i>Z</i>	4	1	4
<i>D</i> _{calcd} , mg m ⁻³	1.191	1.452	1.287
μ , mm ⁻¹	0.601	0.992	0.782
<i>T</i> , K	123(2)	123(2)	123(2)
cryst size, mm	---	---	---
reflns measd	11046	9182	10909
unique reflns	9141	8135	7318
<i>R</i> _{int}	0.0312	0.0173	0.0237
no of params	597	366	432
<i>R</i> (<i>F</i> , <i>F</i> ² > 2 σ)	0.0572	0.0889	0.0398
<i>R</i> _w (<i>F</i> ² , all data)	0.1452	0.2245	0.0937
goodness of fit	1.112	1.075	1.017
max, min $\Delta\rho$, e Å ⁻³	0.978 and -0.515	0.854 and -0.769	0.471 and -0.393